STUDIES ON DOPED AND UNDOPED HIGH TEMPERATURE SUPERCONDUCTING THIN FILMS

A thesis submitted for the award of the degree of
Doctor of Philosophy

by

SATHIRAJU SRINIVAS

School of Physics
University of Hyderabad
Hyderabad - 500 046.
India.

January - 1996.

dedicated to

TO MY MOTHER

who gave me the desire for learning

UNIVERSITY OF HYDERABAD
SCHOOL OF PHYSICS

12th January 1996

CERTIFICATE

This is to certify that I, Sathiraju Srinivas, have carried out the research embodied in the present thesis titled "STUDIES ON DOPED AND UNDOPED HIGH TEMPERATURE SUPERCONDUCTING THIN FILMS" for the full period prescribed under the Ph.D. Ordinances of the University.

I declare to the best of my knowledge that no part of this thesis was earlier submitted for the award of research degree of any University.

S Srinivas

(S. SRINIVAS)
Regn. No. PP5923

AMPath

(A.P. Pathak)
Dean of the School

AK Bhatnagar

(Anil K. Bhatnagar)
Supervisor

Prof. ANIL. K. BHATNAGAR
School of Physics
University of Hyderabad
Hyderabad-500 134, INDIA

Preface

The discovery of superconductivity at relatively higher temperatures (30-35 K) in La-Ba-CuO ceramics by Bednorz and Muller in 1986 was a major forward step in the era of high temperature superconductivity. Within next few years many ceramic oxides with perovskite structures were invented with T_c s as high as 134 K. However, due to their ceramic nature of these materials, immediate technical applications are not possible. The success of thin film technology in achieving excellent superconducting properties than those realized in the bulk form of the superconducting materials has been attributed to the microstructural control and compositional purity attainable with the thin film deposition techniques. Hence, it is important to study the microstructure of superconducting thin films on various substrates that have different structural and chemical properties and having technological application potential. Moreover, successful control of orientation, surface morphology and crystal quality requires a detailed understanding of the issues like of nucleation, growth and epitaxy. These features clearly dependent on the process used for the film deposition, deposition parameters and properties of the materials involved in it.

This thesis deals with the investigations of the early stages of growth process i.e., substrate temperature dependence on the microstructure and superconducting properties of sputter deposited films and Pulsed Laser deposited (Y,Yb)-Ba-Cu-O thin films on various substrates. In addition, substitution effects at Cu site and doping of metal oxides which are having melting points below 800 °C and much above 800 °C are also studied. It was well established by many researchers that HTS films having thickness in between 1000 - 2000 Å will show good microstructural, and superconducting properties (T_c and J_c) and hence in this thesis the above mentioned thickness range was considered for all depositions. Precisely, this thesis attempts to study the microstructural and superconducting properties (like T_c and J_c) dependence on growth conditions of HTS thin

films.

The work embodied in this thesis has been divided into seven chapters. All chapters are self explanatory with individual introduction, review of the literature, description of the experimental procedure, results and discussions, conclusions and list of references. A brief sketch of the thesis chapter wise is given below.

Chapter I consists of the introduction to superconductivity, characteristics of conventional superconductors, a review on HTS research with special reference to Y-123 system and current status of HTS thin films research and motivation for the research work.

Chapter II describes the experimental techniques used in the work reported in this thesis.

Chapter III deals with the design and fabrication of new magnetron geometry for sputter deposition of Y-123 and Y-124 thin films. Preparation of Y-123 and Y-124 thin films on MgO<100> and $SrTiO_3$<100> substrates respectively was discussed in detail.

Chapter IV discusses fabrication of good quality YSZ and STO buffer layers on Si and Sapphire substrates for realizing good quality Y-123 thin films and their microstructural study using SEM and AFM techniques.

Chapter V describes preparation of Y-123 and Yb-123 thin films on $LaAlO_3$ substrates using PLD method and their microstructural properties.

In Chapter VI preparation of $YBa_2Cu_{3-x}Nb_xO_{7-y}$ thin films on $LaAlO_3$ substrates was discussed.

In chapter VII results of the effect of addition of V_2O_5 and Nb_2O_5 to Y-123 in thin films are presented.

Acknowledgments

It is my great pleasure to express my gratitude to my beloved supervisor Prof. Anil K. Bhatnagar, whose constant inspiration and invaluable suggestions always led me towards the right direction. I am grateful to him for the confidence he has shown in me to pursue this project with a free hand and in my own personal style. The extent to which I have benefited both personally and professionally from my interaction with him can not be stated in words.

I wish to express my gratitude to Dr. V.D. Vankar, Prof. L.K. Malhothra and Prof. K. L. Chopra, Thin Film Laboratory, I.I.T. Delhi for introducing me to the Science and Technology of Thin films.

I am indeed grateful to Prof. R.Pinto of the Solid State Electronics Group, TIFR, Bombay who kindly agreed to extend experimental facilities in his well equipped research laboratory for most of the work reported here. His constant encouragement was indeed a great help to me throughout my stay at TIFR, Bombay. I am grateful to Prof. R.Pinto and Dr.P.R. Apte, Prof Roy, Messers S.P.Pai, C.P.D'souza, S.C.Purandare and Dhananjay Kumar in TIFR, Bombay.of the Solid State Electronics Group, TIFR, Bombay for the free access to their laboratories and equipment. Also, I could never forget the encouragement, support and affection that I got from Prof. M. S. Multani and Dr. V.R. Palkar, Materials Research Group, and Prof. L.C. Gupta and Prof. R. Vijayaraghavan and all other research scholars at TIFR. Their personalities and interests provided an atmosphere which helped my work at TIFR both pleasant and productive. I, sincerely express my deep sense of gratitude to all of them.

My sincere thanks are due to the Dean, School of Physics, for extending the facilities of the School to me. My thanks are also due to all teaching and nonteaching members of the School of Physics and CIL staff members for their cooperation.

I owe my gratitude to Prof. S.B. Ogale, Department of Physics, University of Poona, Pune; *Dr* V. S. Raghunathan, Head, Physical Metallurgy Section, IGCAR, Kalpakkam, Dr. M.S.R. Rao, I.I.T, Madras, Dr. M. D. Sastry, BARC, Bombay and Prof. G. V. Subbarao, Director E. C. Labs for their timely help and useful suggestions.

I wish to express my deep sense of gratitude to the Director Dr. S.L.N Acharyulu for allowing me to use DMRL facilities. Also, I would like to express my sincere thanks to Sri Hema Reddy, *Dy* Director; Mrs. Lalitha Kumari, Scientist *C*; Mr. Shankar, SSA; Mrs. T. Nirmala and Sri A.S.R.Nair of DMRL, Hyderabad for showing their genuine interest towards my work.

I wish to thank all of my earlier lab mates and present members *Ms* P. Indira, *Ms* B. Seshu, G. V. Sudhakar, C. Trinath Mohan and lab assistant E. Siriyalu who have never failed to come to my aid when I am in need of their help. I wish to thank my friends Dr. Y.S. Rao, Dr. P.D. Babu, Dr.V.V. Ravi Kanth Kumar and Mr. V. V. Saikumar for their constant cooperation. I wish to thank all the research scholars in the school of Physics for giving me good company.

I am deeply indebted to my sister Dr.S. Annapurna for her affection, constant encouragement and timely help. My sincere thanks are due to my elder brother Mr.S. Venkatachalam, to my elder sisters Ms.S. V. Kameswari, Ms.S. Vijaya kumari, Ms. V. Sarada and Ms. N. Usha Rani, for their love, affection, financial and moral support and who have been most responsible for what I am today. I equally owe to my brother-in-laws for their affection and encouragement.

Finally, I record my thanks to the University Grants Commission, NEW DELHI for the research fellowship and I wish to thank all the people, who are directly or indirectly involved in bringing up this piece of work.

S. Srinivas

Srinivas Sathiraju

Table of Contents

Chapter 1

Overview

A brief introduction to superconductivity, high T_c superconducting materials thin film techniques and motivation for the work presented in this thesis is given in the following sections.

1.1 Introduction

Superconductivity in mercury at temperature 4.2 K was discovered by K. Onnes in 1911 [1]. i.e., electrical resistance of mercury vanished (within measurement accuracy) suddenly at 4.2 K, the superconducting transition temperature T_c, as shown in Fig.1.1. Another breakthrough in the field of superconductors came in 1933 when Meissner and Oschenfeld discovered that a superconductor excluded magnetic flux from its inside completely [2] in a weak magnetic field i.e., a superconductor behaved like a perfect diamagnet (Fig.1.2). This observation was in contradiction to the expected behaviour of a perfect conductor which should maintain a constant internal magnetic field ($dB/dt = 0$) according to the classical electromagnetic theory. The infinite conductivity and perfect diamagnetism (in a weak magnetic field) are two characteristic features of a superconductor. Discovery of

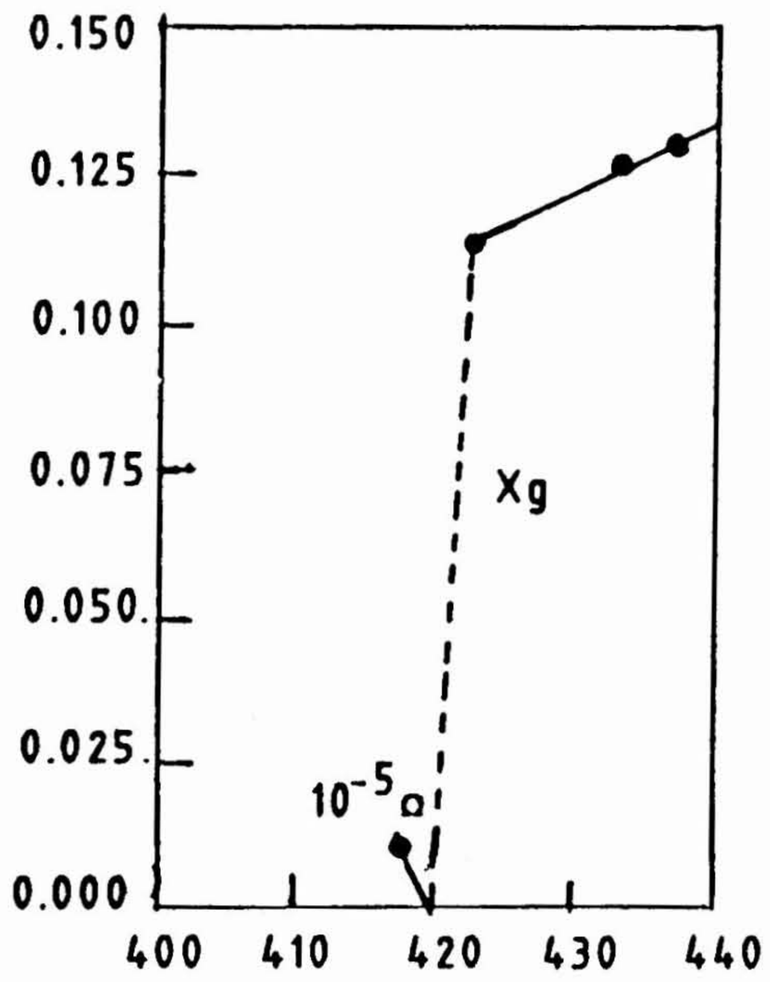

Fig.1.1. Resistance in ohms of a specimen of mercury versus absolute temperature. This plot by Kamerlingh Onnes marked the discovery of superconductivity.

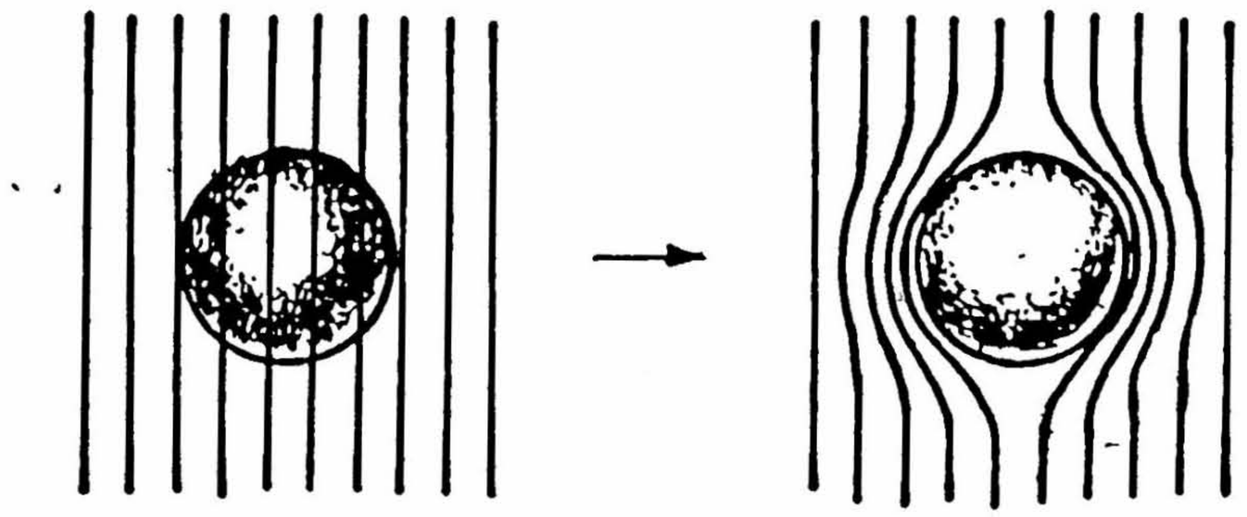

Fig.1.2. Meissner effect in a superconducting sphere cooled in a constant applied magnetic field; on passing below the transition temperature the lines of induction B are ejected from the sphere.

the superconductivity obviously indicated the possibility of a large number of applications based on zero resistivity and diamagnetism but most of these remained economically not viable because of low T_c of superconductors (discovered until 1986), which included elements, alloys, and compounds. The maximum $T_c \simeq 23.2$ K was obtained for Nb_3Ge which reached just above liquid hydrogen boiling temperature at the standard pressure [3].

A feverish activity at a number of centres continued all these years to discover superconductor which will have T_c as high as 100 K or upto room temperature but without success. A real break through came in 1986 when Bednorz and Muller discovered superconductivity in $LaBaCuO$ system at 32 K [4]. Soon after higher T_c in pervoskite type cuprate oxide compounds were discovered one after another; $YBa_2Cu_3O_{7-x}$ (92 K) [5], $Bi_2Sr_2CaCu_2O_x$ (80 K) [6], $Bi_2Sr_2Ca_2Cu_3O_x$ (110 K) [7], $Tl_2Ba_2Ca_2Cu_3O_x$ (125 K) [8] and most recently $HgBa_2Ca_{n-1}Cu_nO_{2+2n+\delta}$ (for n = 3, T_c is 134 K at ambient pressure and 164 K at 30 Gpa pressure) [9,10]. Previously, oxide superconductors, e.g. $Ba_{1-x}Pb_xBiO_3$, had only low T_c ($\leq$ 10 K). [Here after, conventional or LT superconductors (LTS) will be referred to superconductors having $T_c < 25$ K, and cuprate oxide superconductors discovered in 1986 and afterwards as HTS for the brevity]. Fig 1.3 shows the discovery of higher and higher T_c superconductors as a function of years since 1911. It may be added that in 1994 a new family of superconductors RNi_2B_2C ($R = Y$, Ho, Tm etc.) were discovered, but their T_c values are similar to those of LTS (< 30 K) [11,12]. However, importance of the discovery of these borocarbide superconductor is that it is the first time that superconductors having so much of Ni, which is a ferromagnetic metal, have been found.

Discovery of HTS raised enormous hopes of using these superconductors for large scale applications because these devices could be operated using relatively cheaper cryogen liquid nitrogen. However, due to their ceramic nature, technological problems associated with using these HTS for practical applications requires innovative approaches, this is particularly important to large scale applications. However, small scale applications based on HTS thin film devices seem to be not so difficult to prepare and seem to be economically viable. Hence, enormous effort on HTS thin film research and development by various groups has been undertaken.

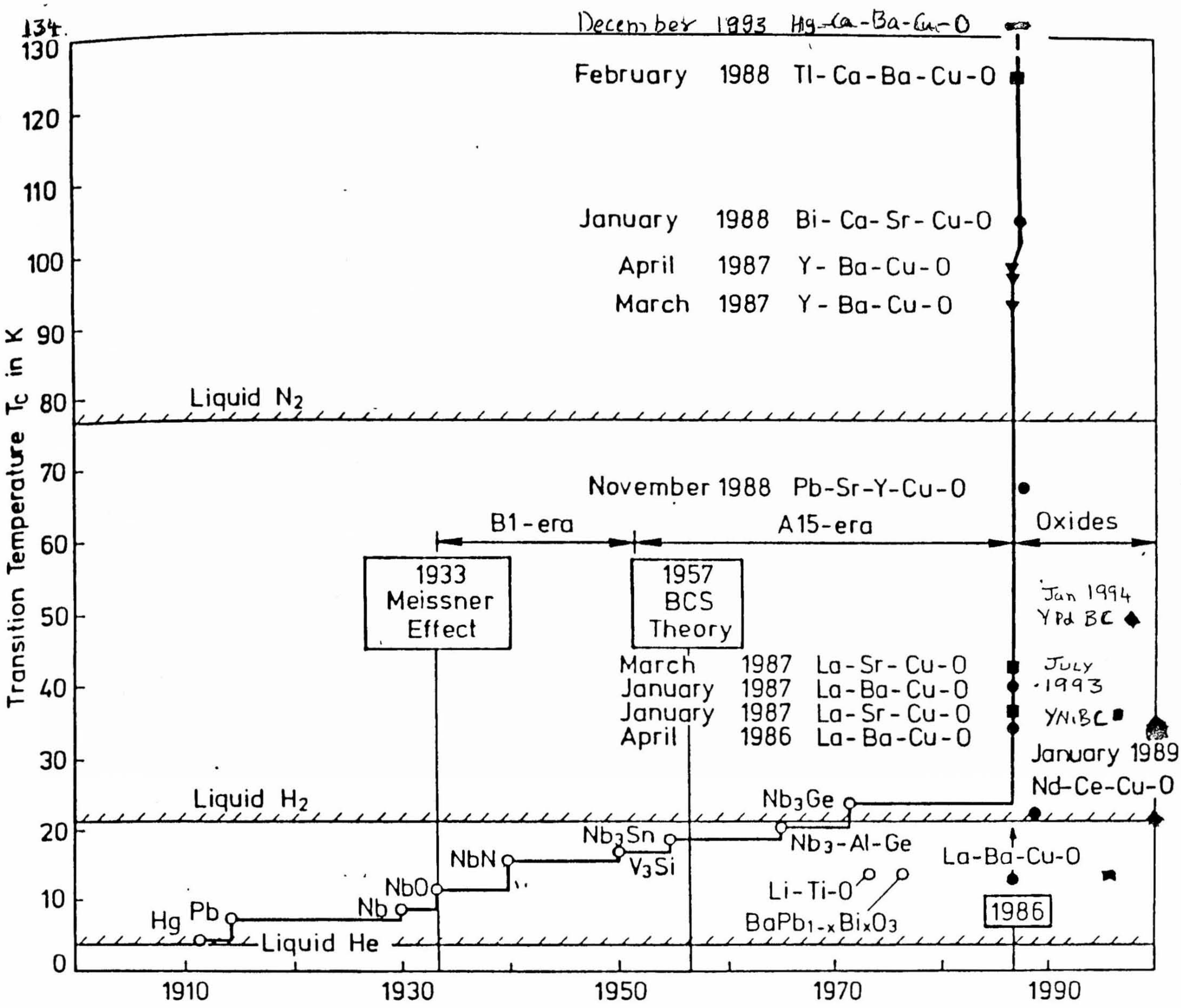

Fig.1.3. The evolution of superconducting materials initially proceeded very slowly after Kamerling Onnes discovery in 1911. Bednorz and Muller's work on La-Ba-Cu-O triggered a world-wide superconductivity fever resulting in the discovery of new superconducting materials and sky-rocketing critical temperature.

Preparation of good quality, stoichiometric and single phase HTS thin films presents its own difficulties because of the multi element nature of the HTS compounds. Superconductivity in these compounds is highly dependent on the correct stoichiometry of the HTS compounds. The broad objectives of the experimental study, reported here, is to prepare good quality $YBa_2Cu_3O_{7-x}$ $(Y-123)$ films. In this work, a *good quality* film will mean that it has T_c close to that of the bulk and the critical current (J_c) is as high as possible, since J_c is an important parameter for various practical applications. Below a brief description of superconductivity, thin film techniques etc., are given.

1.2 Superconductivity

As mentioned before a superconductor is characterized by zero resistivity (inifinite conductivity) and perfect diamagnetism in weak magnetic fields. Superconductivity in a material can be destroyed by raising its temperature above T_c as well as by placing it in a high enough magnetic field ($H \geq H_c$, critical magnetic field) or passing through it a large enough current ($J \geq J_c$, critical current density). Both H_c and J_c are functions of temperature. For most practical applications one would like to have high T_c, high H_c and J_c.

The discovery of Meissner effect lead to application of thermodynamics to superconductors, and to relate thermal properties with the critical field and its derivatives. A jump in specific heat at T_c and $C_v \propto T^3$ were predicted and observed. A large amount of experimental data on various physical properties of superconductors soon became available immediately after the original discovery of superconductivity in mercury, and Meissner effect in 1933. Various theories were put forward to explain these results. The two fluid model tried to explain faster decrease of C_v (in contrast to that of normal metals where $C_v \propto T$) etc. The two fluid model of Gorter and Casimir assumes that below T_c, total number of electrons split between normal electrons having finite conductivity (σ) and superconducting electrons having infinite conductivity [13]. Using an appropriate free energy expression, it was shown that this approach predicted $C_v \propto T^3$; $n_s/n = 1-(T/T_c)^4$, when n_s/n is the fraction of superconducting electrons; and $H_c(T) = H_c[1-(T/T_c)^2]$

which agreed well with the experimental observations.

London developed a theory [14,15] of electrodynamics of superconductors which predicted Meissner effect except that the magnetic inductions $B_{in}(x)$ inside a bulk superconductor, when placed in a magnetic field, does not go to zero suddenly at the surface but drops exponentially inside, i.e.

$$B_{in}(x) = B_o\, e^{-x/\lambda}$$

where λ is a characteristic length known as London's penetration depth given by $(4\pi n_s e^2/mc^2)^{1/2}$. Since $n_s = n_s(T)$, $\lambda = \lambda(T)$.

London's theory was slightly modified by Pippard [16]. Pippard's theory resulted in an additional characteristic length, so called the coherence length ξ, which although temperature independent but depended upon the electron mean free path, l, through the relation $\xi^{-1} = \xi_o^{-1} + \alpha l^{-1}$, where $\alpha \simeq 1$, and $\xi = \xi_o$ as l tends to $\propto$. In this theory, the magnetic penetration depth λ not only depends on T but also on l. Smaller the electron mean path l, larger the penetration depth λ and smaller the coherence length ξ at a given temperature. The concept of coherence in superconductor, therefore, must be attributed to Pippard. The relative magnitudes of λ and ξ determine the magnetic behaviour of a superconductor which will be explained in a later section. These can vary from few tens to thousands of $\mathring{A}$.

Many of the results on LT superconductors remained unexplained even after phenomenological theories of London and Pippard. There was no microscopic theory which could explain most of the properties of superconductors until 1950's. Two ground breaking theoretical advances were made in 1950s which provided the basis for our present understanding of superconductivity. The first was the Ginzburg-Landau (GL) theory, which introduced an order Ψ parameter such that $\Psi^*\Psi$ it gives the local density of superconducting electrons/carriers. The theory is strictly valid near T_c but gives reasonable good agreement with experiments even below T_c but not too far. In this theory also, a superconductor is characterized by two characteristic lengths, magnetic penetration depth $\lambda(T)$, and Ginzburg Landau coherence length $\xi(T)$. $\xi(T)$ is the minimum distance over which Ψ can change appreciably. Again, relative magnitude of λ and ξ determine details of the magnetic behaviour of a superconductor [17].

The real breakthrough in the theory of superconductivity came in 1957 when Bardeen Cooper and Schriefer (BCS) formulated a microscopic theory based on the formation of bound electron pairs (Cooper pairs) at temperatures below T_c because of an attractive interaction between electrons mediated by phonons [18,19]. The BCS theory shows why current carriers move through a superconductor without net scattering, thus avoiding dissipation (resistivity). There is a characteristic difference in energy (the energy gap) between the ground state (Cooper pairs) and the accessible excitations (normal electrons) which is of the order of 10^{-3} to $10^{-4}eV$. The single particle scattering is not possible because of the ordered state consisting of Cooper pairs [20]. In the limit of weak coupling between electron-phonon, the theory predicts T_c of a superconductor by the eqn.

$$k_B T_C = 1.14\hbar\omega_D \exp(-1/N(0)V)$$

where ω_D is the characteristic Debye frequency of phonons, $N(0)$ is the density of states at the Fermi level and V is the attractive effective interaction between the electrons. The highest possible value of T_c in this model (weak coupling limit $N(0)V \ll 1$) is ~ 30 K.

By the time the BCS theory was given, a good amount of experimental data on superconductors was pointing towards the existence of the energy gap. Source of these were :

1. Exponential decrease of the electronic specific heat of a number of superconductors below $T_c/3$;
2. exponential decrease of the thermal conductivity in a number of superconductors below $T_c/3$;
3. decrease in absorption of ultrasonic waves;
4. evidence from transmission of microwaves and long infrared waves through thin films etc.

The energy gap in the electron excitation spectrum comes out naturally in the BCS theory. Thus the prediction of the energy gap by the BCS theory was consistent with the above mentioned experimental results. Later the tunneling experiments provided the direct evidence of the existence of the energy gap in superconductor [21].

Most of the properties of conventional superconductors were well explained by the BCS theory or slight modification of it in specific cases. Therefore, the theory took a firm footing and still continues to be the microscopic theory of superconductivity. The GL theory has been shown to be derivable from BCS theory near T_C. Thus BCS theory confirmed the GL theoretical approach to be correct for $T = T_c$. In the BCS theory also the two characteristic lengths ξ and λ continued to be important parameters of a superconductor. In this theory, ξ is the length over which electrons remain paired. ξ can be reduced, as indicated earlier, by shortening of the electrons mean free path by introducing impurity in a superconductor. When the superconducting state is destroyed, it is destroyed over a region with a minimum dimension ξ.

The observation of flux quantization in a hollow ring with flux quantum $\Phi_o = (hc/e\bar{*})$ where $e^* = 2e$ proved beyond doubt that the current carriers in superconductors are electrons pairs [22]. Another important milestone in the superconductivity was the discovery of Josphson effect in 1962 which predicted tunneling of Cooper pairs between two superconductors separated by a few $\mathring{A}$ [23]. The effect was observed and has become the basis of extremely sensitive voltmeters and magnetometers (so called SQUIDS).

As far as LT superconductors are concerned, there is hardly any property which can not be reasonably explained either by the BCS theory or the G.L Theory (or their extensions). More details can be found in a number of books on superconductivity [24,25]

1.3 Magnetic Behavior of Superconductors

The behaviour of a superconductor in an external magnetic field depends on the size of coherence length ξ to the penetration depth λ. When $\xi > \lambda$, it is called type I superconductor and when $\xi < \lambda$, it is a type II superconductor. For example superconductors tin, lead are type I and superconductors like Nb_3Sn and Nb_3Ge are type II. Type I and type II superconductors have very distinctive magnetization curves which are shown in Fig.1.4. A type I superconductor exhibits perfect diamagnetism for $0 \leq H \leq H_c$. At $H = H_c$, it suddenly switches to the normal state, i.e., diamagnetism disappears and conductivity becomes finite. A type II superconductor exhibits perfect diamagnetism, if

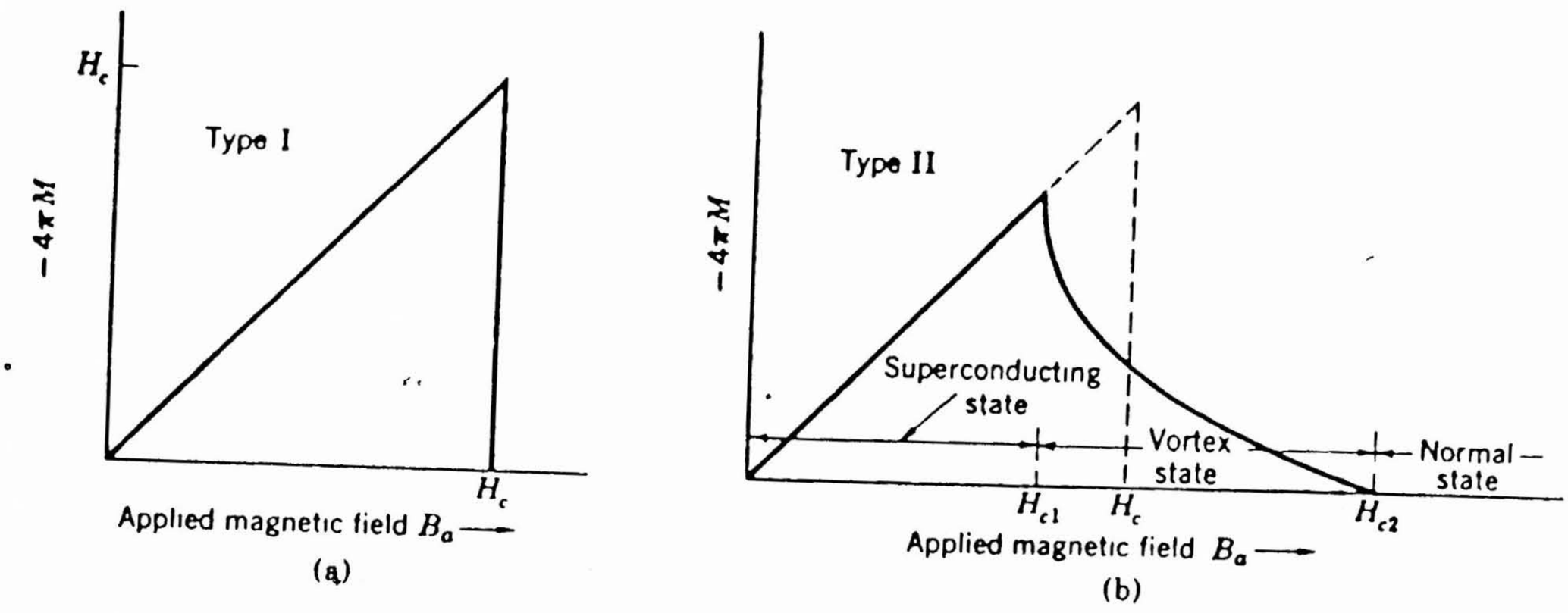

Fig.1.4. Magnetization versus applied magnetic field for a bulk superconductor exhibiting a complete Meissner effect (perfect diamagnetism). A superconductor with this behaviour is called a type I superconductor. Above the critical field H_c the specimen is a normal conductor and the magnetization is too small to be seen on this scale. Note that minus $4\pi M$ is plotted on the vertical scale; the negative value of M corresponds to diamagnetism. (b) Superconducting magnetization curve of a type II superconductor. The flux starts to penetrate the specimen at a field H_{c1} lower than the thermodynamic critical field H_c. The specimen is in a vortex state between H_{c1} and H_{c2}, and it has superconducting electrical properties up to H_{c2}. Above H_{c2} the specimen is a normal conductor in every respect, except for possible surface effects.

$0 \leq H \leq H_{c1}$, but permits penetration of magnetic flux in the region $H_{c1} \leq H \leq H_{c2}$ in form of tube like regions, which are called vortices or fluxon with normal core of diameter ξ aligned with the magnetic field, each containing the quantize unit (ϕ_o) of magnetic flux. The region between $H_{c1} \leq H \leq H_{c2}$ is called the vortex or mixed state. Penetration of flux reduces the net diamagnetism. However, the superconductor in this region continues to have zero resistance. If the vortex density becomes high enough that normal cores overlap, the entire material becomes normal. This field is called H_{c2}. Type I materials are pure metallic elements (except Nb and V) while type II are often alloys and compounds of several metals or thin films (when l is very small so that ξ becomes smaller than λ). Type II materials generally possess higher T_c, J_c and $H_c(H_{c2}$. Table 1.1 lists T_c, H_c or H_{c2} and J_c of some of typical superconductors including those of recently discovered HT-S. Among conventional superconductors, Niobium intermetallic compounds have highest $T_c s$ and are used at present to make state of the art of superconducting solenoids, which of course need to be operated at liquid helium temperature (4.2 K). If one could make magnets and other superconducting devices which would work at Liq N_2 temperatures and higher than there is much to gain. HTS materials have induced this hope. However, technological difficulties due to their ceramic nature are not easy to overcome and a lot of work is being done in this direction.

1.4 High T_c Superconductors (HTS)

In 1986, Bednorz and Muller reported a new system of superconductors $LaBaCuO$ based on CuO with T_c values in the 30 K range [4]. This was the revolutionary finding; not only $T_c \sim 35$ K was obtained but the superconductor was based on cuprate oxide. Besides, that this system had higher T_c than reported before. The HTS are extreme type II ($\xi << \lambda$) and have large $H_{c2} \simeq 150$ T. The coherence length ξ typically is about 20 $\mathring{A}$. (compared to $\xi \sim 10^4 \mathring{A}$ for type I superconductor Al). Assuming that the BCS type theory remains applicable to HTS, the Cooper pairs in HTS are very small, since ξ is small, which overlap much less than Cooper pairs in the conventional superconductors.

In 1987, $YBa_2C_3O_{7-x}$ was discovered having $T_c = 90$ K which was followed by the

Table 1.1
Important superconductors and their critical parameters

Material	$T_c(K)$	H_c $H_{c2}(O)$ (Gauss)	J_c (Transport) Amps. cm^{-2}) (at 4.2 K in appl. field of 4 tesla	Year of Discovery
Hg	4.1	410	—	1911
Pb	7.2	800	—	1913
Nb	9.2	2,000	—	1930
Nb_3Sn*	18.1	2,80,000	2×10^6	1954
NbTi*	9.5	1,60,000	3×10^5	1961
V_3Ga*	14.5	2,50,000	2.5×10^6	1966
Nb_3 (Al,Ge)		4,40,000	10^4	1966
$PbMo_5S_6$	15.0	6,00,000	10^3	1972
$(La,Ba)CuO_4$	35.0	5,50,000**	—	1986
$YBa_2Cu_3O_{7-y}$	92.5	38,00,000**	10^6***	1987
BiTrSrCaCuO	10.0	55,00,000**	10^5***	1988
TlBaCaCuO	125.0	—	10^4***	1988
$HgBa_2Ca_2Cu_3O_y$	164.0	—	10^6***	1993
	30 GPa			

*Available commerically for magnetic fabrication
**Estimated values
***J_c valules are at 77 K and in 0 applied field. in thin films.

whole HTS family $RBa_2Cu_3O_{7-x}$ where R is a rare earth metal (except a few like Pr). All these compounds have similar orthorhombic crystal structure. T_c is found to be independent of R and is 90-92 K. Other copper oxide based HTS have T_c ranging from low values to 135 K. The important HTSs in addition to $YBa_2Cu_3O_{7-y}$, which have T_Cs higher than liquid nitrogen boiling temperature, are $Bi_2Sr_2CaCu_2O_x$, $Bi_2Sr_2Ca_2Cu_3O_x$, $Tl_2Ba_2Ca_2Cu_3O_x$ and most recently a mercury based HTS which has a T_c of 134 K as mentioned earlier. All HTSs are extreme type II superconductors ($\xi \ll \lambda$). The physical properties of HTS materials based on experimental and theoretical review articles edited by Ginsburg gives more understanding about HTS materials [26]

1.4.1 $YBa_2Cu_3O_{7-x}$

Since the work reported in this thesis is on thin films of $RBa_2Cu_3O_{7-x}$ ($R = Y$ and Yb), the brief details of this compound are given below.

The most extensively studied HTS compounds are in the family of $RBa_2Cu_3O_{7-x}$ (where $R = Y$, Nd, Sm, Eu, Gd, Dy, Ho, Er, Tm, Yb, Lu), which is commonly denoted as "123" compound. This system has been studied in detail because it is the first HTS with $T_c = 90$ K, and can be formed in the single crystalline phase, reliably and reproducibly. Further, now good quality single crystals can also grown and studied.

The structure of the 123 compound was determined by a rapid succession of experiments by different groups using x-ray powder, x-ray single-crystal and neutron diffraction [27]. The most striking structural feature, the ordering of the oxygen vacancies giving rise to one dimensional $Cu-O$ chains, was first observed by neutron powder diffraction [28]. The structure consists of two dimpled CuO_2 planes separated by a Y layer which contains no oxygen and intercalated with two BaO and one CuO layers (containing CuO chains) as shown in Fig 1.5. Note that two distinct crystallographic sites are present for the Cu - one in the CuO_2 planes and one in intercalated CuO chain containing layer. The presence of the ordered oxygen vacancies gives rise to an orthorhombic symmetry, Pmmm, because of the existence of the CuO chains ($Cu1$, $O1$ in Fig.1.5).

A formal oxidation state calculation (assuming a valency of +3 for Y, +2 for Ba, +2

Crystal Structure
Of The New High T_c Oxides

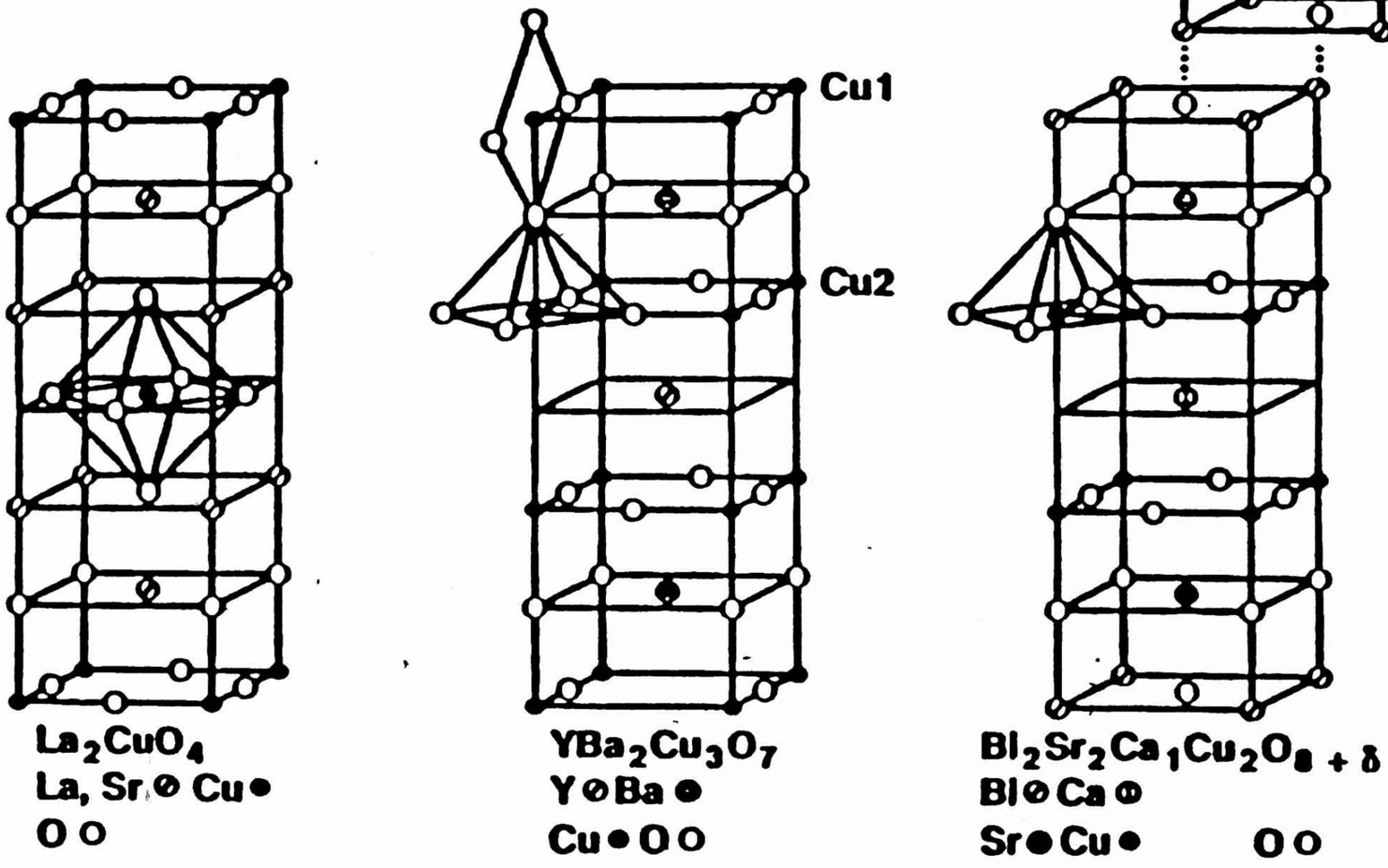

Fig.1.5. Approximate crystal structures of the various high T_c superconductors (courtesy of J.M. Tarascon).

for Cu and-2 for O) requires an oxygen stoichiometry of 6.85. Therefore, the presence of the oxygens in the chain site, producing a total oxygen stoichiometry near 7, implies that in this case the carriers are provided by the excess oxygen. It is also possible to change the number of carriers in the system by doping at the metal ion sites. Generally, metal ions that do not change the formal oxidation state and preserve the structure have a pronounced effect on the superconductivity only if they substitute in the CuO_2 plane and a small effect if they substitute in other sites [29]. This is true, unexpectedly, even for substitutions of R-magnetic ions, which undergo long-range ordering (Dy, Er, Ho) in the Y site. [30]. A notable exception is the substitution of Pr in the Y site, which gradually suppresses the superconductivity to zero transition temperature when 60% of Y is substituted by Pr [31].

Changes in oxygen stoichiometry have been found to strongly affect superconductivity in the 123 systems [32]. In $Y-123$, as oxygen is removed from the chains, some of the remaining oxygen atoms move to sites between the chains, eventually resulting in a transition to a disordered tetragonal structure [33]. T_c drops with decreasing oxygen content and reaches zero near the orthorhombic-to-tetragonal transition which corresponds to a composition near $YBa_2Cu_3O_{6.4}$ [34].

The common conclusion drawn from experiments where T_c in the 123 system has been modified by metal-site substitution or changes in oxygen stoichiometry is that the superconductivity depends on the degree of charge transfer from the intercalating layers, which act as "reservoirs" of charge, to the conducting $Cu-O_2$ planes [35]. However, a variety of studies suggest that the existence of one dimensional $Cu-O$ chains (perhaps only locally ordered in the structures with average tetragonal symmetry) may also play an important role in the superconductivity [28,29,34,35].

1.4.2 Current Status Of HTS Materials

During the last 9 years extensive studies have been made on the various aspects of HTS materials. A cursory glance of the summary of the experimental results was given below.

1. Although greater values of T_c have appeared, presently 135 K is the accepted highest T_c occuring reproducibly in Hg-based superconductors at ambient conditions.

2. J_c at 77 K is about $10^6 A/cm^2$ in $YBa_2Cu_3O_{7-\delta}$ thin film and $10^5 A/cm^2$ in the melt grown textured bulk $YBa_2Cu_3O_{7-x}$ system.

3. An upper critical field $H_{c2} \sim$ 150-200 T has been obtained resistively along ab-plane and $\sim$ 60 T along the c axis in the presence of a magnetic field by extrapolation. However the complicated magnetic field effect on resistivity introduces a large uncertainty to the H_{c2} so obtained.

4. The lower critical field H_{c1} is estimated to be 10-100 Oe. Again the anomalous macroscopic magnetic properties of HTS makes difficult an accurate determination H_{c1}.

5. The coherence length at 0 K, $\xi = 0.5 - 6\mathring{A}$ along c direction and 15-75 Åin the ab plane have been indirectly extracted. The value of ξ normally depends on the materials examined, the models used, and the assumptions made.

6. The electron density of states $N(0) \sim 1 - 50\ mJ/moleK^2$ determined calorimetrically. The high T_c and large H_{c2} make it difficult to determine $N(0)$ accurately.

7. Electric charge carriers form pairs below T_c as is evident by observations of Shapiro steps flux quantization and vortex lattice image.

8. The energy gap $2\Delta/KT_c$ is 2-20 and converges toward 8. It is also found that it is anisotropic.

9. The resistivity is proportional to T along ab-plane and proportional to $1/T$ when perpendicular to the ab plane, However there are some cases with significant deviations from $\rho \propto \frac{1}{T}$ behaviour.

10. The macroscopic magnetic properties exhibit an irreversibility line, magnetic relaxation and flux creeping and melting. Recent systematic studies have shown that extreme care has to taken to obtain meaningful data for analysis.

11. Acoustic, Positron life time, structural, Raman, and channeling anomalies have been reported at T_c.

12. The carrier concentration $n = 10^{21}$ per cm^3 of holes was determined from Hall measurements.

From the above, the high T_c, short ξ, low $N(0)$, low n and large structural and electric anisotropy appear to distinguish the HTS from LTS. These unusual characteristics have profound impact on understanding and applications of HTS materials.

Before discussing HTS thin film deposition techniques a brief introduction to thin films and the conventional techniques available in literature is given. A special attention is drawn on sputtering and laser ablation techniques due to their popularity in the area of HTS thin films.

1.5 HTS Thin Films

Many of the potential applications of superconductivity lie in the field of electronics, power and magnetic field generation. A strong focus of the HTS development has been on thin films in recent years. After an initial period of excitement about the possibility of obtaining higher and higher transition temperatures, the field of high T_c superconductors has now nearly matured and stabilized, and identification of some specific goals of practical importance. A number of small scale applications can be realized if good quality films of these material can be produced. Besides their ceramic nature, these high T_c superconductors have three or more elements. Therefore preparation of good quality films of these materials requires special experimental innovative approaches. Preparation of devices based on thin films, whether superconducting or semiconducting requires developments of well controlled, reliable thin film technology particularly suited to a device in question.

Over the past few years, it has become clear that preparation of stoichiometric and good quality of HTS thin films is not an easy task due to their multi-element compound nature and incorporation of sufficient oxygen in the film. Most of the studies related to HTS films have been confined to $Y-123$ films and perfecting them in order to use them for device applications besides understanding underlying physics of these materials.

The first report an high T_c superconducting thin film, although with a reduced T_c, was published in April 1987 [36]. The first films which show at high T_c and J_c were reported by Enomoto et al in July 1987 [37]. Various growth techniques were tried and reported by large number of groups world wide [38-42].

Humphrey [43] has reviewed the fabrication and properties of $YBa_2Cu_3O_{7-x}$ ($Y-123$) films made by various physical vapor deposition techniques on various substrates. Schieber [44] reviewed fabrication methods for $Y-123$ and Bi based and Tl based films and compiled useful information on lattice parameters of superconducting oxides on various substrate materials. Alarco et al [45] reported films made by laser deposition and co-evaporation and discussed device fabrication techniques and progress in Josephson weak link technology. Singh and Narayan [46] explained laser deposition of $Y-123$ on various substrates in some detail. A book edited by Conwell and wolf [47] consists much of the early pioneering work on film fabrication. Simon presented [48] a popular review of film fabrication and possible device applications. Finally, R. Ramesh et al [49] have reviewed the synthesization, structure-property relationships of the thin films of HTS specifically $Y-123$ system and discussed some of the applications that have been invisaged.

T.R. Lemberger has reported the over all work done in HTSC thin films during the period 1987-1991 [50]. It is well established that three conditions must be satisfied to produce good quality superconducting thin films. They are, (a) the right constituent atoms must be transported on to a substrate in the correct stoichiometry, (b) the right structure phase must be formed, and finally (c) the correct amount of oxygen must be incorporated into the structure.

The deposition techniques for films may be broadly classified into two types. They are physical vapor deposition and chemical vapor deposition.

1. Physical vapor deposition : It is again classified in to two categories, (a) thermal evaporation and (b) sputtering.

2. Chemical vapor deposition : This method can also be classified in two categories, (a) Electroplating and (b) Chemical vapor deposition.

In this work physical vapour deposition techniques, i.e., sputtering (DC and RF) and

pulsed laser ablation, have been used. In order to get good HTS films one needs a single crystal substrate which has reasonable lattice and thermal expansion matching with the HTS material to be deposted as a film. Other experimental parameters like the nature of a target, substrate temperature and oxygen pressure during the deposition etc. are important in producing a good HTS films, therefore, these need to be optimized in each case. Details of the techniques used and optimization of other parameters are discussed in detail in later chapters.

1.5.1 Possible Technological Applications

All applications proposed so far for HTS are basically the same as those of LTS based on the unique features of superconductivity namely zero resisivity, the Meissner effect and macroscopic quantum phenomenon except that devices based on HTS can be operate at LN_2 temperature. As a result very energy efficient devices may be built and ultra sensitive and ultra fast electronics become possible.

Some of possible applications are given below.

(a) Small current applications :

Josephson devices, SQUIDS superconducting strips or other configurations all using the HTS materials in the form of thin or thick films. They include ultra fast components for computers, efficient interconnects for semiconductor chips, ultra sensitive detectors for magnetic field wide band sensors for EM waves (IR - mm), bolometers, wide band A/D converters, loss less matched filters, microwave antennas, microwave cavities, opto-electornics. etc.

(b) Large Current Applications :

Superconducting magnets wires or ribbons using the HTS in bulk form. They include particle accelerators, magnetic energy storage, controlled fusion, magnetic levitated trains, magneto hydrodynamics motors, power generators, power transmissions lines, magnetic

shielding magnetic separations.

(c) Novel HTS Applications :

The novelty of applications of this type stems from those characteristics of the HTS materials in superconducting state which are rather different from their LTS counter parts. But the low n may offer of possibility for optical switching through a direct photon-superconducting-pair interaction deep inside the HTS material for ultra fast efficient devices. The exhibition of magnetic, insulating and superconducting properties with out major change of the cations in a HTS material provides us with extra leverage for multi layer devices. The low pining potential of HTS materials may be used for low cost simple magnetic field sensors.

1.6 Motivation and Scope of this Thesis

Preparation of good quality films of HTS materials stresses on special experimental innovative approaches preparation of devices based on thin films, whether superconducting or semiconducting, requires development of well controlled reliable thin film technology particularly suited to device is in question yet. Over the last few years it has become clear that preparation of stoichiometric and good quality HTS thin films is not an easy task. Most of the studies related to HTS thin films have been confined to $YBa_2Cu_3O_{7-y}$ films and perfecting them in order to use them for device applications besides understanding underlying physics of these HTS materials. However, there are numerous companies in US developing microware filters, antennas etc using high T_c Thin films.

Even though pulsed laser deposition has been successfully exploited for HTS thin films, still sputtering is the only alternative for depositing large area films with uniformity. Another problem faced in obtaining good quality HTS film on a given substrate is the lattice mismatch and chemical reactivity between the film and the substrate on which it is deposited. For many electronic applications, HTS films may need to be deposited on silicon < 100 > or other semiconducting substrates, i.e., $GaAs$, and for microwave applications on sapphire substrates. But Si and Sapphire are not good substrates for

obtaining good quality of HTS films due to their lattice mismatch, chemical reactivity and thermal expansion coefficient mismatch [51,52]. To overcome this, one needs to deposit buffer layers. Yittria stabilized Zirconia is the popular choice among the buffer layers during the last few years. In addition $SrTiO_3$ (STO) can also act as a good buffer layer on the above mentioned substrates [53]. For better understanding the growth condition of YSZ and STO buffer layers and also to explore the possibility of sputtering high quality films of $Y-123$ on Si $< 100 >$ and Sapphire $< 1102 >$ substrate for technical application a detailed study on the preparatory conditions for reproducible results is needed.

Current research trends have aimed at studies of changes in the superconducting properties by substitution or addition of other elements with an aim to understand the physics of these compounds as well as with a hope to improve these properties. The superconducting properties of widely investigated $Y-123$ have revealed that the assembly of $Cu-O$ plane and chain is primarily responsible for superconductivity and the main contribution to the density of states at the Fermi level comes from the $Cu-3d$ and $O-2p$ hybridization states. Hence, the substitution for Cu by transition metals is expected to produce substantial changes in the superconducting properties of orthorhombic $Y-123$ system [54].

It is well estabilished that the superconducting transition temperatures of orthorhombically distorted oxygen deficient perovoskite $RBa_2Cu_3O_{7-y}(R = Y$, rare earth) are nearly independent of a rare-earth element regardless of their magnetic behaviour. The early efforts to prepare single phase $123-Yb$ and $123-Lu$ were not successful and difficulty in getting a single phase 123 compound for these rare earths were ascribed to their smaller ionic radii. While $Y-123$ system has been widely studied in bulk as well as in thin film form there are a few reports on other rare-earth bulk 123 systems. However, there are reports that one can form $La-123$ and $Lu-123$ in thin film having orthorhombic structure which show superconductivity at $T_c = 70K$ and $88K$ respectively [55,56]. Many R-123 thin films have been made using the PLD technique except $Yb-123$ films. Even though Yb-123 film was tried using other techniques like sputtering and MOCVD but the quality of those films are not upto the mark [57-59]. Formation of $Yb-123$ thin films thought to be interesting to try to see if good quality single phase superconducting films of $Yb-123$ can be prepared by the PLD technique. Hence, $Yb-123$ system in addition to the $Y-123$ system was also chosen to study the effect of film growth conditions on

the superconducting properties in chapter V.

Considering the above, the aim of the present work is

- To design a simple and efficient planar magnetron sputtering for in situ ($Y-123$) thin films from stoichiometric single target.
- To study the growth and micro structural properties of buffer layers for depositing high quality $Y-123$ films on Si $<100>$ and sapphire $<1\bar{1}02>$ substrates.
- To study the synthesis of $RBa_2Cu_3O_{7-y}$ ($R = Y$, Yb) thin films using laser ablation techniques and to study their growth temperature dependence on superconducting properties.
- To study Niobium (Nb) substitution at Cu site in thin films ($YBa_2Cu_{3-x}Nb_xO_{7-x}$ where $x = 0$ to 1) and variation of transport properties with Nb concentration.
- To study the addition effects of V_2O_5 and Nb_2O_5 systems in thin films.

The thesis presents details on the experimental work listed above. Each chapter contains individual introduction, review of literature, description of the experimental procedure, results and discussions and list of references.

References

[1] H.Kammerlingh Onnes, Akad Van Wetenschappen, **14** (1911) 818.

[2] W.Meissner and R.Oschsenfeld, Natuwin 21 (1933) 787.

[3] J.R. Gavaler, Appl. Phys. Lett. **23** (1973) 480.

[4] J.G. Bednorz K.A.Muller Z. Phys. B **64** (1986) 189.

[5] M.K. Wu, J.R. Asburn, C.T. Torng., P.H. Hor, R.L. Meng, L.Gao, Z.J. Huang, Y.Q. Wang and C. W. Chu, Phys. Rev. Lett **58** (1987) 908.

[6] H. Maeda, Y.Tanaka, M. Tuktomi and J. Asano Japn. J. Appl. Phys. **27** (1988) L209.

[7] R.M. Hazen, C.T. Preuitt, R.J. Angl, N.L. Ross, L.W. Finger, C.G. Hadidescos, D.R. Veblen, P.J. Heaney, P.H. Horn, R.L. Merg, Y.Y. Sun, Y.Q. Sun, Y.Y. Yue, Z.J. Huang, L. Gao, J. Bechtold and C.W. Chu, Phys. Rev. Lett. **60** (1988) 1174.

[8] Z.Z. Sheng and A.M. Hermann, Nature **332** (1988) 1174.

[9] A.Schilling, M.Cantoni, J.D. Guo and H.R. Oh, Nature **363** (1993) 56.

[10] C.W. Chu, L. Gao, F. Dhen, Z. H. Huang, R.L. Meng and Y.Y.Y. Lu, Nature 365 (1993) 323.

[11] Chandan Mazumdar, R. Nagarajan, C. Godart, L. C. Gupta, M. Latroche, S. K. Dhar, C. Levy-Clement, B. D. Padalia and R. Vijayaraghavan, Solid Stat. Com. 87(1993)413.

[12] R.J. Cava, H. Takagi, B. Batlogg, H.W. Zandbergen, J.J. Krajewski, W.F. Peck Jr., R.B. Van Dover, R.J. Felder, T. Siegrist, K. Mizuhashi, J.O. Lee, H. Eisaki, S.A. Carter and S. Uchida, Nature **367** (1994) 146.

[13] C.J. Gorter and H.B.G. Casimir, Phys. Z. B **35** (1934) 963.

[14] F.London and H.London, Proc. Roy.Soc. A, **149** (1935) 72.

[15] F.London and H.London, Phisca, **2** (1935) 341.

[16] A.B. Pippard, Proc. Roy. Soc. A **191** (1947) 370, 385, 399.

[17] V.L. Ginzburg and L.D. Landau, Zh.Eksperim. Teor Fiz. **20** (1950) 1064.

[18] J. Bardeen, L.N. Cooper, J.R. Schrieffer, Phys. Rev. **106** (1957) 162.

[19] J.Bardeen, L.N. Cooper, J.R. Sschrieffer, Phys. Rev. **108** (1957) 1175.

[20] L.N. Cooper Phys. Rev. **104** (1956) 1189.

[21] I. Giaever, Phys. Rev. Lett. **5** (1960) 147, 464.

[22] B.S. Deaver and W.M. Fairbank, Phys. Rev. Lett. **7** (1961) 43; R. Doll and M. Näbauer, Phys. Rev. Lett. **7** (1961) 51.

[23] B.D. Josephson advanc. Phys. **14** (1965) 419; *ibid* Phys. Lett. **1** (1962) 251.

[24] Introduction to superconductivity ed. by M. Tinkham, Mc Grawhill Book Co., 1975.

[25] Introduction to superconductivity ed. by A.C. Ross-innes and E. H. Rhorerick, Pergamon Press, 1969.

[26] Physical Properties of HTSC Vol I, II and IIIed. by Donald M. Ginsburg, World Scientific, 1988- 1990- 1992.

[27] J.D. Jorgensen Japn. J. Appl. Phys. **26** (1987) 2017.

[28] M.A. Beno, L.Soderholm, D.W. Capone II, D.G.Hinks, J.D. Jorgensen, J.D. Grace, I.K. Schuller, C.V. Serge, K. Zhang, Appl. Phys. Lett **51** (1987) 57.

[29] G.Xiao, M.Z. Cieplak D.Musser, A. Garvin, F.H.Strietz, C.L. Chien, J.J. Rhyne and J. A. Gotaas, Nature **332** (1988) 238.

[30] L. Soderholm, K. Zhang, D.G.Hinks, M.A. Beno J.D.Jorgensen,C.U. Segre and I.K.Schuller, Nature **328** (1987) 604.

[31] I.K. Schuller, D.G.Hinks, M.A. Beno, D.W. Capone II, L.Soderholm, J-PLocquet, Y.Bruynseraede,, C.U. Segre and K.Zhang, Solid State Commn. **63** (1987) 385.

[32] J.D. Jorgensen, M.A. Beno, D.G.Hinks, L.Soderholm, J.P. Locquet, Y. Bruynseraede, C.U. Segre, K. Zhang, and M.S. Kleefisch, Phys. Rev. B. **36** (1987) 3608.

[33] R.J. Cava, B. Batlogg, C.H. Chen, E. A. Rietman, S.M. Zahurak, and D. Werder, Phys. Rev. B **36** (1987) 5719. ibid Physica C **153-155** (1988) 360.

[34] Y. Tokura, J.B. Torrance, T.C. Hang, and A.I. Nazzal, Phys. Rev. B **38** (1988) 7156.

[35] C.U. Segre, B. Dabrowski, D. G. Hinks, K.Zhang, J.D. Jorgensen, M.A. Beno and I.K.Sculler, Nature **329** (1987) 227.

[36] R.E. Somekh, M.G. Blamire, Z.H. Barber, K. Butter, J.H. James, G.W.Morris, E.J. Tomlenson, A.P.Schwarzen berger, W.M.Stobbs, J.E. Evetts, Nature, **326** (1987) 857 .

[37] Y. Enomoto, Muraku T, T, Suzuki M and Moriwakik, Jpn. J. Appl. Phys **26** (1987) L1248.

[38] M. Naito, R.H. Hammond,Oh.B.Hahn M.R.,T.W.P.Hsu, P.Rosenthal, A.F. Marshall, M.R. Beasley, T.H. Geballe and Kapitulnik, Jl. Mat. Res. A **2** (1987) 713.

[39] P. Choudhari, J. Mannhart, O.Dimos, C.C. Tsuei, J. Chin, M.M. Oprysk and M. Schcucrmann, Phys. Rev. Lett. **60** (1988) 1653.

[40] J. Mannhart. P.Chaudhari, D.Dimos,C.C. Tsuei and T.R. McGuire Phys. Rev. Lett. **61** (1988) 2476.

[41] P.M. Mankiewich, Schofield .J.H, Skocpol.W.J., Howrd R.E., Day em A.H., E. Good, Appl. Phys. Lett., **51** (1987) 1753.

[42] R.L. Sandstram, W.L. Gallagher, T.R. Dinger, R.H. Koch, R.B. Laibowitz, A.W. Kleinsanes, R.J. Gambino, B. Umble and M.F. Chism, Appl. Phys. Lett. **53** (1988) 444.

[43] R.G. Humphreys, J. s. satchell, N.G. Chew, J.A. Edwards, S. W. Goodyear, S. E. Blankisop, O.D. Dosser and A. G. Cuills, Supercond. Scie. and Tech. **3** (1991) 401.

[44] M. Schieber, J. Cryst. Growth. **109** (1991) 401.

[45] J. A. Alarco, B. Broson, T. Claeson, Physica Scripta **44** (1991) 95.

[46] R.K. Singh and J. Narayan , J. Mat. Sci. **26** (1991) 13.

[47] Science and Technology of thin film superconductors ed by E. M. Conwell and S. A. Wolf (Polonum Ny 1989).

[48] R.W. Simon, Physics Today **44** (1991) 64.

[49] R. Ramesh, A. Inam T.Sands and C.T. Rogers, Materials Science and Engineering B **14** (1992) 188.

[50] Films of High temperature oxide superconductors by T.R. Lemberger, Physical Properties of HTSC III ed by Donald M. Ginsburg, 1992.

[51] A.Inam, X.D. Wu, T.Venkateshan, D.M. Humg, C.C.Change, R.Ramesh, S.Mirua, S. Matsubaro, Y. Miyabska and N. Shohata Sold State Technology, Feb (1990) 113.

[52] D.K. Fork, D.B. Fenner, G.An. Connel, J.M. Phillips and T. H. Ge, App. Phys. Lett. **57** (1990) 1137.

[53] K. Char, N. Newman, S.M. garrison, R.W. Bartor, R.C. Taber, S.S. Laderman and R.D. Jacowitz, Appl. Phys. Lett. **57** (1990) 407.

[54] J.M. Tarascon, P. Barboux, P.F. Miceeli, L.H. Greene, G.W. Hull, M. Eibschutz and S.A. Sunshine, Phys. Rev. B **37** (1988) 7458.

[55] M.Suzuki, T. Fuji, K. Mori, K. Muta and T.Watari, Jpn. J. Appl. Phys. **27** (1988) 2003.

[56] R. Pinto, S.P. Pai, A.S. Tamhane, P.R. Apte, L.C. Gupta, R. Vijayaraghavan, K.I. Gnanasekher, H.V. Keer, Phys. Rev. B **46** (1992) 14242

[57] H.S. Chen, S.H. Liar, A.R. Kortan and L.C. Kimerling Appl. Phys. Lett. **53** (1988) 705.

[58] H.G. Lee, S.D. Park, C.J. Kim, G.W. Hang, H.S. Chang and D.Y. Wan, J. Appl. Superconduc. **1** (1993) 807.

[59] J.L.M. Driscoll, J.A. Alonso, P.C. Wang, T.W. Geballe and J.C. Bravmun, Physica C **232** (1994) 288.

Chapter 2

Experimental Techniques

The experimental techniques used for the research work presented here are briefly described in this chapter. In later chapters, more details are given at the appropriate places.

2.1 Materials Preparation, Targets and Substrates

High T_c superconductors $Y-123$ and $Yb-123$ were prepared by the well established solid state reaction method [1,2]. Purity of oxides varied between 99.99% and 99.999%. The furnace used for preparation of the materials was Eurotherm (U.K.) company make. Its temperature could be controlled within $\pm 1°C$. For grinding and mixing the powder, a zirconia ball mill was used. Raw material grinding was done for 1 hr to 2 hrs. Each sintering was done at 930°C for 48 hrs. Grinding between two sinterings was done for 30 to 60 minutes. Every pellet after preparation was subjected to the energy dispersive X-ray analysis (EDAX) at several places to ensure the uniform stoichiometry through out the sample. Oxygenation of the bulk samples was done at 550°C using 99.99% pure oxygen. Depending upon sample to sample, the oxygenation time varied from 24 hrs to

48 hrs.

Targets in the form of pellets of half inch diameter and 4mm thick for PLD method and one inch diameter and 4mm thickness were prepared using a pressure of 15,000 to 18,000 pounds and sintered at 950°C. The density of these pellets was found to be 80 to 90 %. of the bulk density. $R-123$ ($R = Y$, Yb) films were deposited using either sputtering or PLD technique. The crucial deposition parameters which need to be controlled are (i) nature of the substrate, (ii) substrate temperature (iii) partial oxygen pressure in the film deposition chamber and (iv) target-substrate distance.

The choice of a substrate for deposition of a HTS film depends upon various factors. Single crystal substrates are preferred so that almost single crystal HTS film may grow on it or atleast the grain size may be large and aligned. The substrate should also be lattice matched with the HTS material, and the HTS film coefficient of thermal expansion should also match with that of the substrate. Moreover, the HTS film should not react with the substrate. Single crystal substrates of MgO, $LaAlO_3$, $SrTiO_3$, YSZ etc with $< h00 >$ orientation are generally preferred for HTS films. Table 2.1 gives physical properties of various substrates and HTS materials.

Based on previously published results on preparation of HTS films, substrates for deposition of $Y-123$ and $Yb-123$ films were chosen to be single crystal $< h00 >$ thin plates of Yittria stabilized Zirconia (YSZ), Strontium Titanate ($SrTiO_3$), Magnesium Oxide (MgO) [3,4] and Lanthanum Aluminate ($LaAlO_3$) obtained commercially. Typical size of the substrates was (1 cm × 1 cm × 0.5 cm). For the buffer layer work, the substrates used were Si $< 100 >$ p-type and Sapphire $< 1102 >$ R-plane cut. All substrates were well polished.

For in situ growth of any HTS film there is an optimum substrate temperature at which the required orthorhombic phase grows, preferentially, and below which intermediate phase formation takes place. For $R-123$ films it is 750-800°C, while for Bi and Tl based HTS films it is about 800°C.

In the $Ar+O_2$ gas mixture in the film deposition chamber, the partial oxygen pressure is a very crucial parameter and needs to be optimized for each case. In the case of the sputtering technique, if it is more than 30 m torr which destroys the growing film and also reduces the sputtering yiield which in turn results in deviation from he stoichiometry

Table 2.1

Physical Properties of substrates and HTS materials

Material	Cyrstal system	Structure	Lattice constants (A°)	Coefficient of thermal expansion 10^{-6}/K
$La_{1.8}Sr_{0.2}CuO_4$	Tetragonal	K_2NiF_4	a = 3.78 c = 13.23	10-15
$YBa_2Cu_3O_{7-x}$	Orthorhombic	Oxygen deficient pervoskite	a = 3.82 b = 3.89 c = 11.68	10-15
$Bi_2Sr_2Ca_2Cu_3O_{10}$	Pseudo-teragonal	Bi-layered structure	a = 5.4 c = 30	12
$Tl_2Ba_2Ca_2Cu_3O_{10}$	-do-	-do-	a = 5.4 c = 36	
$SrTiO_3$	Cubic	Pervoskite	a = 3.91	10.8
$LaAlO_3$	Rhombohedral	-do-	a = 3.78	10
CaF_2	Cubic	Fluroite	a = 5.4	-
MgO	-do-	Rock-salt	a = 4.2	13
YSZ	-do-	Fluorite	a = 5.16	10
Al_2O_3 (Sapphire)	Trigonal	Corundum	hex. axes a = 4.73 c = 13.00	q=8.0 7.5
Si	Cubic	Diamond	a = 5.43 3a = 16.3	4.4
GaAs	-do-	-do-	a = 5.65	4
$CoSi_2$	-do-		a = 5.43	9.4

and intermediate phase formation [5-7]. Off axis sputtering [8-10] is one possible way to avoid backsputtering. Similarly, distance between the target and the substrate needs to be optimized to get a good HTS film. Normally, it is 3 - 5 cm for the DC sputtering and 1 - 5 cm to the RF sputtering and 4 - 5 cm for the PLD technique. Since in each film deposition case, these parameters need to be optimized, further details on these parameter adjustments are given in each chapter.

2.2 Sputtering

When the surface of a material (target) is bombarded with energetic particles then atoms will be ejected out. This is called sputtering. If ejection is due to the positive ions then it is known as cathodic sputtering. Ejected atoms can be condensed on a substrate to form a thin film. The technique has certain advantages over thermal evaporation. In this method, conducting and insulating materials, which have high melting points can be easily deposited, since deposition parameter can be controlled with ease.

A sputtering unit consist of two electrodes kept in a relatively low vacuum. One of these electrodes is a target and the another one has a substrate attached to it on which the film deposition takes place. If the electric potential applied between the two electrodes is DC, then it is called the DC sputtering technique, and if a RF potential is applied between the electrodes, then it is called the RF sputtering technique. Only metal targets can be used for the DC sputtering while either metal or semiconductor/insulator targets can be used for the RF sputtering. Usually the growth of a film, when prepared using any of two sputtering techniques, is slow in 'average' sputtering conditions. One can increase the yield (growth of the film) by applying appropriate magnetic field (magnitude and direction) near the target. Such an arrangement is called a magnetron. We describe below experimental arrangements directly related to the work presented here. More theoretical and experimental details on the sputtering technique, including the magnetron technique, can be found in a number of excellent books [11-13].

In this work two sputtering units were used for the preparation of thin films. They are (a) home made one inch dia hollow cathode magnetron system for preparing RF/DC

sputtered superconducting thin films and (b) commercially made 4 inch dia NORDICO 2000 RF magnetron sputtering system (UK) for fabricating large area buffer layers.

(a) Lab made Magnetron Sputtering System :

The block diagram of the home made magnetron sputtering system is shown in Fig.2.1. It basically consists of two planar electrodes. The target to substrate distance can be varied between 1 cm - 6 cm depending on the requirement. A transverse magnetic field of 150 Oe was applied in the plasma region i.e by keeping permanent U shaped ALNICO magnets in transverse position surrounding plasma region between the two electrodes. The substrate heater is made from a Kanthal wire and the maximum temperature it can go is 800°C. The temperature on the surface of the substrate is measured using another dummy substrate of the same dimensions. The accuracy of the temperature measurement is ±5°C. The variation of the substrate temperature during deposition is ±5°C. Every deposition has been made 4 to 5 times, and all the results reported in this thesis are based on nearly 100% reproducibility. A Diffusion pump has been used for creating Vacuum in the sputtering system.

(b) Nordico 2000 :

This is a commercially available RF magnetron sputtering system with a CTI (USA) cryopump. Since the pump is oil free, one has a carbon free atmosphere in the chamber which is otherwise present in the diffusion pumping system due to the backstreaming of the oil. The ultimate pressure one can get at the mouth of the baffle is $\sim 1 \times 10^{-8}$ Torr. The chamber pressure goes to 1×10^{-7} Torr. The maximum RF power is 200 Watts at 13.56 MHz frequency. The system has a halogen lamp substrate heater which can go up to 850^{0}C. Figure 2.2a shows Nordico sputtering unit and 2.2b shows the Argon + oxygen plasma between the target surface and substrate heater assembly.

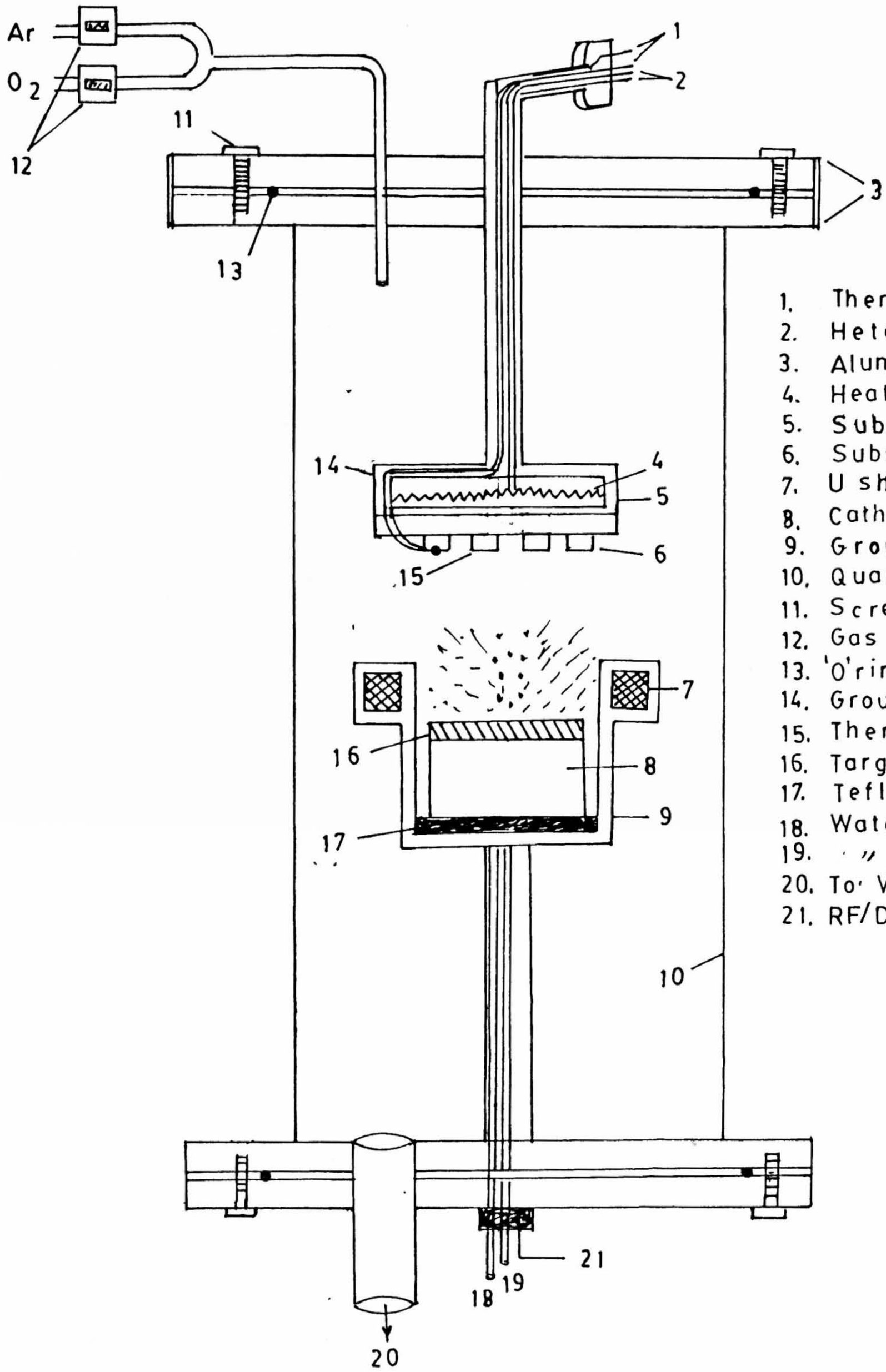

1. Thermo couple connections
2. Heter connection
3. Aluminium flanges
4. Heater
5. Substrate holder
6. Substrates
7. U shaped Magnet
8. Cathode
9. Ground shield
10. Quartz chamber
11. Screw
12. Gas flow meters
13. 'O'ring
14. Ground shield
15. Thermo couple
16. Target
17. Teflon spacer
18. Water in
19. " out
20. To Vacuum System
21. RF/DC power connection

Fig.2.1. BLOCK DIAGRAM OF MAGNETRON SPUTTERING SYSTEM

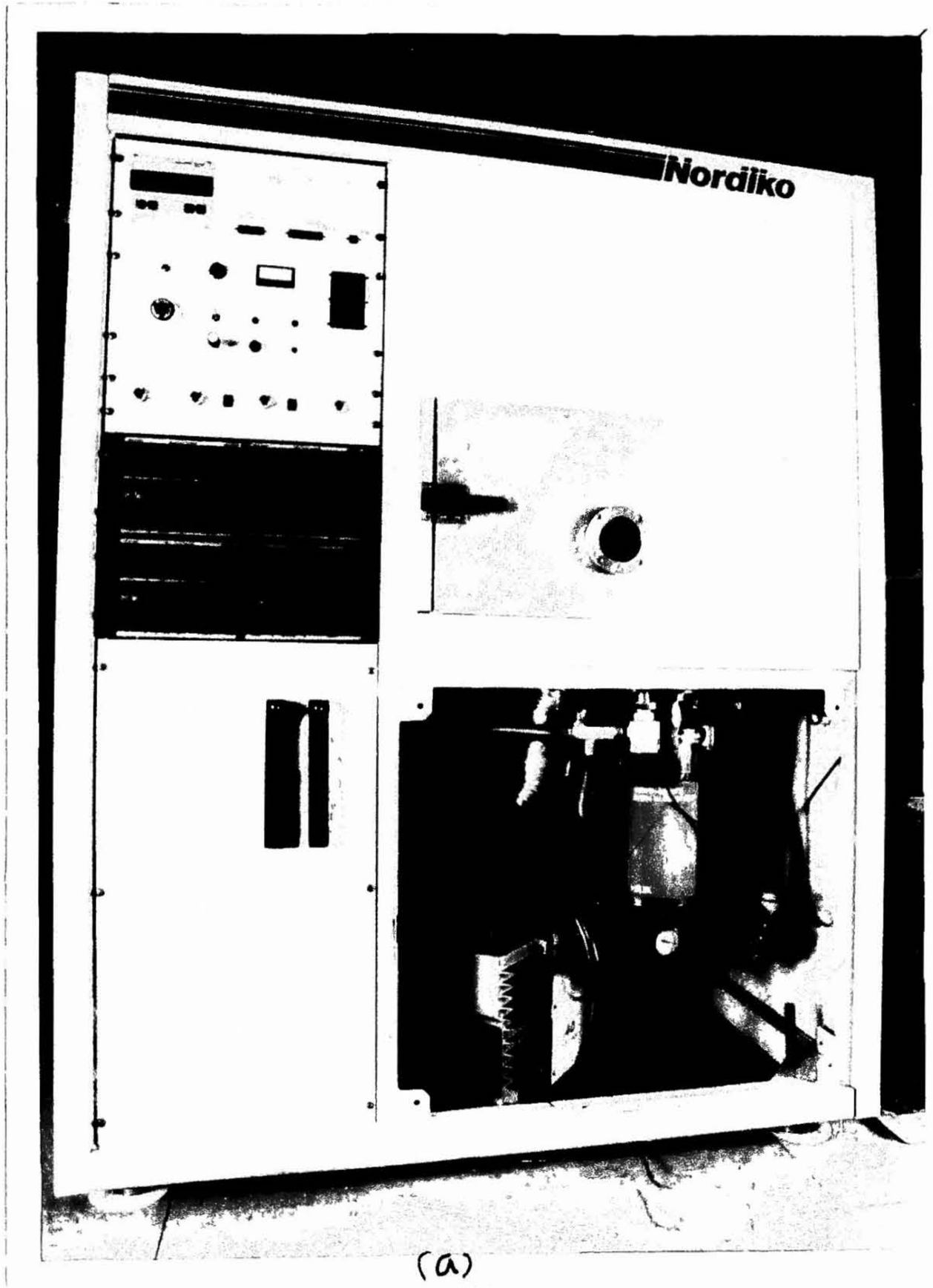

(a)

Fig.2.2. Sputtering: $Ar+O_2$ plasma between the target surface and substrate heater assembly in Nordico 2000 System.

(b)

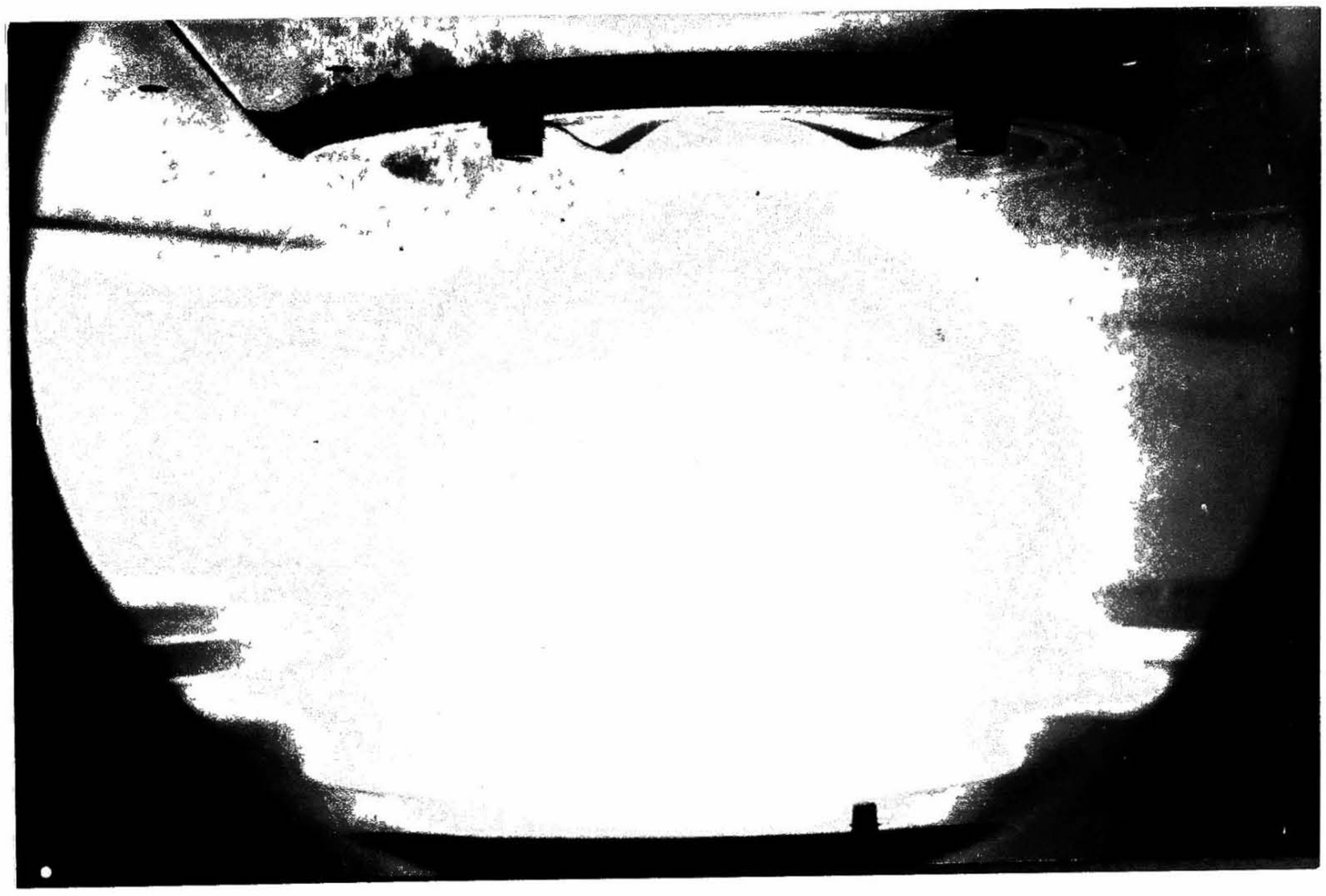

2.3 Pulsed Laser Deposition (PLD) Method

Due to multi-element HTS $R-123$ compounds and their reactive nature, efforts to deposit high quality HTS film using the conventional film deposition techniques encountered a number of difficulties. Laser have been used in the last three decades to produce high temperature and high density plasmas (in device applications) by vaporizing a small amount of material with high powered nano second pulses. The use of high power lasers in materials science is now very common either to prepare materials or modification of materials etc. [14]. The pulsed laser ablation technique has been extensively used to deposit thin films. Due to high energy density pulses of an appropriate laser when incident on a material, whether single or multicomponent, produces extremely high temperatures locally and evaporates the material instantaneously and forms a plume around the target. This property of high energy density lasers is used in the deposition of HTS films. This technique will be referred hereafter as the PLD technique. Excimer lasers are now extensively used for the deposition of good quality HTS films by the PLD technique [15]. More details are given in chapter V.

Basically the critical parameters in the pulsed laser deposition technique for HTS thin films are (i) energy density (ii) substrate - target distance, (iii) oxygen partial pressure (iv) nature of the substrate and (v) substrate temperature. Based on the reported work on the growth of HTS films, particularly those of $R-123$ compounds, optimum laser pulse energy density is found to be around 2 - 3 J/cm^2. The laser beam spot size as well as the target to substrate distance need to be adjusted for the optimum growth of a film. Usually 4 - 5 cm target to substrate distance is ideal for HTS thin films depending on the spot size ($3x0.8mm^2$). The substrate should not be in the plume region; it should be placed at the tip of the plasma. Oxygen partial pressures of 200 mTorr is reported to be usually optimum for good quality deposition of $Y-123$ thin films [16]. It has been established that the PLD technique produces very good quality small area HTS films especially that of $Y-123$ [16].

HTS films in this work were also prepared by the PLD technique in addition to the sputtering technique. The laser ablation depositions of $Y-123$ and $Yb-123$ films were done using a Lambda Physik 301:KrF 248 nm excimer laser and 300 mm focal length

quartz lens for laser beam focusing. The excimer laser pulse had a maximum energy of for good quality 1200 mJ with a pulse width of 25 ns and a 1-10 Hz variable repetition rate. The optimized spot size and the pulse energy for good quality $YBa_2Cu_3O_{7-x}$ $(Y-123)$ films were found to be 3 mm × 0.8 mm and 2 J/cm^2. The angle between the laser beam and the normal to the target was 45°.

Fig.2.3. shows the top view of the pulsed laser deposition chamber and related arrangements for the PLD deposition of 123 films. It consists of a 300 mm diameter stainless steel chamber having a quartz window and pumped with a turbo-pump module. A Platinum strip heater with a temperature capability upto 900 °C. was used for the in situ growth of the films. The chamber was initially pumped to a base pressure of 10^{-6} Torr, and later high pure oxygen was introduced. The chamber pressure was stabilized at 200 mTorr. The target was rotated at a rate of 15 rpm. The substrate temperature was measured using an optical pyrometer. Most of the films studied were grown on single crystal substrates heated to temperature between 650 - 750 °C.

2.4 Film Thickness Measurement

Film thickness was measured using a surface profilometer (STYLUS) on patterned films. The accuracy of the measurement is estimated to be $\pm 2\mathring{A}$.

2.5 X-ray Diffraction Studies

The X-ray data for both bulk and thin films were obtained on a JEOL 8030 XRD powder diffractometer in the Bragg mode with $Cu-K_\alpha$ radiation using 0.02° step angle and 1 sec-count time. The current and the voltage of the X-ray tube was kept at 25 mA and 35 kV respectively during all the measurements.

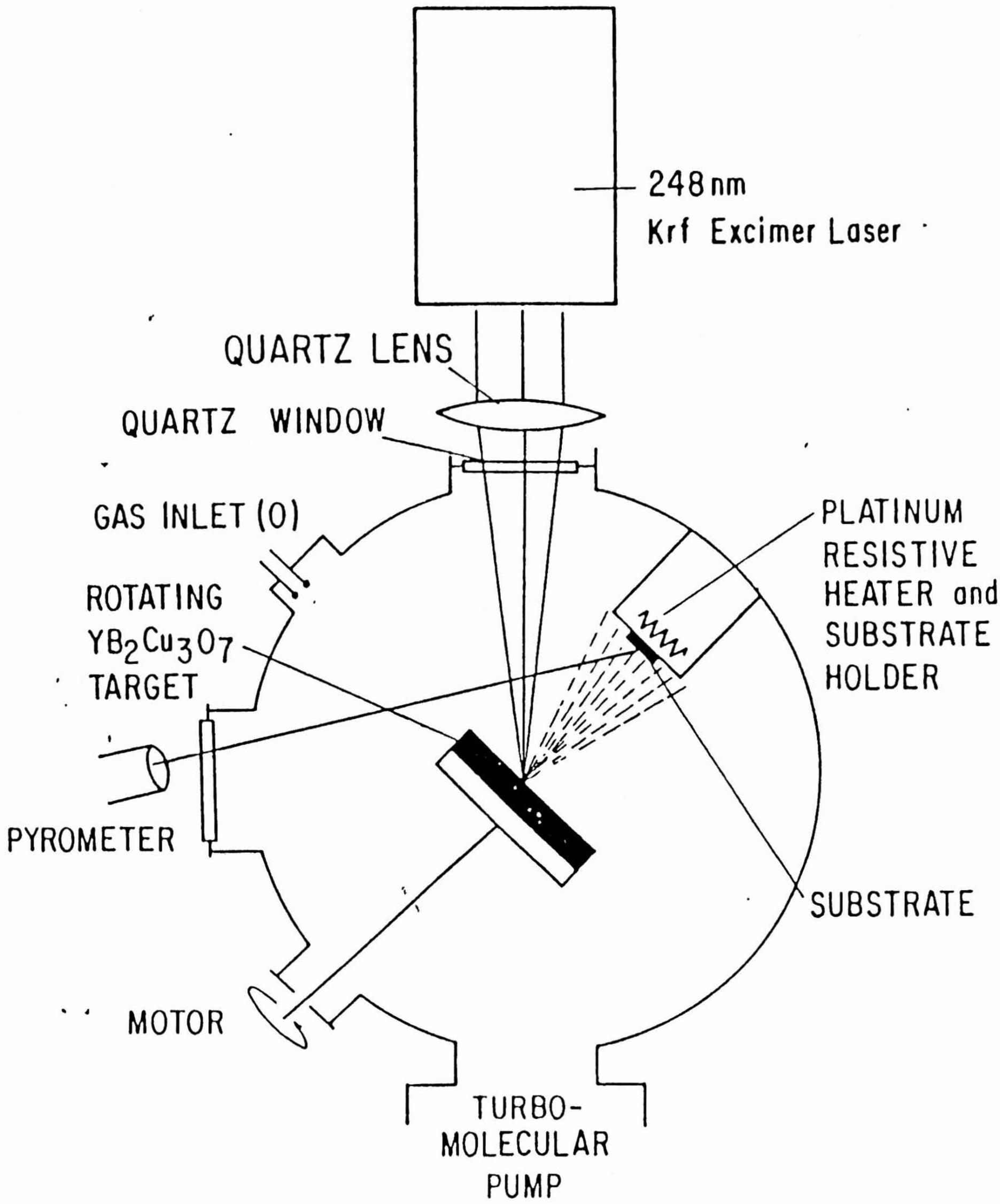

Fig.2.3. Schematic of pulsed laser deposition system

2.6 DC Electrical Resistivity Measurements

The resistivity was measured using the standard four probe method. A schematic of the setup is shown in Fig.2.4. The current source was a Keithely 224 programmable constant current source and voltage across each sample was measured using a 196 DMM voltmeter. A closed cycle refrigerator, capable of going down in temperature upto 10 K, was used for temperature variation. A Lakeshore DRC 91C temperature controller was used to stabilize the temperature within ± 0.05 K. The set-up was interfaced with a PC-XT computer for automatic data collection. The sample was mounted on the cold head using a cryo-grease to provide a good thermal contact between the two. The helium exchange gas in the chamber and a good thermal stabilization ensured temperature differences between the cold head and the sample chamber to be negligible.

2.7 Patterning of Films for J_c Measurements

The methods used to pattern a film were either (a) Photolithography or (b) Pulsed Laser Etching.

(a) Photolithography :

Photolithography is most widely used technique for patterning high T_c thin films in order to measure the critical current densities. The first step in lithography is to coat a sample by a thin layer of an organic polymer, called photoresist, which is sensitive to ultraviolet light. A photomask, generally a quartz plate on which there is a metal pattern, is placed in contact with the photoresist coated on the surface of the sample and the sample is exposed to ultraviolet light. The metal on the mask is opaque to ultra-violet light whereas quartz is transparent. The radiation causes a chemical reaction in the exposed areas of the photoresist. In the patterning of high T_c films, a positive photoresist (PPR) is used which upon exposure to ultraviolet light gets weakened due

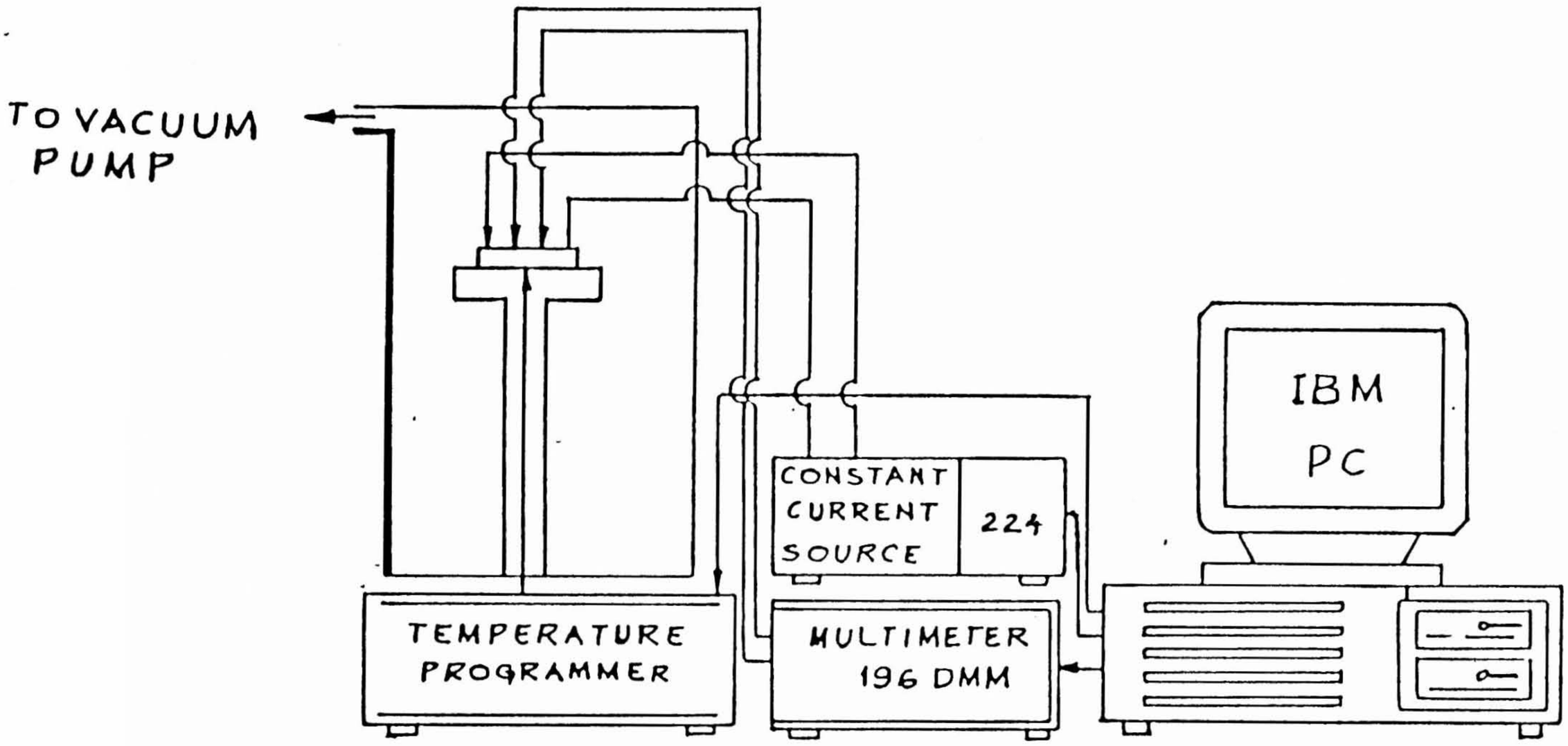

Fig.2.4. SCHEMATIC DIAGRAM OF FOUR PROBE INSTRUMENT

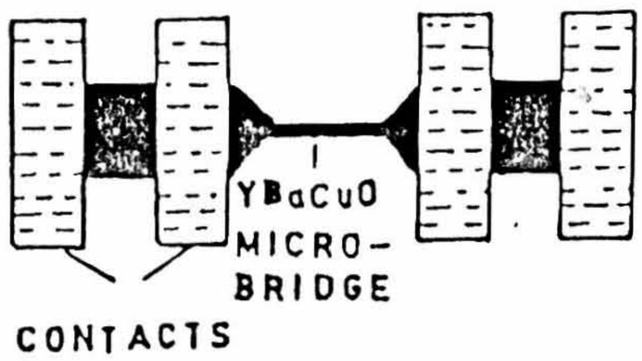

Fig.2.5. Systematic diagram of the micro bridge of Y-123 films.

to chemical reaction. The sample is then rinsed in developing solution that removes the exposed areas of PPR, leaving the pattern of bare PPR coated surface of the sample. The steps involved in the patterning of high T_c superconductor samples are mentioned below in sequence.

1. Spin on positive photoresist (Micro Posit 1350) at 3000 rpm for 30 sec. 2. Bake at 100 °C for 10 min. 3. Align the photomask over the sample, positioning the photomask so that the contact pads are over the silver deposits. 4. Expose to UV light for 20s. 5. Develop in Micro posit developer for 45 s. 6. Rinse in distilled water. 7. Spin for 10 sec 3000 rpm (to get rid of water on the surface). 8. Bake at 100 °C for 10 min. 9. Etch in a solution of ferric nitrate or orthophosphoric acid. 10. Stop etch in distilled water. 11. Remove photoresist with acetone.

Fig 2.5 shows the schematic representation of the micro-bridge patterned using the photolithography technique.

(b) PULSED LASER ETCHING

This technique has been used for patterning thin films employing a pulsed laser system. A 10 μm bridge mask was kept on the film and exposed to laser shots of frequency 2-4 Hz with 100-150 mJ laser power. The part of the film which is masked was unetched and rest of the portion which is exposed to pulsed laser beam was etched away. In this way one can produce highly accurate geometrical configurations for appropriate physical measurements like critical current density. This is a simple and time saving procedure for patterning High T_c thin films.

to chemical reaction. The sample is then rinsed in developing solution that removes the exposed areas of PPR, leaving the pattern of bare PPR coated surface of the sample. The steps involved in the patterning of high T_c superconductor samples are mentioned below in sequence.

1. Spin on positive photoresist (Micro Posit 1350) at 3000 rpm for 30 s.
2. Bake at 100°C for 10 min.
3. Align the photomask over the sample, positioning the photomask so that the contact pads are over the silver deposits.
4. Expose to UV light for 20s.
5. Develop in Micro posit developer for 45 s.
6. Rinse in distilled water.
7. Spin for 10 sec 3000 rpm (to get rid of water on the surface)
8. Bake at 100°C for 10 min.
9. Etch in a solution of ferric nitrate or orthophosphoric acid.
10. Stop etch in distilled water.
11. Remove photoresist with acetone.

Fig.2.5 shows the schematic representation of the micro-bridge patterned using the photo lithography technique.

(b) Pulsed Laser Etching :

Using a 10 μm bridge mask on the film and exposed to a low power pulsed laser one can pattern the film for current density measurements. This dry technique avoids usage of chemicals which affects a film quality to a certain extent.

2.8 Scanning Electron Microscopy (SEM) Studies

Scanning electron Microscopy is a powerful technique for studying the surface morphology of bulk samples as well as thin films. But only metallic films deposited on conducting substrates can be studied using this technique. In this thesis SEM was used to study film surface morphology as well as cross sections of the fractured substrates.

SEM studies of the samples studied in this thesis were done with the help of a JEOL JSM 840 (nano scale resolution) equipped with an Energy Dispersive X-ray Fluorescence (EDX) attachment. The samples were investigated for grain size, changes in grain morphology and for changes in the image contrast.

2.9 Atomic Force Microscopy (AFM) Studies

Surface characterization techniques like SEM and Scaning Tunneling Microscopy (STM) are limited to conductive samples. To overcome this limitation G. Binning C. Gerber and C. Quate invented the Atomic Force Microscopy (AFM) for non conducting samples in 1985 [17]. AFM can image nonconducting samples as well, because it uses an optical technique to sense the position of the tip realtive to the sample. The AFM provides the ability to acquire three-dimensional data with angstrom resolution from conducting and nonconducting surfaces. AFM made by digital instruments company model III nanoscope was used for analysing our samples. The block diagram of AFM front view was shown in the Fig.2.6. Further details on the AFM and its mode of functions are described in Chapter 4.

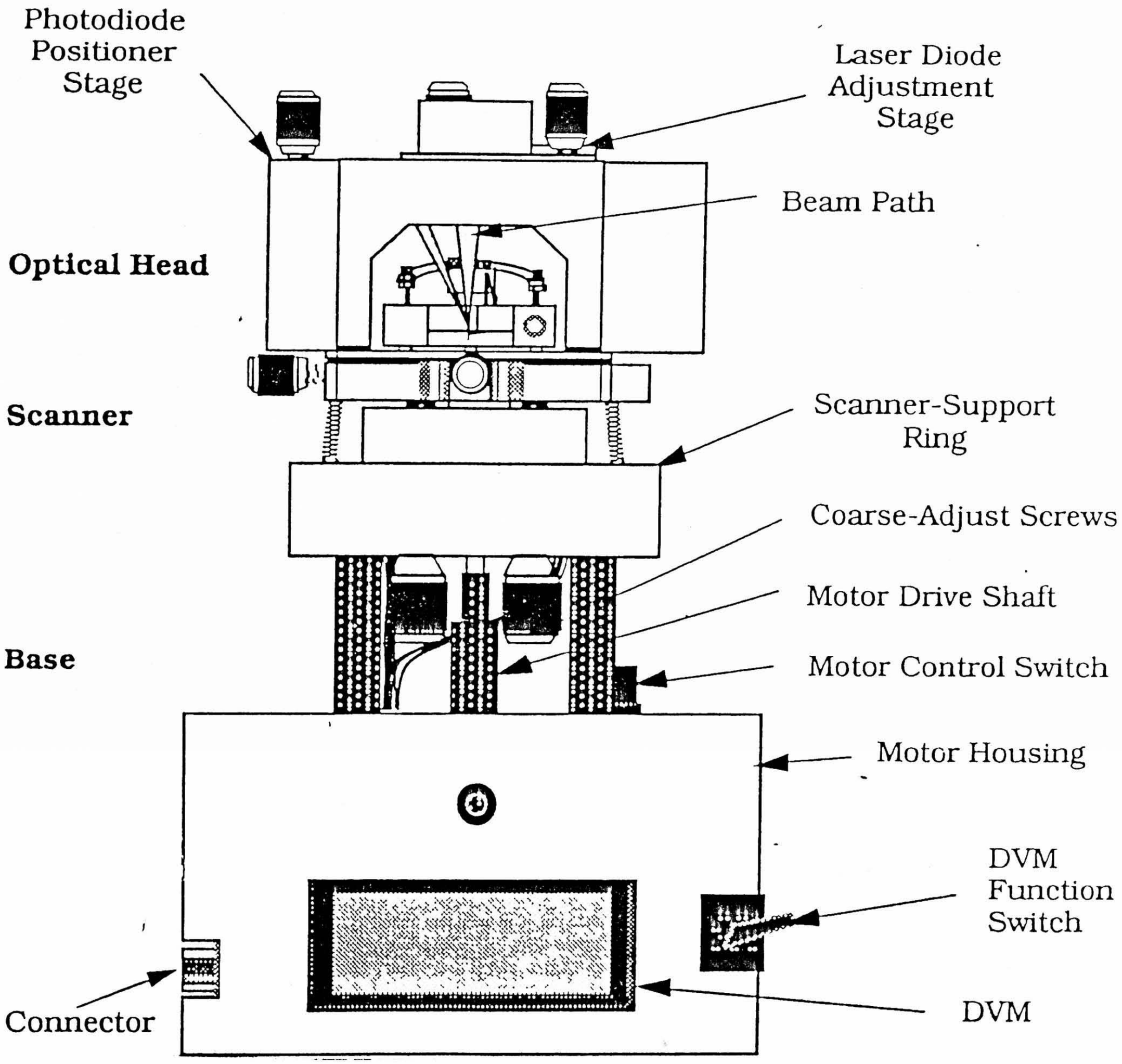

Fig.2.6. AFM (Front View)

References

[1] J.M. Tarascon, L.H. Greene P. Barboux, W.R. Mc Kinoon, G.W. Hull, T.P. Drlands, K.A. Dehn, S. Fopner and E.J. Mc Kiff, Phys. Rev. B **36** (1987) 8393.

[2] P. Gupta Sarma, V.R. Palkar and M.S. Multani, Solid State Commn. **177** (1991) 337.

[3] S.B. Ogale, R.D. Vispute and S.M. Kanetkar, Ind. J. Pure and Appl. Phys. **30** (1992) 666.

[4] R. Pinto and R. Vijayaraghavan, Ind. J. Pure and Appl. **30** (1992) 692.

[5] R.Ramesh, A. Inam T.Sands and C.T. Rogers, Materials Science and Engineering B **14** (1992) 188.

[6] Films of High temperature oxide superconductors by T.R. Lemberger, Physical Properties of HTSC III ed by Donald M. Ginsburg, 1992.

[7] S. Tanaka and H. Itozak, Japn. Jl. of Appl. Phys. **27** (1988) L622.

[8] C.B. Eom, J. S. Sun, K.Yamamoto, A.F. Marshall, K.E. Luther, T.H. Geballe, Appl. Phys. Lett. **555** (1989) 595.

[9] N.Terada, H.Ihara, J. Mastoshi, H.Masayuki, Y.Kimur, K. Matsutami, K. Hirata, E. Onno, R.Sugire and F.Kawashima, Japn. Jl. Appl. Phys. **27** (1988) L639.

[10] R. Pinto, L.C. Gupta, R. Vijayaraghavan, A.G. Chourey, V.S. Shirodkar, Physica C **171** (1990) 131.

[11] L.I. Maissel and R. Glang, *Hand Book of Thin Film Technology*, Mc Graw Hill Book Co. (1970).

[12] J.L. Vossen and W. Kern, *Thin Film Processes*, Mc Graw Hill Book Co. (1978).

[13] K.L. Chopra, *Thin Film Phenomenon*, Mc Graw Hill Book Co.

[14] Conf. Proc. of the MRS Symposium on Laser Ablation for Material Synthesis, eds. D.C. Paine and J.C. Brarman, Mat. Res. Soc. group, Pitsburg (1990).

[15] D. Dijkkamp, T. Venkatesan, X.D. Wu, S.A Shaheen, N. Jisrawi, Y.H. Min-Lee, W.L. McLean, M. Croft, Appl. Phys. Lett. **51** (1987) 619.

[16] X.D. Wu, B. Dutta and M.S. Hegde, Appl. Phys. Lett. **54** (1989) 179.

[17] G. Bing, C.F. Quaste and Ch. Gerber, Phys. Rev. Lett. **56** (1986) 930.

Chapter 3

Magnetron Sputtered Y-123 and Y-124 Thin Films

In this chapter, after a brief review of the literature on HTS thin film work, the following research work is presented.

1. Design and performance of a planar magnetron system to minimize the back sputtering to improve the stoichiometry of deposited HTS films, and hence their quality.

2. Sputter deposition of $YBa_2Cu_3O_{7-y}$ $(Y-123)$ films on single crystal MgO $< 100 >$ substrates using the planar magnetron system and their evaluation with respect to T_c and J_c.

3. Formation of $YBa_2Cu_4O_8$ $(Y-124)$ phase in sputtered deposited films on $SrTiO_3$ $< 100 >$ substrates using the planar magentron system, and their evaluation.

3.1 Introduction

Many difficulties faced in HTS R & D arise due to their ceramic/granular nature, short coherence length and anisotropy. Most applications of superconductors require high J_c which depends upon the microstructure of HTS superconductors[1-4]. Therefore, extensive studies have been done on microstructure controlling/grain alignment/grain

boundary minimization to improve the critical current density (J_c). The same remains true for HTS films. For this reason HTS films are deposited on single crystal substrates to improve grain alignment and size. However, HTS thin films deposited on single crystal substrates are not truly epitaxial; the microstructure of these films, grain size, grain orientation, and grain boundary weak links varies from film to film, which critically depends upon complexity of the growth process and the type of a substrate used, and other parameters.

The first report on $Y-123$ thin films prepared using a sputtering technique was by R. E. Somekh et al [5] and followed by others using several sputtering deposition methods [2-6]. There are, however, several common problems in the sputtering deposition methods. In this process the highly energetic ions as well as neutral particles, and secondary electrons emitted from the target surface, are accelerated towards the substrate by the electric field applied to the target. This leads to back sputter of the growing film components selectively and causes stoichiometric deviation from that of the target. It also leaves various crystalline defects in the films, resulting in amorphization in extreme cases [5,7,8]. In the case of oxide materials, the resputtering is due to oxygen anions and highly energetic neutral particles. Formation of O^- and O^{-2}, and resputtering due to oxygen anions has been reported previously by Hanak [10]. However, films growth experiments with pure Ar sputtering still show considerable amount of resputtering most probably due to oxygen anion from an oxide target on sputtering.

Several groups have used non stoichiometric targets for compensating the selective backsputtering [8,9]. One possible solution is the off axis sputtering which was originally developed by Hoshi et al [11]. It is the most promising sputtering arrangement as the plasma can be confined almost completely in the space between the targets facing each other. Sandstorm et al have used off-axis sputtering in which substrates were placed on the side of and at an angle (45 to 90 °) to the sputter gun. They used low gas pressures (6 mTorr), a rotating substrate block to obtain uniformity and an off-stoichiometric target adjusted to improve the film composition. Eom et al have developed a high pressure off axis sputtering technique in which almost the exact composition of the target is obtained over large areas without a need for the substrate rotation [12]. Sputtering in relatively high pressure of oxygen as reported by Poppe et al [13] for on axis sputtering also resulted in stoichimetric $Y-123$ films. Li et al have also made similar observations at 600 mTorr

[14]. The frequent collisions at high pressure results in a reduction of the kinetic energy of the particles and consequently a reduction in back sputtering. This approach also enables the use of high oxygen pressure for in situ film growth but the uniformity of the resulting film is has been reported to be poor. A better uniformity has been achieved by the same group [15] by optimizing the deposition parameters. Magnetron sputtering offers high at rates of deposition, low bombardment of the substrates and convenient control of film composition for all types of targets. Terada et al have reported that transverse magnetic field can minimize back sputtering and hence stoichiometric deviation [7] in HTS films. By applying a transverse magnetic field of about 150 Oe they found that the bombardment of the secondary electrons on the growing film are minimized considerably. However, resputtering due to highly energetic neutral particles still continue to exist in this method.

Many researchers have reported on sputtering of 2 inch dia targets only. But cost wise they are very expensive and preparation of high density 2" targets in the normal research laboratories is also not easy. One inch diameter targets one obviously should be preferred in order to minimize the preparation cost and labour. Infact it is very easy to prepare 80% – 90% dense targets of one inch diameter and 3 - 4 mm thick through a standard solid state method. There is a report by Kuppuswamy and Raghunathan which discusses preparation of $Y-123$ films by dc sputtering using one inch target and high pressure oxygen and on axis geometry [16]. A study, therefore, was taken to prepare a planar magnetron system [17] (with transverse magnetic field) suitable for one inch diameter target and use the same to prepare stoichiometric $Y-123$ films using the on-axis sputtering geometry. A preliminary report of the design of the magnetron system has been reported earlier [18].

A new high T_c superconductor $YBa_2Cu_4O_8(Y-124)$ containing double $Cu-O$ chains was first discovered as a planar defect in the $Y-123$ superconductor with a single $Cu-O$ chain [19]. Unlike $Y-123$ high T_c $Y-124$ compound has thermally stable oxygen content up to 800°C [20], and therefore, it is more suitable for technological applications. However, its lower superconducting transition temperature (T_c) of 80 K is not favorable for practical devices operating at liquid nitrogen temperatures or higher. A subsequent discovery that a substitution of Ca for 10% of Y in this compound increases its T_c to 90 K [21], almost the same T_c as that of $YBa_2Cu_3O_{7-y}$ $(Y-123)$, improved the situation

with respect to its $(Y/Ca-124)$ applicability in superconducting devices. However, there is an additional difficulty with respect to the $Y-124$ compounds. While it is trivial to synthesize a $Y-123$ compound, a phase pure $Y-124$ compound is not easy to prepare. It has to be either synthesized under a high oxygen pressure or very long time is needed to prepare it in single phase at 1 atm. oxygen pressure due to very slow kinetic reactions of the constituent oxide at $830°C$, above which $Y-124$ is unstable [22].

It seems that although the $Y-124$ phase is difficult to prepare in bulk, it is not so difficult to obtain it in thin film form by e-beam or sputtering methods [23-26] or other physical methods. P.Gupta Sarma et al. have reported that the solution derived complex untreated targets can produce single phase $Y-124$ thin films by a pulsed laser ablation method [27]. $Y-124$ films have also been grown by sputtering [28], thermal evaporation [26], molecular beam epitaxy [29], and CVD [30]. Ca doped 124 films have been prepared by sputtering [31,32]. Recently Y. Yoshida et al have reported growth of $Y-124$ films, with c-axis in plane, by in situ annealing of precursors deposited by the hybrid plasma sputtering [33]. They confirm that amorphous precursor is the best candidate for growing $Y-124$ thin films.

There were several research reports on the effect of deposition conditions such as target composition, substrate material, substrate temperature and total pressure of sputtering gas mixture and partial pressure of oxygen gas etc. [1-9,34,35] for in situ deposition of high quality $Y-123$ and $Y-124$ thin films. This chapter also presents a study on the phase formationof $Y-124$ films on $SrTiO_3$ < 100 > substrates using the magnetron system and their growth dependence on the target nature, and deposition conditions including variation of oxygen partial pressure and the substrate temperature.

3.2 Theory and Design of Magnetron

The basic physical principles of magnetron sputtering are discussed by Thornton and Penfold [36], Thornton [37-39] and Thornton et al. [40]. Waits has reviewed the technology of planar magnetrons [41,42]. Different practical aspects related to magnetrons, like magnetic field geometry, magnet material, discharge characteristics and thickness are discussed by Almeida [43]

(a) Physics of Magnetron :

In a uniform magnetic field and in zero electric field, an electron moves in circular orbit whose radius is given by [44]

$$r_g = m\,v/q\,B \qquad \ldots 3.a$$

where m is its mass, v is its veloctity, B is the magnetic field, and r_g is the radius of the orbit called gyro or Larmor radius. In presence of an electric field, $\vec{E}$, this takes the form

$$r_g = m\,v\,\sin\theta/q\,B \qquad \ldots 3.b$$

where θ is the angle between $\vec{B}$ and $\vec{E}$. Thus an electron spends more time in a region in presence of a magnetic field perpendicular to its motion.

A magnetron arrangement in a sputtering system, makes electrons confined near to the target and the plasma near to it. The energetic electrons produce higher ionization due to repeated collisions. As a result, the thickness of the cathode dark space, working pressure and voltage (because fewer secondary electrons are needed) are reduced and the sputtering flux is increased.

The advantages of a planar magnetron source are as follows: follows.

1. A high rate of sputtering is obtained due to the confinement of the plasma close to the target surface.

2. The heating of the substrate by stray electrons is low. In many cases this is the limiting factor for high rate conventional sputtering.

3. Sputtering can take place at a low gas pressure because of the increased path length of electrons within the plasma and prevention of their escape.

Considering these advantages, a magnetron arrangement was designed to prepare the better quality $Y-123$ and $Y-124$ films.

3.3 Description of the Magnetron Sputtering System

Figure 3.1 shows a schematic diagram of the cross section of the planar magnetron source for the deposition of high T_c thin films. It consists of a water cooled cathode (A) made of copper on which planar targets (B) of any materials bonded to a copper backing plate can be easily mounted. The cathode is insulated from a water cooled aluminum shield (C) with Teflon spacer (D) and is kept in position using a stainless steel nut (I). The magnets (J) are mounted outside the shield. The whole assembly is affixed to a stainless steel base plate (G) which is placed on a bell jar in which sputtering is carried out.

Figure 3.2 shows a schematic arrangement of U shaped permanent magnets as viewed from a direction normal to the cathode plate. This figure also shows the magnetic field lines. The electric field lines between the cathode, shield and substrate holder (both are grounded) are always perpendicular to the magnetic field lines in this geometry. A schematic view of the electric and magnetic field lines is shown in figure 3.3

3.4 Magnetron System Performance

The system performance of the magnetron source in terms of uniformity and rate of deposition to verify the magnetron mode of operation are discussed here. For evaluation of the performance of the system, target materials of different yields (copper and aluminum) are considered. Thin sheets of the target materials were affixed to copper backing plates with a conducting epoxy. The backing plate was in mechanical and thermal contact with water cooled cathode holder. A water flow of 1.5 liter/ min was found to be adequate at the power used. A *RF* power supply operating at 13.56 MHz was used for *RF* sputtering (power 1 kwatt) and for DC sputtering 2 KV with 500 mA variable current was used. *Ar* gas pressure during sputtering was 10^{-2} Torr for sputtering and cathode to target distance is 5 cm and flow rate of argon is 20 cm^3 per minute. The

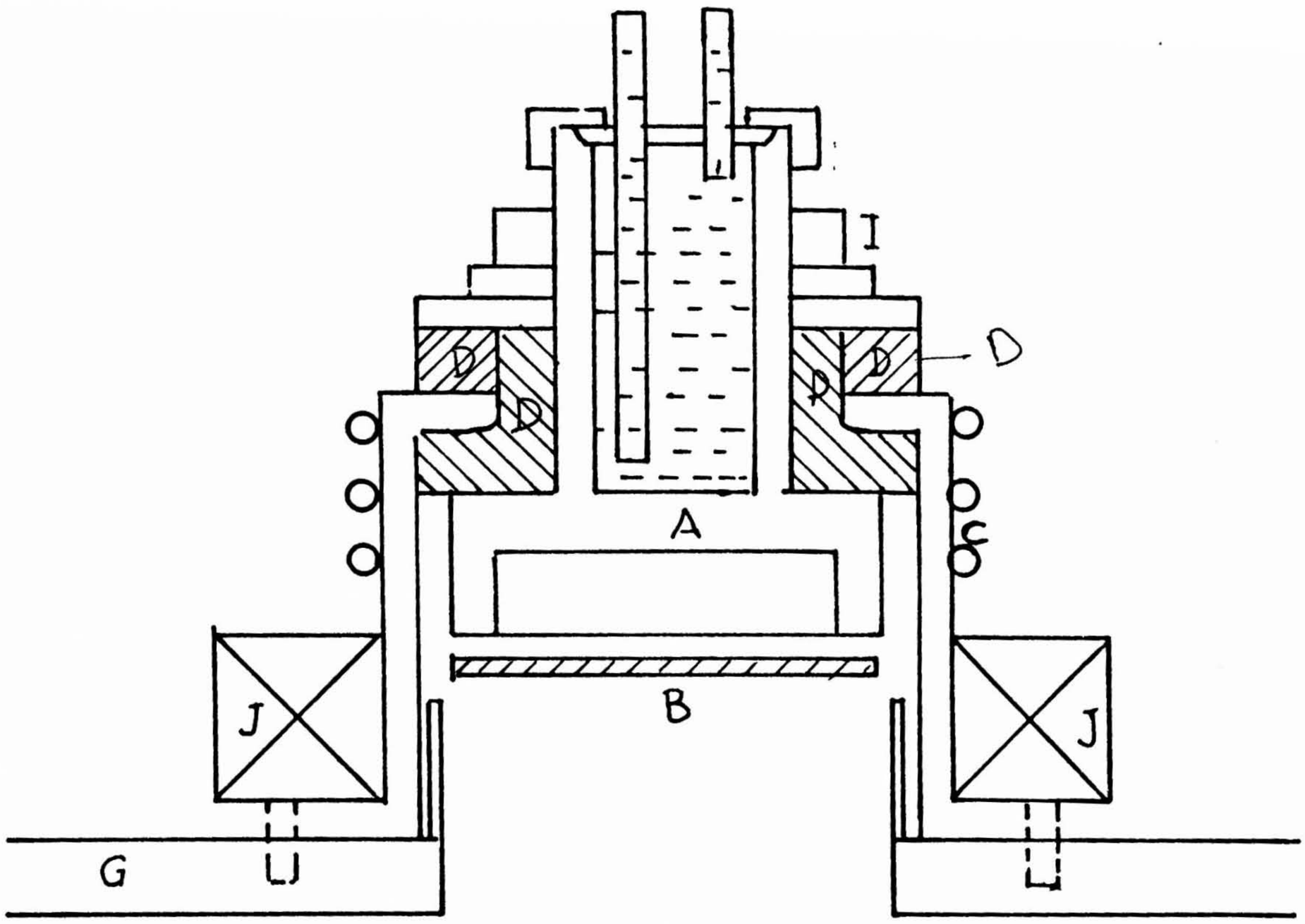

Fig.3.1. Cross-sectional view of the planar magnetron sputtering source. (A) Cathode; (B) Planar Target; (C) Aluminium Shield; (D) Teflon Spacer; (I) Stainless Steel Nut; (J) Magnets and (G) Stainless Steel Base Plate.

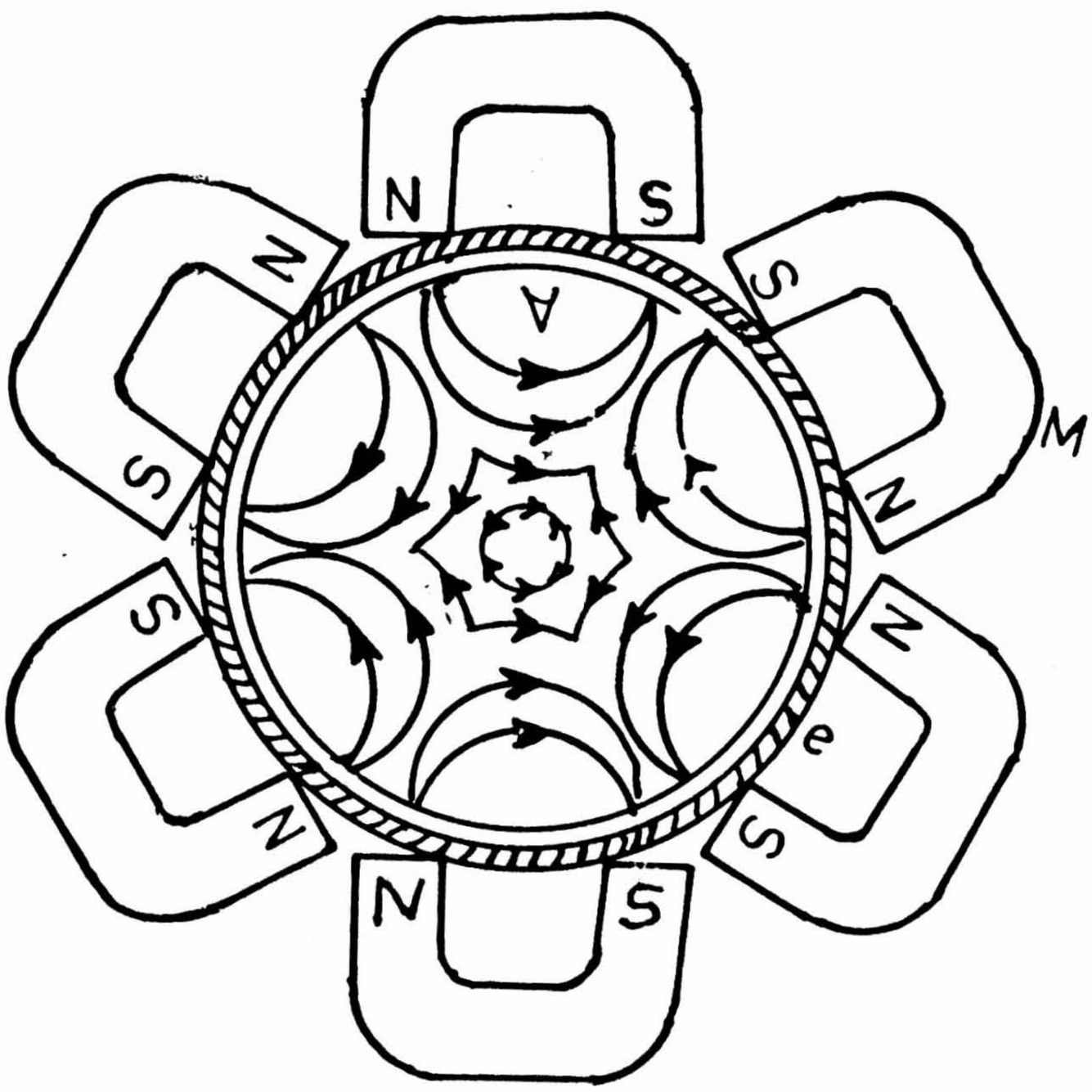

Fig.3.2. Schematic arrangement of the magnets and magnetic lines of forces viewed from a direction perpendicular to the of the target showing (A) Target; (B) Shield and (M) Magnets.

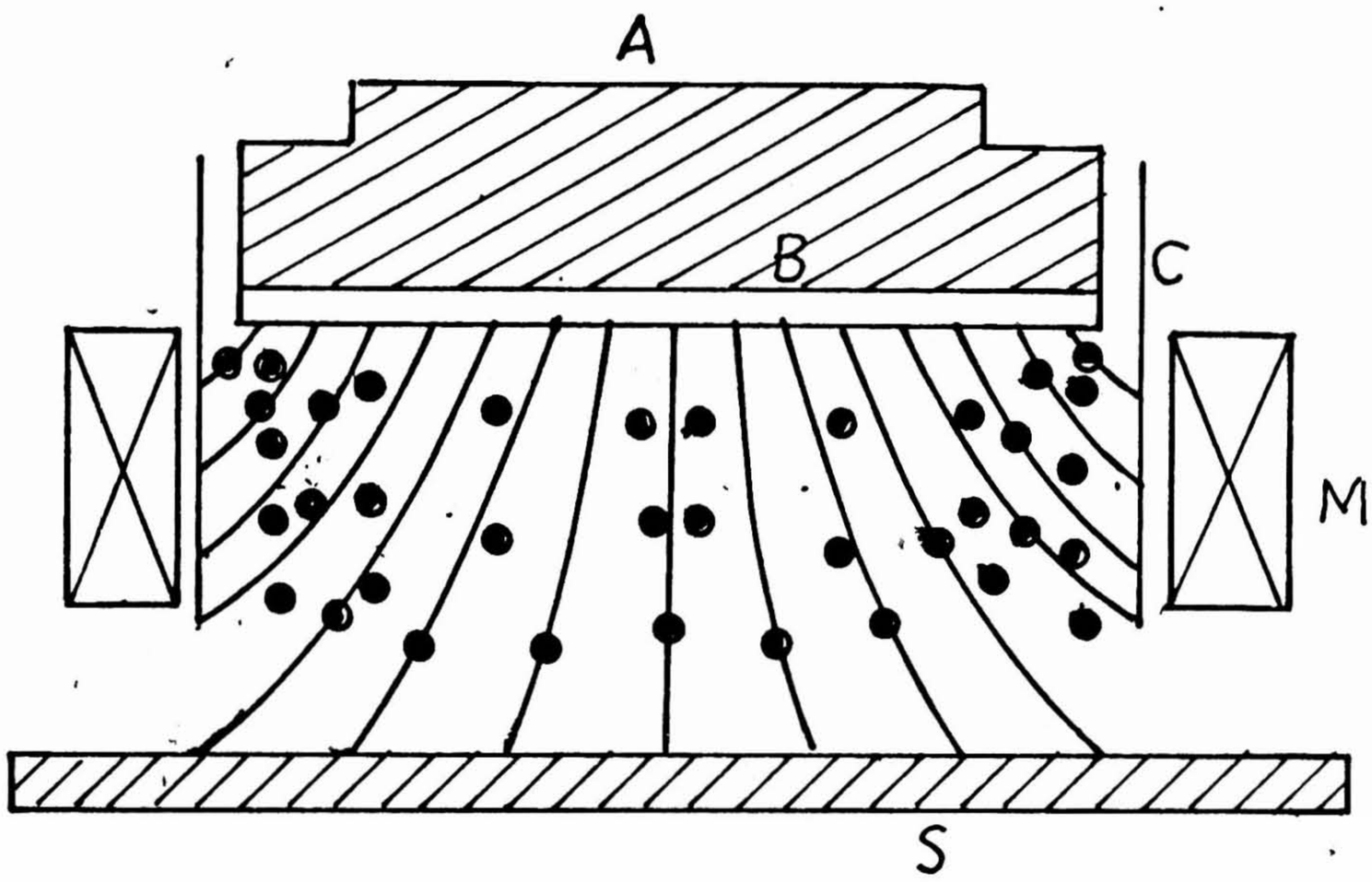

Fig.3.3. Schematic Cross Section of the Magnetron Source showing electronic field lines (continuous) and Magnetic field lines (•) perpendicular to electric field lines and showing (A) Cathode; (B) Target (C) Shield; (S) Substrate and (M) Magnets.

maximum magnetic field obtained in the present case with the available four magnets is 100 Oe on the target surface.

Presputtering for 10 min was enough to clean the target surface. Films were then deposited on clean glass substrates using copper or aluminium targets. The thickness of the deposited metal films at various positions on the substrate holder was measured with the help of a talystep (STYLUS) measuring instrument. Films were formed to have the thickness uniformity of better than 95% across a length of 1.5 cm which normally is not there without the magnetism arrangement. The high uniformity of the deposition is due to a combination of electrostatic focusing effects and magnetic field geometry employed in this system. The erosion of the target surface was also found to be quite uniform from the visual appearance. The results are summarized in Table 3.1. The rates obtained are nearly two times higher as compared to rates obtained in simple diode sputtering system with out magnetron. By introducing more magnets, field can be increased effectively resulting in higher yield. For our work, the present system was found satisfactory. The rates can be further improved with a stronger magnetic field. However, the uniformity of deposition may be affected due to magnetic field variations across the total cross section in a stronger mangetic field design which must be considered while selecting a magnetic design. This system is used to prepare $Y-123$ and $Y-124$ films as described in the next section.

3.5 Y-123 Films

One inch diameter $Y-123$ targets were prepared by the standard method. The density of the targets was in between 80 to 90%. The $Y-123$ thin films were deposited by dc as well as RF magnetron sputtering techniques using a single stoichiometric target (T_c = 90 K). The sputtering chamber was pumped to a base pressure of 10^{-6} Torr and the sputtering pressure was controlled in the range 60 mTorr to 120 mTorr with $80:20 Ar/O_2$. The substrates were heated to 750°C using a lab made heater. The deposition rate was about 12Å/min. The sputtering conditions of both RF and DC are listed in Table 3.2a and 3.2b respectively. Films were characterized using XRD, four probe DC electrical

Table 3.1

Performance of targets of various materials in terms of deposition rate and uniformity of the deposition at 25 m Torr. Ar pressure and 5 cm Target to Substrate Distance.

Sl.	Target Material	Power applied (Watts)	Deposition rate Å/min. with field 100 Oe	Deposition rate Å/min. without field	Uniformity of Deposition (%)/1.6 cm^2
1.	Aluminium	50 (RF)	120	10-12	95
		50 (DC)	18	8	90
2.	Copper	25 (RF)	30	14	100
		25 (DC)	32	18	95
3.	$YBa_2Cu_3O_{7-y}$	25 (RF)	15	10	80
	metallic target)	10 (DC)	12	8	85

Table 3.2a
DC Sputtering Conditions

1.	Target	$YBa_2Cu_3O_{7-y}$ (1 cm dia; 4mm thick, 90% dense; $T_{co} \sim 90$ K).
2.	DC Power	7-10 Watts.
3.	Substrate Temperature	650-750°C.
4.	Substrate-traget distance	4-5 cm
5.	Substrate	MgO < 100 > (0.5×0.5 cm^2)
6.	Sputtering gas	Ar+O_2 mixture (4:1 and 1:1)
7.	Sputtering gas pressure	60 - 120 mTorr

3 2b

1.	RF Power	25 Watts.
2.	T-S distance	5 cm
3.	Sputtering gas pressure	90 mTorr; Ar+O_2 (9:1)
4.	Sputtering temperature	650, 700, 750°C.
5.	Substrate	MgO < 100 > (0.5×0.5 cm^2)

resistance and Scanning Electron Microscope studies. Critical current density J_c of the films was measured using 10 μm $\times$ 2 mm $\times$ 200 nm microbridges prepared by laser etching.

The effect of sputtering parameters both in *RF* and *DC* sputtering and substrate temperature on microstructure and superconducting properties have been studied under identical deposition conditions of other parameters for the comparison sake. Effect of the sputtering gas pressure was studied keeping the substrates at 750°C. Oxygen partial pressure was also varied keeping other optimized conditions fixed. The effects of the varied sputtering parameters on the microstructure and superconducting properties are discribed below.

3.5.1 Structure of the Y-123 Films

Figure 3.4 shows the typical X-ray diffraction patterns of the six $Y-123$ films prepared at different substrate temperatures for six films. Films a, b, c are RF sputtered while d, e, f films are DC sputtered. All XRDs are presented in one figure. Each XRD trace has been displaced by 1°. The 2θ scale indicated belongs to the sample 'a'. For all the films no XRD peaks other than those of $Y-123$ compound were detected indicating that ihere is no XRD detectable segregation of impurity phases, i.e., all films were XRD pure 123 phase. Further, the XRD patterns of all the films show only $< 00l >$ peaks indicating that all grains in the film are perfectly c-axis oriented in nature. It is usual that, the intensities of the relfections at very low 2θ Bragg angle in thin films have a large contribution from the matrix of the surface layers owing to the effect of X-ray diffraction. These reflections are also sensitive to the geometry of the sample setting inside the diffractometer. As a result, the intensities of these reflections are difficult to measure accurately. With increase in the 2θ Bragg angle, however, the influences of surface conditions and setting geometry on the reflection intensities become negligible. Thus relatively an accurate measurement of the reflection intensities at the high Bragg angles becomes meaningful. The XRD intensities of <004, 005, 006 and 007> peaks are compared with each other. From the Fig.3.4 one can see that intensities of $< 004 >$ and $< 006 >$ reflections seem to vary among the films prepared at different substrate

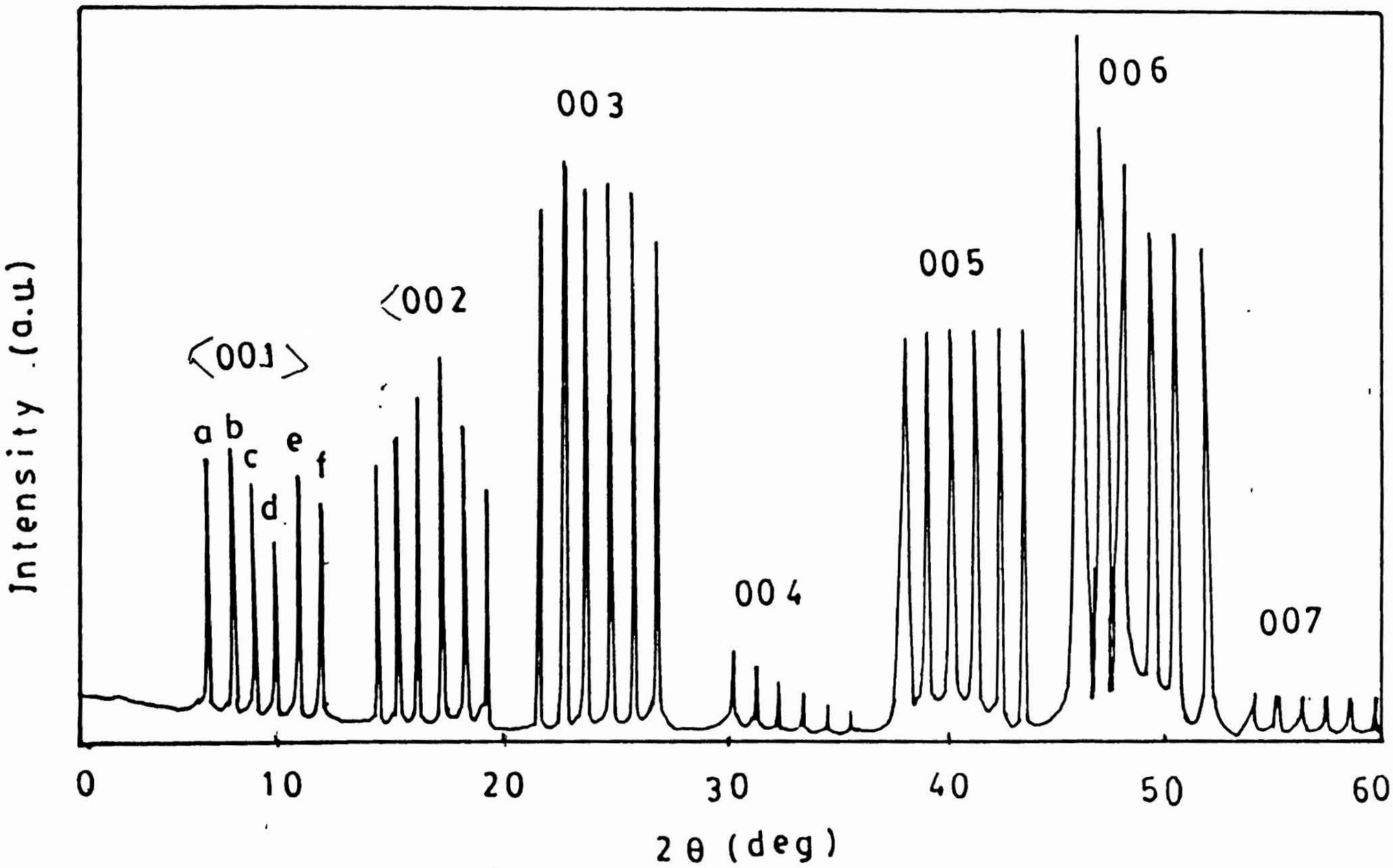

Fig.3.4 Typical X-ray diffraction patterns of Y-123 thin films prepared at (a, c) 650°C (b, d) 700°C and (e, f) 750°C substrate temperatures. Peaks were shifted by 1° from each other for comparison sake and intensities were normalized by their <005> reflections. a, b, c indicates RF sputtered films and d, e, f indicates DC sputtered films. The Scale in X axis refers to film 'a'.

temperatures, while the 007 reflection changes very little but this observation may be due to low intensities of this reflection that we are unable to observe the changes. The variation of crystallinity of the films with substrate temperature can be assessed from the full width at half maximum (FWHM) values of the maximum peak intensity, i.e., the < 006 > reflections. The FWHM values of < 006 > peaks of the films deposited at $650°C$, 700 $°C$ and 750 $°C$ are 0.53 °, 0.39 °and 0.22 °, respectively. Smaller FWHM values indicates better crystalline, hence, it is clear that the films deposited at higher substrate temperatures give better crystallinity in films. The FWHM values of XRD peaks reflect information about the grain size and the lattice strain along the deposition direction i.e, the c-axis. The results indicate larger defects and structure disorder in films deposited at lower substrate temperatures. Further, EDAX measurements on all the six films showed good 123 stoichiometry to films deposited on the substrate held at 750°C. However, a slight deviation from the stoichiometry was observed for some films which were deposited at substrate temperature 600^0C in both RF sputtering as well as in DC sputtering.

Fig 3.5 was drawn to show the substrate dependence of the c-lattice parameters of the as grown thin films. It is obvious that the c lattice parameters expand considerably if the films are prepared at lower substrate temperatures. With increase of the substrate temperature, the c parameters decrease. At the highest temperature of the present research range, as-grown films showed the smallest c value, but still longer than $11.68\mathring{A}$, the 'c' value of bulk $Y-123$. Increase in the c parameter is not because of oxygen deficiency as films were well oxygenated after the deposition is over. The expansion in c - axis of the films may be from crystallographic defects introduced due to the lattice mismatch with the (MgO) substrate , deposition faults like netural particle bombardment etc. The present study is not enough to confirm these explanations. However, the data obtained shows similar trends as observed many researchers earlier [2-9].

3.5.2 Effect of Sputtering Gas Pressure

At the optimized substrate temperature sputtering gas pressures were varied from 60 mTorr to 120 mTorr using $Ar + O_2$ gas mixture in 4:1 ratio. Fig 3.6 shows the T_c vs.

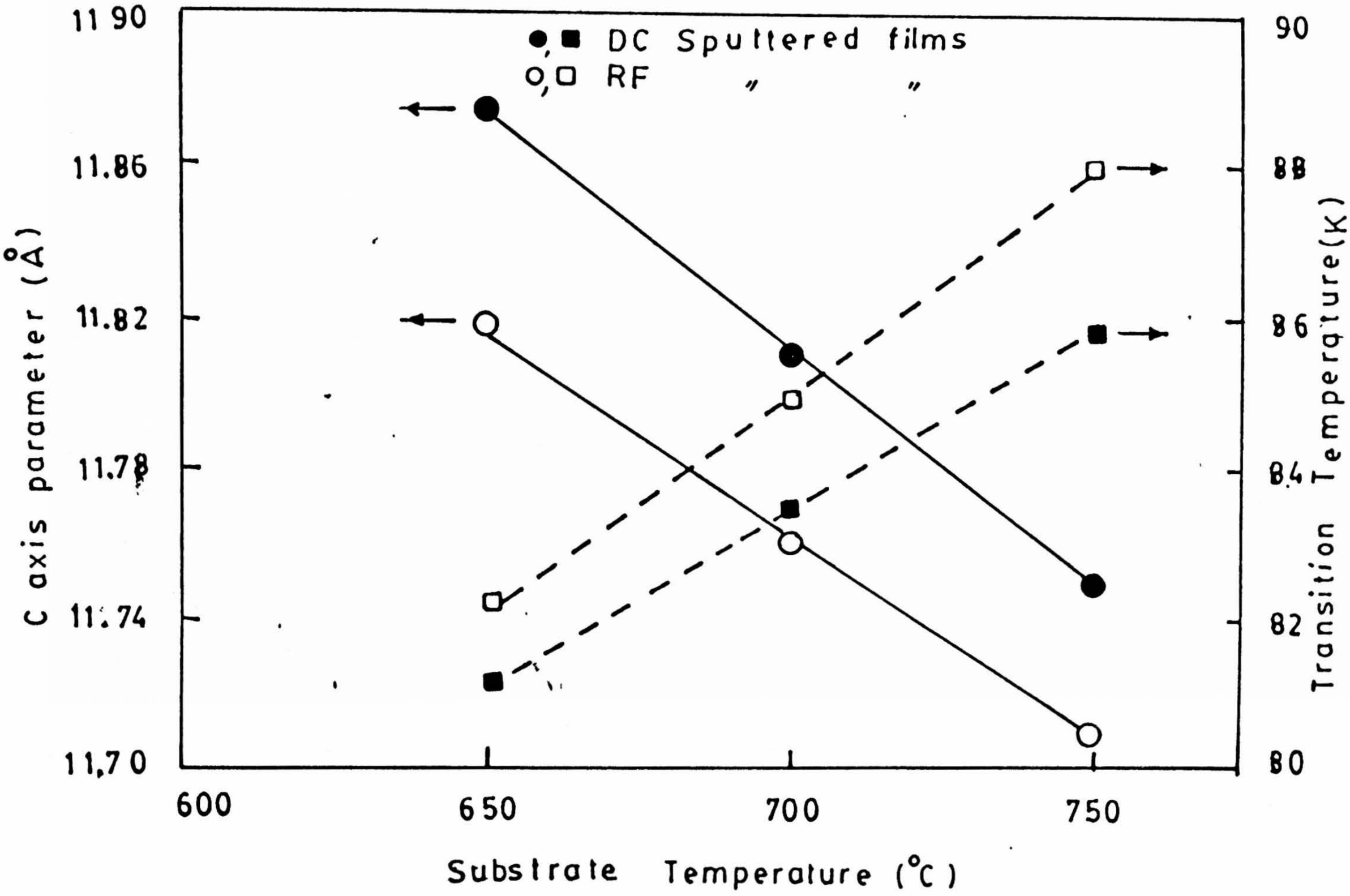

Fig.3.5. C axis parameter vs substrate temperature plots for R.F. and D.C. sputtered Y-123 films.

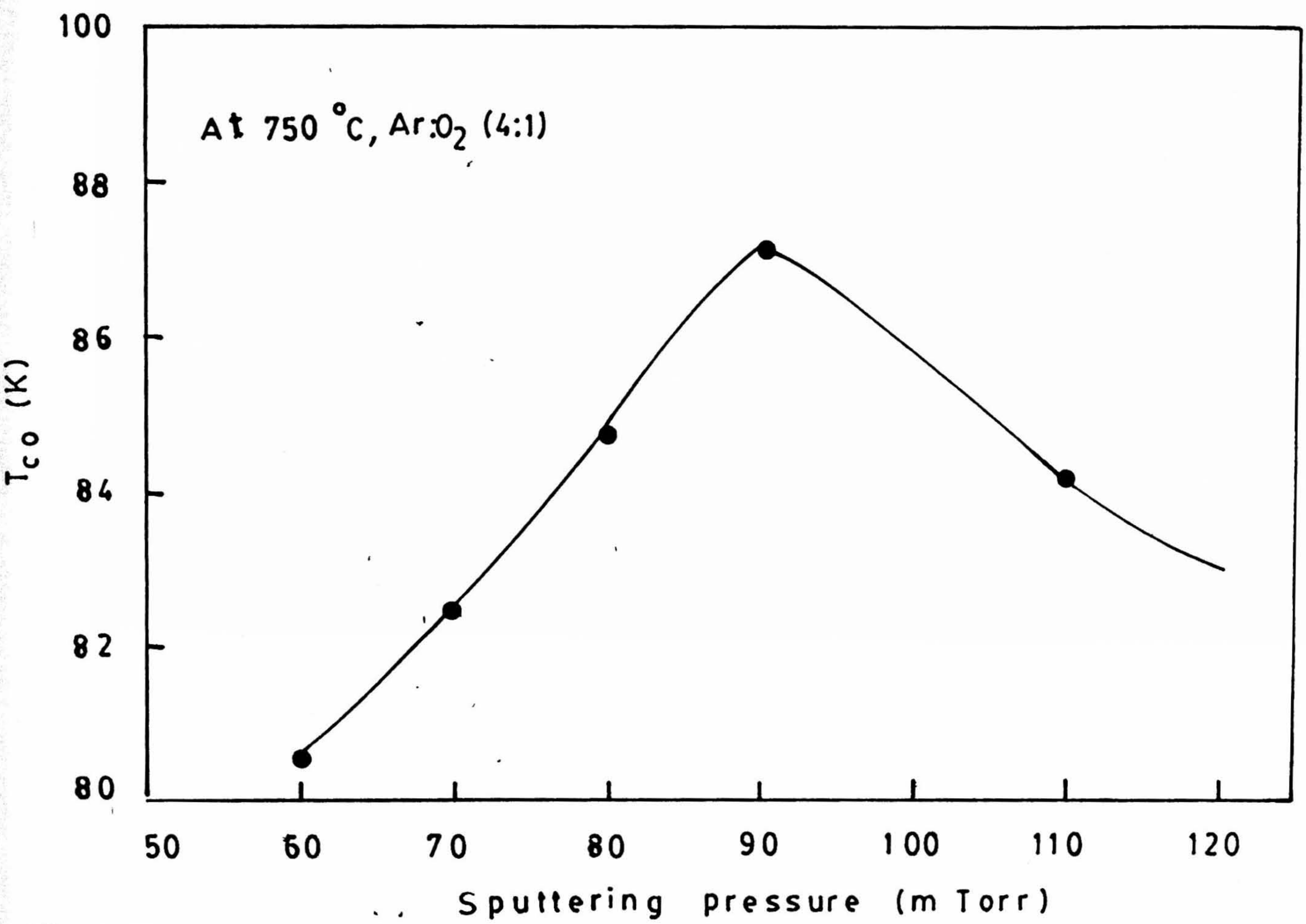

Fig. 3.6. Tco vs Sputtering gas pressure plot for RF sputtered Y-123 films deposited at 750°C and Ar + O_2 gas mix. in 4:1 ratio.

sputtering gas pressure. It indicates a sputtering gas pressure of 90 mTorr ($Ar + O_2; 4:1$) is optimum for the magnetron geometry used. Oxygen partial pressure was also varied at 90 mTorr sputtering pressure and 750°C substrate temperature. Fig. 3.7 shows the $R-T$ curves of the $Y-123$ films deposited using 4:1 and 1:1 ratio of $Ar : O_2$ gas mixture. It was found that 4 :1 ratio of $Ar : O_2$ gas mixture is optimum for one inch dia target system, since films deposited at this ratio shows resistivity at room temperature and higher T_c.

3.5.3 T_c Dependence on Substrate Temperature

Fig 3.8 shows the results of electrical resistivity measurements of DC sputtered $Y-123$ films. The $R-T$ curves shows the linear behavior of resistance above T_c as observed earlier by others. Table 3.4 shows the results on $R-T$ curves of the $Y-123$ films deposited on MgO < 100 > substrates at various substrate temperatures and sputtering gas pressures. The resistivity $\rho(300)$ was found to decrease with increase in the substrate temperature. Films deposited at 750 ° substrates give minimum resistivity and higher T_{co} as shown in the Fig. 3.9. The highest T_{co} obtained, i.e., 88.2 K, is still much lower than the bulk T_{co} (90 - 92 K) of $Y-123$. There are a number of possibilities which can affect lowering of T_c from the bulk value, especially for the HTS thin films. Two of these are:

1. Higher surface to volume ratio can lead to desorption of oxygen from the film. In addition, there could be some other surface related problem [45].

2. Structural disorder, defects and X-ray undetectable impurity phases since these may vary from film to film even when almost similar deposition condition are maintained.

Therefore, ours as well as others [46] observations of lower T_{co} in $Y-123$ films is something which is expected unless one grows perfect films using molecular bean epitaxy (MBE) technology. Normally even T_{co} of thin films of conventional supercoductors are different than the bulk T_{co}. Hence this observation in HTS films is not very surprising.

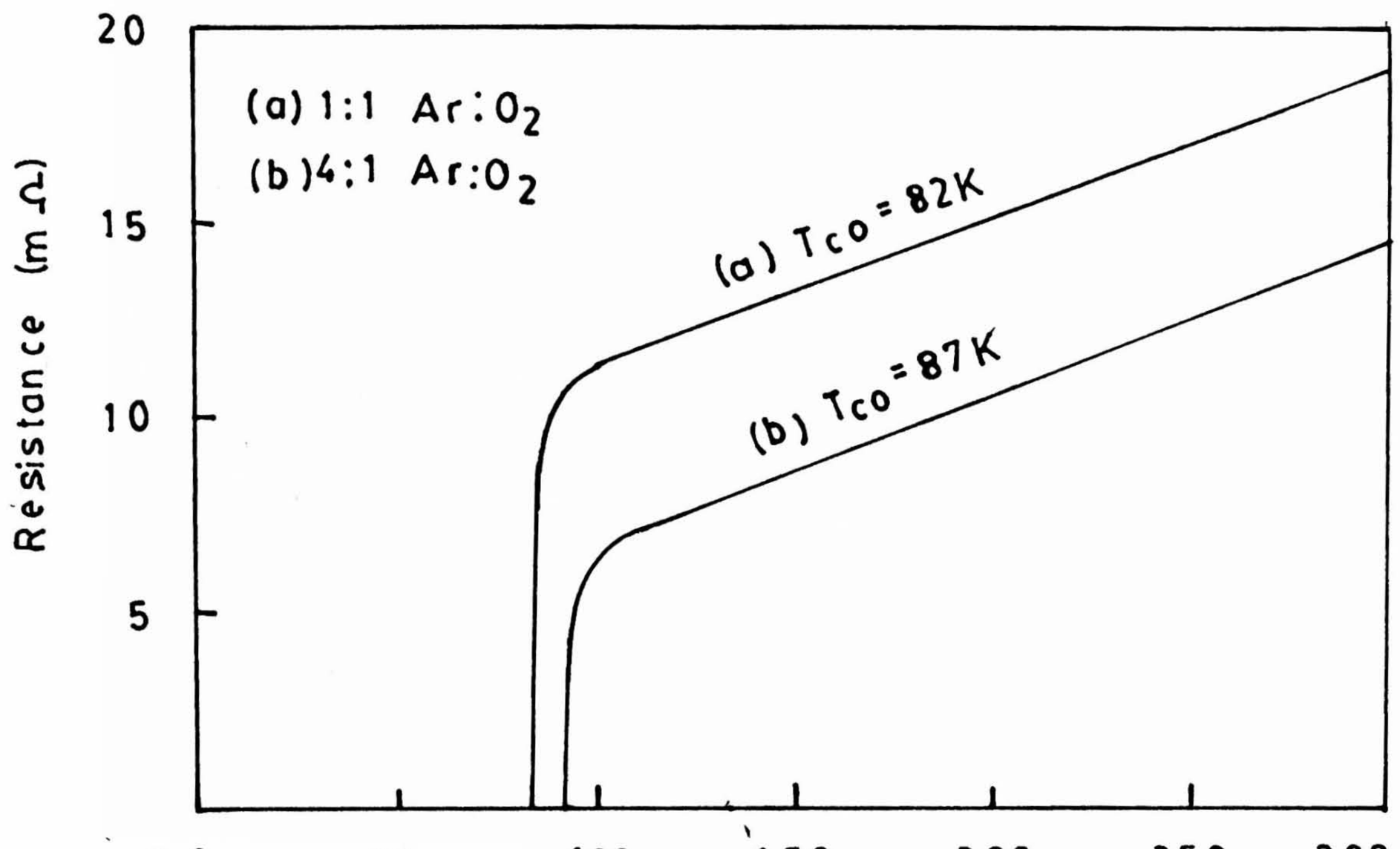

Fig. 3.7. A comparative spectral of R-T curves of deposited Y-123 films deposited at (a) 1:1 (b) 4:1 Ar = O_2 ratio gas mix.

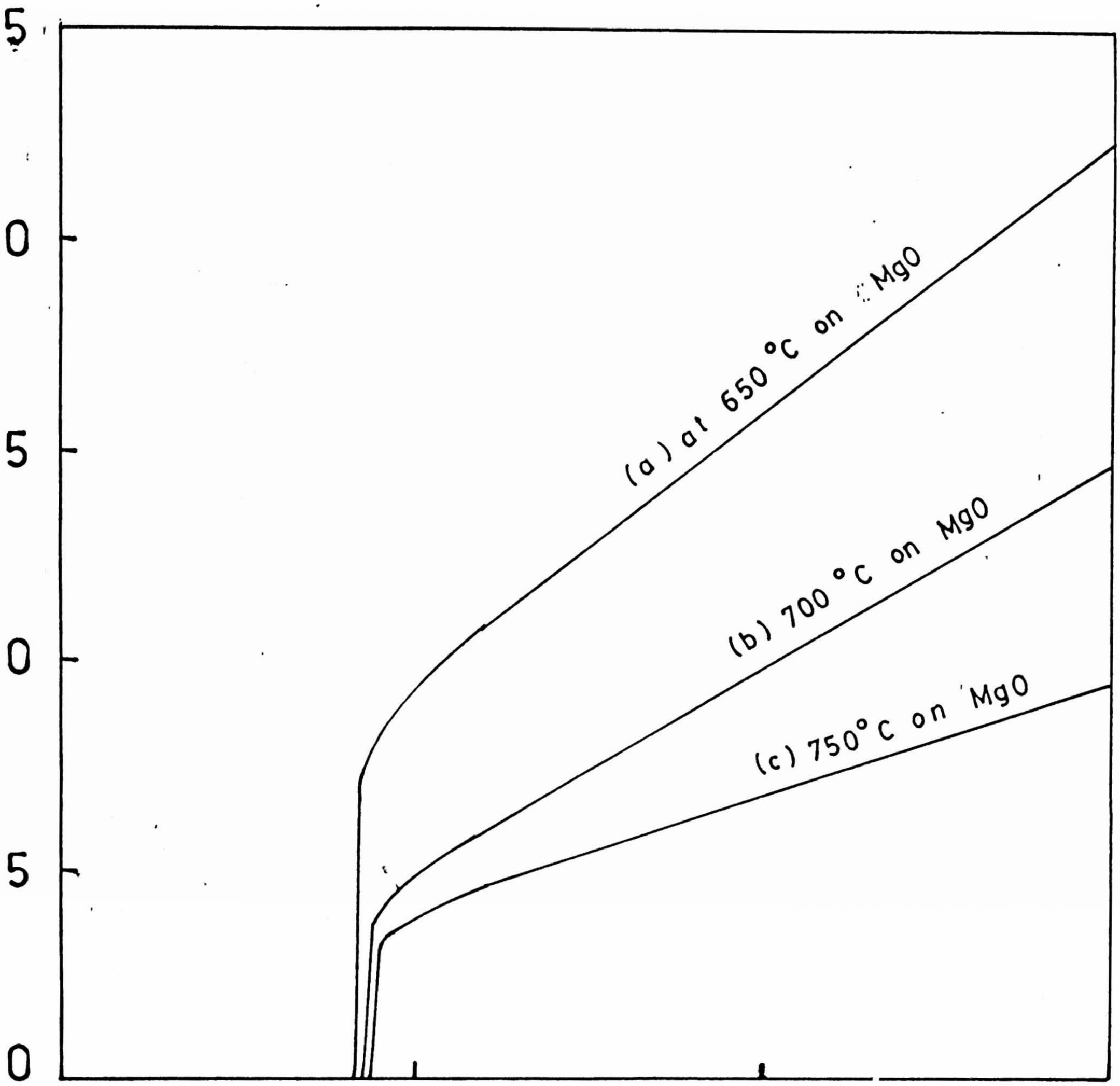

Fig.3.9. R-T curves of D.C. Sputtered Y-123 films deposited at three substrate temperatures (a) at 650° and Tco 81.2 (b) at 700° and Tco 83.5 (c) at 750° and Tco 85.8.

Table 3.4

Restults of $Y-123$ films deposited by RF and DC sputtering.

Sl. No	Preparation method	Sub Temp. (°C)	thickness (Å)	ρ_300 (ohm-cm)	T_{co} (K)	J_c at 77 K (10^4 A/cm^2)
		$[Ar:O_2]$				
1	RF	700	1840	0.0885	82.8	4
		[1:1]				
2	RF	700	1828	0.0502	87.2	50
		[4:1]				
3	DC	650	1848	0.0854	81.8	2.5
		[4:1]				
4	DC	700	1800	0.0637	83.8	3.9
		[4:1]				
5	DC	750	1852	0.0431	85.6	13
		[4:1]				
6	RF	650	1724	0.0931	84.3	3.3
		[4:1]				
7	RF	700	1831	0.0843	86.7	12
		[4:1]				
8	RF	750	1790	0.0403	88.2	47
		[4:1]				

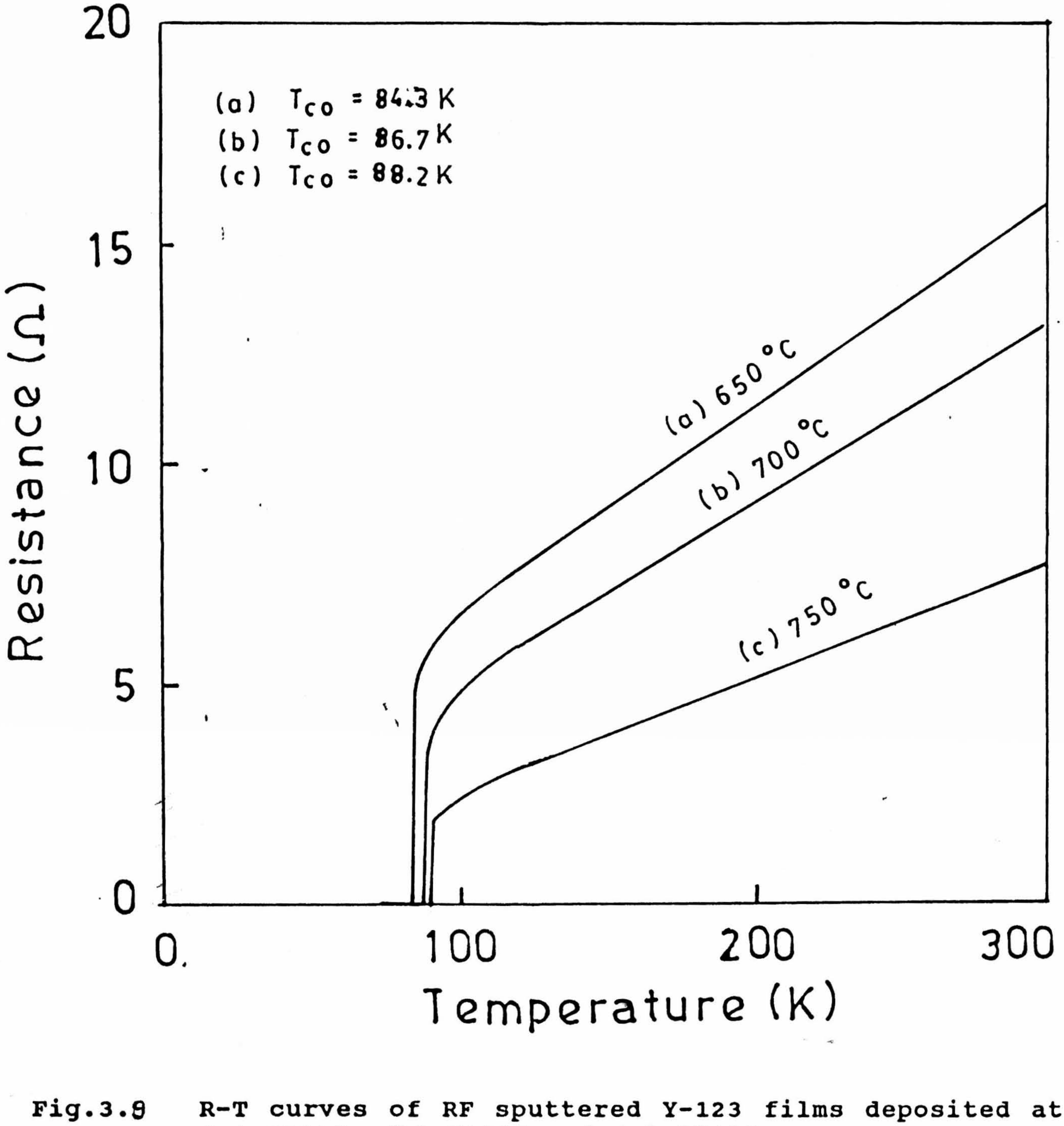

Fig.3.8 R-T curves of RF sputtered Y-123 films deposited at (a) 650°C; (b) 700°C and (c) 750°C.

3.5.4 Models for J_c of HTS and J_c Measurements on Y-123

The critical current density depends upon the flux pinning centers as well as the grain boundaries, both of which depend upon epitaxial quality and microstructure of the films. The nature of the grain boundaries is expected to depend upon the lattice match between the film and the substrate.

It is important to understand the mechanism which limits the critical current density in these granular high T_c superconducting films. The variation of J_c with temperature of these films was explained using models prepared by earlier researchers for granular superconductors. The basic reason for choosing molecular model is due to their microstructure which confirms the existence of well aligned grains. These grains are homogeneous but are connected by weak links. These weak links can be either grain boundaries, or superconducting regions of poor quality, or even normal conducting or insulating barriers.

One of the main problems is the temperature region where the models are valid. In fact the models based on the Ginzburg-Landau (GL) theory are strictly applicable only near the transition temperature (T_c). The differences between the various models are relatively small and moreover the subtle differences among them are difficult to detect experimentally.

Since the high T_c superconductors are all of extreme type II. We will limit our discussions to this limit only. It is of importance to realise how the critical current is actually measured. When a transport current is passed through the superconductor a voltage drop (ΔV) appears at a certain value of the current density, denoted as the critical current density (J_c). In the granular superconductor (ΔV) is caused by a voltage drop over the junction between grains and it corresponds to the normal conducting state of the junctions. One the other hand, in a homogeneous type II superconductors a voltage drop is measured due to the motion of magnetic flux lines.

Clem et al [47] have assumed that in granular superconductors the order parameter is depressed by the supercurrent that flows through the sample. It is assumed that the grains lie on a cubic lattice with lattice parameter a_0 and that the junctions are identical . This means that the sample is considered as a single junction. Of course, in reality there

will be a contribution of junctions of varying strength. Still the temperature dependence of J_c will be determined mainly by the type of junctions. The Gibbs free energy relative to the normal state (ΔG) per grain near T_c is given by

$$\Delta G = \left(\frac{H_c^2}{4\pi}\right) V(-f^2 + \frac{1}{2}f^4) + \left(\frac{\hbar}{2e}\right) I_0 f^2(1 - \cos\phi) - \left(\frac{\hbar}{2e}\right) I\phi \qquad (3.1)$$

The first term is the condensation energy of the grains and the second term is the coupling energy between the grains. H_c is the thermodynamic critical field, V is the volume of the grain. ϕ the phase difference over a junction and I_o the maximum spercurrent near T_c. The factor f represents the fraction by which the gap and the order parameter are reduced by the current, i.e.,

$$I = I_0 f^2 \sin\phi \qquad (3.2)$$

Next, (δG) is minimized at constant ϕ and I with respect to f, which gives

$$f^2 = 1 - \epsilon(1 - \cos\phi), \qquad (3.3)$$

where $\epsilon = E_J/2E_S$ is the ratio of the coupling energy between the grains ($E_J = \hbar I_o/2e$) to twice the condensation energy of a grain ($E_S = H_c^2 V/8\pi$)

(a) Granular (S-I-S) superconductors :

If the barrier between the superconducting grains are of an insulating nature, the maximum supercurrent (I_o) is given by the expression of Ambegaokar and Baratoff (AB) [48]. The AB theory gives for a Josephson junction between two identical superconductors.

$$I_o(T) \propto \Delta(T) \tanh \frac{\Delta(T)}{2k_B T}\ , \qquad (3.4)$$

where $\Delta(T)$ is the superconducting gap parameter from the BCS theory. The temperature dependence of I_o according to above equation is shown (dashed curve) in Fig.3*10* The parameter ϵ is written as

$$\epsilon(T) = \epsilon_o \frac{[\Delta(T)/\Delta(0)] \tanh[\Delta(T)/2k_B T]}{[H_c(T)/H_c(0)]^2} \qquad (3.5)$$

substituting the Eqs.(3.4)-(3.5) into Eq.(3.2) gives an expression that can be used to analyze the critical current density.

It was shown [48] that the parameter ϵ is also equal to the ratio $\xi^2(T)/2a_o^2$. When $\epsilon \gg 1$, the condensation energy of a grain is much smaller than the coupling energy and the current-induced gap suppresion is important. In this case one finds the critical current density expression which is the same as obtained in the GL theory. This also implies that the coherence length is larger than the distance between the junctions. Then the order parameter is reduced throughout the sample and close to T_c one has $j_c(t) \propto (1-t)^{3/2}$, where $t = T/T_c$. On the other hand, when $\epsilon \ll 1$, one finds the AB expression and $\xi \ll a_o$. In this case, gap suppression is rather significant. Near T_c one finds

$$j_c \propto (1-t) \tag{3.6}$$

for $\epsilon = 1$ a crossover takes place between the two cases.

Fig.3.10ashows the results of calculations for various values of ϵ_o. Close to T_c the cross-over from one model to the other model can be observed. Strictly speaking the above model for granular SIS- suerpconductors is valid only near T_c.

(b) Granular (S-N-S) superconductors :

In the work by Clem et al [47] it was already recognized that the temperature dependence of I_o given Eq.(3.4), where $I_o(T) \propto \Delta(T) \tanh \frac{\Delta(T)}{2k_BT}$ should be modified when the non-superconducting barriers are for instance, normal metals.

According to BCS theory of superconductivity a superconductor is characterized by the parameter NV where N is the density of states at the Fermi level and V the effective electron-electron interaction. Within the frame work of BCS theory this quantity does not vary spatially. It was pointed out that the density of superconducting electrons cannot change abruptly at the boundary of two super-imposed metals, but only over a distance of the coherence length. Thus in the case of superconductor-normal metal interface (S-N) interface, the BCS theory can no longer be applied.

DeGennes [49] used spatially dependent pair potential ($\Delta(t)$) to describe boundary effects in superconductors ($\Delta(r) = V(r) \times F(r)$; where $F(r)$ is the dependent electron-electron interaction. In a simplified form of this model Clarke [50] gave an expression for J_c of an S-N-S junction. In a superconductor in contact with a normal metal, $F(r)$

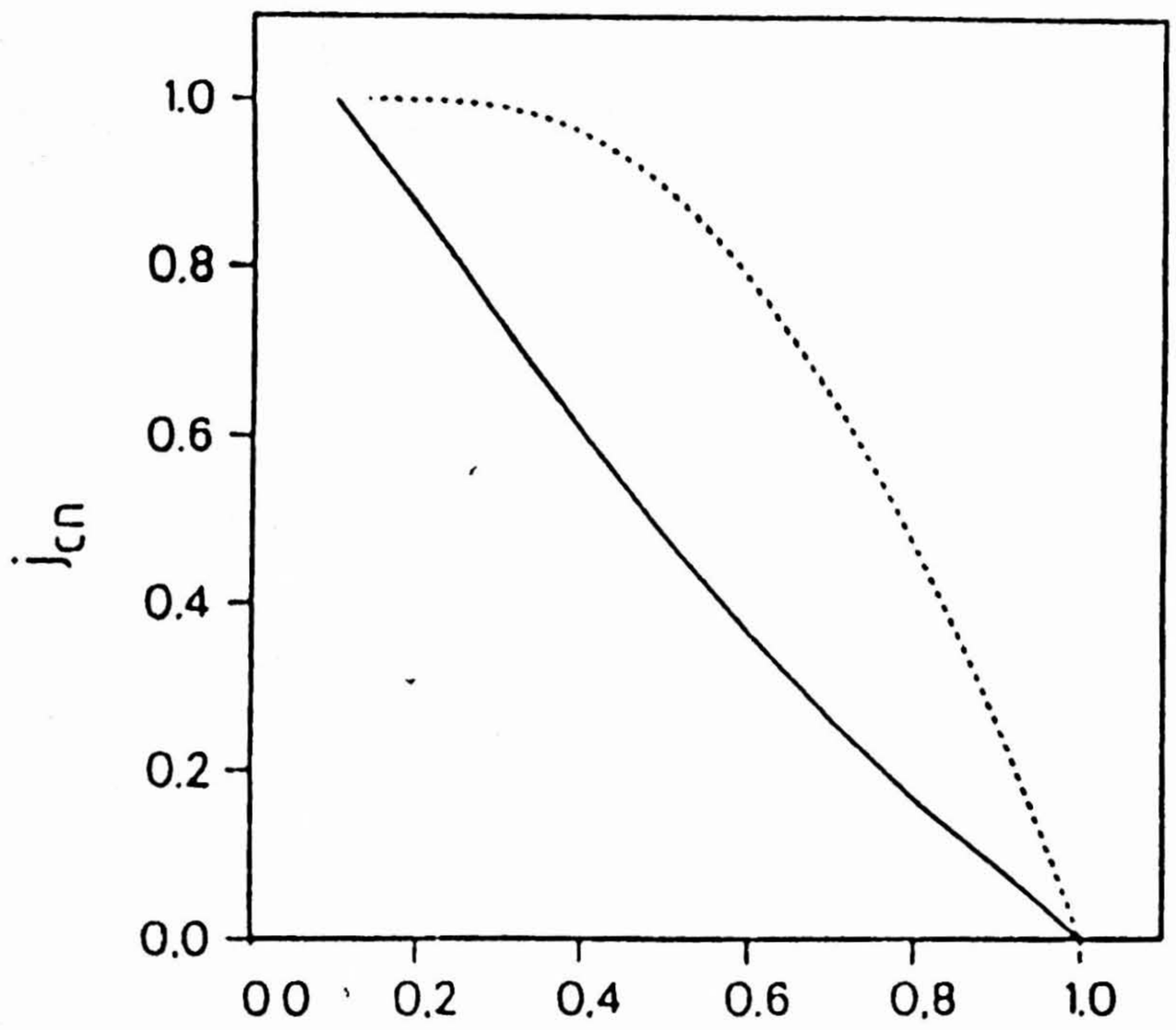

Fig.3.10. Normalized values of the critical current density J_{cn} versus reduced temperature (t) according to the flux motion model (-) and the Ambegaokar Bartof model for SIS JUNCTIONS (----).

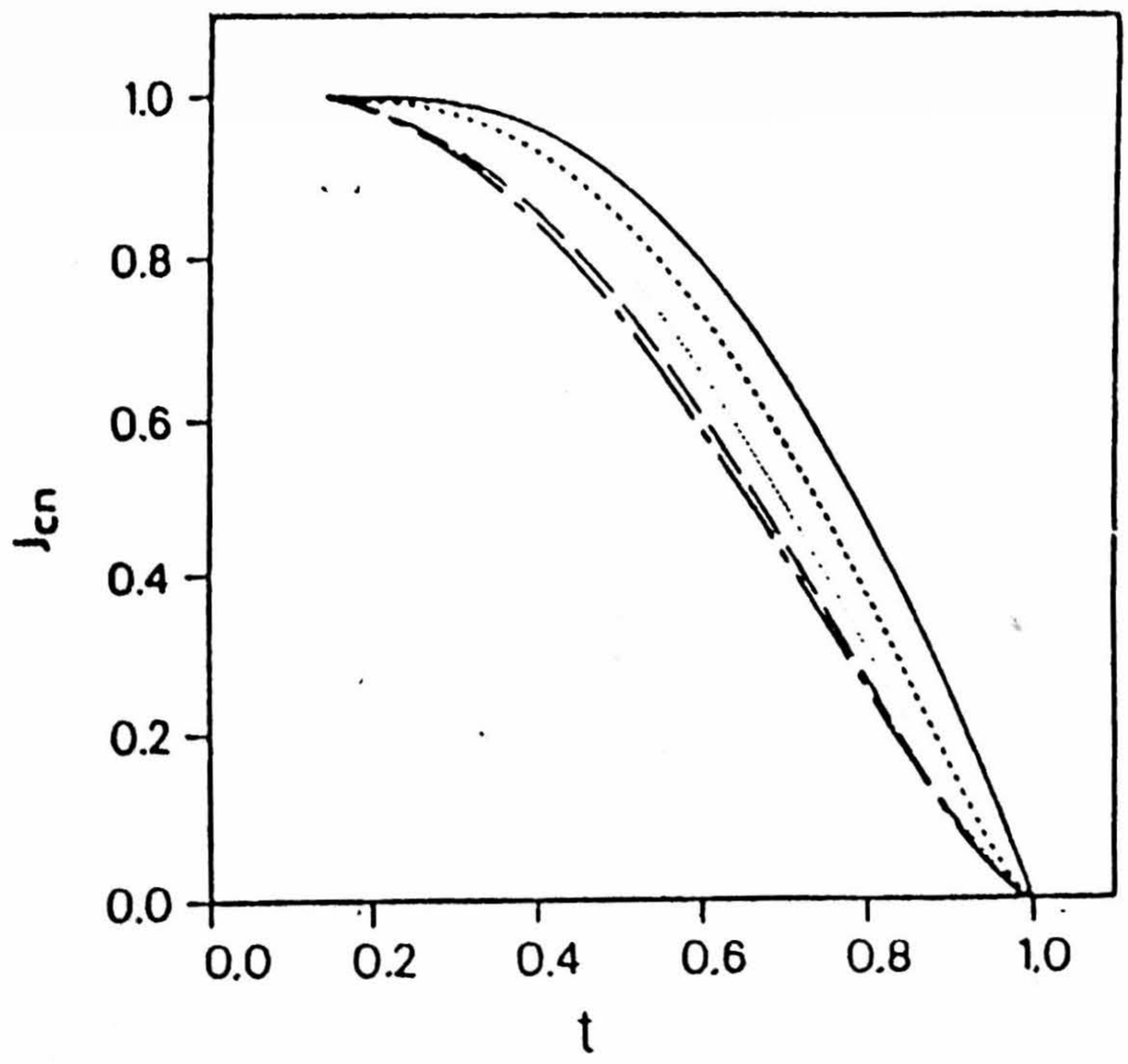

Fig.3.11. (a) Jcn vs t calculated with the model of granular super conductors with STS junctions: $\epsilon_o = 0$ (-), $\epsilon_o = 0.1$ (---), $\epsilon_o = 0.3$ (...) $\epsilon_o = 1$ (-. -. -. -) and $\epsilon_o = 10$ (_. _. _)

is depressed over a distance of the order of the GL coherence length (ξ_{GL}) and in the normal metal the electron pairs penetrate over a distance $\xi_N \simeq \sqrt{h\nu_{FN}l_N/6\pi k_B T}$ or $\xi_N \propto (1/T)$ (V_{FN} is the Fermi velocity in the normal metal and l_N the mean free path). The temperature dependance of the maximum supercurrent is then given by

$$I_o(T) \propto \mid F_o(T) \mid^2 \frac{\xi_N(T)}{\xi_{GL}^2(T)} \exp\left\{\frac{-a}{\xi_N(T)}\right\} , \tag{3.7}$$

where $F_o(T)$ is the bulk value of the superconducting electron density and a is the thickness of the normal metal barrier. For temperature close to T_c we have $\xi_{GL}(t) \propto (1-t)^{-1/2}$ and $F_o(t) = (1-t)^{1/2}$, where $t = T/T_c$ and realizing that $\xi_N(T)$ does not depend on temperature as strongly as the other parameters do, for a proximity effect junction I_o varies as given below [51].

$$I_o \propto (1-t)^2 \exp\left\{-\frac{a}{\xi_N(T)}\right\} . \tag{3.8}$$

Substituting the expression for $\xi_N(T)$ we find

$$I_o(t) \propto (1-t^2) \exp\left\{\frac{-a}{\xi_N(T_c)}\sqrt{t}\right\} . \tag{3.9}$$

This relation can now be used in the expression for the parameter $\epsilon = hI_o/eH_o^2V$ and $I = I_o f^2 \sin\theta$, in the same way as for the granular S.I.S. samples. Although eq.(4) is strictly valid only close to T_c, it will approximately hold at lower temperatures as well [47].

Fig.3.11 shows the calculated curves of J_c for various values of ϵ_a for $a/\xi_N(T_c) = 1$. One sees that the temperature dependence of the critical current does not change much as a function of ϵ_o. Fig.3.12 shows the J_c vs. T. dependence as a function of the barrier width $a/\xi_N(T_c)$ for $\epsilon_o = 0$; where the variations are much more pronounced.

Close to T_c, the temperature of a SNS junction a dependence of J_c is markedly different from the linear temperature dependence of J_c in S.I.S. junctions, and is given as

$$J_c \propto (1-t)^2 \tag{3.10}$$

as near to T_c, the exponential term can be neglected. So here the coupling between the superconductors is through metallic regions via proximity effect. This situation can be

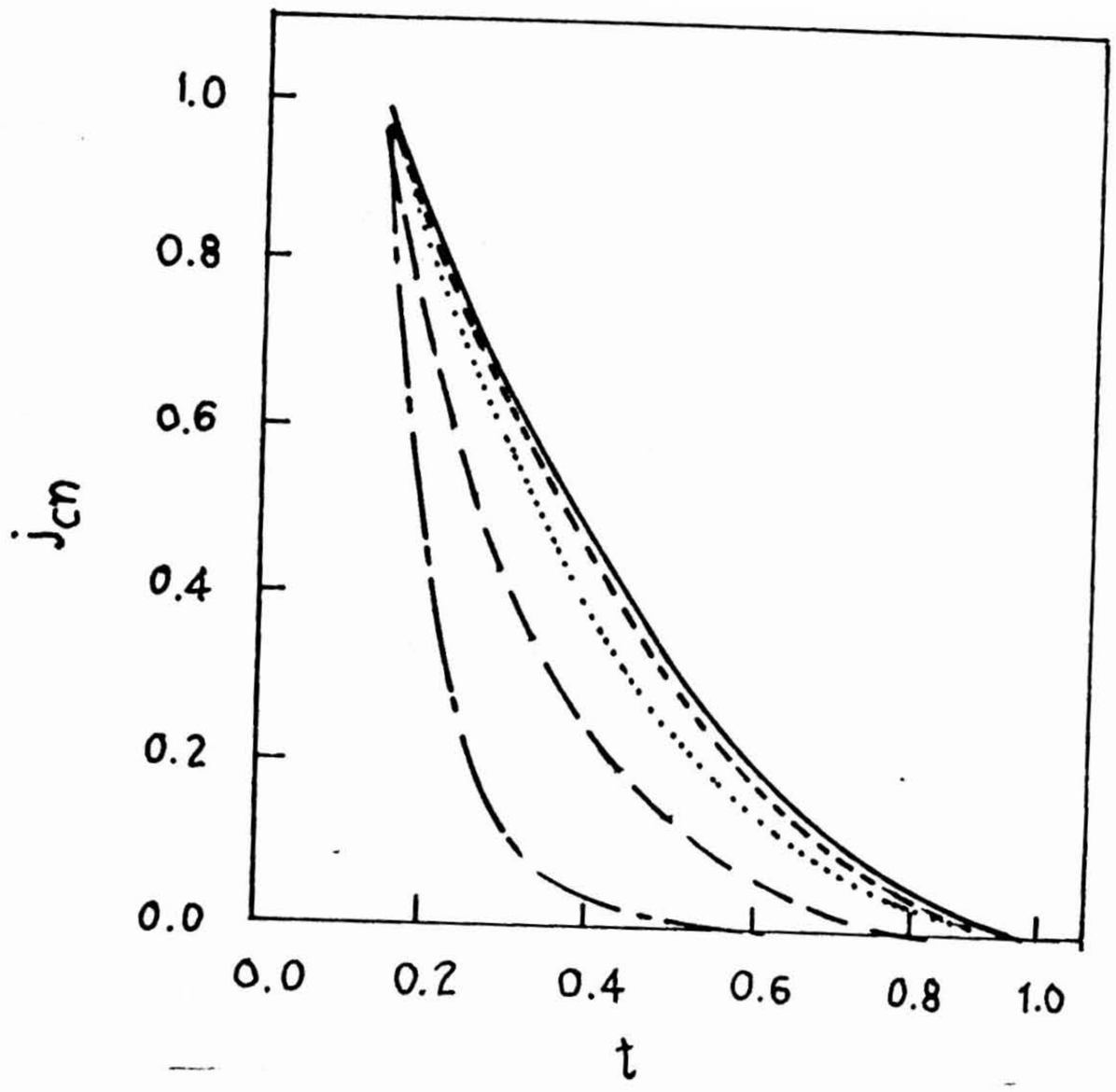

Fig.3.12 (a) J_{cn} vs t calculated with the model of granular super conductors with S-N junctions for ϵ_0=0:$a/\xi_N(T_c)$= 0.1(-), $a/\xi_N(T_c 0)$ 0.3 (---), $A/\xi_n(T_c)$=1 (...) $a/\xi_N(T_c)$=3 (-. -. -.) and $a/\xi/_N(T_c)$=10 (_. _. _)

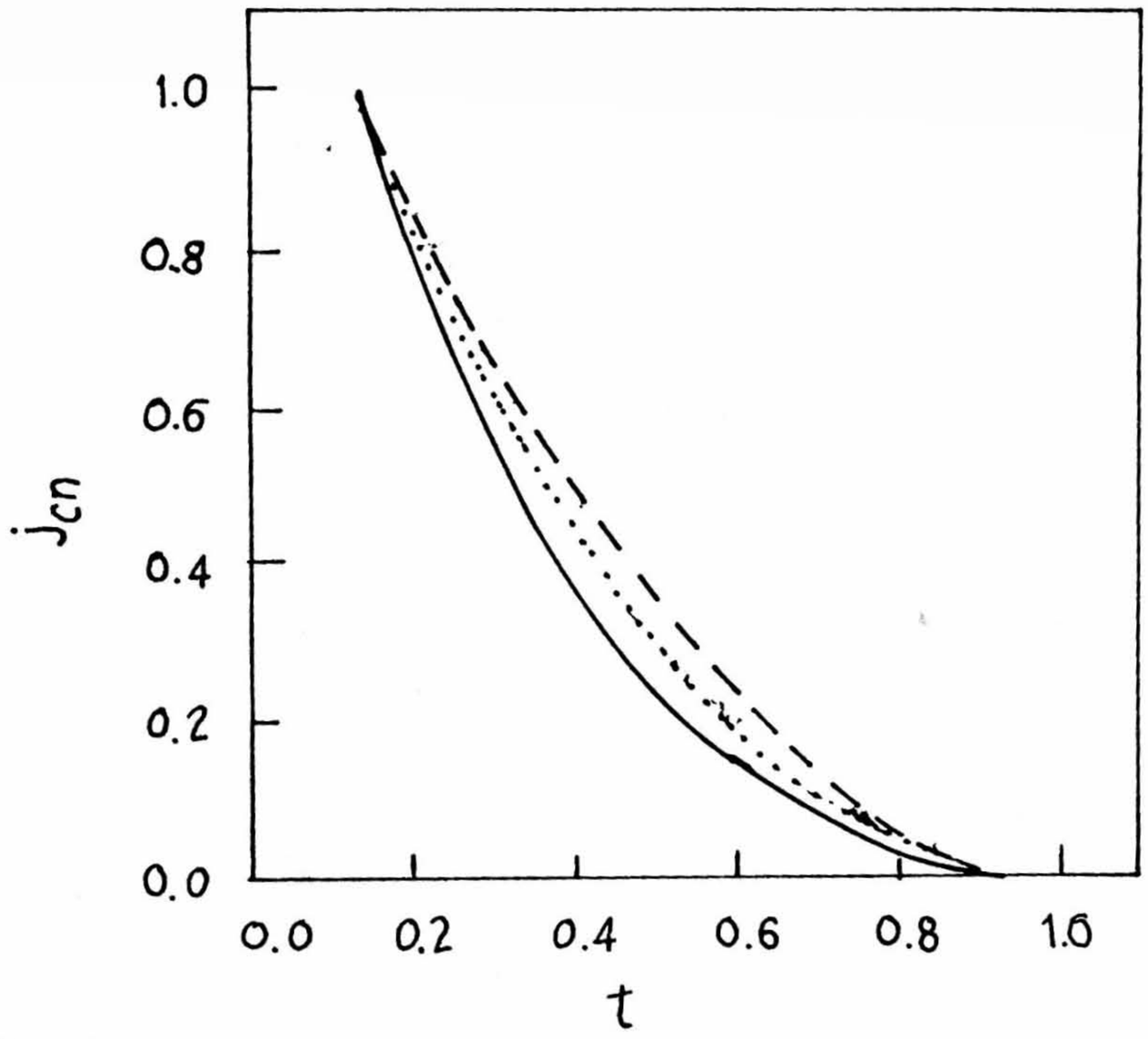

Fig.3.11. (b) (a) J_{cn} vs t calculated with the model of granular super conductors with S-N junctions for $a/\xi_N(T_c)$ = 1, ϵ_0 = 0.1 (-), (...), ϵ_0=3 (...) and ϵ_0=10 (_. _. _.)

expected in HTS fims prepared by sputtering or any other technique when the boundaries between the superconducting grains consists metal like material. The model for such junctions developed by DeGennes and Clarke can be expressed in the present case as

$$J_c(T) \propto (T_c - T)^2 \exp\left\{-\frac{a}{\xi_N(T)}\right\} . \qquad \ldots 3.11.$$

where a is the thickness of the grain boundary domain between the superconducting grains consisting metal like material. xi_N is the grain boundary coherence length. Ignoring the weak temperature dependance of xi_N compared to the the $(T_c - T)^2$ then the above expression be rewritten as

$$\sqrt{J_c} \propto (T_c - T) \qquad \ldots 3.12$$

In Fig.3.13(a,b) are shown the $\sqrt{J_c}$ vs. $T_c - T$ plots for films grown at 650, 700, 750°C. Although there is some scatter in the data all plots show linearity indicating that the SNS models J_c of these films is more appropriate. It is also interesting to note that the plot of the film grown at $750°C$ shows highest slope. This may indicate that the grains in the films grown on MgO at $750°C$ are more aligned than those in the films grown at 600 and 650°C. So far the J_c achieved on MgO using sputtering technique (Rf/DC) is around 10^6 A/cm^2 at 77K. Only with pulsed laser abalation technique it is possible to grow good quality $Y - 123$ film on MgO. In the present case the J_c obtained on MgO is upto state of art.

3.5.5 Y-124 Thin Films

Both RF/DC sputtering methods were used to grow $Y - 124$ films. For the DC sputtering method, a 1" diameter target of $Y - 124$ was prepared from stoichiometric ratios of high purity chemicals (99.99%) of Y_2O_3, $BaCO_3$ and CuO using a chemical coprecipitation method similar to that described in Ref.[52]. This target showed a metallic resistivity behavior and $T_c = 80$ K. For the RF sputtering technique, a 1" diameter target was used and it was prepared through a solution derived untreated complex [52] RF/DC Power (10/25 Watts), and target to substrate distance (5 cm) were kept constant through out all film preparations. Sputtering gas was a mixture of $(Ar + O_2)$ and its

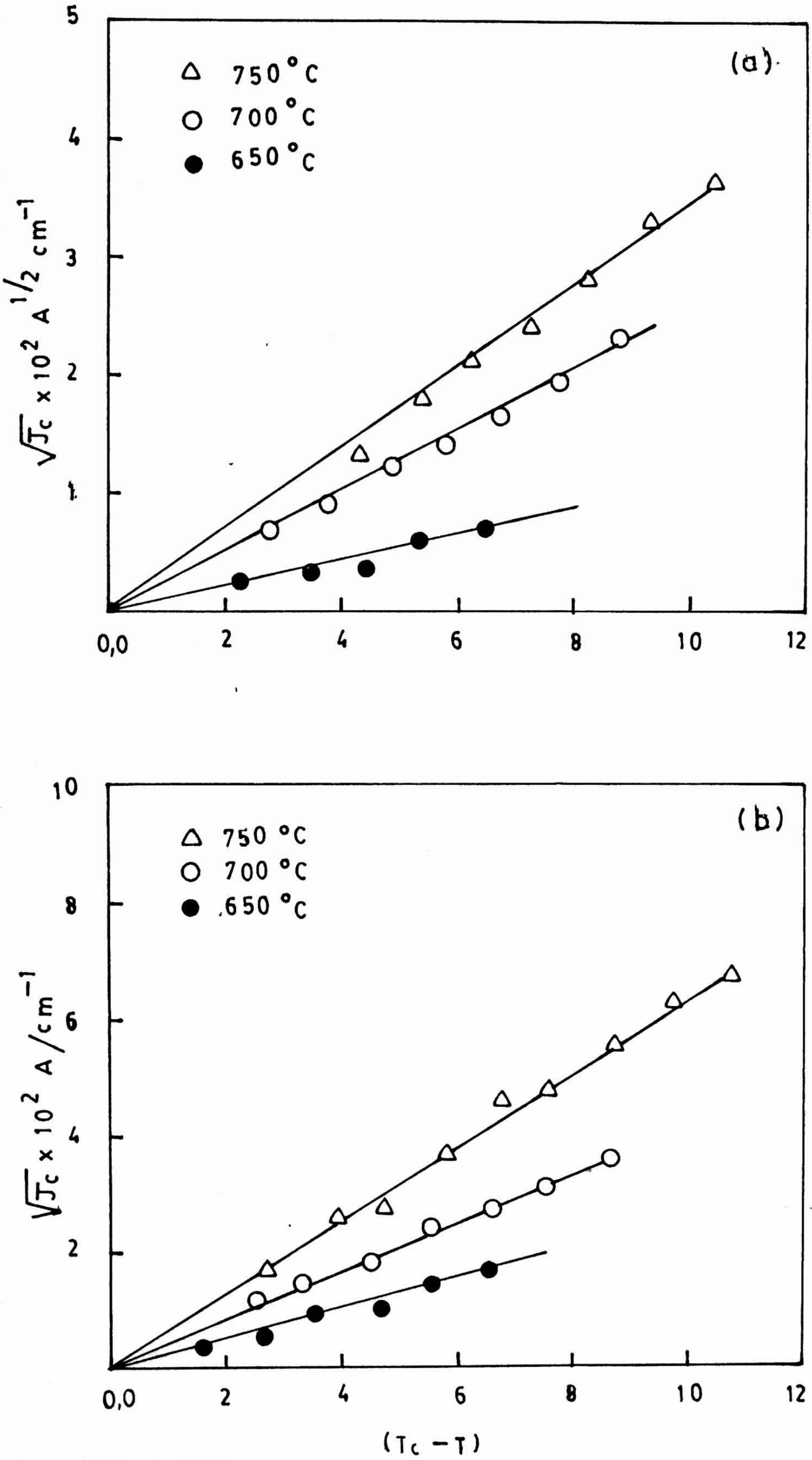

Fig.3.13. $\sqrt{J_c}$ vs (Tc-T) plots for Y-123 films deposited at (a) for D.C. sputtered (b) R.F. sputtered Y-123 films deposited at different substrate temperatures.

pressure was kept between 60 -120 mTorr pressure. A lot of trial and error experimentation determined the optimal sputtering conditions as summarized in Table 3.3 - . The substrates used were single crystals of $SrTiO_3$ < 100 >. Sputtering was done for long enough to get films of 2000 Å(±5%) within 10% accuracy. Each film was black and had a metallic lustre. A set of films were post-annealed at different temperatures between 550 - 750 °C in one atmosphere oxygen pressure for 2 to 24 hrs to remove oxygen deficiency, if any, and also to stabilize the $Y-124$ phase. Structural studies were done by the XRD. Four probe resistivity measurements were made using a computer controlled CTI closed cycle refrigerator working between 12 K - 300 K. Critical current density measurements (J_c) were made on 20 μm wide, 1.5 mm long and 200 nm thick microbridges prepared by a laser patterning technique.

Extensive studies were done to study deposition of $Y-124$ films by RF/DC sputtering and PLD techniques on single crystal $SrTiO_3$ < 100 > substrate. Only a few reproducible results are presented here.

A stoichiometric $Y-124$ target was used for the DC sputtering technique. Films deposited on $SrTiO_3$ substrates, kept at 550°C, and with the sputtering conditions as listed in Table 3.5, resulted in highly c-axis oriented $Y-123$ films as shown in Fig. 3.14(a) by the XRD of such a typical film. A post-annealing of the film at 650°C for 24 hrs in 1 atm oxygen pressure $Y-123$ changed into a single phase $Y-124$ film as shown by its XRD in figure 3.14b. It is surprising that the XRD Fig.3.14b does not show any impurity phase, hence, it is reasonable to assume that CuO must be distributed over grain boundaries in extremely small quantities.

Films deposited by the RF sputtering of an untreated target on $SrTiO_3$ < 100 > substrates, held at 500°C, turned out to have almost single phase $Y-124$ structure with some small $Y-123$ impurity phase. A post annealing of films at 550°C for 12 hrs. at 1 atm. oxygen pressure resulted in single phase $Y-124$ thin films as confirmed by the XRD pattern shown in figure 3.15a. Films deposited at a substrate temperature of 550°C and post annealed at 600°C temperature for 6 hrs, also resulted in films having $Y-124$ phase as the major one with a little $Y-123$ phase as displayed in figure 3.15b. Films deposited at higher substrate temperatures, i.e., 600°C, resulted in mostly $Y-123$ phase. A post annealing of a film at 650°C for 2 hrs did not make much difference in structural changes

Table 3.3
Sputtering Conditions

1.	Target	Y-124
2.	Target Substrate Distance	5 cm.
3.	DC Power	10-25 Watts
4.	RF Power	15-25 Watts
5.	Substrate Temperature	500-700°C
6.	Substrates	$SrTiO_3$ < 100 >

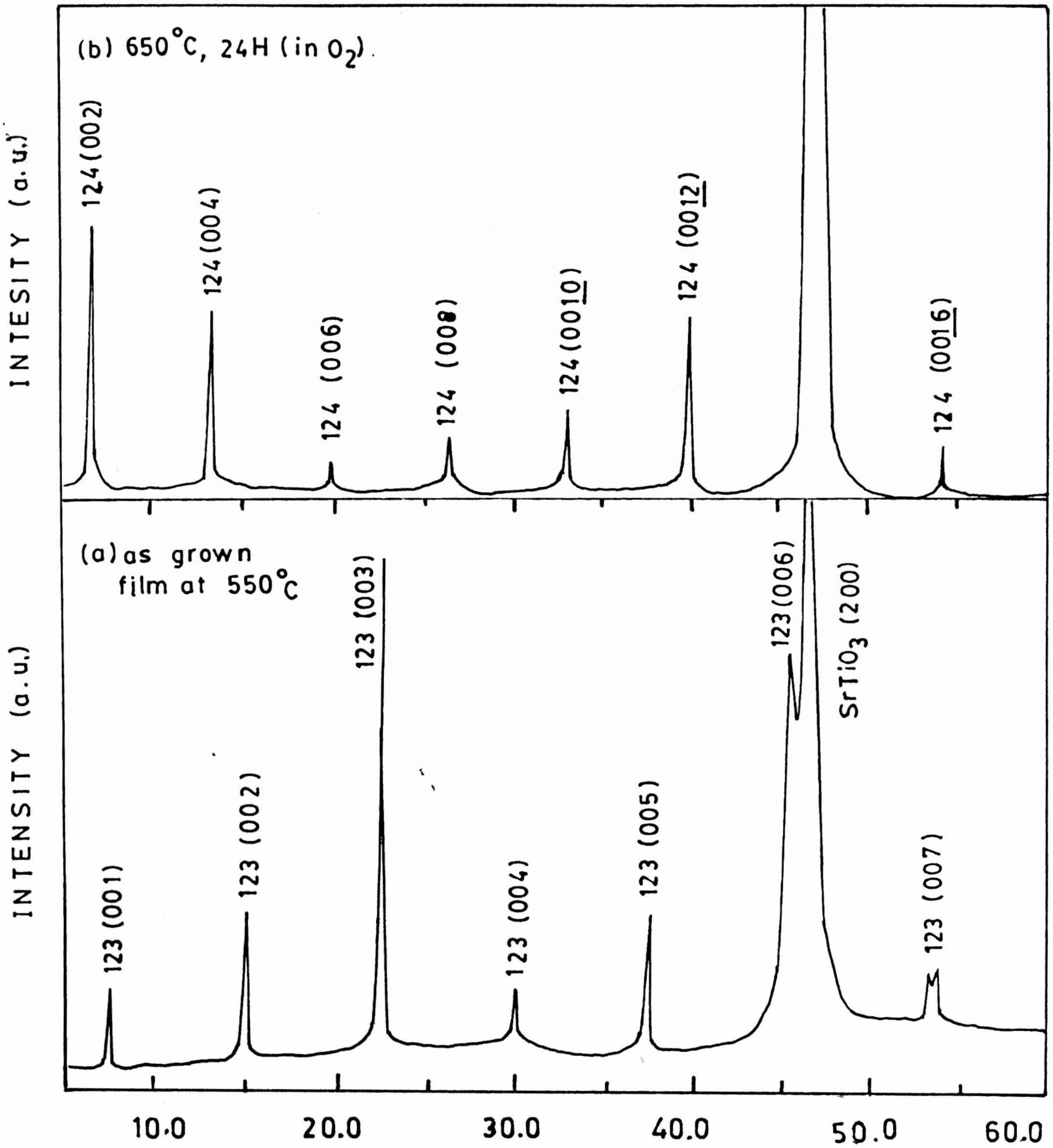

Fig.3.14. . XRD patterns of D.C. sputtered Y-124 thin films (a) as deposited films at 550°C and (b) post annealed film of (a).

Table 3.5
Results of Y-124 Films Deposition on $SrTiO_3$ < 100 > substrates.

Sl. No.	Sputtering gas pressure Ar:O_2			Sub. Temp °C	T_c in K		Post annealed film T_{co}K	XRD Phase
	m Torr	ratio	tech.		T_c	T_{co}		
1.	80	80: 20	(DC)	700	88	86.0	-	123
2.	80	50: 20	(DC)	600	86	82.0	-	123
3.	90	80: 20	(DC)	650	82	78.0	80.0	123+124
4.	90	75:25	(DC)	600	83	76.5	78.0	124
5.	90	60:40	(RF)	550	80	62.0	65.0	123+124
6.	90	50:50	(RF)	550	70	40.0	45.0	123+124
7.	120	80:20	(RF)	600	83	72.0	75.0	123+124
8.	120	80:20	(RF)	600	81	50.0	61.0	123+124
9.	90	80:20	(RF)	550	80	78.0	78.5	124

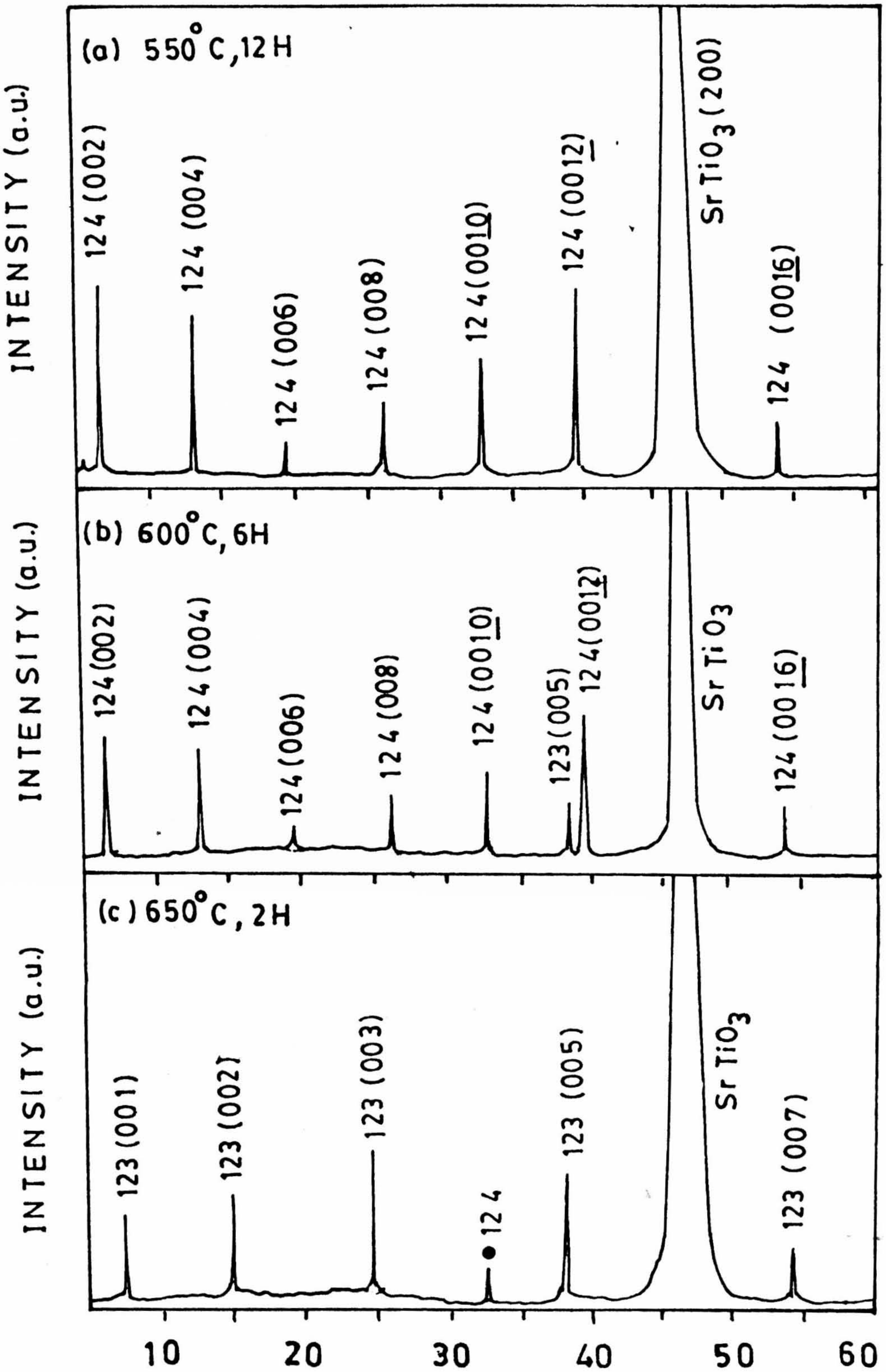

Fig.3.15. XRD patterns of Y-124 films deposited at (a) 500°C and post annealed at 550°C for 12 hrs; (b) deposited at 550°C and post annealed at 600°C for 6 hrs; (c) deposited at 600°C and post annealed at 650°C for 2 hrs.

of the film as shown in figure 3.15c Thus, our studies show that the probability of 124 phase formation is higher than that of $Y-123$ phase if films are sputtered-deposited at relatively low temperatures i.e., between $550-600°C$, on single crystal $SrTiO_3$ < 100 > substrates. Post annealing at different substrate temperatures between $550-750°C$ were tried for different durations (1 hr to 24 hrs). It was noticed that 2-6 hrs post annealing in between $550-650°C$ of the films deposited on $SrTiO_3$ using RF sputtering technique with unreacted chemically co precipitated $Y-124$ target gives single phase $Y-124$ films.

Wada et al [53] have studied the stability of the $Y124$ phase with respect to oxygen partial pressure $P(O_2)$ and temperature by XRD, thermogravimetry and differential thermal analysis. From this $P(O_2)-T$ phase diagram of 124 composition, it is noted that about 75 mTorr oxygen is necessary at $600°C$ for the formation 124 phase. In order to see the effect of oxygen partial pressure for the sputtered 124 films we varied the total pressure of the sputtering gas $(Ar + O_2)$ between 80 mTorr to 120 mTorr. For each pressure of sputtering gas oxygen partial pressure was varied between 10% to 50%. It was observed that when the oxygen partial pressure was above 30%, it enhanced back sputtering and reduced the sputtering yield which resulted in formation of intermediate phases in films. Most of films with almost single 124 phase were grown with the sputtering gas having 3:1 ratio of Ar to O_2 at 90 mTorr. These films although contain major 124 phase, when deposited on $SrTiO_3$ < 100 > substrates held at 500°C - 600°C, a minor 123 phase was always found to be present. Post annealing of these films around $700°C$ in one atm oxygen reduces and eventually removed the minor impurity phase in otherwise single phase $Y-124$ film. From this study it is inferred that the post annealing of films at an appropriate temperature is a must in the case of sputter deposited films to grow almost single phase $Y-124$ structure. Details of deposition conditions for eight films and XRD results are summarized in Table 3.5

(c) T_c and J_c Measurements :

One of among various parameters which can be used to evaluate quality of a superconducting film is its resistive transition to superconductivity. Figure 3.16 shows resistive transition to superconductivity of two films deposited on $SrTiO_3$ substrates by RF and

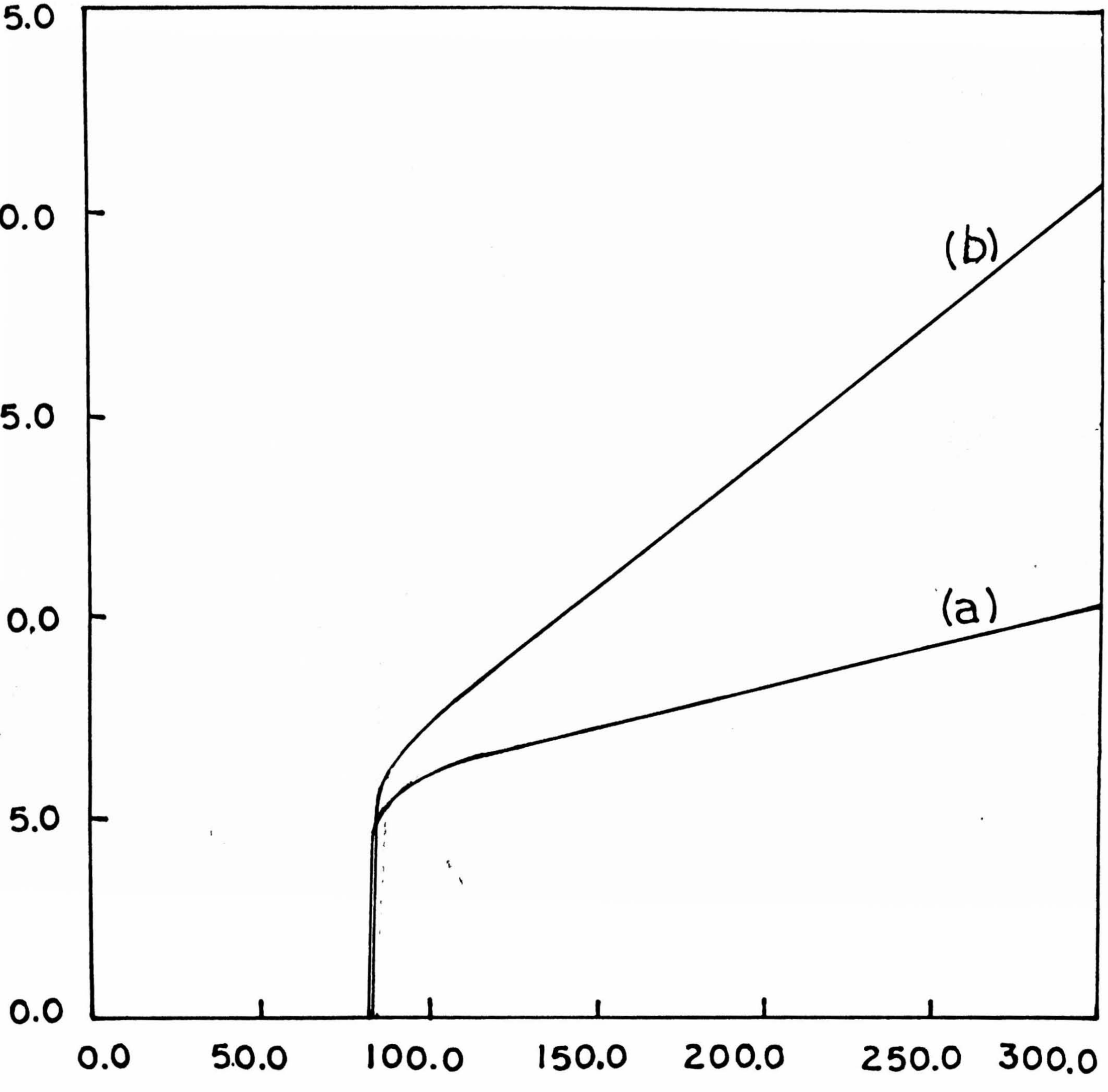

Fig.3.16. R-T plots for (a) R.F. and (b) D.C. sputtered Y-124 films with Tco ≈ 79 and 77K respectively.

DC sputtering technique. Both films show linear temperature dependence of the resistance above T_c. Their room temperature resistances (hence resistivities as all films had similar length, width and film thickness) are different, indicating two films having microstructural differences. *DC* sputtered film showed higher resistivities. However, the transition width in each case was less than 2 K although T_{co} varied slightly from film to film within a few degrees. The highest T_{co} is found to be 79.3 K. Quality of a film, as determined by its critical current, is also found to be reasonably good. A typical measured value of J_c is $1 - 2 \times 10^5 A/cm^2$ at 65 K for the best films (highest T_{co} and smallest room temperature resistivity).

To determine wheter SNS model of J_c is valid for $Y - 124$ films. $\sqrt{J_c}$ vs. $(T_c - T)$ is plotted for *RF* sputtered and *DC* sputtered $Y - 124$ thin films. It shows linear behavior nearer to T_c which indicates SNS type microstructure in Fig. 3.17 The *DC* sputtered films have low slope when compared with *RF* sputtered films. It indicates *DC* sputtered $Y - 124$ films have grain boundaries having less metallic nature when compared with that of *RF* sputtered films. The suppression of T_c in $Y - 124$ is due to the double chains of $Cu - O$ bonds and due to the excess oxygen content. Finally, our results indicate that *RF* sputter deposited films tend to have better superconducting properties when compared with those of *DC* sputter deposited $Y - 124$ thin films with respect to microstructure T_c and J_c properties.

3.6 Conclusions

A one inch sputtering system with transverse magnetron geometry was fabricated in ordered to minimize the back sputtering effects in on axis sputtering of oxide materials. The system has served its purpose and back sputtering is minimized. HTS oxide superconducting $Y - 123$ and $Y - 124$ films were successfully grown using the system by *RF* and *DC* methods. The results were summarized as follows.

(a) $Y - 123$ *thin films :*

1. **Back sputtering was minimized and stoichiometry of the films was achieved by**

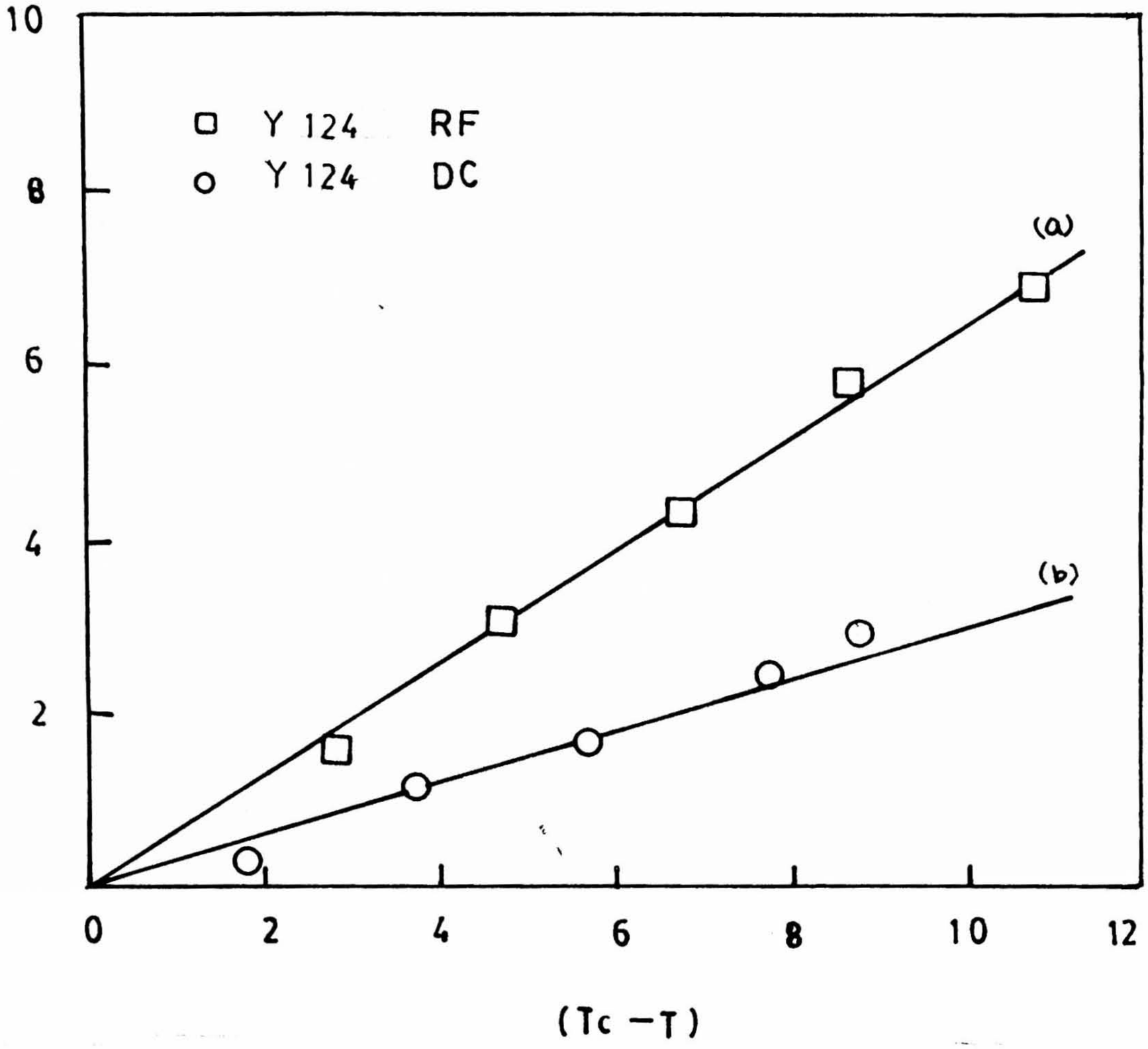

Fig.3.17. . $\sqrt{J_c}$ vs (T_c-T) plots for Y-124 films prepared by (a) RF; (b) D.C.

using optimized deposition conditions.

2. The optimized conditions for $Y-123$ thin film deposition in the case of DC as well as RF sputtering methods are 90 mTorr, $Ar + O_2$ (4:1), 5 cm Target to substrate distance. 10 watts DC Power was used for depositing all films prepared by DC sputtering and RF power 25 Watts.

3. $Y-123$ films deposited below $700°C$ have shown relatively inferior quality superconducting properties when compared with the films deposited at $750°C$ on $MgO < 100 >$ substrates in both RF as well as DC sputtering.

4. The best T_c and J_c realized in RF sputtered $Y-123$ films are $6 \times 10^5 A/cm^2$ for the films deposited at $750°C$ on $MgO < 100 >$.

5. From $(T_c - T)$ vs. $\sqrt{J_c}$ plots it is concluded that RF sputtered films show higher slope when compared with that of the DC sputter deposited films. Hence it is understood that RF sputtered $Y-123$ films show better crystalline and microstructure and superconducting properties when compared with that of DC sputtered films using the same magnetron geometry.

6. Through a systematic investigation of a series of $Y-123$ films deposited at three substrate temperatures it is concluded that there is an intrinsic relationship between the microstructure, T_c and J_c which are strongly dependent on the growth temperature.

(b) $Y-124$ Thin Films :

It has been realized that the phase formation of $Y-124$ thin films depends on deposition technique, substrate temperature and oxygen partial pressures and therefore, one has to optimize the conditions to deposit single phase $Y-124$ films either by RF or DC sputtering techniques.

1. Even though, films deposited at $500°C$ substrate temperature in sputtering are having 123 phase initially, they get completely transformed to $Y-124$ phase after post annealing at $650-700°C$ for 2 - 12 hrs depending on deposition technique.

2. The transport J_c for theY-124 film deposited by RF sputtering is $2x10^5$ A/cm^2 at 65 K on $SrTiO_3$ (100) substrate. DC sputtered films have shown relatively inferior quality films with respect to T_c as well as J_c.

3. It is another insitu process for depositing Y-124 films. Moreover, for the first time J_c measurements are reported in thin films prepared using sputtering technique. These films are much superior in quality than films reported by earlier workers.

2. The transport J_c for the $Y-124$ film deposited by RF sputtering is $2 \times 10^5 A/cm^2$ at 65 K on $SrTiO_3 < 100 >$ substrate. DC sputtered films have shown relatively inferior quality films with respect to T_c as well as J_c.

References

[1] P. Choudhary, R.H. Kock, R.B. Laibowitz, T.R. McGuire and R.J. Gaubino Phys. Rev. Lett. **58** (1987) 2684.

[2] Y. Enomoto, T. Mara Kami, M. Suziki and K. Moriwaki Jpn. J. Appl. Phys. **26**(1987)*L*1248.

[3] D. Dijkkamp, T. Venkatesan, X.D. Wu, S.A. Shaheen, N. Jisrawi, Y.M. Min Lee, W.L. McLean and M. Croft Appl.Phys.Lett. **51** (1987) 619.

[4] R.Bormann and J. Nolting Appl.Phys.Lett. **54** (1989) 2148.

[5] R.E. Somekh, M.G. Blamire, Z.H. Barber, K. Butler, J.H. James, G.W. Morris, E.J. Tomlinson, A.P. Schwarzenberger, W.M. Stobbs, J.F. Evetts Nature **B26** (1987) 857.

[6] M.Naito Hommond R H Oh B, Hahn M R, Hsu J W P, Rosenthal P, Marshall A F, Beasley M R, Geballe T H and Kaptalnik A J. Mat. Sci. **2** (1987) 713.

[7] N.Terada, Ihara H, Jo M, Hirabayashi M, Kimura Y, Matsutani K, Hirata K, Ohno E, Sugise R and Kawashima F, Japn. J. Appl. Phys **27** (1988) L639.

[8] X.X. Xi, H.C. Li, J. Geerk , G.Linker, O.Meyer, B.Obst, F. Ratzel, R. Smithy, F.Wechsenfelder, Physica C **133** (1989) 794.

[9] C.B. Eom, J.Z Sun, K. Yamamoto, A. F. Marshall, K. E. Luther, T. H. Geballe and S.S. Laderman, Appl. Phys. Lett, **55** (1989) 595.

10 J. J. Hanak and J. P. Pellicane, J. Vac. Sci. Technol. **13** (1976) 406.

[11] H. Adachi, K. Hirochi, K. Sestune, M. Kitabatake and K. Waser, Appl Phys. Lett. **57** (1988) 2263.

[12] Y. Hoshi, M. Naoe and S. Yamanika, Japn. J. Appl. Phys. **16** (1977) 1715.

[13] U. Poppe, J. Schubert, R R Hrons, W. Evers, C.H. Freiburg, W. W. Reichert, K. Schmidth , W. Sybertz and K. Urban, Sol. State. Comm. **66** (1988) 661.

[14] H. C. Li, G. Linker, F. Ratzel, R. Smithey, J. Geerk, Appl. Phys. Lett. **52** (1989) 1098.

[15] X. Xi, J. Geerk, G. Linker, Q. Li and O. Meyer, Appl Phys. Lett. **54** (1989) 2367.

[16] P. Kuppuswamy and V. S. Raghunathan, Matals Materials and Process **3** (1991) 147.

[17] R.S. Rastogi, V. D.Vankar and K. L. Chopra, Rev. Sci. Instruments **58** (1987) 1505.

[18] S. Srinivas, DAE SSP symposium 1990 Conf. proceedings vol. **56c**. page 454.

[19] H.W Zandbergen, R. Gronsky, K. Wang and G. Thomas, Nature, **331** (1988) 506.

[20] J. Karpanski, E. Kalidas, E. Jielk, S. Rusieki and B. Butcher, Nature **341** (1989) 1.

[21] T. Miyatake, S. Gotoh, N. Koshizuka and S. Tanaka, Nature, **341** (1989) 41.

[22] R. J. Kawa, J. J. Krajewski, W. F. Peck, Jr. B. Batlogg, and L. W. Rupp, Jr. R.M. Fleming, W. P. James and P.Marsh, Nature **338** (1989) 328.

[23] A. F. Marshall, R. W. Barton K. Char, A. Kapitulnik, B.Oh, R. H. Hammond and S.S. ladermann Phys. Rev. B **37** (1988) 207.

[24] K. Char, Mark Lee, R.W. Bartan, A.F. Marshall, R. H. Hammond, M. K. Beasley, T. H. Geballe, A. Kapitulnik and S.S.Ladermann : Phys. Rev. B **38** (1988) 5031.

[25] M. L. Mandich, A. M. Desantolo, R. M. Sunshine, J. Kwo, M. Hong, T. Boone, T.Y. Komehaehani and L. Martinez - Miranda, Phys. Rev. **38** (1988) 5031.

[26] R. C. Budhani, M.W. ruckman, R. L. Sabatani, M. Suenaga and D. O. Welch Solid St. Comm. **7** (1990) 337.

[33] P. Guptasarma, V.R. Palkar, M.S. Multani R.Vijayaraghavan, S.T.Bhindre and S.B. Ogale : Solid State Communications **79** (1991) 851.

[28] D.D. Barkely, D. H. Kim, B. R. Johnson and A. M. Goldman, Appl. Phys. Lett. **53** (1988) 708.

[29] J. Kwo, M. Hong, R.M. Fleming, A. F Heburd, , M.L.Mandich, A.M. Desentolo, B. A davidosn, P. Marsh and N.D hobbins, Appl. Phys. Lett. **52** (1995) 1625.

[30] K. Kuroda, K. Kojima, M. Tamoku, K. Yokoyama and K. Hamanka, Jpn. J. Appl. Phys. **29** (1990) L1439.

[31] Y. Terashima, M. Saga, T. Mima, J. J. Appl. Phys. **30** (1991) L816.

[32] H. Hayashi, Y. Yamada, T. Sugimoto, Y. Shiohara and S. Tanaka, Jpn. J. Appl. Phys. **30** (1991) L725.

[33] Y.Yoshida, J.g.Wen, . Watanabe, W. Ito, N. Koshizuka and T. Morshita, Appl. Supercond. **1** (1993) 333.

[34] R.H. Hammond and R. Bormann, Physica C **162-164** (1989) 703.

[35] V. Matijaenic, P. Rosenthal, K. Shinohara, A. F. Marshall, R.H. Hammond and M. Bealey, J. Mat. Res. **6** (1991) 682.

[36] J. A. Thornton and A. S. Penfold, In thin film processes Ed J. L. Vossen and W. Kern, Academic press, New York, (1978)

[37] J. A. Thornton, J. Vac. Sci. Technol. **15** (1978) 171.

[38] J. A. Thornton, Mat. Finish, **77** (1979) 45.

[39] J. A. Thornton, Thin Solid Films **80** (1981) 1.

[40] J.A. Thornton, J. Tabock and D. W. Hoffman, Thin Solid Films **64** (1979) 111.

[41] R. K. Waits, J. Vac. Sci. Technol. **15** (1978) 179.

[42] R. K. Waits in Thin film Processes, Ed J. L. Vossen and W. Kern **131** (1978).

[43] S. B. Alneida Vacuum. **37** (1989) 717.

[44] Y. Tokura, J. B. Torrance, T. C. Huang and A. I. Nazzal, Phys. Rev B **38** (1988) 7156.

[45] P. F. Miceli, J.M. Tarascon, L. H. Greene, P.Barbour, F.J. Rotella and J. D. Jorgensen, Phys. Rev. B **37** (1988) 5932.

[46] T. M. Shawl, D. Dinos, P. E. Batson, A.G. Schrott, D.R. Clarke and P.R. Duncombe, J. Mat. Res. **5** (1990) 1176.

[47] J. R. Clem, B. Bumble, S. I. Raider, W.J. Gallagher and Y. C. Shih, Phys. Rev. B **35** (1987) 6637.

[48] V.Ambegaokar and A. Baratoff Phys. Rev. Lett. 10 (1963) 486 ibid 11 (1963) 104 (E)

[49] P.G. De Gennes, Res. Mod. Phys. **36** (1964) 225.

[50] J. Clarke, Proc. R. Soci. London A **308** (1969) 442.

[51] W.Y. Shih, C. Ebner and D. Stroud, Phys. Rev. B **30** (1984) 134.

[52] P. Guptasarma, V.R. Palkar and M. S. Multani : Solid state communications 77 (1991) 769.

[53] T. Wada, N. Suzuki, A. Ichinose, Y. Yaegashi and S. Tanaka, Appl. Phys. Lett. **57** (1990) 81.

Chapter 4

YSZ and STO Buffer Layers

4.1 Introduction

In the previous chapter $YBa_2Cu_3O_{7-x}(Y-123)$ thin films have been prepared by using magnetron sputtering technique directly on single crystal MgO substrates. The effect of the growth on the substrate temperature on the crystallinity and superconductivity have been presented. For many electronic applications it may be necessary to deposit film on Si or Sapphire. However, earlier work has shown that one is unable to get good HTS films on Si/Sapphire substrates directly. Hence one needs to have buffer layers in between HTS film and Si/Sapphire substrate to obtain a good quality film. Therefore, a study of buffer layer of YSZ and STO on Si/sapphire substrates was taken up. The present chapter deals with the fabrication of epitaxial buffer layers for depositing high quality $Y-123$ films on Si and Sapphire substrates using the RF magnetron sputtering technique.

$Y-123$ thin films have been epitaxially grown on oxide single crystal substrates such as $SrTiO_3$, MgO and $LaAlO_3$ with superior quality superconducting properties ($T_c \simeq= 90$ K and J_c exceeding $10^6 A/cm^2$ at 77 K) [1-3]. However, these oxide substrates

are not suitable for device applications because they are relatively expensive and the substrate size is restricted. The integration of high temperature superconductor (HTS) with the conventional semiconductor-based technology would have important consequences for micro-electronics with the promise of high performance hybrid circuits incorporating the best of what superconductors and semiconductors have to offer as well as possibilities of novel devices. Adding to the well known advantages of semiconductors, passive superconductive elements such as transmission lines offer the possibility of low loss, dispersionless signal transmission active devices. Josephson junctions make it possible to achieve very fast switching speeds with limited generation of heat. HTS superconducting films on sapphire (Al_2O_3) are found to be useful in high Q resonators, delay lines and infrared bolometers [3,4]. Hence, investigation of HTS thin films on Si and Sapphire single crystal substrates are of great interest and importance due to their possible wide technological applications.

Difficulties in fabricating high quality $Y-123$ thin films directly on substrates like Si or sapphire arise from three main factors (1) intermixing and chemical reaction at the $Y-123$/substrate interface, (2) thermal expansion mismatch between the $Y-123$ and the substrate and (3) the mismatch in the lattice constants of the two materials [5-11].

The above three factors limit quality of films that can be obtained directly on Si and sapphire substrate. One possible solution is the use of an intermediate buffer layer between the Si/Sapphire and the $Y-123$ film. The desired properties of such a buffer/barrier layer are,

1. It must be an effective barrier against diffusion of Si/Sapphire into the film and must itself be chemically stable at the buffer/$Y-123$ interface.

2. Any stresses arising from thermal cycling should be absorbed in the buffer layer or the buffer/substrate interface rather than at the $Y-123$/buffer interface.

3. The buffer layer should be lattice matched as nearly as possibly for both Si/Sapphire and $Y-123$ such that the $Y-123$ thin film is orientationally locked to a given crystalline direction.

These are very stringent requirements on intermediate layers to have such a combination of properties, but not impossible to achieve with proper selection of material and

depositing conditions. In the present work these requirements have been nearly achieved for YSZ buffer layers.

4.1.1 Buffer Layers

A brief introduction about Yittria Stabilized Zirconia (YSZ) and $SrTiO_3$ (STO) buffer layers which were chosen for the present study is given below.

(a) Yittria Stabilized Zirconia (YSZ) buffer layers :

The most suitable choice and promising buffer layer is of yittria stabilized zirconia (YSZ) for the growth of $Y-123$ thin films on Si and sapphire substrates. When Yittria (Y_20_3) is substituted in ZrO_2, then zirconia stabilizes to the cubic structure. Hence, it is known as Yittria stabilized zirconia or YSZ. Not only the structure but also the dielectric properties change drastically with Yittria concentration as shown below.

Mole % of Y_2O_3	Structure	Dielectric constant	Dielectric loss
0	Monoclinic	17.9	0.0007
1 – 2%	Tetragonal	34.5	0.0009
2.2%	Cubic+Tetragonal	32	0.0012
9% -15%	Cubic	27.2	0.0047

YSZ can be grown epitaxially on Si or sapphire substrates inspite of a -6% lattice mismatch with them. Moreover, $Y-123$ films also can grow with c-axis orientation even though a +6% lattice mismatch exists between YSZ and $Y-123$ film [9,10].

Lee et al are among first few to report work on YSZ buffer layers on Si using RF diode sputtering [11]. As deposited films were found to be polycrystalline with microvoids between the grains. Annealing of these films at higher temperatures ($800-1100°C$) eliminated the microvoids and the grain size became larger. $Y-123$ fim deposited on such a buffer layer was not found to be of good quality ($T_c \approx 40$ K and $\Delta T = 50$ K,

where ΔT is the transition width). Fork et al have reported growth of the YSZ cubic phase on Si and sapphire heated to 780 to 800°C using the PLD technique [12]. Schmidt et al were successful in growing highly textured $< hoo >$ YSZ films on $< 1\bar{1}02 >$ sapphire substrate by the planar RF magnetron sputtering. DC sputtered $Y-123$ films grown on this buffer layer registered the superconducting onset temperature of 90 K [13,14]. A number of other workers have repeated similar results on YSZ buffer layers.

(b) $SrTiO_3$:

$SrTiO_3$ is the first substrate which yielded high T_c and J_c for $Y-123$ films directly deposited on it due to its lattice and thermal expansion coefficient match with $Y-123$. Therefore, $SrTiO_3$ as a buffer layer should be considered ideal for deposition of $Y-123$ films. There are a few reports on STO buffer layer deposition on Si or sapphire substrates [15-17]. Char et al have reported the properties of $Y-123$ thin films deposited on STO buffer layer on sapphire substrates. Their $Y-123$ films deposited on Si with STO as buffer layers yielded a very high J_c ($4.5 \times 10^6 A/cm^2$ at $77K$) and microwave surface resistance R_s of $65\mu\Omega$ at 10 K [15]. Jeffrey et al have reported on the growth of high quality $Y-123$ film on MgO (100) with a STO buffer layer by the PLD method [16] with reproducible superconducting properties.

A brief review on the initial work done on depositing $Y-123$ thin films on Si and Sapphire substrates with and without buffer layers is given below.

4.1.2 Y-123 Thin Films on Si Substrates

Sputter deposited $Y-123$ thin films with T_c of about 10 K [18], 64 K [19], 76 K [20] and 84 K [21] directly on Si have been reported earlier. Plasma assisted laser deposition resulted in $Y-123$ films on Si substrate with 45 K [22], 63 K [23], 67 K [24], 70 K [25] and 78 K [26]. HTS films obtained by coevaporation method exhibited T_c of 81 K [27] and 84 K [28].

Schieb et al [29] have done insitu X-ray diffraction to study the crystallization and

film-substrate reaction of amorphous $Y-123$ thin films on Si with and without buffer layers. They observed that above $700°C$, Ba diffuses into Si substrates and forms $BaSiO_4$ and also initiates the formation of $Cu_2Y_2O_5$ and CuO in the barium depleted thin films. Similar observations were reported by Harada and coworkers using Auger electron spectroscopic depth profile studies [30].

There are reports of HTS films deposited on buffer layers of metals such as as silver, gold and niobium on Si substrates. These buffer layers can be easily formed on silicon or oxidized silicon, but HTS films deposited on them are found to be a polycrystalline. These films show low T_c and there has been some success in producing good quality HTS films with oxide buffer layers such as that of ZrO_2, Yittria Stabilized Zirconia (YSZ) and Y_20_3 on Si.

Initially using a silicon nitride buffer layer on Si $Y-123$ films yielded 46 K T_c [29]. Bouteloup et al have reported a T_c of 70 K with silicon nitride buffer layer [31]. Migliuolo et al have first reported the usage of Yittria stabilized Zirconia buffer layers and achieved a T_c of 70 K by sputtering [32]. By sequential evaporation of a Silver buffer layer [33], by laser ablation on to silicon with AlN buffer layer [34] and with a MgO buffer layer [22] a T_c of 70 K have been reported. Ma et al have reported T_c of 79 K which is above 77 K using a silver buffer layer [35]. 80 K T_c was reported using a Zirconia buffer layer [36]. By using several physical vapor deposition techniques T_cs ranging from 82-88 K have been reported [37-39]. However, J_c is observed to be very low due to the polycrystallinity of the buffer layer. Highest J_c reported on such buffer layers is $5 \times 10^5 A/cm^2$ at 10 K [39]. The next advancement was to prepare on epitaxial buffer layer in order to grow an epitaxial HTS film on it which was expected to show better superconducting properties.

Epitaxial buffer layers like Yittria Stabilized Zirconia have been grown successfully on silicon by various techniques. $Y-123$ films deposited on epitaxial YSZ buffer layer show T_c of 62 K to 86 K and values of J_c vary from 10^4 to $10^6 A/cm^2$ at 77 K [39-42], which is two orders of magnitude better than the J_c obtained on polycrystalline buffer layers. Moreover, it has been well established that insitu deposition and thickness of the buffer layer and thickness of the $Y-123$ thin film play important role in obtaining high T_c and J_c irrespective of the technique [42].

Other buffer layers such as $CoSi_2$, RuO_2 and CeO_2 have also been tried [43-45].

Double epitaxial buffers have been tried and the first successful deposition of $Y-123$ films on double epitaxial buffer layer of $MgAl_2O_4$ and $BaTiO_3$ has been reported with T_c between 70-86 K and J_c about $6 \times 10^4 A/cm^2$ at 77 K [46,47]. $Y-123$ films deposited on double epitaxial layer combination of YSZ and Y_2O_3 resulted in a T_c between 82 -84 K and J_c of $10^4 - 10^6 A/cm^2$ at 77 K and reported by H. Myoren et al [38]. However, a trilayer combination of YSZ/Y_20_3/YSZ showed a very high J_c of $10^6 A/cm^2$ at 66K [48].

4.1.3 Y-123 Films on Sapphire Substrates

At present it seems that the most immediate applications of HTS material is in the area of passive microwave devices such as resonators, filters, delay lines etc [3,49]. One, therefore, has to chose a substrate for HTS films suitable for such applications. Sapphire has low dielectric constant ($\in' \approx 6$) and dielectric loss tangent ($\tan\delta < 10^{-4}$), as compared to that of other commonly used substrates $LaAlO_3$ and YSZ. Hence, sapphire is the most suitable substrate material for the growth of $Y-123$ films for microwave device applications. Moreover, High Debye temperature, high thermal conductivity, low microwave loss, high mechanical strength and easy availability (commercially cheap) of thin (25μm) sapphire substrates make these substrates popular for microwave device applications. However, it has a large lattice mismatch ($\approx 13\%$) with $Y-123$. Besides it has been found that aluminium diffuses into $Y-123$ lattice from the substrate during the film growth process at elevated temperatures ($750-800°C$), which is detrimental to T_c as well as J_c of $Y-123$ film, hence, a direct deposition of $Y-123$ films on sapphire substrates is not useful.

The very first report of a direct deposition of $Y-123$ films with $T_c = 40$ K on sapphire using Nb buffer layer was by Katoh et al [50]. Other buffer layers like Pt, MgO, CeO_2, YSZ, $SrTiO_3$ have been tried by many researchers. Although considerable amount of work has been done on the growth of $Y-123$ films on YSZ [51-54] and other buffer layers [5,6] on sapphire substrates the critical current densities obtained so far have not been very high ($1-2 \times 10^6$ power A/cm^2 at 77 K) as compared to those realized on LAO and STO substrates ($6-10 \times 10^6 A/cm^2$ at 77 K) [54,55]. R. Pinto and his coworkers have reported the growth of Ag doped $Y-123$ films with superior quality ($T_c = 90$ K

and $J_c \approx 1 \times 10^6 A/cm^2$) directly on Sapphire with out any buffer layer [56].

4.1.4 Scope of the Present Work

Even though considerable amount of work has been done on YSZ buffer layers on Si or sapphire substrates the effect of growth conditions on microstructural changes in films have not been studied in detail. Moreover, J_c is strongly dependent on the $Y-123$ microstructure which itself is determined by the buffer layer microstructure. Since the microstructure of YSZ films grown on Si and sapphire substrates depends on the growth conditions, it is important to study the microstructural changes with deposition conditions for reproducible results and to improve the HTS film quality for technological applications. In view of this, a systematic study was taken up on the effect of variation of growth conditions on the microstructure of YSZ films suitable for $Y-123$ film growth by using RF magnetron sputtering technique, and subsequent $Y-123$ film growth by PLD method on these buffer layers. The microstructure of films has been studied using scanning electron microscopy and atomic force microscopy and an assesment of its bearing on J_c of $Y-123$ films deposited on these (YSZ) buffer layers is reported. Further, some work on STO buffer layers was taken up which is also reported here.

4.2 Deposition Details of Buffer Layers

Growth of YSZ buffer layers on single crystalline $Si < 100 >$ and R-plane (1102) sapphire were carried out using RF magnetron sputtering, and subsequent $Y-123$ film deposition on these buffer layers was done by a pulsed laser deposition (PLD) technique described in chapter 2. A parallel plate RF magnetron system (NORDICO 2000) was used to grow YSZ films. Commercially obtained YSZ and $SrTiO_3$ targets of 100 mm dia, 3 - 4 mm thickness and 99.9% purity were used for sputtering. Argon gas and $Ar + O_2$ gas mixtures of high pure gases were used as sputtering mediums and sputtering gas pressure was varied between 5 mTorr to 50 mTorr. To study the effect of oxygen

partial pressure two Ar/O_2 ratios were used viz., 9:1 and 1:1. The Ar/O_2 gas mixture was introduced into the chamber using flow meters fitted with fine control valves. A halogen lamp heater assembly was used to heat substrates up to temperatures 800° C. During buffer layer depositions, the substrate holder temperature was monitored with appropriate corrections applied to give a more realistic substrate temperature. RF power power was varied between 75 - 150 watts. $Si < 100 >$ wafers of 10 mm × 5 mm were used for YSZ deposition. Each Si wafer is rotated, flushed with high-purity alcohol, and etched with several drops of 1:10:1 mixture of HF, ethanol and distilled water all of high purity. This process produces oxide-free wafer covered by one monolayer of hydrogen which is passive to the effects of brief exposure to room air.

YSZ films were deposited on Si Substrates held at room temperature (RT), 600, 700 and 800°C. Other deposition parameters were kept constant. Table 4.1a gives details of the deposition parameters. Films deposited at RT, 600 and 700 $°C$ were post annealed 800 to 900 $°C$ for 30 minutes in ambient oxygen atmosphere. Table 4.1b gives the deposition conditions on sapphire substrates. The post annealing temperature 850 $°C$ and 30 minutes annealing in ambient pressure oxygen flow were found to be optimum for obtaining good quality $Y - 123$ film. Film thickness was measured using a stylus profilometer.

The following conditions were used for the PLD growth of $Y - 123 + 5\% Ag$ doped films on the buffer layers : 248 nm laser wavelength (UV, excimer), 600 mJ laser energy, 2 J/cm^2 laser fluence, 10 Hz repetition rate, 5 cm target- substrate distance and 750°C substrate temperature. Laser deposition conditions are shown in Table 4.2.

The structural investigation was carried out with X-Ray diffraction (XRD), microstructural studies were done using Scanning Electron Microscopy and Atomic Force Microscopy (AFM :Digital instruments Nanoscope III model). Fractured sections of YSZ buffer layers deposited on $Si < 100 >$ substrates were used for cross sectional SEM studies. Resistance - Temperature ($R - T$) measurements on $Y - 123 + 5\% Ag$ superconducting films deposited by the PLD technique were carried out using a four probe method using a CTI cryocooler in the temperature range 12 K to 300 K. Critical current density measurements were carried out on 15μm wide patterned microbridges of films.

Table 4.1

(a) YSZ Deposition Conditions on Si < 100 >

	Target	YSZ ($Y_2O_3$10%) (99.9% pure)
1.	RF Power	75-150 watt
2.	Substrate target distance (ST)	4-8 cms
3.	Base Pressure	10^{-7} Torr
4.	Sputtering gas mixture	Ar + O_2 (9:1 and 1:1)
5.	Sputtering pressure	10, 20, 25 and 50 mTorr.
6.	Substrate temperature	RT, 600°C, 700°C and 800°C
7.	Rate of deposition	12 Å/min
8.	Substrates used	Si < 100 > P type.
9.	Best Conditions	800°C, 10 mTorr, Ar+O_2(9:1)
		125 watts, 5 cm (T-S)

(b) YSZ Deposition Conditions on Sapphire

1.	RF Power	125 watt
2.	(S-T) distance	5 cms
3.	Base Pressure	10^{-7} Torr
4.	Sputtering gas mixture	Ar + O_2 (9:1 and 1:1)
5.	Substrate temperature	800°C
6.	Sputtering pressure	5 mTorr, 10 mTorr and 20 mTorr
7.	Rate of deposition	12 Å/min
9.	Best Conditions	800°C, 5 mTorr, Ar+O_2(9:1)
		5 cm (T-S) 125 Watts

Table 4.2
Laser Deposition Condition

1.	Laser Power	600 mJ
2.	Rep. rate	10 Hz
3.	Target-Substrate distance	4.5 cm
4.	Target	Y-123
5.	Spot Size	3.0×0.8 mm^2
6.	Sub. Temperature	$725°C$ on Si 750°C on sapphire
7.	Base Pressure	10^{-6} Torr
8.	O_2 partial pressure	200 mTorr

4.3 Results and Discussion

4.3.1 Yittria Stabilized Zirconia Buffer Layers

Besides the substrate used for the the growth of sputtered YSZ layers, sputtering parameters such as RF power density, substrate temperature and sputtering gas pressure (especially oxygen partial pressure in the sputtering gas mixture) significantly affect the microstructure of YSZ buffer layers. Moreover, the substrate temperature plays an important role by influencing the density of the microstructure, and hence, the intrinsic strength of the films. The following gives the effect of variation of these parameters on the quality of YSZ films. Only when the deposition parameters were optimized, good quality $Y-123$ thin films were obtained.

(a) RF Power :

The RF power was varied between 50 - 150 watts and found that the power between 100- 125 watts is the best for getting good quality buffer layers with maximum deposition rate. Fig.4.1 shows the RF power vs. deposition rate plot at $800°C$ and RT. Fig.4.2 shows the deposition rate and substrate temperature at 125 Watts. An RF power of 125 Watts was used for all depositions. Eventhough, deposition rate is low optical YSZ buffer layers were grown at this power at 800 °C. When RF power is above and/or below 125 watts, polycrystalline YSZ films were obtained.

(b) Substrate to Target Distance :

The substrate to target $(T-S)$ distance was varied between 4 cm to 8 cm. It was found the maximum deposition rate ($\sim 16A/\min$) with large area (nearly 154 cm^2) of uniform thickness was obtained when the distance was between 5-6 cm. Figure 4.3 shows deposition rate vs, $T-S$ distance. For all the depositions 5 cm $(T-S)$ distance was

Fig.4.1.

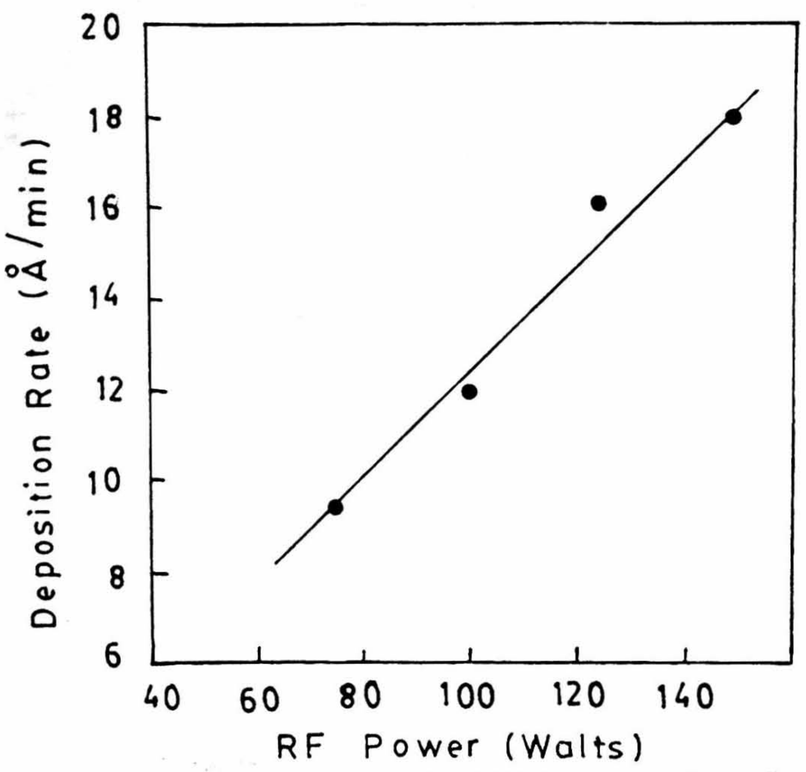

Fig.4.2.

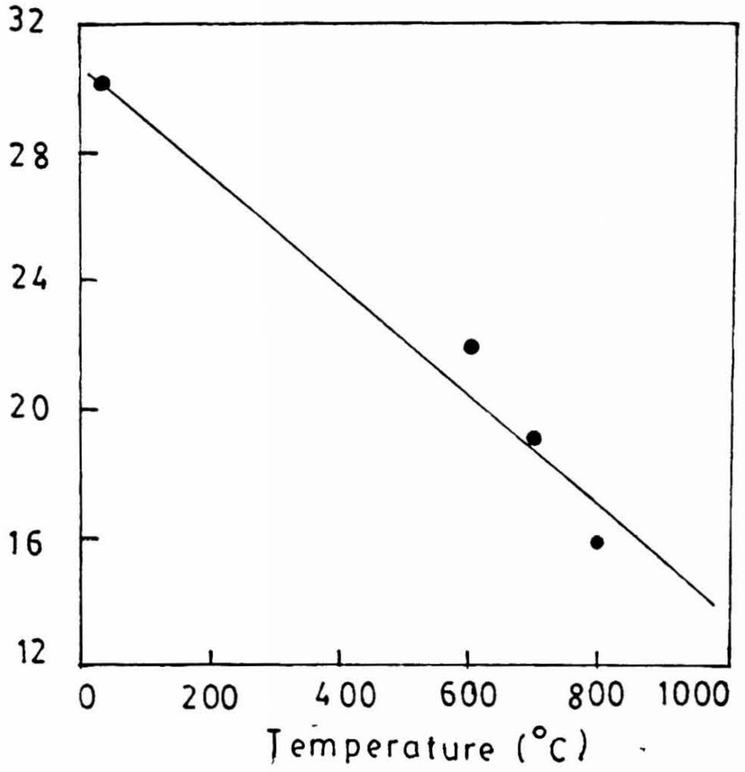

Fig.4.3

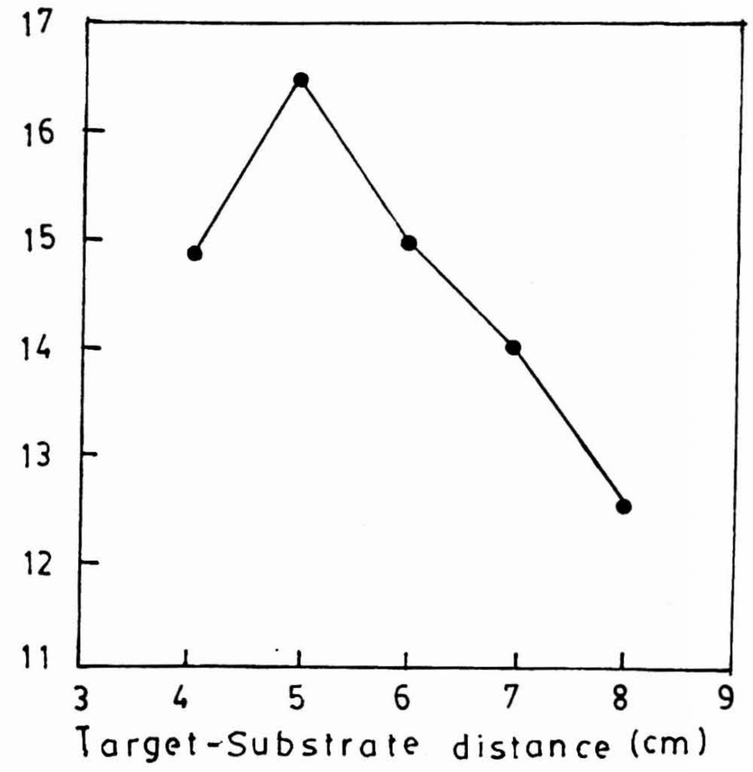

Fig.4.1. R.F. Power vs Deposition Rate of YSZ films deposited on Si <100>.

Fig.4.2. Substrate Temperature vs Deposition Rate of YSZ films deposited at 125W RF power.

Fig.4.3. Target substrate distance vs Deposition Rate of YSZ films at 800°C substrate temperature..

kept constant.

4.3.2 YSZ Buffer Layers on Si<100> Substrates

Films deposited on substrates held at RT were amorphous as evident by XRD shown in Fig.4.4a1. Those deposited at 600°C and 700°C resulted in polycrystalline nature as indicated by XRDs shown in Fig.4.4b1 and 4.4c1. Films deposited at 600°C show strongly $< 200 >$ oriented YSZ along with some satellite peaks which correspond to tetragonal YSZ phase (Fig.4.4b1). $< 111 >$ orientation of YSZ phase is also very strong in these films. Films deposited at 700°C also show similar features but the intensity of the peaks is very strong when compared to the same with YSZ films deposited at 600°C (Fig.4.4c1). To improve the crystallinity of the buffer layer, they were post annealed at 850°C for 30 minutes in oxygen. $< 220 >$ orientation along with minor $< 200 >$ orientation has been observed in the post annealed YSZ films which were deposited at RT (Fig.4.4a2). It is clear that the crystallinity has improved i.e. the intensities of $< 111 >$ and $< 200 >$ and other orientations (Satellite peaks) increased for films deposited at 600°C and 700°C after post annealing. $< 111 >$ orientation has relatively higher intensity than $< 200 >$ orientation in the post annealed YSZ film which was deposited at 600°C (Fig.4.4b2). On the other hand $< 200 >$ peak intensity and tetrogonal YSZ satellite peak intensity has been observed to increase (Fig.4.4c2) more than that of the $< 111 >$ peak in the case of post annealed film which was deposited at 700°C substrate temperature. The polycrystalline nature in these films may be due to the stabilization of tetragonal YSZ phase whose growth temperature is around 600°C, along with a cubic YSZ phase.

It is found, as observed earlier by other researchers, that YSZ films deposited at 800°C result in cubic single phase. Fig.4.5a shows $< h00 >$ oriented YSZ film on Si. The tetragonal phase reflections of YSZ, as observed in the case of films deposited at 600 and 700°C, were absent in the present case. However, the $< 111 >$ orientation of cubic YSZ grows larger with increase in film thickness. This may be due to the reoxidation of silicon substrate surface at higher temperatures in presence of oxygen in the sputtering gas [14] and hence perfect epitaxy may not be possible. Whereas laser ablated films show higher order of epitaxy when compared with sputter deposited YSZ films [42]. Here the oxygen

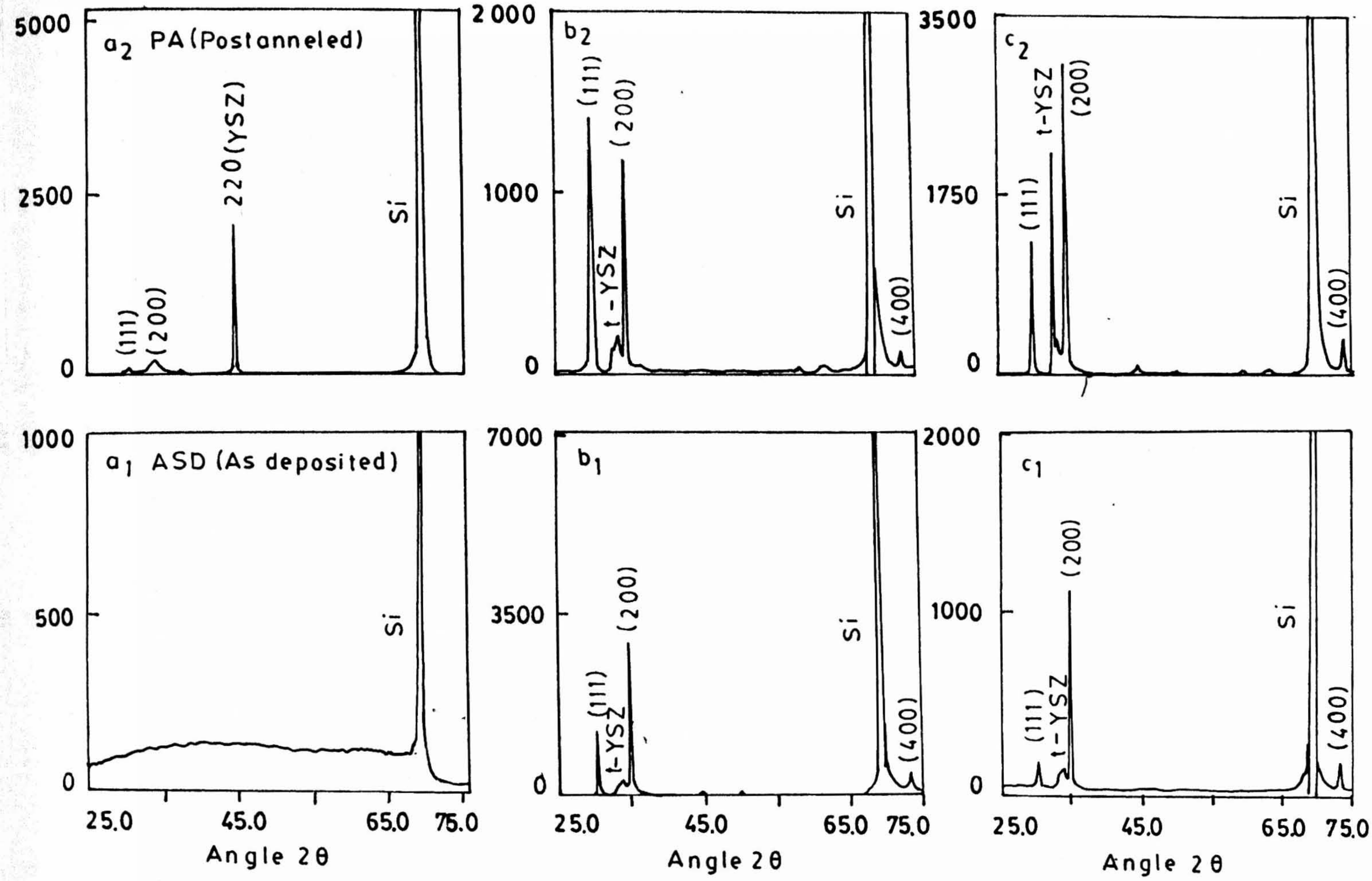

Fig.4.4. XRD Patterns of deposited and Post Annealed YSZ films on Si <100>.

a_1 As deposited at room temperature.

a_2 Post Annealed YSZ film of a_1.

b_1 YSZ film deposited on Si <100> at 600°C temperature.

b_2 Post annealed YSZ film of b_1.

c_1 YSZ film deposited on Si <100> at 700°C temperature.

c_2 Post Annealed YSZ film of b_2 t-YSZ = Tetragonal YSZ.

content in the sputtering gas was maintained less than 10^{-2} Torr in order to avoid the reoxidation of Si surface.

The primary requirement of oxide buffer layer is that the grains should be highly oriented and dense. Moreover, oxygen deficiency in the YSZ buffer has to be minimized so that it does not effect the oxygen content in the $Y-123$ films. Otherwise YSZ buffer takes oxygen from growing $Y-123$ film during $Y-123$ deposition. Hence, partial pressure of oxygen is essential for growing stoichiometric YSZ films. However, high oxygen partial pressure during the growth process decrease the sputtering rate due to resputtering of the film by highly energetic oxygen anions. So the processing parameters become sensitive to high oxygen environment during sputtering. Four sputtering gas pressures 10 mTorr, 20 mTorr , 25 mTorr and 50 mTorr in each case $Ar + O_2$ with 9:1 ratio were studied for the comparison sake. Fig.4.5a-d shows the XRD patterns of the films deposited at various sputtering gas pressures at $800°C$ substrate temperature and 125 watts RF power. With the increase of sputtering gas pressure it was observed that intensity of the $< 200 >$ and $< 400 >$ peaks started decreasing. Broadening of these peaks is also observed with the increase of the sputtering gas pressure. The full width at half maxima (FWHM) values of $< 200 >$ reflection in XRD of these films are 0.24, 0.32, 0.35 and 0.44 for 10, 20, 25 and 50 mTorr respectively. Since FWHM increases with the sputtering gas pressures, crystalline quality of the YSZ film decreases relatively. Films deposited at 10 mTorr sputtering pressure (Ar/O_2 ratio 9:1) resulted in highly $< h00 >$ nature with small FWHM values.

4.3.3 Microstructure of the YSZ Buffer Layers

This study is mainly aimed at understanding how the microstructure of YSZ film changes with the sputtering gas pressure and thickness of the buffer layer which in turn effects the quality of superconducting $Y-123$ film. Therefore, for this study Si substrates were held at $800°C$(which is the YSZ cubic phase formation temperature) and $600°C$ for depositing YSZ buffer layer. At each substrate temperature two different sputtering gas pressures ($Ar/O_2 = 9:1$) of 10 mTorr and 20 mTorr were used for the present study.

Figs.4.6(a-d) show the cross sectional SEM micrographs of fractured surface of YSZ

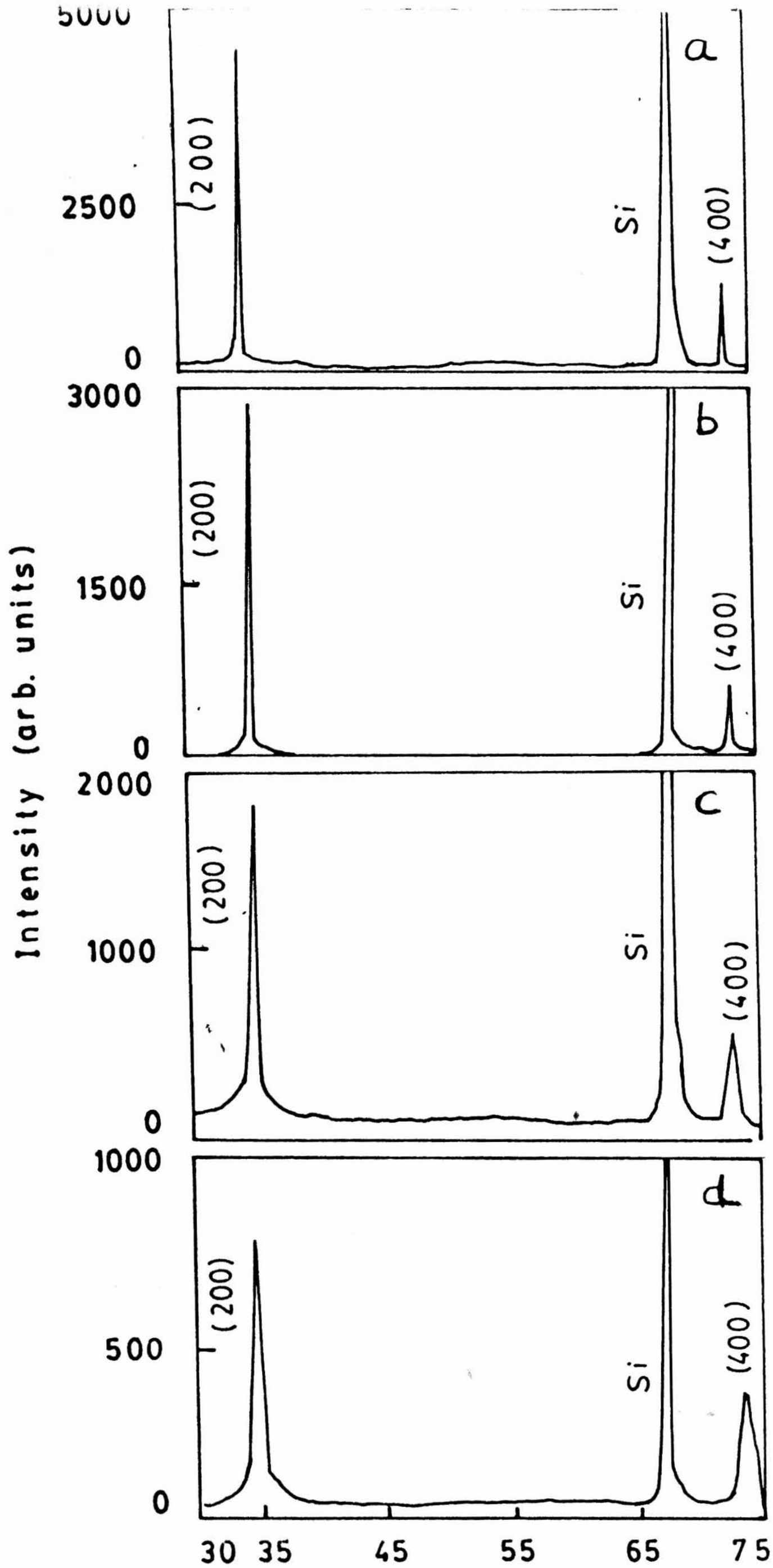

Fig.4.5. XRD patterns of YSZ films on Si <100> deposited at 800°C temperature and at (a) 10 mTorr Ar+O_2 (9:1); (b) 20 mTorr Ar + O_2 (9:1); (c) 25 mTorr Ar + O_2 (9:1); (d) 50 mTorr Ar + O_2 (9:1).

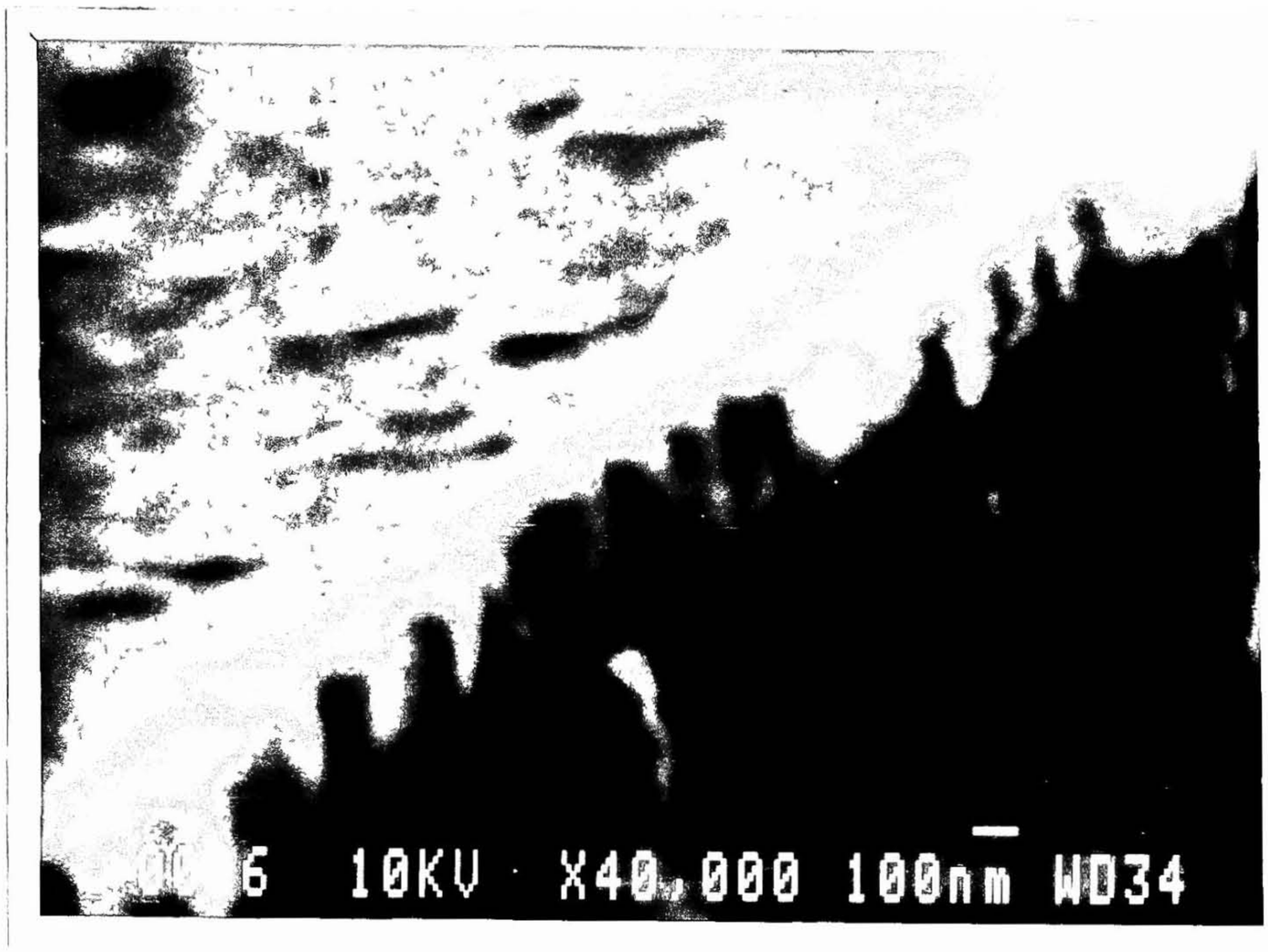

Fig.4.6 (a) Cross sectional SEM micrograph of fractured surface of YSZ film grown on Si(100) at 600 C and 10 mTorr Ar/O_2 gas mix in 9:1 ratio - smooth Columnar growth can be seen at the cross section.

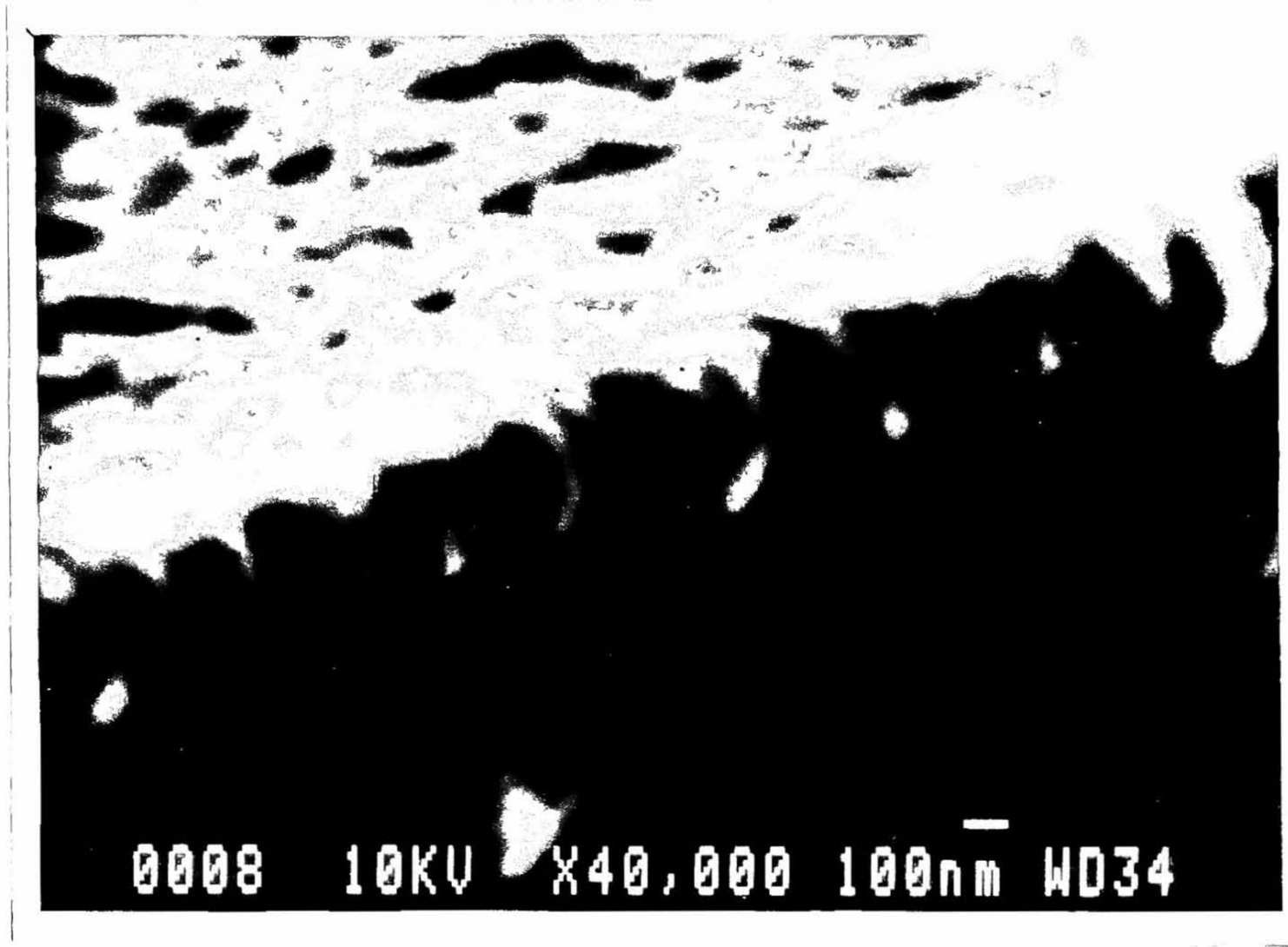

Fig.4.6 (b) Cross sectional SEM of fractured surface of YSZ grown at 600 C and 20 mTorr (9:1) on Si - increased surface roughness and Columnar structure can be seen at the cross section.

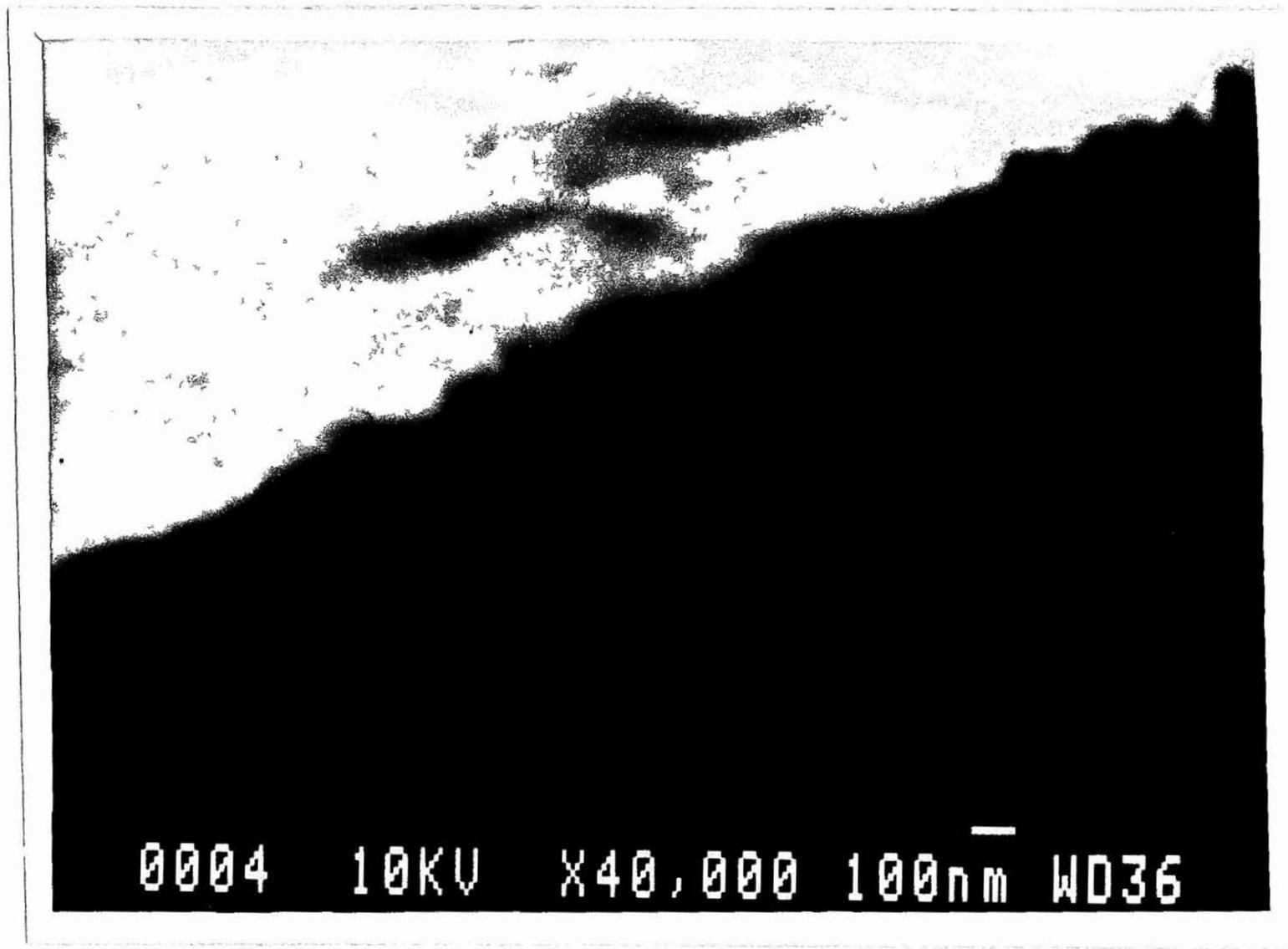

Fig.4.6 (c) Cross sectional SEM of fractured surface of YSZ film deposited at 800 C and 10 mTorr Ar/O_2 (9:1) gas on Si substrate - reduced Columnar growth can be seen at the cross section.

Fig.4.6 (d) Cross sectional SEM of fractured surface of YSZ film deposited at 800 C and 20 mTorr (9:1) on Si - increased Columnar growth and surface roughness can be seen at the cross section.

films deposited at 10 and 20 mTorr for 600 and 800°C. Films deposited at 800 and $600°C$ with 10 mTorr have shown relatively smooth and densified microstructure and show much lower tendency for columnar growth (Figs.4.6a,c). YSZ films deposited at 20 mTorr have shown microstructure of highly packed columnar grains (Figs.4.6b,d) irrespective of deposition temperature. The tendency for columnar growth has been found to be strong at high sputtering gas pressures and has been found to persist to higher substrate temperatures too. This observation is consistent with the structure zone model proposed by Movchan and Demchishin [57] and later by Thornton [58]. They reported that the tendency for columnar growth is more for higher substrate temperatures and high sputtering gas pressures. Although, the YSZ films sputtered on silicon may not have the same structural pattern as that observed by Thornton in sputtered metal films, significant similarities are expected. However, when the sputtering pressure was lowered, the coating was found to be denser by SEM but these were still slightly columnar. At high T/T_m the intergrain voids begin to fill in and the structure passes in to a transition zone of tightly packed fibrous grains which generally do not extend throughout the film thickness. This could be the reason YSZ films deposited at 20 mTorr pressure have shown strong tendency for columnar growth for both the temperatures. Another possible explanation for columnar growth probably due to the relatively low adatom surface mobility which is limited by sputtering gas at high pressures. As there is large coefficient of thermal expansion mismatch between YSZ and Si, the films having a columnar structure will have low lateral strength, generate microcracks at higher thickness than the films grown at higher $T/T_m(0.3)$ which have higher density and have little tendency for columnar structure. Another speculation for higher tendency for columnar growth may be due to the reoxidization of Si substrate at higher substrate temperatures due to the presence of oxygen in sputtering gas. However, the YSZ films deposited at $800°C$ and 10 mTorr have the relatively smooth and densified microstructure.

4.3.4 Y-123 Films on YSZ Buffered Si Substrates

$Y-123$ thin films were deposited using PLD method on YSZ buffered Si substrates held at 750 °C. Postannealed buffer layers were used for $Y-123$ films deposition. Fig.4.7

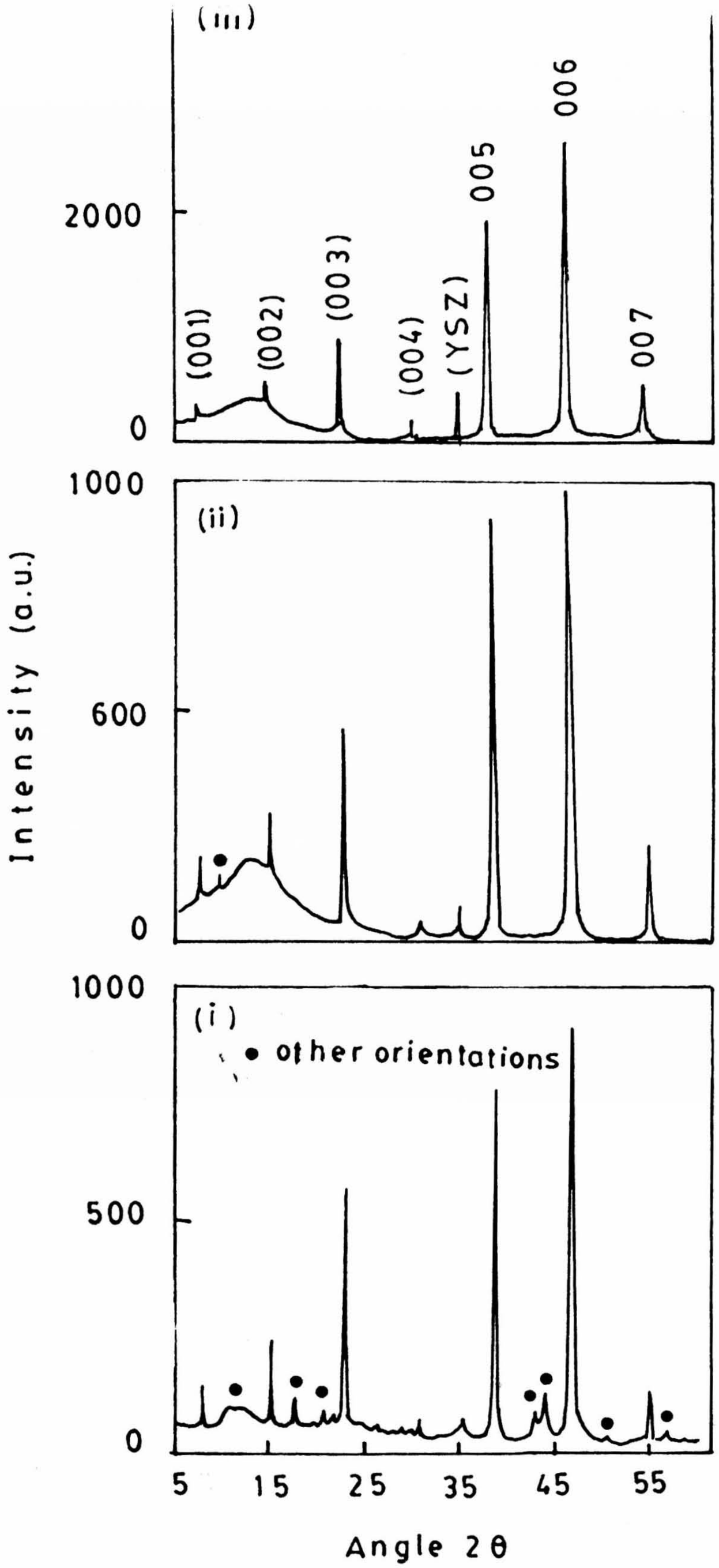

Fig.4.7. XRD patterns of Y-123 films deposited on (i) Post Annealed YSZ buffer layer deposited at RT. (ii) Post Annealed YSZ buffer layer deposited at 600°C temperature and (iii) Post Annealed YSZ buffer layer deposited at 700°C temperature.

shows the XRD pattern of the $Y-123$ thin films deposited at $750°C$ on post annealed buffer layers deposited on Si at RT, 600 and $700°C$ respectively. The large FWHM values of $< 00l >$ oriented reflections confirm the granular nature of the $Y-123$ thin films. Fig.4.7b shows the XRD of the $Y-123$ film deposited on YSZ buffered prepared at $800°C$ and 10 mTorr $Ar + O_2(9:1)$ gas pressure on Si. This $Y-123$ film show the best superconducting properties than the other films. Fig.4.8 shows the resistance vs temperature curves of $Y-123$ thin films deposited on the YSZ buffer layers prepared at above mentioned temperatures on Si. The room temperature resistance varies from 25 ohms to 12 ohms and T_c ranges from 82 K to 88 K. J_c was measured for all $Y-123$ films at 77 K and was found to be low ($\sim 8 \times 10^5 A/cm^2$). Table 4.3 shows the results on $Y-123$ deposited on polycrystalline YSZ buffer layers on Si. The reason for the poor J_c on the polycrystalline buffer YSZ films is the large coefficient of thermal expansion and lattice mismatch which results in polycrystalline $Y-123$ films having small grains with large number of weak links, as indicates by the XRD - FWHM values.

To study YSZ film thickness dependence on J_c of $Y-123$, single phase $< hoo >$ oriented YSZ films of thicknesses 40 nm and 80 nm were deposited on $Si < 100 >$ substrate at the optimized parameters. Over these buffer layers nearly 100 nm $Y-123$ films were deposited and their critical current densities were measured. XRD patterns of the $Y-123$ films deposited on the buffer are shown Fig.4.9. Fig.4.10 shows the Resistance vs. Temperature curves of the above mentioned $Y-123$ films. $Y-123$ film deposited on $40nm$ YSZ buffered Si substrate has a T_c of 86 K and J_c of $4 \times 10^5 A/cm^2$ at 77 K and the $Y-123$ film deposited on 80 nm has a T_c of 84 K and a J_c of $8 \times 10^4 A/cm^2$ at 77 K. Table4.4shows the results on YSZ buffered $Y-123$ thin films and their T_c and J_c values of $Y-123$ thin films deposited over them. Obviously, J_c values are very low. The thermal cycling of the YSZ buffer might have developed microcracks due to a large thermal expansion mismatch between Si and YSZ buffer as well as oxygen loss in the YSZ film which might be responsible for lower quality of $Y-123$ thin films. Hence YSZ buffer layer and $Y-123$ film have to be grown simultaneously without cooling the Si substrate. However, these results were found to be highly reproducible.

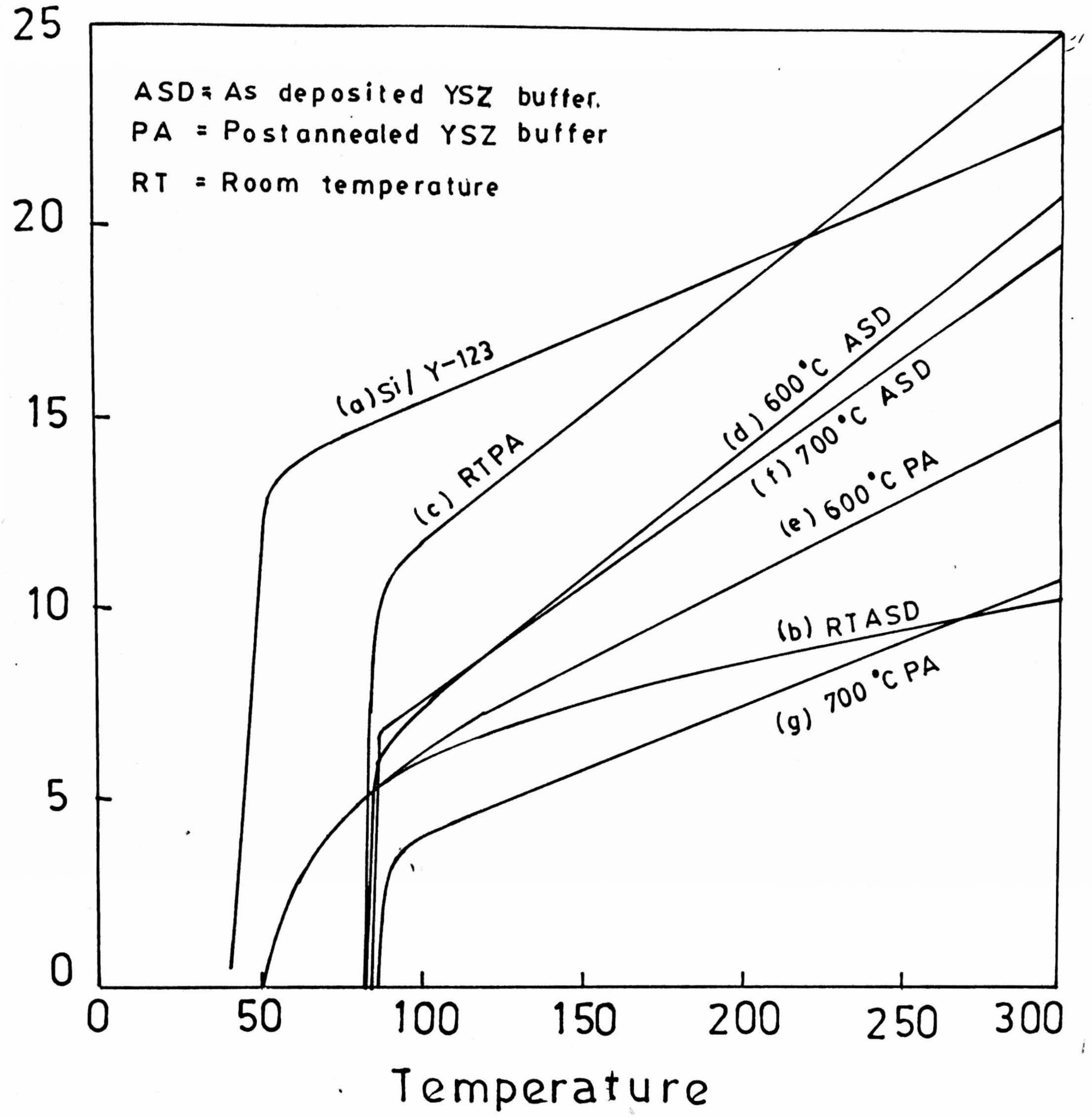

Fig.4.8. R-T Curves of Y-123 films deposited on Si <100> using YSZ buffer layers deposited at different substrate temperatures.

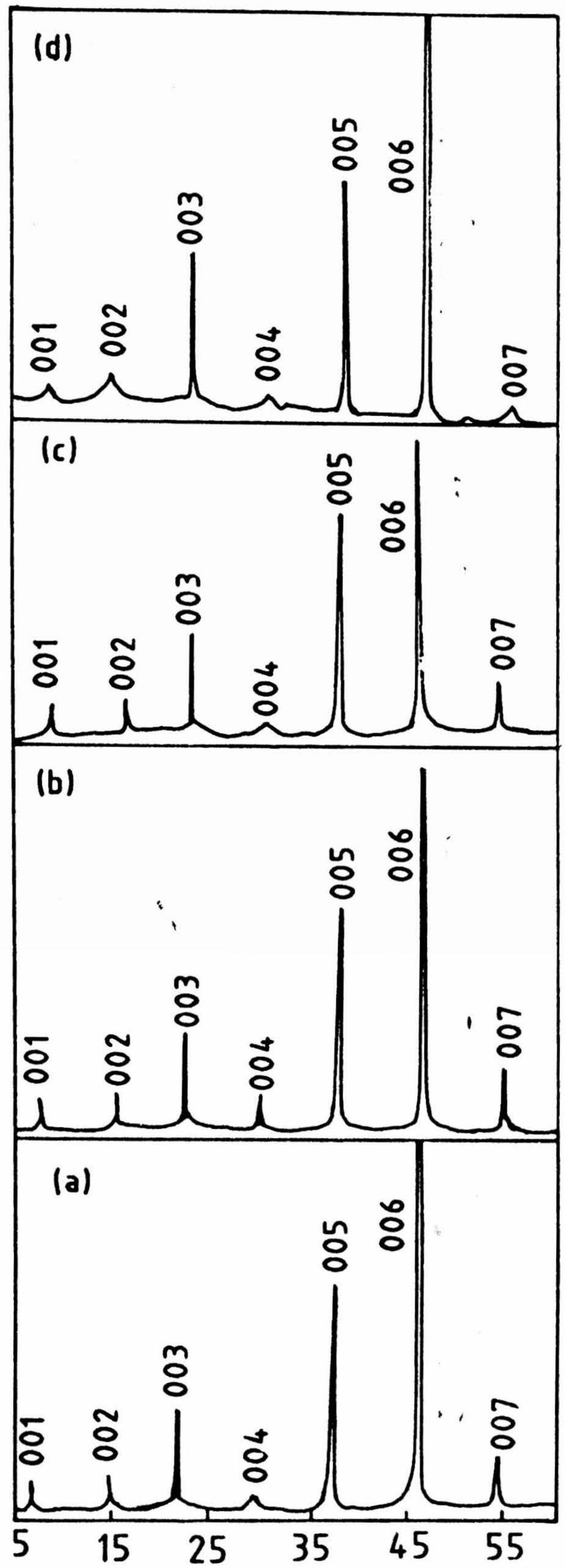

Fig.4.9. Y-123 films deposited on Si <100> using YSZ buffer layers deposited at 800°C and at (a) 10 mTorr; (b) 20 mTorr; (c) 25 mTorr and (d) 50 mTorr sputtering gas ($Ar+O_2$) pressures.

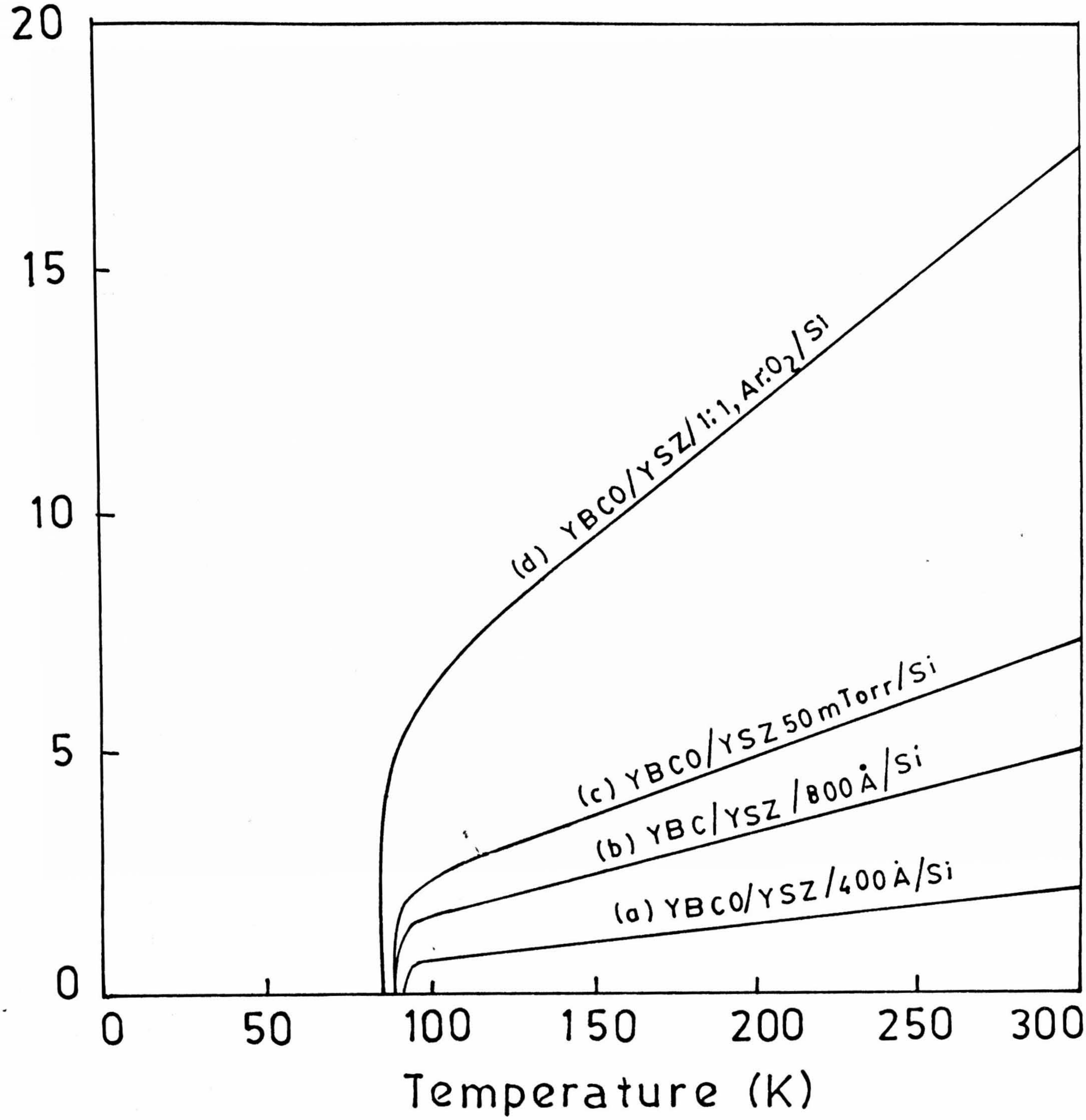

Fig.4.10. R-T curves of Y-123 films deposited on Si <100> using YSZ buffer layers of thickness (a) 400Å; (b) 800Å (c) 800Å (50 mTorr) and (d) 800Å(1:1).

Table 4.3
Y-123 films R-T Results on YSZ Buffered Si< 100 >

Sl. No.	YSZ filmn Deposition temperature °C	Post annealing temperature of YSZ buffer	YSZ Buffer thickness Å	Y-123 thickness Å	Y-123 deposition temperature °C	R_{300} Resistance Ω	T_cK T_{co}	Residual resistance Ω	J_c at 77 K A/cm^2
1.	Si (no buffer)	—	680	1200	780	21	38	12	5.2
2.	RT	—	528	1576	760	24	49	6.8	8.6
3.	RT	850 for 1 hr	516	962	758	7.5	78	4.2	12.5
4.	600	—	509	964	760	19	80	32	200
5.	600	860 for 30 hr	520	920	758	17	81	2.4	950
6.	700	—	495	958	775	16	82	1.6	2560
7.	700	855 for 1 hr	515	910	750	8	84	1.5	8450

Table 4.4
Results of Y-123 films deposited on YSZ buffered Si< 100 >

Sl. No.	YSZ filmn Deposition temperature °C	Sputtering Gas pressure Ar:O_2	YSZ Buffer thickness Å	Y-123 thickness Å	Y-123 deposition temperature °C	ρ_{300} Resistivity Ω/cm	T_cK T_{co}	Residual resistance Ω	J_c at 77 K A/cm^2
1.	800	(9:1)	828	860	750	0.0688	84.5	0.6	3×10^3
2.	800	(9:1)	412	900	750	0.0396	86.2	0.25	4×10^5
3.	800	(1:1)	580	1100	752	0.3740	81.0	2.5	8×10^4
4.	800	50	556	1200	765	0.4080	87.0	1.1	4×10^4

4.3.5 YSZ Buffer Layers on Sapphire Substrate

It is well established that [14] epitaxial YSZ buffer layers can be grown at 800°C on Sapphire substrates. Present work was aimed at studying the effect of sputtering gas pressure on microstructure of the YSZ buffer. Three different sputtering pressure conditions viz. 5 mTorr, 10 mTorr and 20 mTorr were chosen for this investigation. Two Ar/O_2 ratios 9:1 and 1:1 were studied for the comparison sake. In all the cases a presputtering for 5 minutes was done and the film thickness was in the range of 50-70 nm.

Figure 4.11 shows the XRD of the YSZ buffer layers grown on sapphire single crystalline substrate using different growth conditions. For films grown using $9:1 Ar/O_2$ gas mix, XRD shows sharp $< h00 >$ reflections which is indicative of good crystalline nature of films. FWHM of $< 200 >$ reflection was 0.22, 0.26 and 0.3 for films grown using 5, 10, 20 mTorr chamber pressures respectively. On the other hand for films grown using $1:1 Ar/O2$ gas mixture, XRD showed very low intensity $< 200 >$ reflections and the FWHM are higher (0.28, 0.32 and 0.45 for 5, 10 and 20 mTorr sputtering pressures). The higher angle reflections were not seen in this case. Thus XRD confirms that films grown using a chamber pressure of 5 mTorr and $9:1 Ar/O_2$ gas mixture ratio have better crystallinity as compared to those grown using other conditions. The YSZ lattice parameters calculated from XRD study were found to vary from 0.513 to $0.516nm$ when the sputtering pressure varied from 5 to 20 mTorr. This variation in the lattice parameter shows that there is a change in the YSZ composition for films grown using higher O_2 partial pressure. This means in $(Y_2O_3)_m(ZrO_2)_{1-m}$, m tends to increase from an optimum value (0.08-0.1) to higher values which is not good for the stability of the film. Since the surface morphology of YSZ buffer layers deposited on sapphire can not be detected by SEM due to its nonconducting nature of the substrate, detailed studies with a new surface analytical technique based on atomic force microscopy (AFM) were carried out to visualize the microstructural details of the YSZ buffer layers grown with different growth conditions on Sapphire.

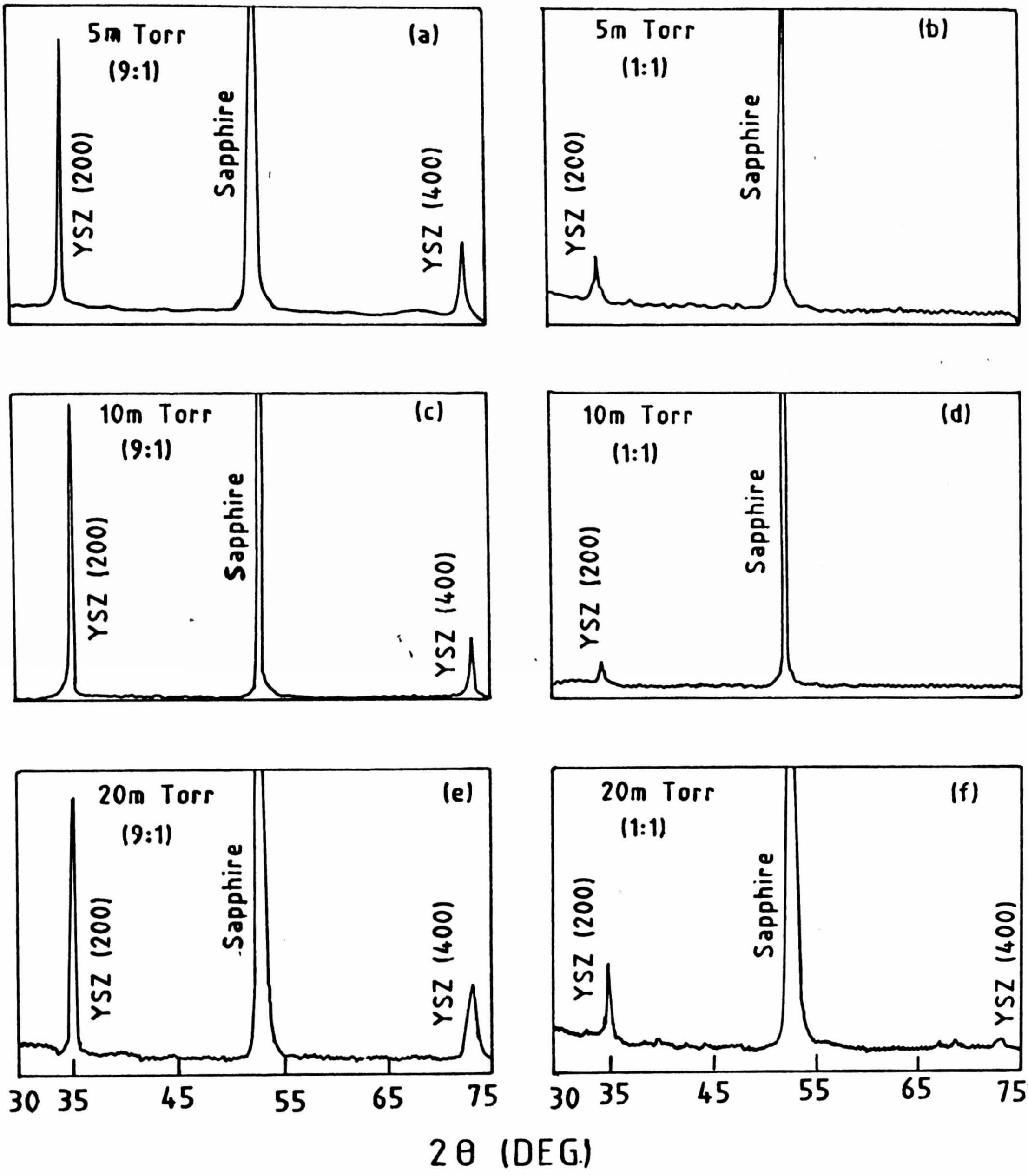

Fig.4.11. XRD traces of YSZ buffer layers grown on r-plane (1102) sapphire using different growth conditions. Value in parenthesis indicates Ar/O_2 ratio.

4.3.6 Atomic Force Microscopy Studies on YSZ Buffer Layers

AFM is a simple but versatile technique that has been found to be extremely useful in visualizing the true microstructure of the YSZ films. The AFM a very recent invention [59], produces images that are much closer to simple topographs and can image nonconducting surfaces as well. Thus it has a promise for imaging biological materials and other substances that do not readily conduct electrons.

The AFM records interatomic forces between the apex of a tip and atoms in a sample as the tip is scanned over the surface of the sample when the AFM is operated in a mode that senses the repulsive forces between tip and sample. The tip actually touches the sample much like the stylus of a record player touches the surface of a record. For the AFM, however the tip is much sharper and the tracking force is much smaller, about one millionth as great as for a record plyaer. At these small tracking forces, the tip can trace over individual atoms without damaging the surface of the sample. The AFM can also be operated so that it senses the attractive forces between the tip and the sample. The feed back system then prevents the tip from touching and damaging the sample. But this mode of operating an AFM comes at the cost of decreased lateral resolution. So far, most images obtained in this way are micrometer scale objects. Schematic view of the force sensor for an AFM is shown in Fig.4.12. The essential features are a tip, shown as a rounded cone, a spring and some device to measure the deflection of the spring. In practice, the spring deflection sensor can be either based on electron tunneling to the back of the spring, on optical interference between the back of the spring and a reference plate, or by deflection of a laser light beam reflected off the back of the spring. In any case the tip follows a path that is an accurate topograph of the surface. No voltage is applied between the tip and the sample, and no current needs to flow between the tip and the sample. Thus the AFM can image nonconducting samples also.

The tip can be made of a small fractured diamond fragment attached to a spring in the form of a cantilever. The small repulsive tracking forces between the tip and the sample susally in the range of 10^{-6} to 10^{-9}N, are recorded by measuring minute deflections of the cantilever. A typical spring constant for a cantilever would be about 1 N/m. If a delfection as small as 1 nm can be sensed for a cantilever with a spring constant of 1 N/m,

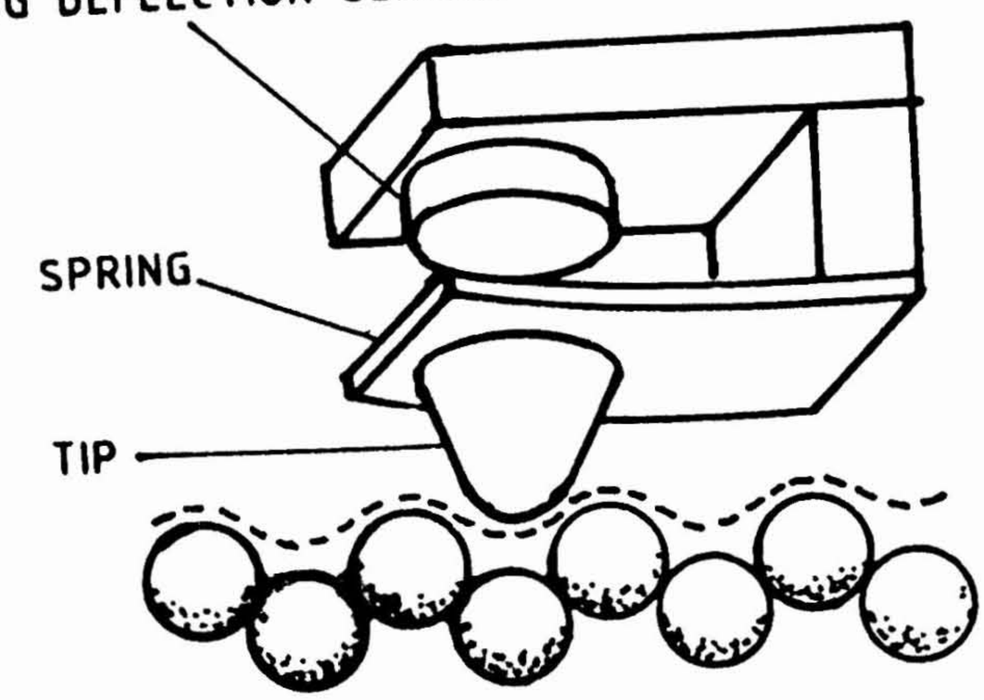

Fig.4.12. (a) Schematic diagram of atomic force micro sensor.

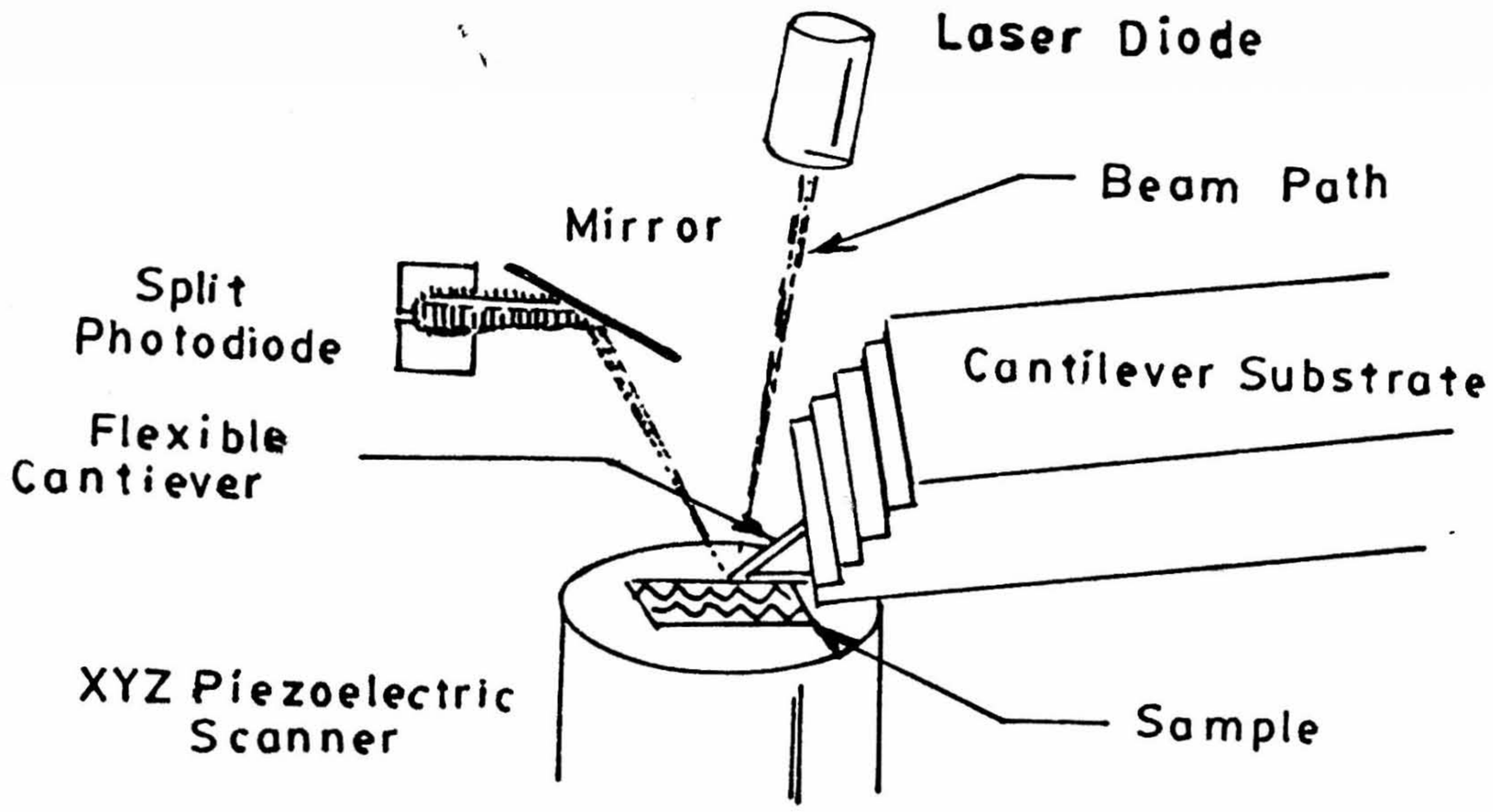

Fig.4.12(b) AFM Optical Sensing System

then a tracking force as low as 10^{-9}N can be applied between the tip and the sample. Microcantilevers made of silicon oxide or silicon nitride with silcon etching technology [60] are even lighter and have resonant frequencies as high as 100 KHz. The higher the resonant frequency, the less sensitive the cantilever is to vibrations, and the more stable it is for atmoic force microscopy. The vibration of one end of the cantilever relative to the other in response to an external vibration of magnitude A and frequency ν_g is approximately $A(\nu/\nu_r)^2$, where ν_r is the resonant vibration frequency of the cantilever. For a typical laboratory room, A would be of order 1 μm and ν_r of order 20 Hz. Thus a cantilever with a vibration frequency of 10 KHz would have a vibration amplitude less than 0.01 nm and be suitable for atomic resolution imaging with minimal vibration isolation. A commercially available, Digital Instruments company model III nanoscope with Silicon Nitride tip was used in the present case for studying the microstructure of buffer layers deposited on Sapphire substrate.

This technique has yielded a great deal of information for a very good understanding of the growth process of the buffer layers as well as the $Y-123$ films with regard to variations in growth parameters. Fig.4.13a shows the AFM image of the YSZ buffer layer grown using 5 mTorr (Ar/O_2 ratio = 1:1) pressure, Fig.4.13b shows its $3D$ surface plot which clearly shows outgrowths on the film surface with an average roughness (AR) of 0.6 nm. In comparison, microstructure of the films grown using the same pressure (5mTorr) and a gas mixture ratio of 9:1 indicates very smooth surface morphology (AR = 0.3 nm) as shown in Fig.4.13c. Figure 4.13d shows the 3D surface plot of the same. Similarly, out growths with an average roughness of 1 nm are seen on the films grown using 10 mTorr (1:1) sputtering conditions as shown in Fig.4.14a. However, although no such outgrowths are seen in Fig.4.14b for films grown using 10 mTorr (9:1) growth conditions, the average film roughness has increased to 0.6 nm from that of 0.3 nm observed for 5 mTorr (9:1) growth conditions. Figures 4.15a and 4.15b depict the surface morphology of films grown using chamber pressure of 20 mTorr and Ar/O_2 gas mixture (1:1). The outgrowths that have started to appear in the case of films grown using pressures 5 and 10 mTorr and Ar/O_2 gas mixture (1:1) have increased to the extent that the surface morphology of the film appears granular (average grain size $0.3\mu m$). Grain boundaries separating out the grains can be clearly seen. Some of the grains are oriented at tilt angles with respect to neighboring grains and the average surface roughness is 5 nm. On the other hand, as

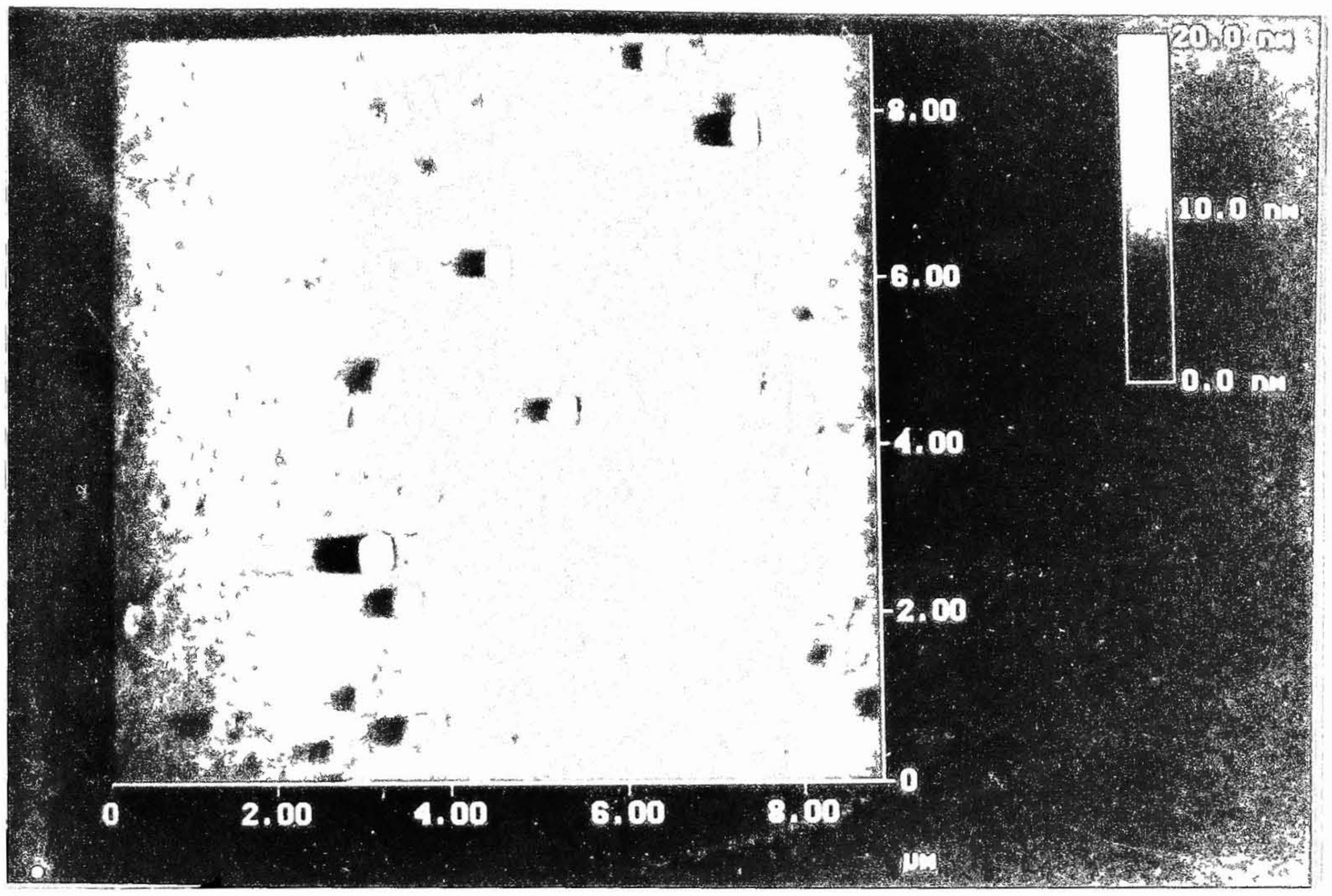

Fig.4.13. AFM images of YSZ buffer layers grown using a 5 mTorr Ar/O_2 gas mix ratios of 1:1 (a) 5 mTorr (1:1) - outgrowths can be seen and the average surface smoothness is 0.6 nm

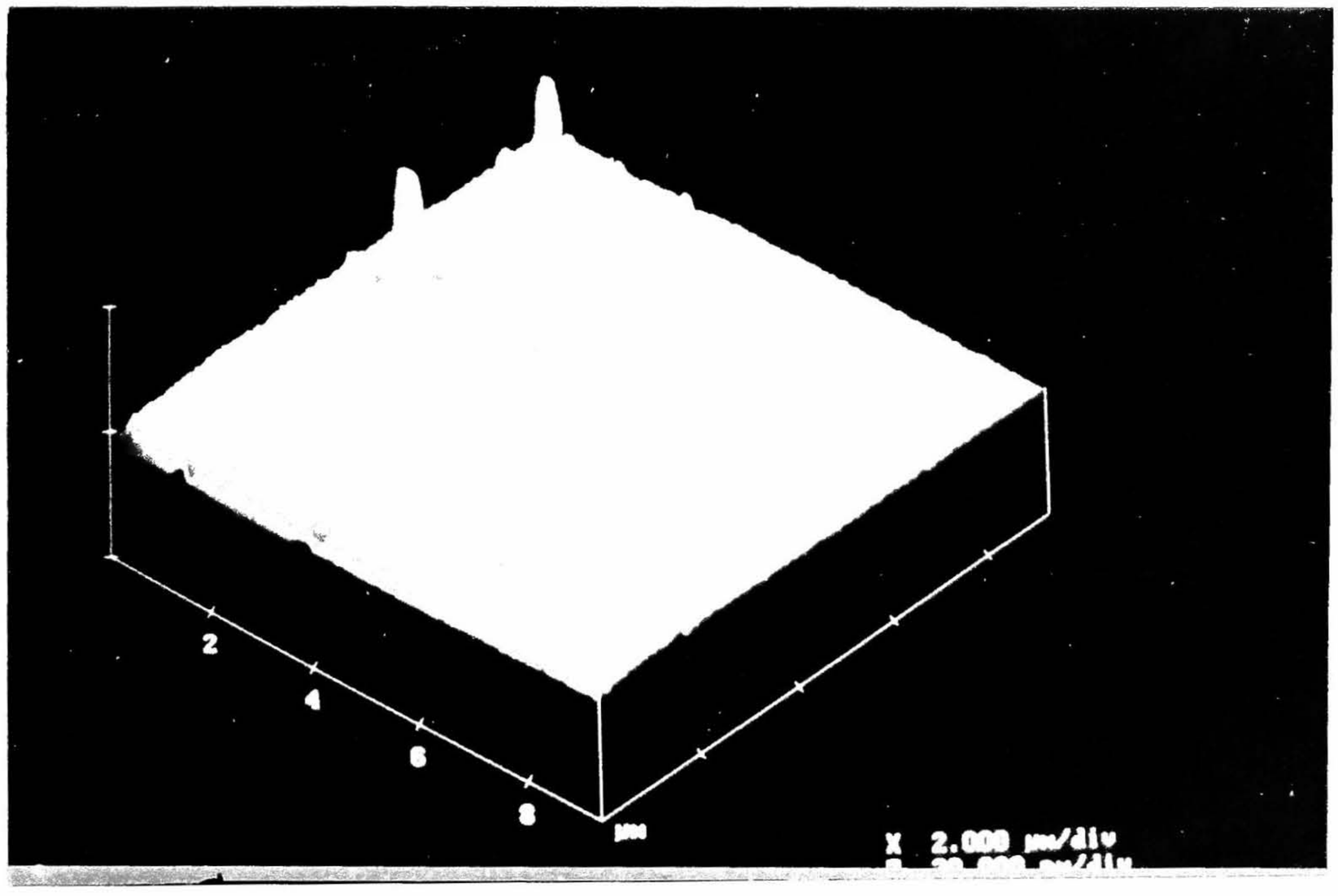

Fig.4.13 (b) a 3D plot of the above AFM image

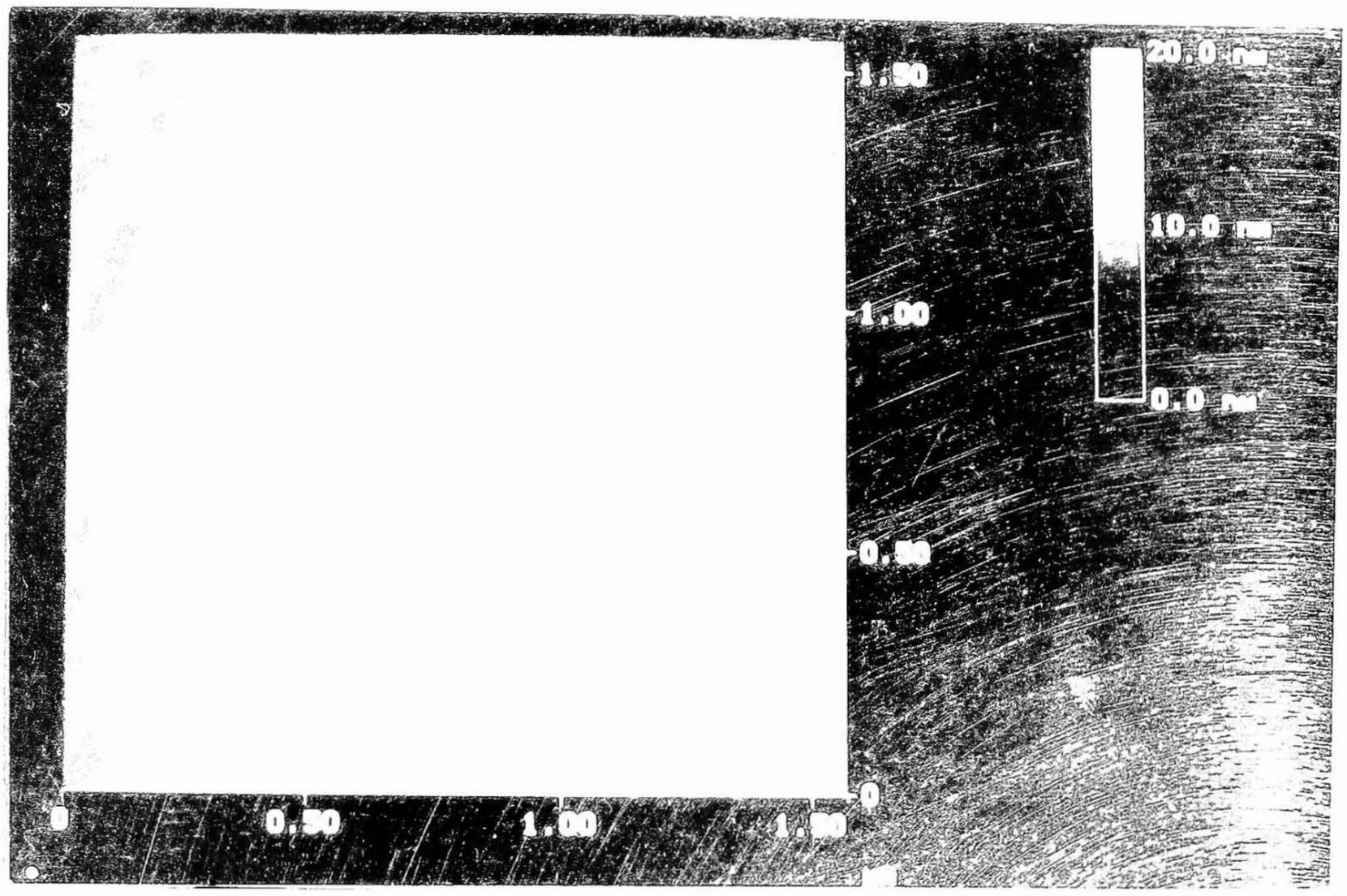
1.50
1.00
0.50
0
0.50
1.00
1.50
20.0 nm
10.0 nm
0.0 nm

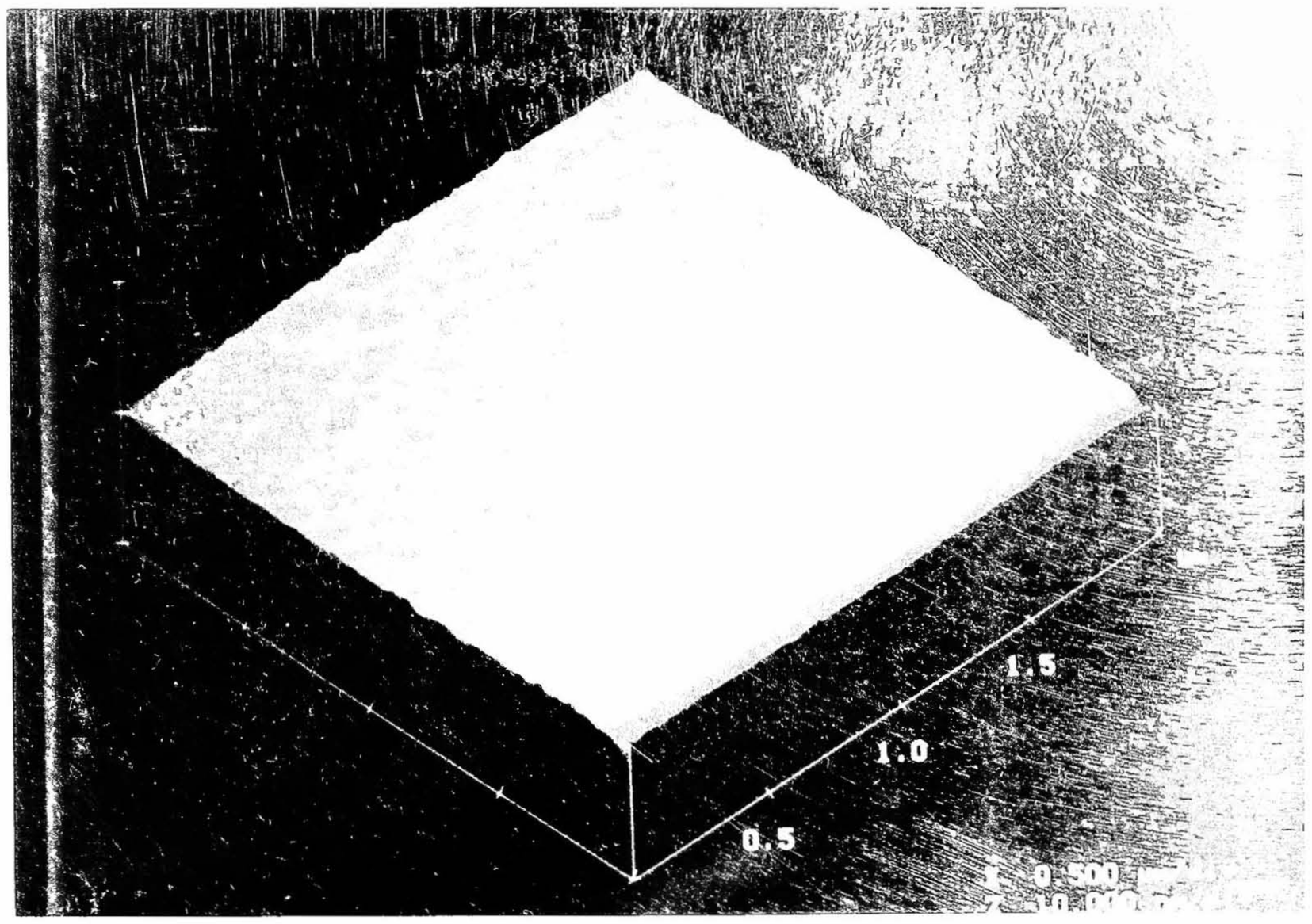
1.5
1.0
0.5

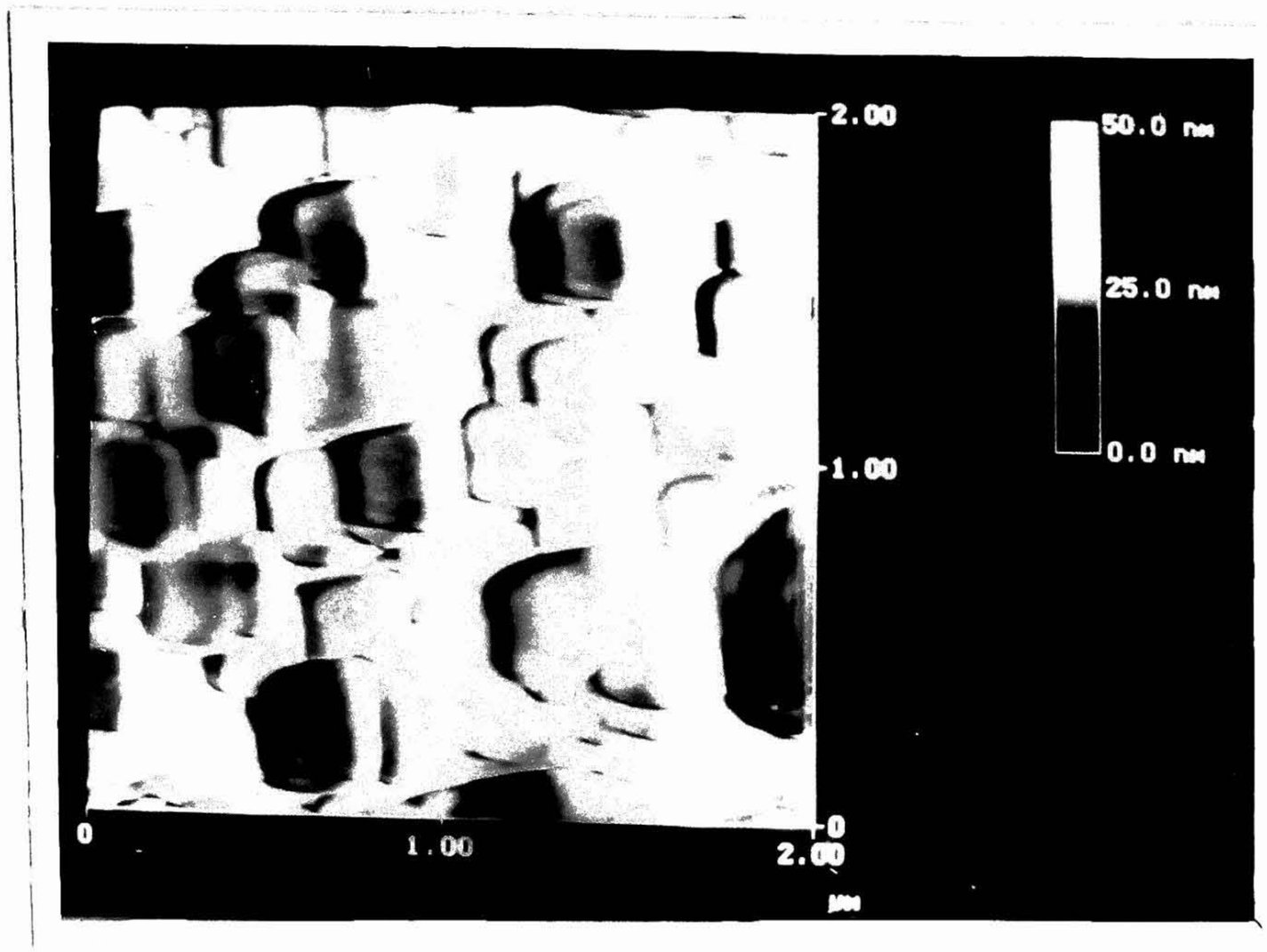

Fig.4.15 (a) AFM image of YSZ buffer layer grown using a pressure of 20 mTorr and Ar/O_2 (1:1) - the surface morphology of the film appears granular with average surface roughness = 5 nm and average grain size 0.3 micron meters

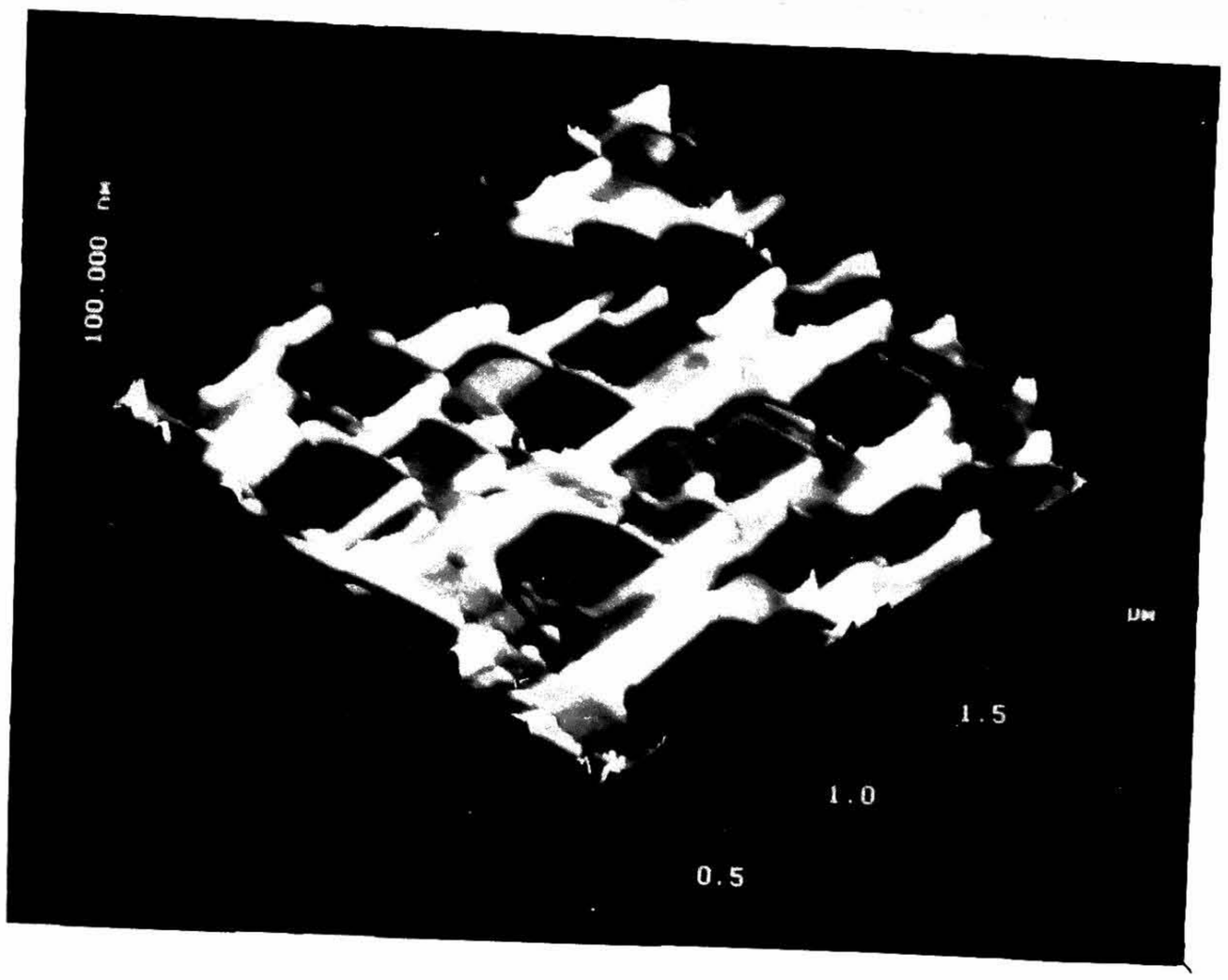

Fig.4.15 (b) a 3D plot of the above AFM image

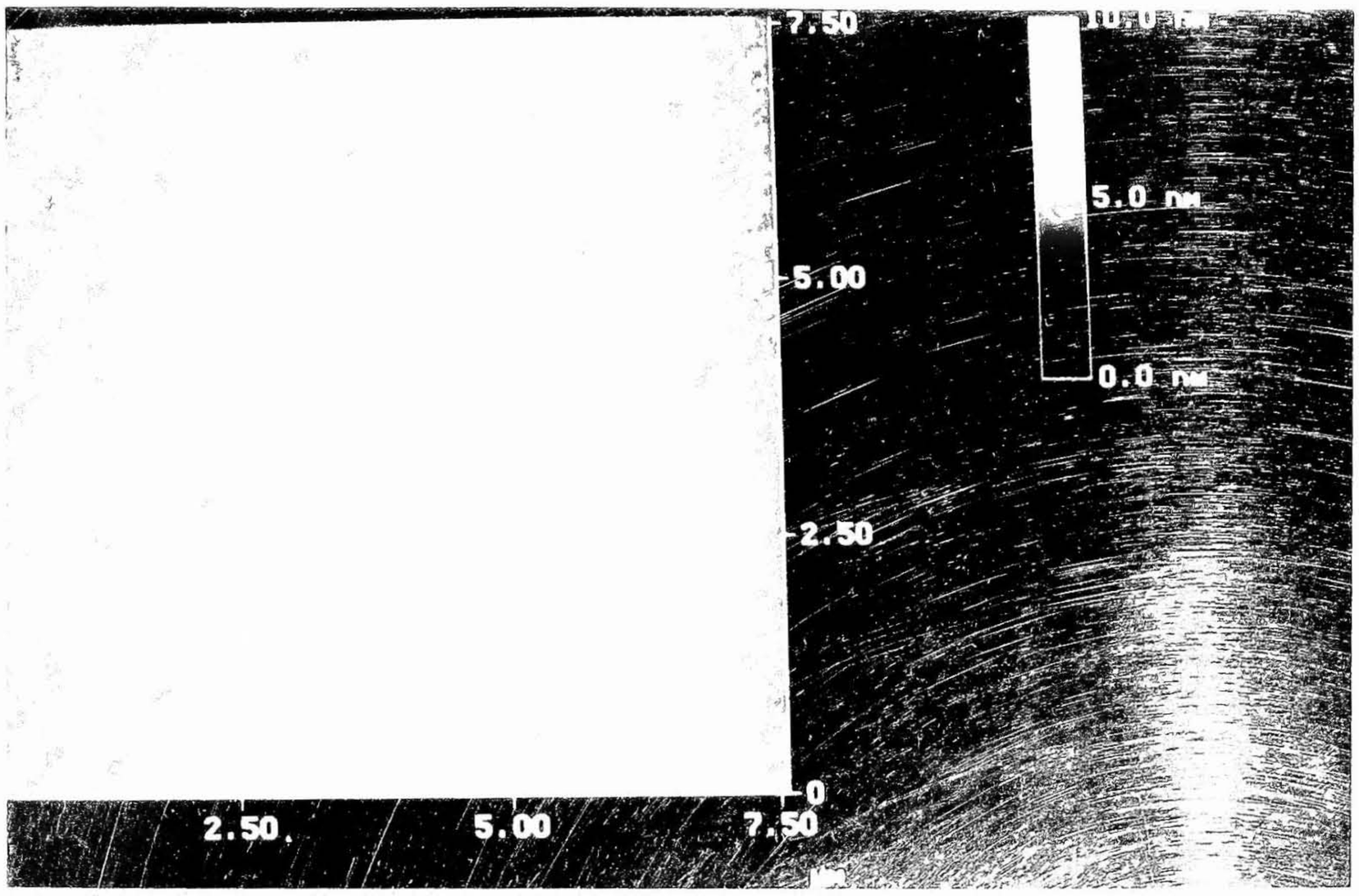
7.50
5.00
2.50
0
5.0 nm
0.0 nm
2.50
5.00
7.50
0

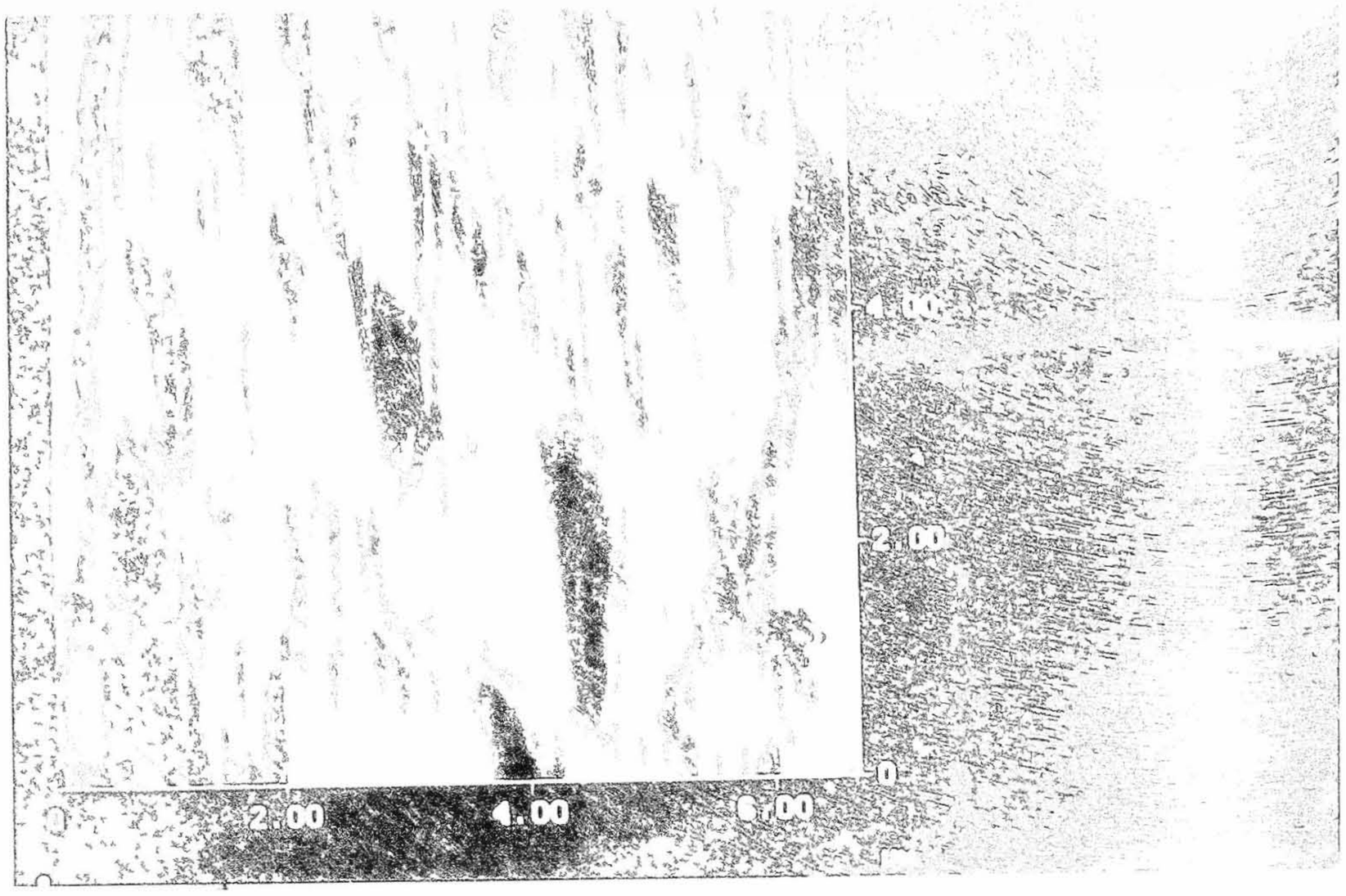
2.00
4.00
6.00
0

seen in Figs.4.15c and 4.15d films grown using 20 mTorr (9:1) growth conditions have shown a surface roughness of 1 nm. The average roughness of the YSZ films deposited at various sputtering gas pressures are shown in Table 4.5

The, AFM results on the microstructure of YSZ buffer layers can be summarized as follows :

1. Average film roughness increases with increase in chamber pressure (5 to 20 mTorr) for $Ar/O2$ gas mixture ratio of 9:1.

2. For films grown using Ar/O_2 gas mixture (1:1), large number of outgrowth process has a drastic effect on the microstructure of the films. Increase in O_2 partial pressure increases the number of negative ions ($O-, O_2-$) generated in the plasma [61]. These negative species are accelerated away from the target towards the substrate kept at a positive potential. Spatial variation in the film composition results due to negative ion backsputtering, and hence, the quality of the film is affected as seen in the present study. Films deposited at higher O_2 partial pressure have yielded films with slightly lesser thickness ($\approx$ 60 nm) as compared to that of (70 nm) grown using lower oxygen partial pressure. This shows that the sputtering rate is reduced with increase in oxygen partial pressure. Films grown to thicknesses of the order of 100-200 nm resulted in extremely large rough surfaces.

4.3.7 Y-123 Films on YSZ Buffered Sapphire Substrate

YSZ buffered sapphire substrates grown using the above six different growth conditions were used for the deposition of $Y-123$ thin films using PLD. It has reported earlier that addition of 5 wt% Ag to $Y-123$ superconductor dramatically improved the microstructure, J_c and microwave surface resistance (R_s) compared to pure $Y-123$ films [62]. Hence 5 Wt% Ag added $Y-123$ targets were used in this study and hither to, refer $Y-123+5\%Ag$ for simplicity. The growth parameters used for realizing high quality $Y-123+5\%Ag$ films on LAO AND STO [54,55] were optimized earlier ($J_c = 8 \times 10^6 A/cm^2$ at 77 K)

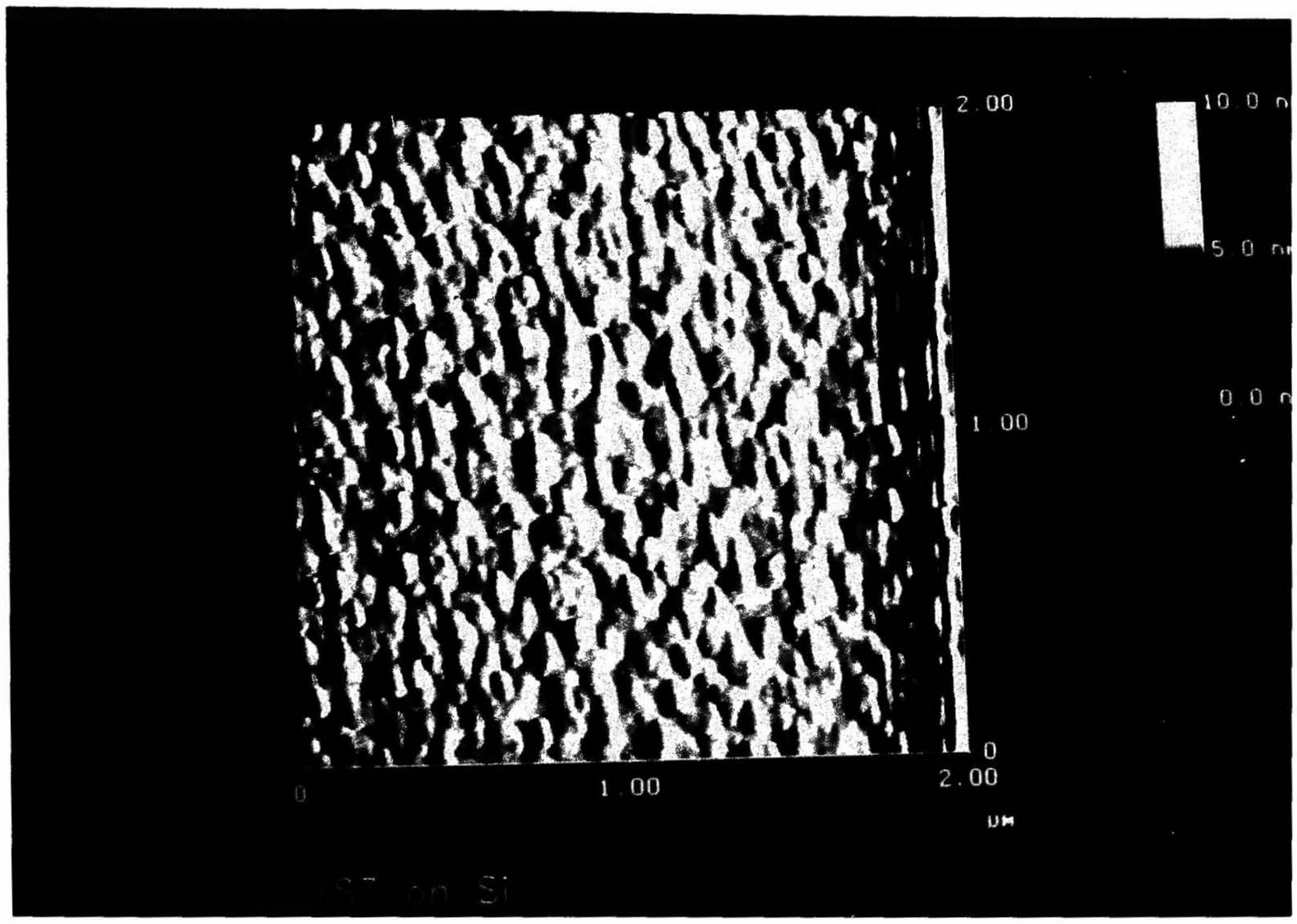

Fig.4.15 (c) AFM image of YSZ buffer layer grown at 20 mTorr (9:1) Ar/O_2 gas mix - the increase in the average surface roughness (=1 nm) is seen as compared to that for films grown using low oxygen partial pressure

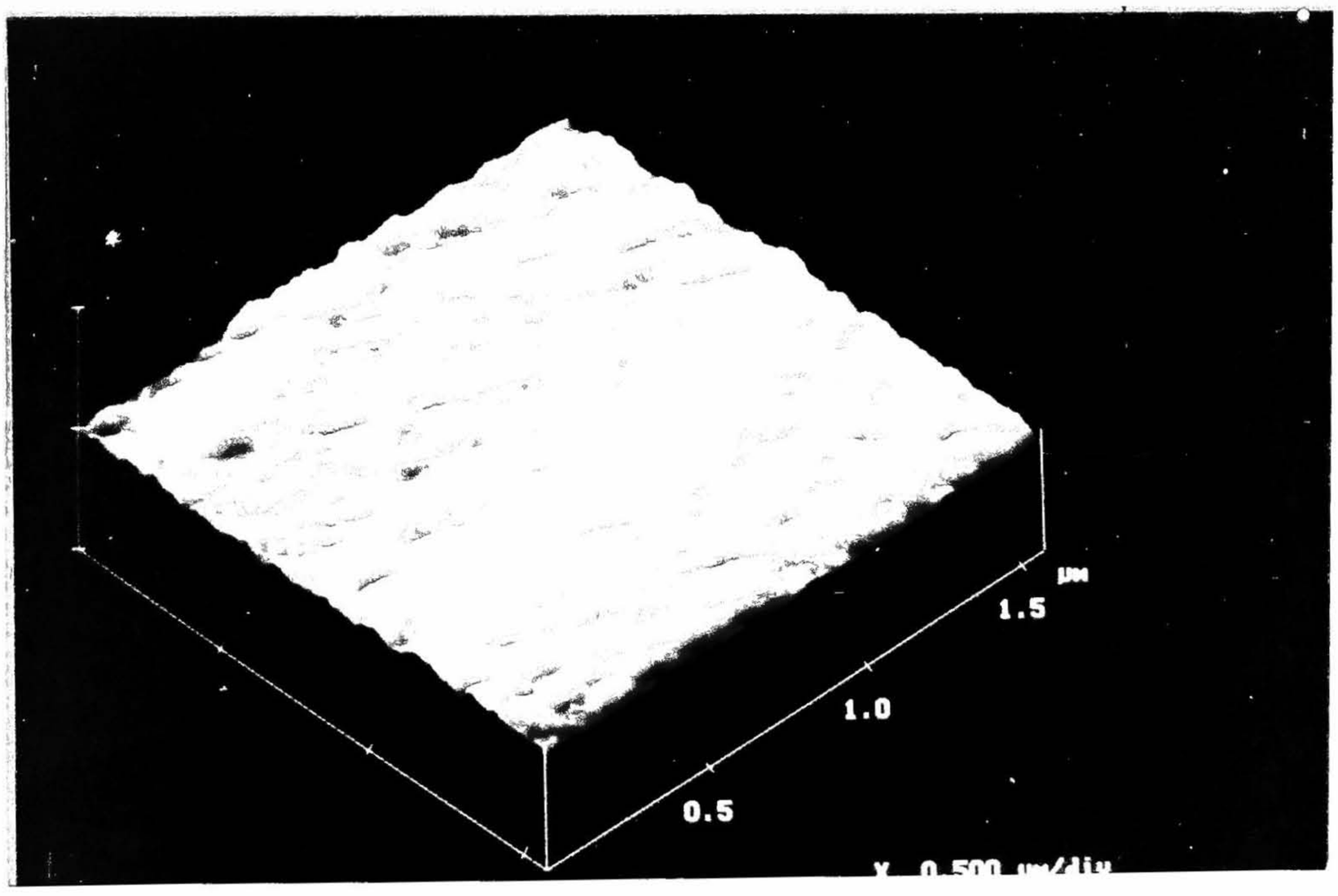

Fig.4.15 (d) a 3D plot of the above AFM image

Table 4.5

Average raoughnes of YSZ films grown on Saphhire deposited at various Sputtring gas pressures.

Sl. No.	Sputtering gas pressure $Ar+O_2$ (9:1) (mTorr)	YSZ Film Thickness (Å)	Scan length (μm)	Average rougness estimated from AFM study (nm)
1a.	5 (9:1)	410	2	0.25
1b.	5 (9:1)	410	8	0.35
2a.	5 (1:1)	385	2	0.34
2b.	5 (1:1)	385	10	0.41
3a.	10 (9:1)	395	2	0.53
3b.	10 (9:1)	395	8	0.63
4a.	10 (1:1)	382	2	0.15
4b.	10 (1:1)	382	8	0.75
5a.	20 (9:1)	386	2	0.37
5b.	20 (9:1)	386	10	0.86
6a.	20 (1:1)	373	2	0.29
6b.	20 (9:1)	373	10	0.80

To realize high quality superconducting films on a YSZ buffered sapphire substrate, it is very important that the surface morphology of the YSZ buffer layer be very smooth to facilitate the growth of highly textured superconducting films. The fact that lattice parameters of $Y-123$ (0.382 - 0.388 nm) and YSZ (0.513 - 0.518 nm) are quite different, good crystalline growth of films results only when the diagonal of the ab-plane of the $Y-123$ film grows along the YSZ axes, i.e., azimuthal rotation by 45° of the $Y-123$ ab-plane with respect to YSZ a-axis as shown in Fig.4.16. Even in such a configuration, there exists a lattice mismatch (5%) between $Y-123$ and YSZ as compared to substrates with lesser lattice mismatch viz LAO (3%) and STO (1.2%).

XRD shows c-axis oriented $Y-123$ film growth in all the cases. Fig.4.17 shows the XRD traces of $Y-123$ films insitu grown on sapphire with YSZ buffers grown using the sputtering parameters : 10 mTorr (9:1) and 5 mTorr (1:1). FWHM of $< 005 >$ reflection for 5 mTorr (9:1) is 0.3° which is indicative of good crystallinity of the films. Similarly, FWHM of $< 005 >$ reflections of the films grown on buffers using 10 mTorr pressure are comparatively good (0.32 - 0.4). On the other hand, $Y-123$ film deposited on the buffer grown using sputtering conditions 20 mTorr (1:1) shows the highest FWHM value of 0.48. Further microstructure differs markedly for $Y-123$ films deposited on buffer layers grown using different growth parameters. Figures 4.18a & 4.18b show the microstructure of $Y-123+5\%Ag$ films grown on the buffer layer with very smooth surface morphology obtained using the growth conditions of 5 mTorr sputtering pressure and 9:1 gas mixture ratio. The microstructure appears similar to that observed on the $Y-123+5\%Ag$ films grown on LAO substrates that yielded high J_c. This indicates that the base film YSZ, which acquired smooth surface morphology, must have facilitated easy alignment of the $Y-123$ ab-axis diagonal with the a-axis of YSZ. In a similar way, $Y-123-Ag$ films deposited on buffer layers grown using a $Ar/O2$ gas mixture of 9:1 and chamber pressures 10 mTorr (Fig.4.18c) and 20 mTorr have resulted in similar grain structure growth, although the average surface roughness in these cases is higher. However, films deposited on buffer layers grown with higher oxygen ratio (1:1) have shown no proper grain structure and the surface morphology is very rough with the appearance of undesirable voids on the surface as can be seen in Fig. 4.18d.

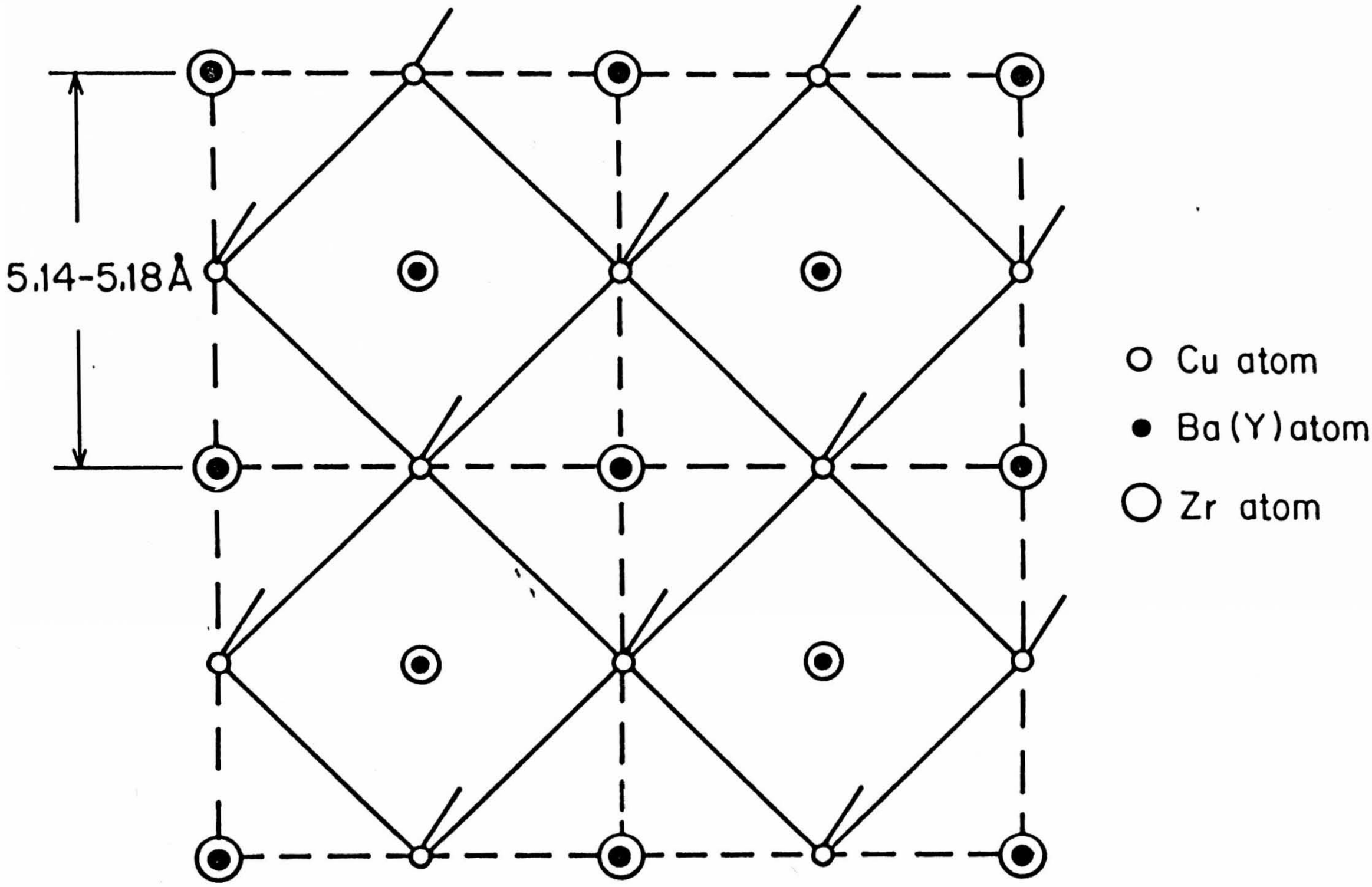

Fig.4.16. YSZ has a cubic structure [a≈0.514-0.518 nm]. Good crystalline growth of YBCO films results only when the diagonal of a-b plane of the films grows along the YSZ axis; i.e. azimuthal rotation (by 45° of the YBCO a-b plane with respect to YSZ a-axis).

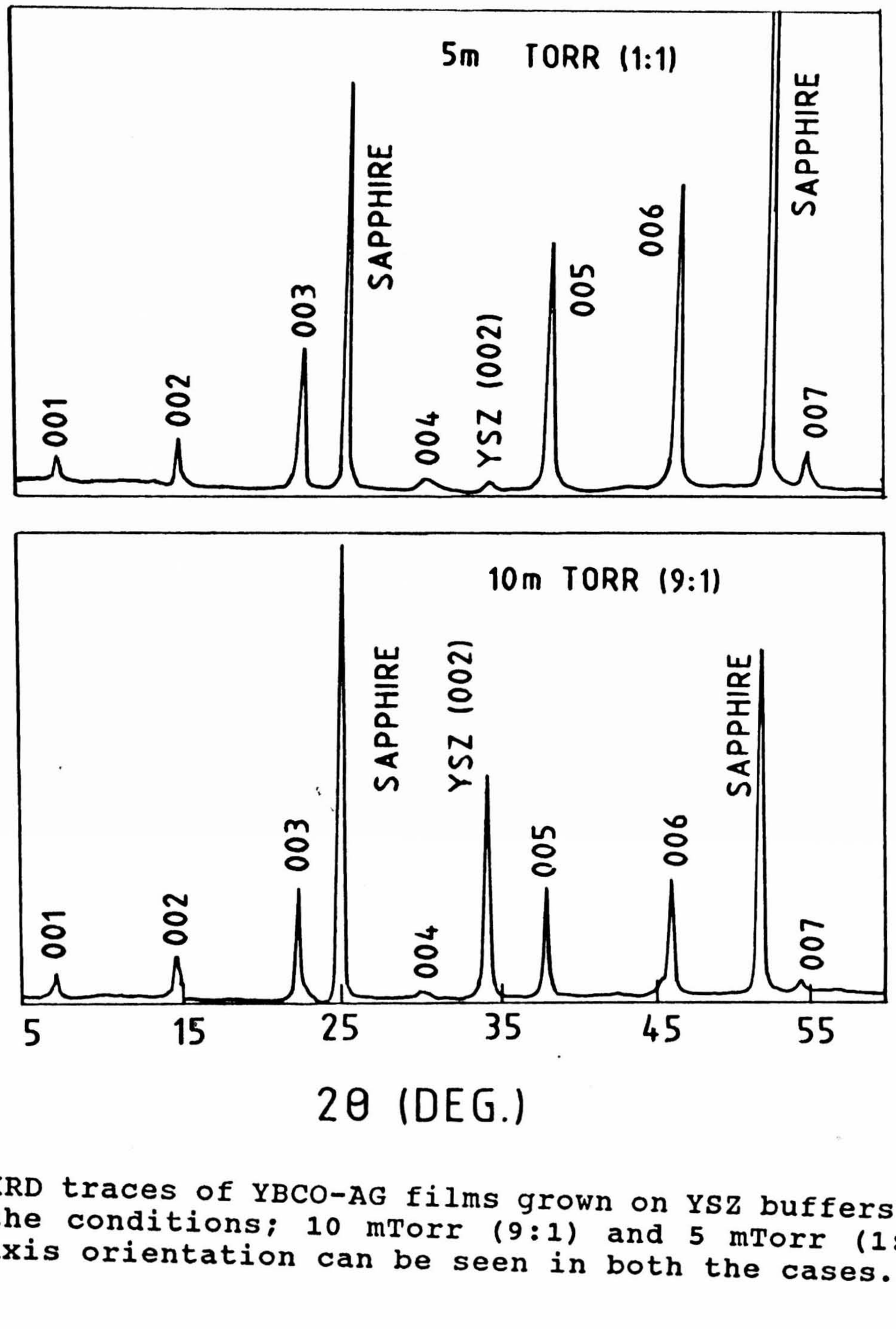

Fig.4.17. XRD traces of YBCO-AG films grown on YSZ buffers using the conditions; 10 mTorr (9:1) and 5 mTorr (1:1) c-axis orientation can be seen in both the cases.

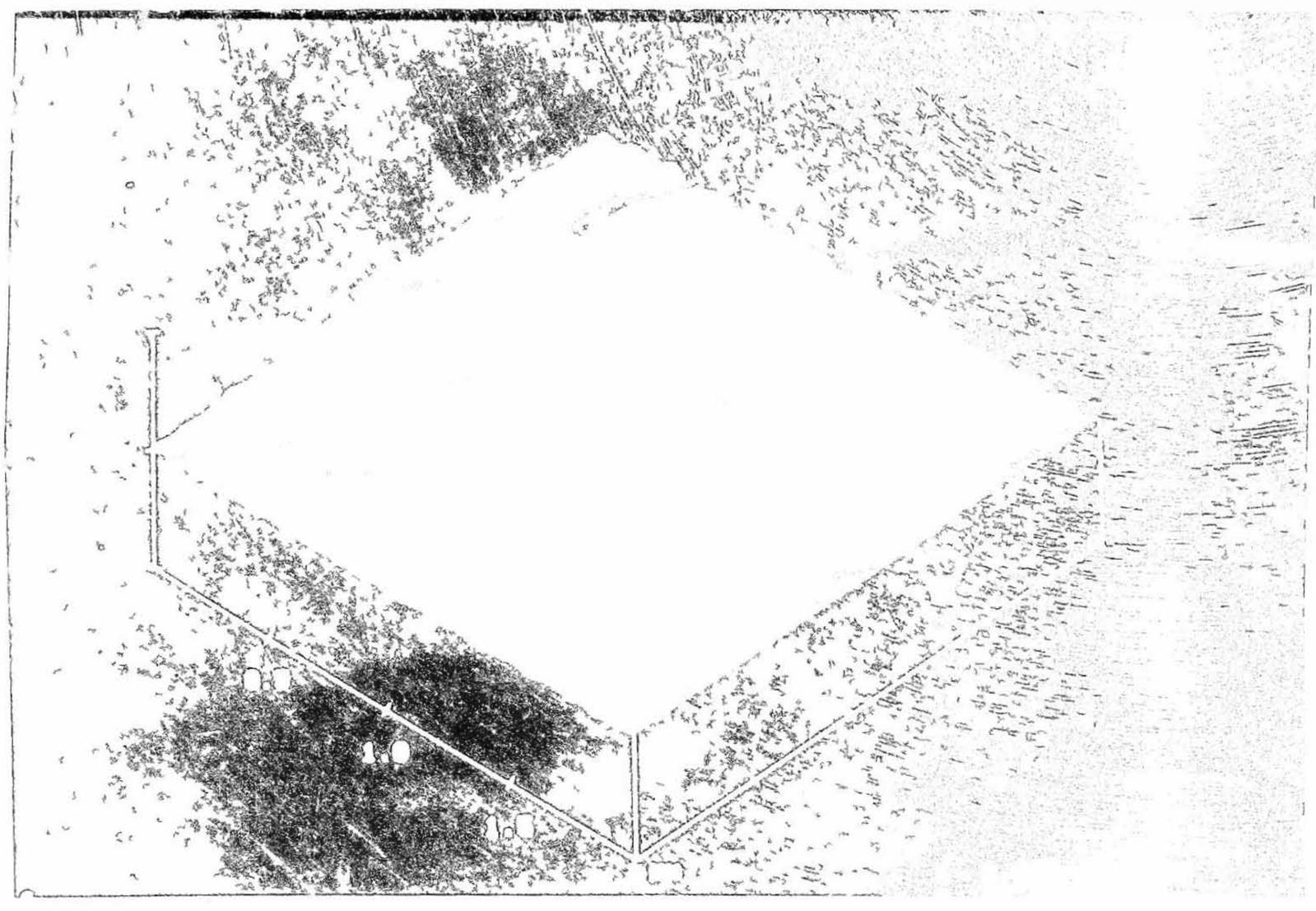
1.0

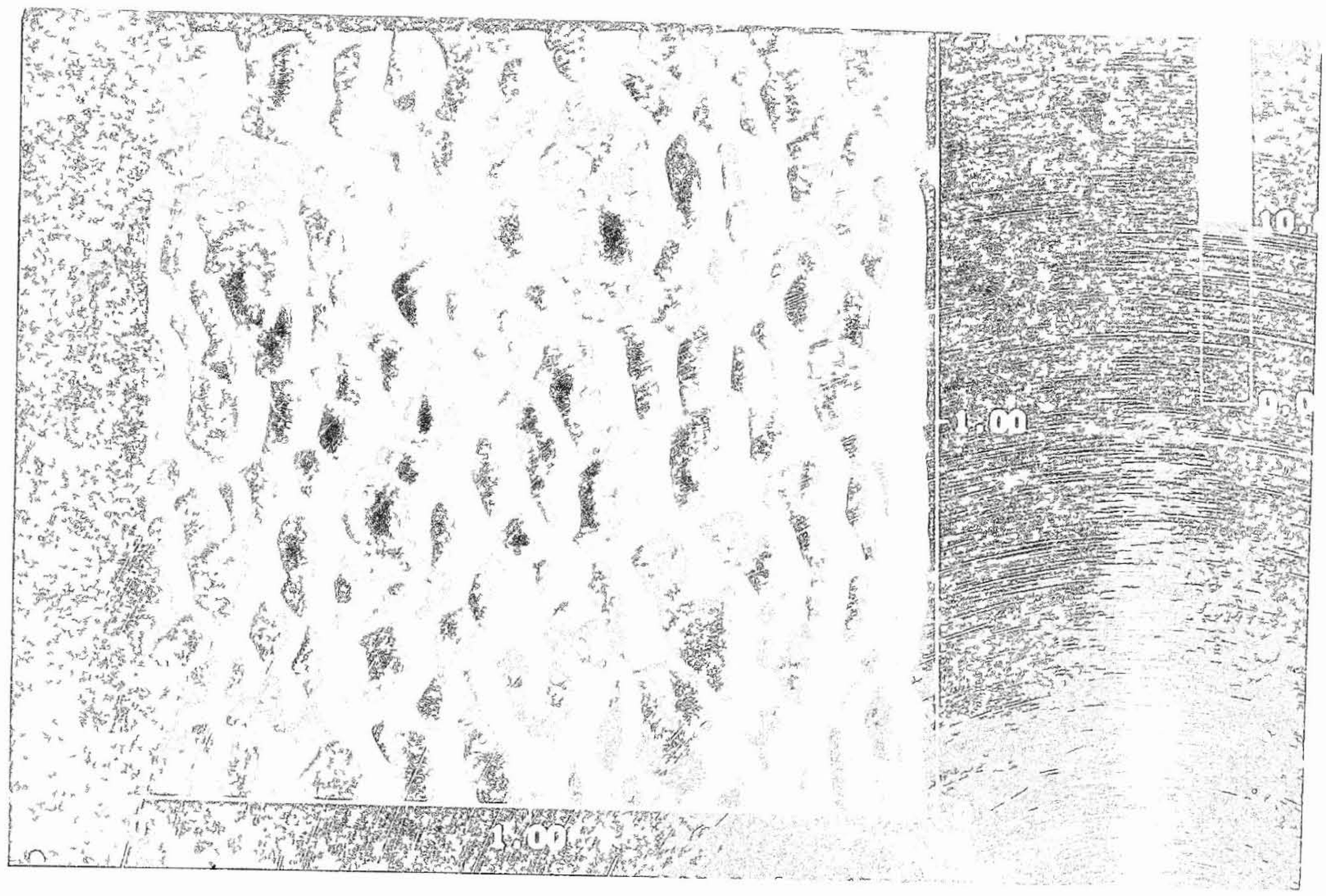
1.00
1.00

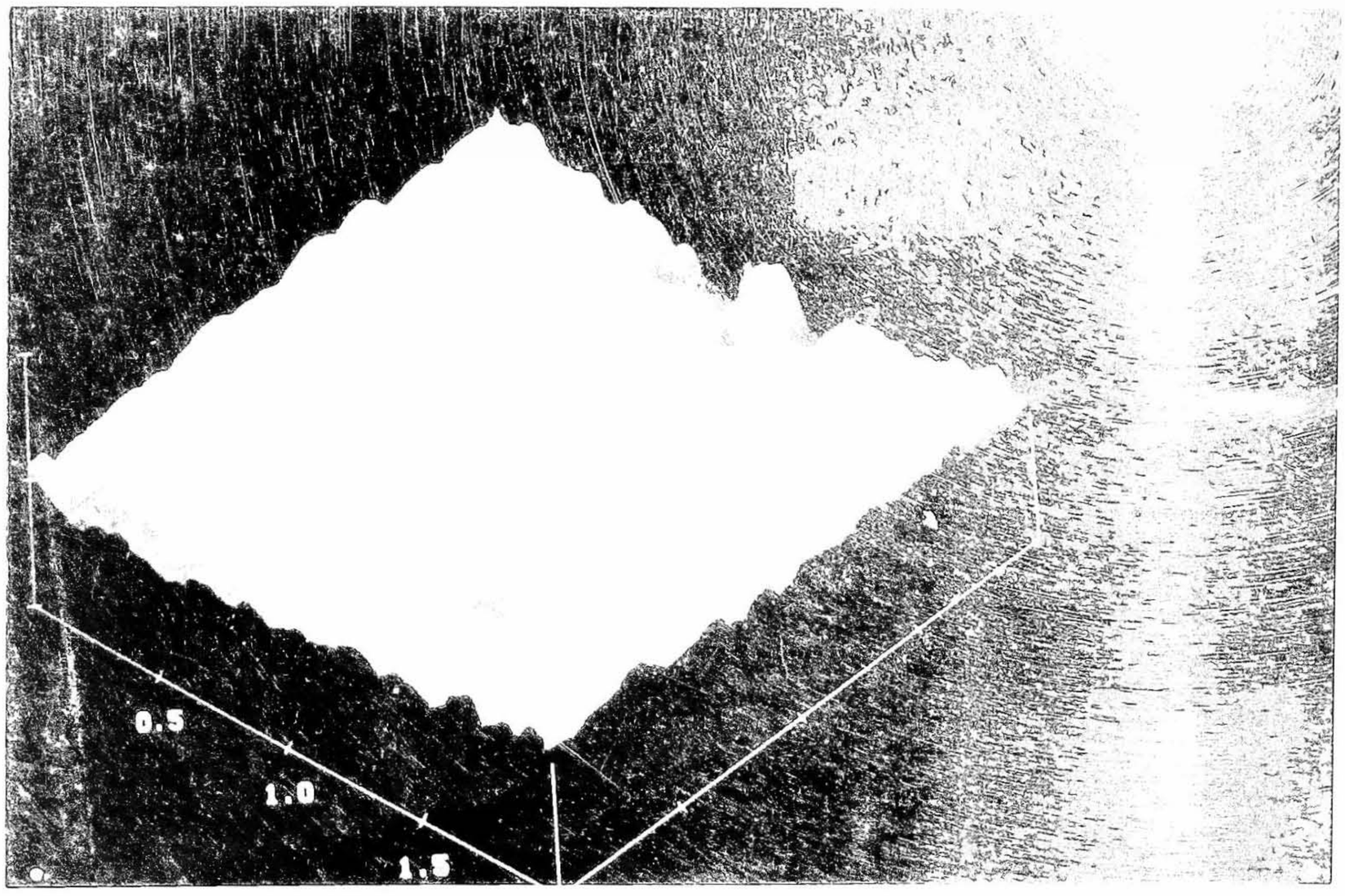
0.5
1.0
1.5

4.3.8 T_c and J_c Measurements

Although, $T_c(= K)$ has been found to be constant in all the cases, films deposited at higher oxygen ratios (1:1) have shown higher R_{300K}, large transition width ΔT_c = 3 - 4 K and higher residual resistance R_o ($\approx$ 4.4 ohms), compared to those of films deposited on buffer layers grown using lower oxygen ratios (9:1) as shown in Fig.4.19. Table 4.6 gives summary of the results of Y-123 films deposited on YSZ buffered sapphire. Highest $J_c = 4.5 \times 10^6 A/cm^2$ at 77 K has been realized on YSZ buffered sapphire grown using 5 mTorr (9:1) sputtering conditions. This is, by far, the highest J_c reported on $Y-123$ films deposited on YSZ buffered sapphire substrates [51,52]. Critical current densities of the $Y-123+5\%Ag$ films deposited on buffer layers grown using other parameters are inferior compared to that realized on buffer layer grown with optimized parameters (5 mTorr 9:1 Ar/O_2). This shows the direct correlation of microstructure and J_c.

Superconductor-normal metal-superconductor (S-N-S) model proposed by DeGennes [63] and Clarke [64] gives a good account of the quality of of the superconducting films with respect to estimating the grain boundary widths which limit the J_c values. This model has been extensively used in understanding and judging the quality of the films in our previous studies (Chapter 2). The nature of the grain boundary separating the individual grain in general is the superconductor itself with inferior superconducting grains these grain boundaries act as metallic regions thereby forming superconductor-normal metal- supeconductor (SNS) junctions. However, at lower temperatures these weakly-superconducting grain boundary regions do not offer much resistance to higher current flow as they become fully superconducting. On the other hand, when the grain boundary volume is very small the current tunneling by proximity effect improves and it is possible to realize high J_c values even at temperatures close to T_c.

It is shown in Chapter 3.that J_c is proportional to $(T_c - T)^2$ for S-N-S type junctions. Near T_c the equation that governs the S-N-S type junction is

$$J_c \propto (T_c - T)^2 \exp(-d/\xi_N)$$

or

$$\sqrt{J_c} \propto (T_c - T) \exp\{(-1/2)d/\xi_N\}$$

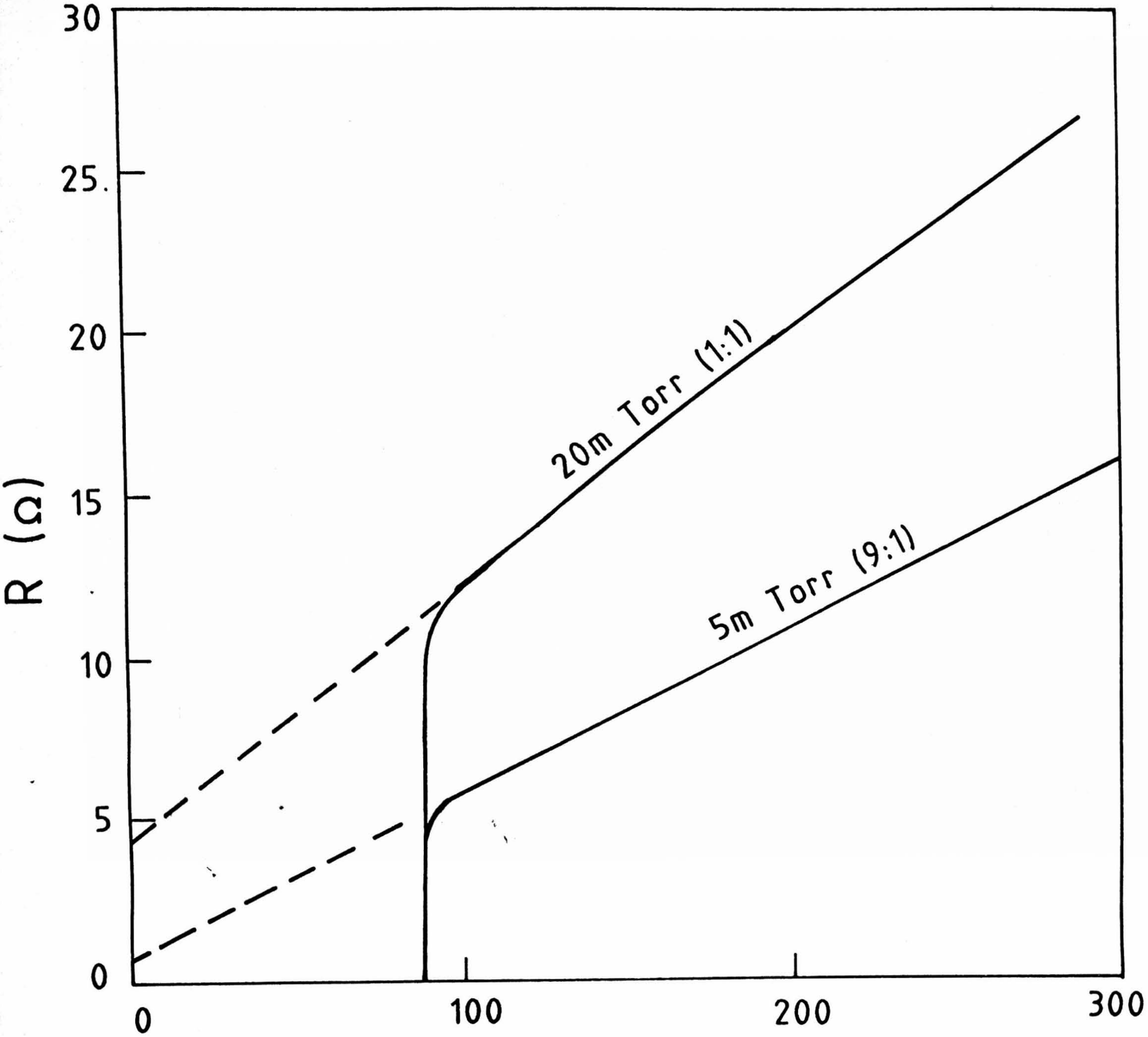

Fig.4.19. R-T plot of YBCO-AG deposited on YSZ buffer grown using 2 different conditions 5 mTorr (9:1) and 20 mTorr (1:1).

Table 4.6
Best Results of Y-123 films deposited on YSZ buffer sapphira

Sl. No.	YSZ deposition condition	YSA buffer thickness Å	Y-123 film thickness Å	ρ_{300} T_c mΩ	T_c(K) T_c on set	T_{co}	ΔT	Residual Resistance R_o	J_c at 77 K (A/cm^2)
1.	5 mTorr (9:1)	410	992	0.282	90.5	88.7	1.8	0.982	1.80×10^6
		816	1020	0.355	90.2	87.1	2.12	1.453	0.8×10^6
2.	5 mTorr (1:1)	385	1006	0.326	89.8	87.6	2.21	2.562	1.2×10^6
3.	10 mTorr (9:1)	395	994	0.368	89.4	88.5	0.90	0.959	1.30×10^6
4.	10 mTorr (1:1)	382	985	0.387	84.1	87.6	1.53	1.757	0.72×10^6
5.	10 mTorr (9:1)	386	970	0.398	89.2	86.8	2.45	2.438	0.94×10^6
6.	20 mTorr (1:1)	373	945	0.424	89.0	86.8	2.17	4.478	0.68×10^6
7.	5 mTorr (9:1)	408	5% Agopted Y-123 film 982 Å	0.181	90.4	89.1	1.24	0.752	4.51×10^6

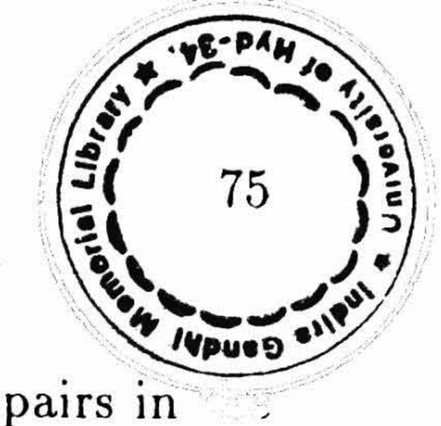

where d is the grain boundary width and ξ_N^{-1} is the decay length of Cooper pairs in grain boundary (N) region. Considering the S-N-S type of coupling between the grains, K, is given by

$$\xi_N = (\hbar D_N / 2\pi K_B T)^{1/2}$$

Where D_N is the diffusion coefficient and is the coherence length in normal region.

At lower temperatures, when N becomes fully superconducting, K becomes large and higher currents can flow through the junction. A straight line plot of $\sqrt{J_c}$ vs. $(T_c - T)$, which goes through the origin, shows that the coupling between superconducting grains is S-N-S like at temperatures few Kelvin below the transition temperatures. Slope of $\sqrt{J_c}$ vs. $(T_c - T)$ plot which is an inverse exponential function of a gives an estimate of the grain boundary width.

Fig.4.20 shows $\sqrt{J_c}$ vs. $(T_c - T)$ plots of $Y - 123 + 5\%Ag$ films deposited on buffer layers grown using optimized parameters [5 mTorr 9:1].Films with highest J_c, also give the highest slope. An increase in slope indicates decrease in grain boundary width, which is also evident from the microstructural study. A systematic decrease in the slope values for films deposited on buffer layers grown at different conditions shows the versatility of this model in estimating the film quality. These results again corroborate very well with the microstructural study [65].

4.3.9 $SrTiO_3$ Buffer Layers

$SrTiO_3$ (STO) buffer layer were deposited by RF magnetron sputtering on Sapphire substrate at 700 and 800°C. Fig.4.21a and b shows the XRD pattern of STO film deposit at 700 and 800°C on sapphire substrate. Films deposited at 800°C show $< h00 >$ oriented nature as shown in figure 4.21b, and films deposited at 700°C show other orientations $< 110 >$ along with $< h00 >$ orientations (Fig.4.21a). The STO epitaxy is found to increase with the substrate temperature. The crystallinity of the films deposited at 800°C is observed to be the highest. AFM pictures of STO films deposited at 5 mTorr ($Ar + O_2$) and 10 mTorr are shown in Fig.4.22a,b, respectively. These pictures clearly indicates that films deposited at 5 mTorr show better surface microstructural properties

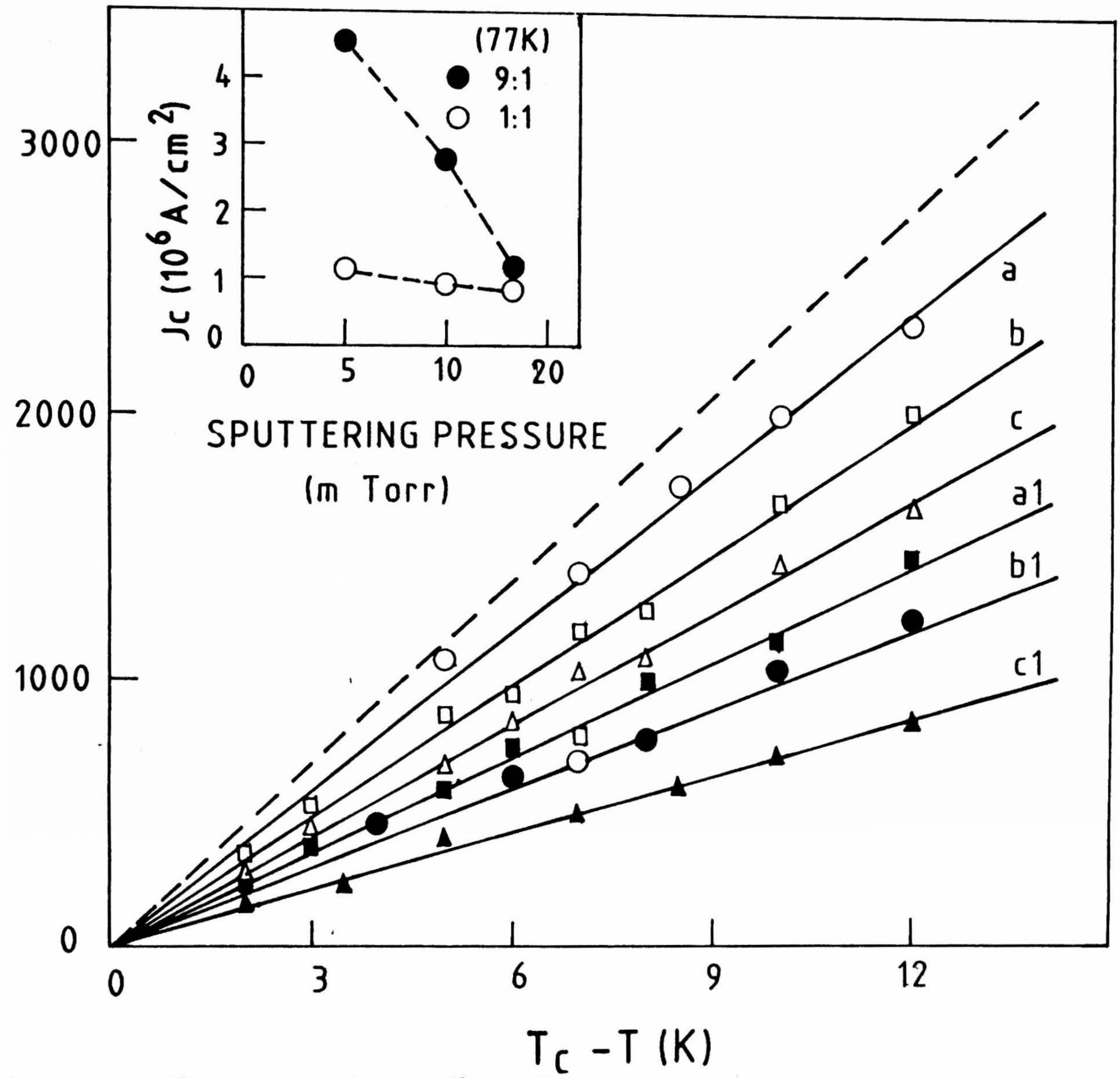

Fig.4.20. $(J_c)^{½}$ Vs T_c-T plots of YBCO-AG films grown on YSZ buffer layers grown using different growth conditions; (a) 5 mTorr (9:1); (a'): 5 mTorr (1:1); (b) 10 mTorr (9:1); (b'): 10mTorr (1:1); (c) 20 mTorr (9:1); (c'): 20 mTorr (1:1) YBCO-AG films deposited on YSZ buffer layers grown with optimized conditions 5 mTorr (9:1) have yielded the highest $J_c \approx 4.5 \times 10^6$ Acm^{-2} @ 77K (see inset) and highest slope as compared to others which means a much reduced grain boundary width. Dashed line shows the plot of YBCO-AG film grown on LAO for comparison.

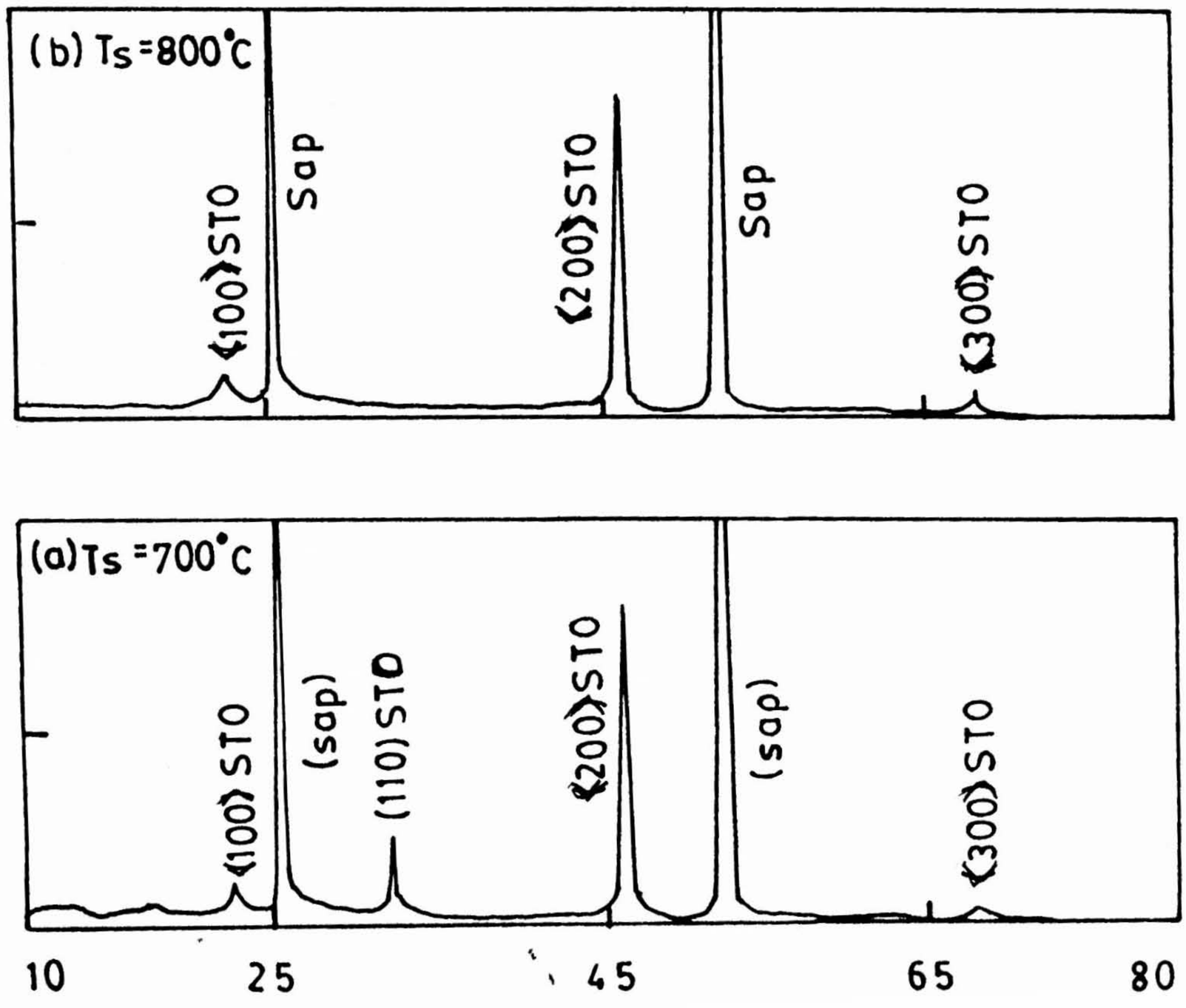

Fig.4.21. XRD patterns of $SrTiO_3$ films deposited on Sapphire substrates at (a) 700°C and (b) 800°C temperature.

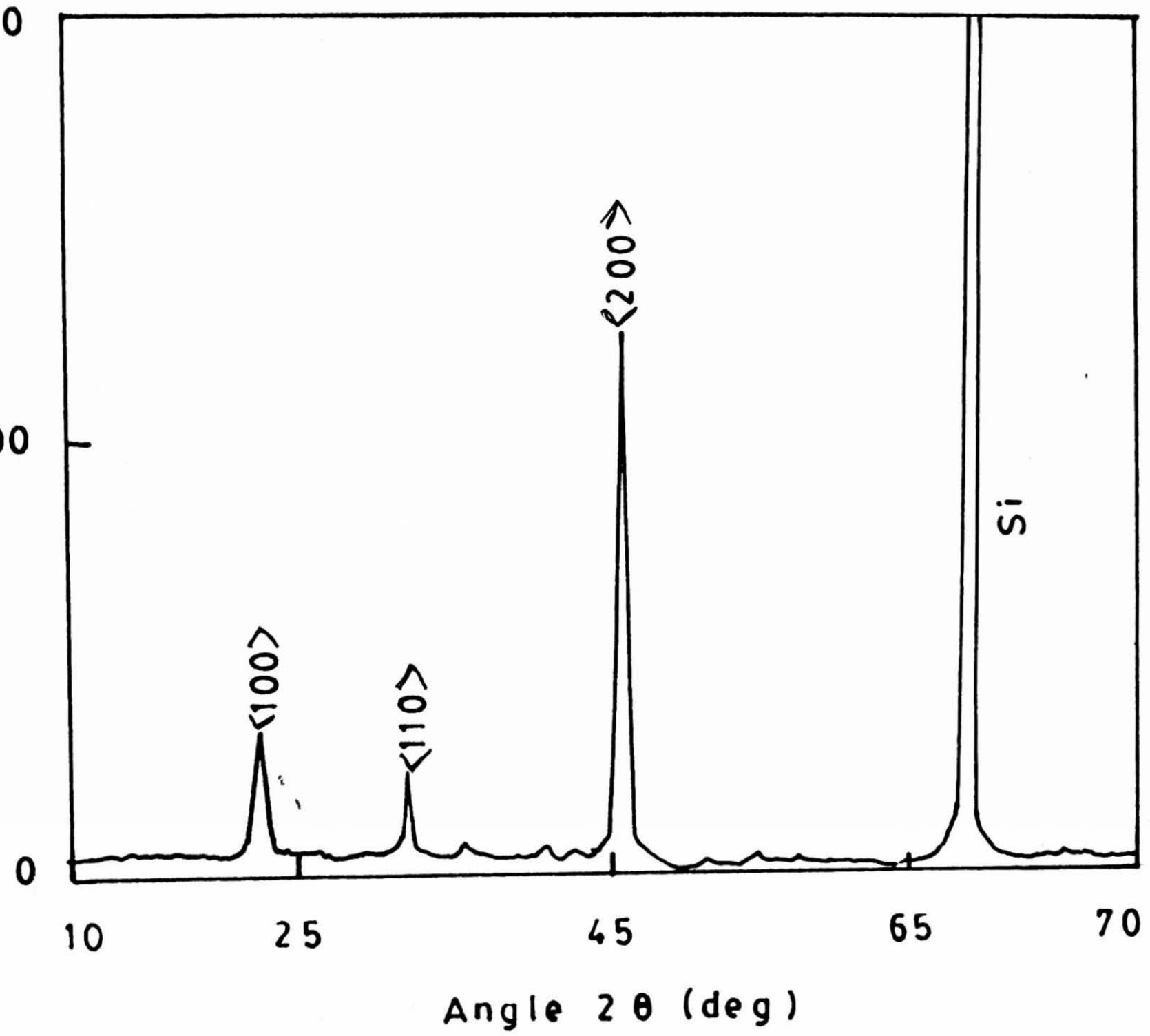

Fig.4.22. $SrTiO_3$ films on Si <100> deposited at 800°C and at 5 mTorr Ar+O_2 gas mix in 9:1 ratio.

i.e, smooth surface, whereas the films deposited at 10 mTorr show increased surface roughness and poor quality microstructure as seen from AFM photographs. The average roughnesses estimated from AFM studies are 0.28 nm and 0.4 nm for film thicknesses of 500 $\mathring{A}$.

$Y-123$ films were deposited on STO buffered saphhire substrates using the PLD method. Buffer thicknesses used were 50 nm and 100 nm. $Y-123$ film deposited on the 50 nm buffer layer has a T_c of 87 K and $J_c = 1.2 \times 10^6 A/cm^2$ at 77 K.

STO films deposited on Si substrate at $800°C$ resulted in single phase but polycrystalline films. This may be due to a large lattice and thermal expansion coefficent mismatch between Si and STO buffer layer. The XRD of a typical STO film deposited on Si at $800°C$ is shown in Fig.4.23. Table 4.7 shows the results of $Y-123$ films deposited on STO buffered Si and sapphire substrates. Fig.4.24a,b shows $Y-123$ thin films deposited on STO buffered Si and Sapphire substrates, respectively. The XRD of both the films show these to be strongly c-axis oriented. But $Y-123$ film deposited on Sapphire buffered with STO has better crystalline quality than that of the film deposited on STO buffered Si as indicated by the FWHM values for the $< 006 >$ reflections of $Y-123$ deposited on Saphhire and Si are 0.27° and 0.59° respectively. The $R-T$ curves of $Y-123$ thin films deposited on STO buffered Sapphire and Si substrates are shown in Fig.4.25. T_c obtained in either of films are similar.

From these studies it is clear that good crystalline and almost epitaxial of films STO films can be deposited at 5 mTorr and $800°C$ on sapphire substrate and it is difficult to grow $< h00 >$ oriented STO films on Si.

4.4 Conclusions

In conclusion, the effect of growth conditions on the micro-structure of YSZ buffer layer for realizing high quality $Y-123$ superconducting thin films on Si and Sapphire substrates. At the same time, the growth conditions for STO buffer layer were optimized on Sapphire substrate only. $Y-123$ films were deposited on the YSZ/STO buffered Si or sapphire substrates. Some important results of these studies were mentioned below.

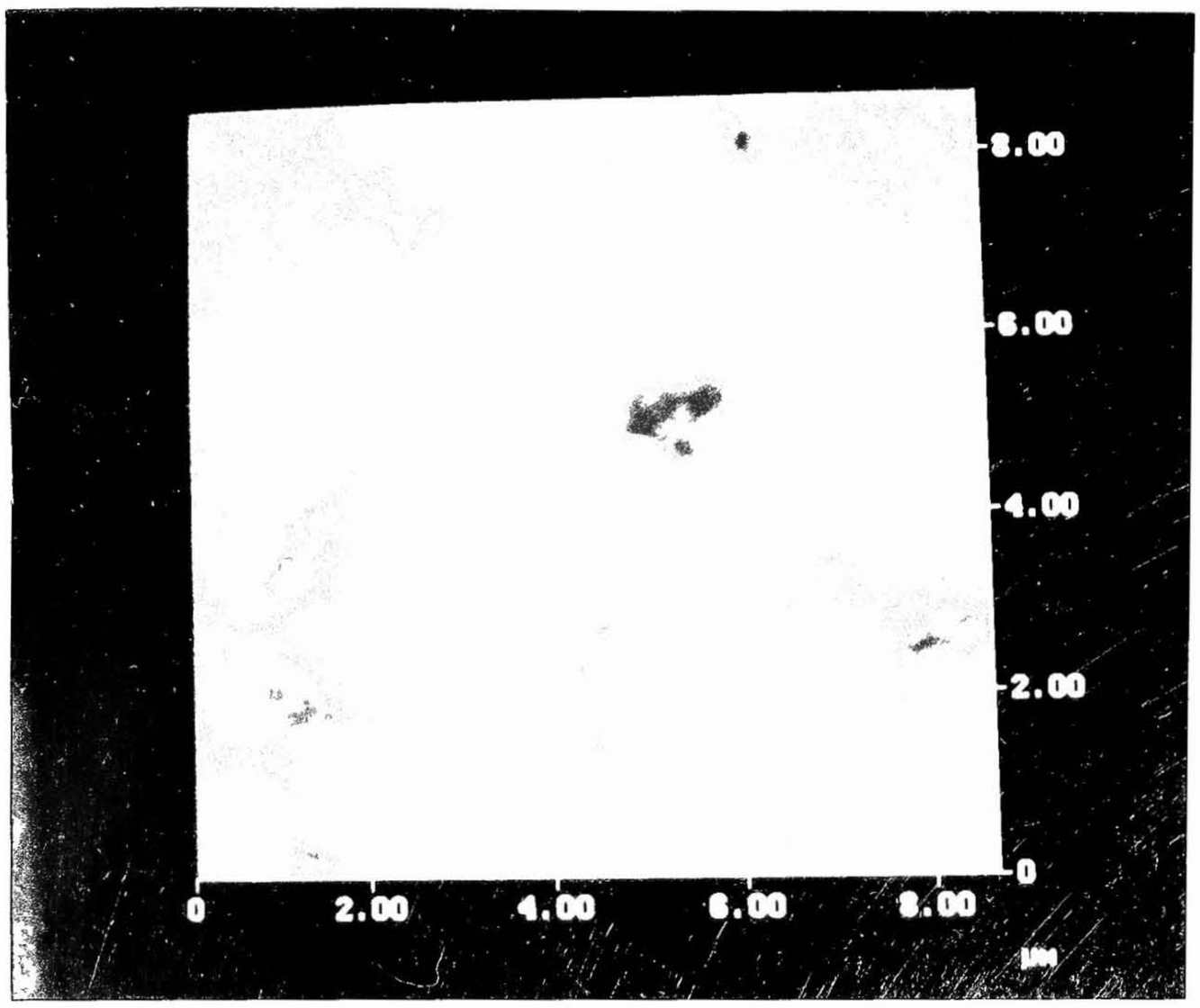

Fig. 1. (a):

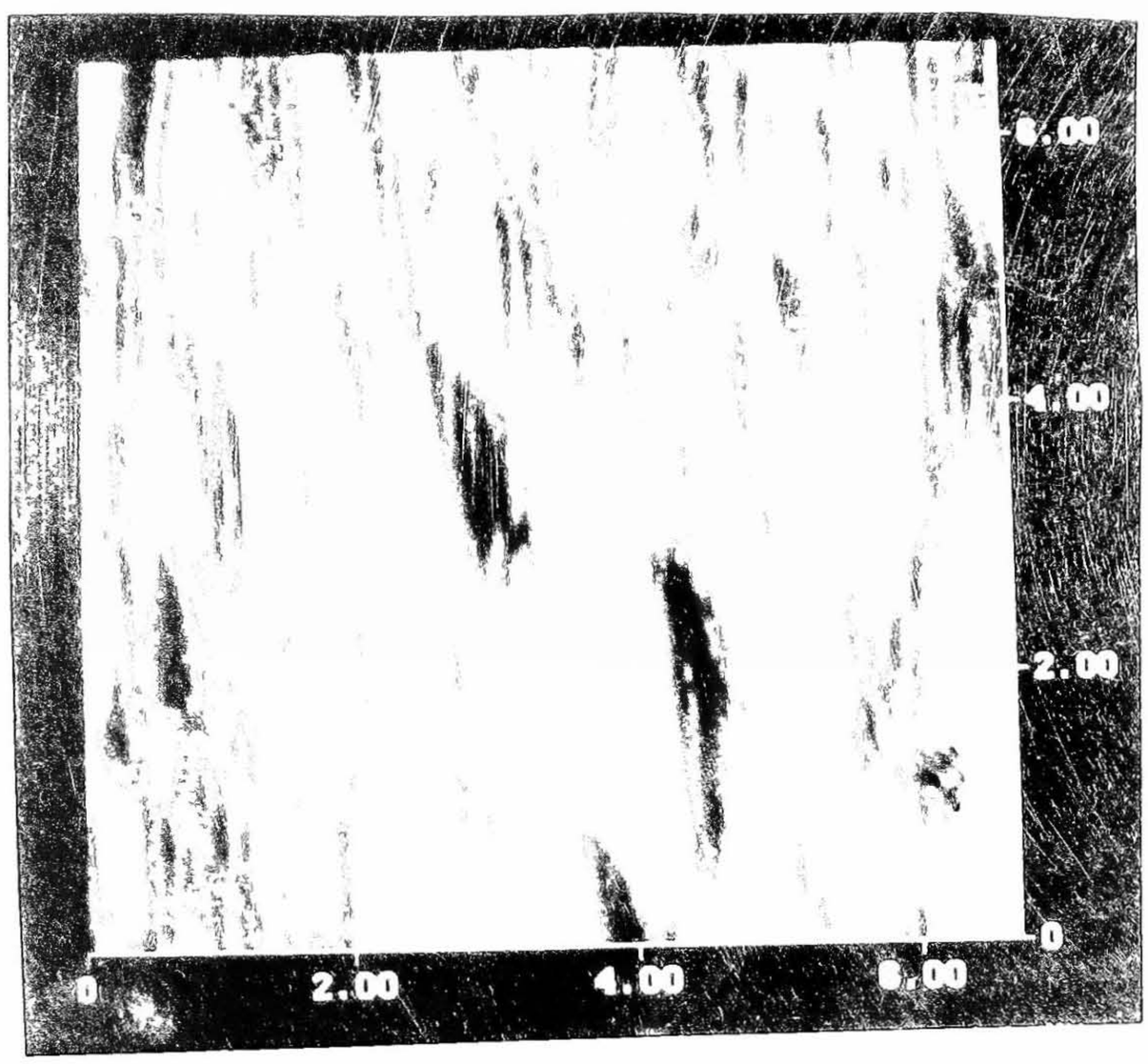

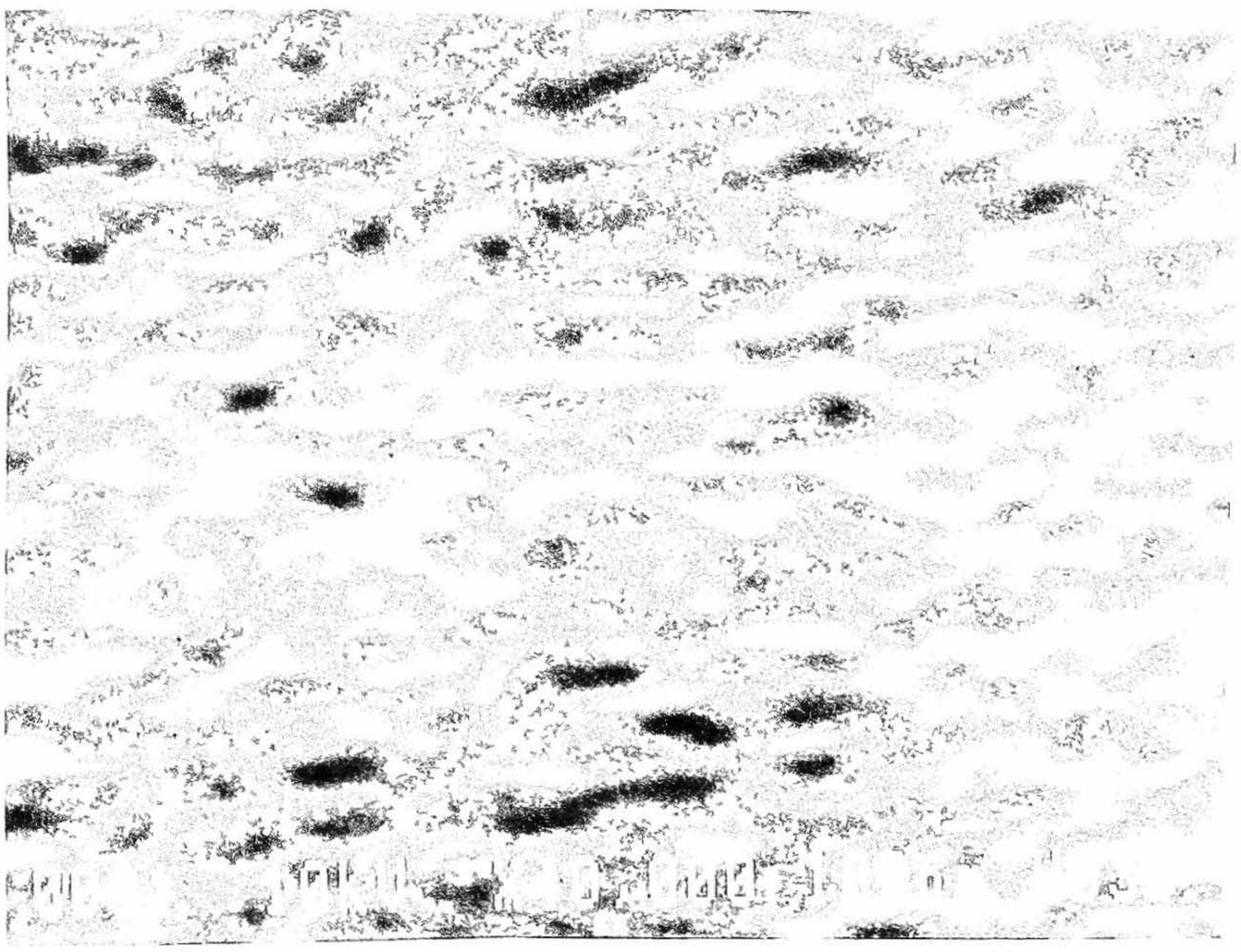

Fig. 1.

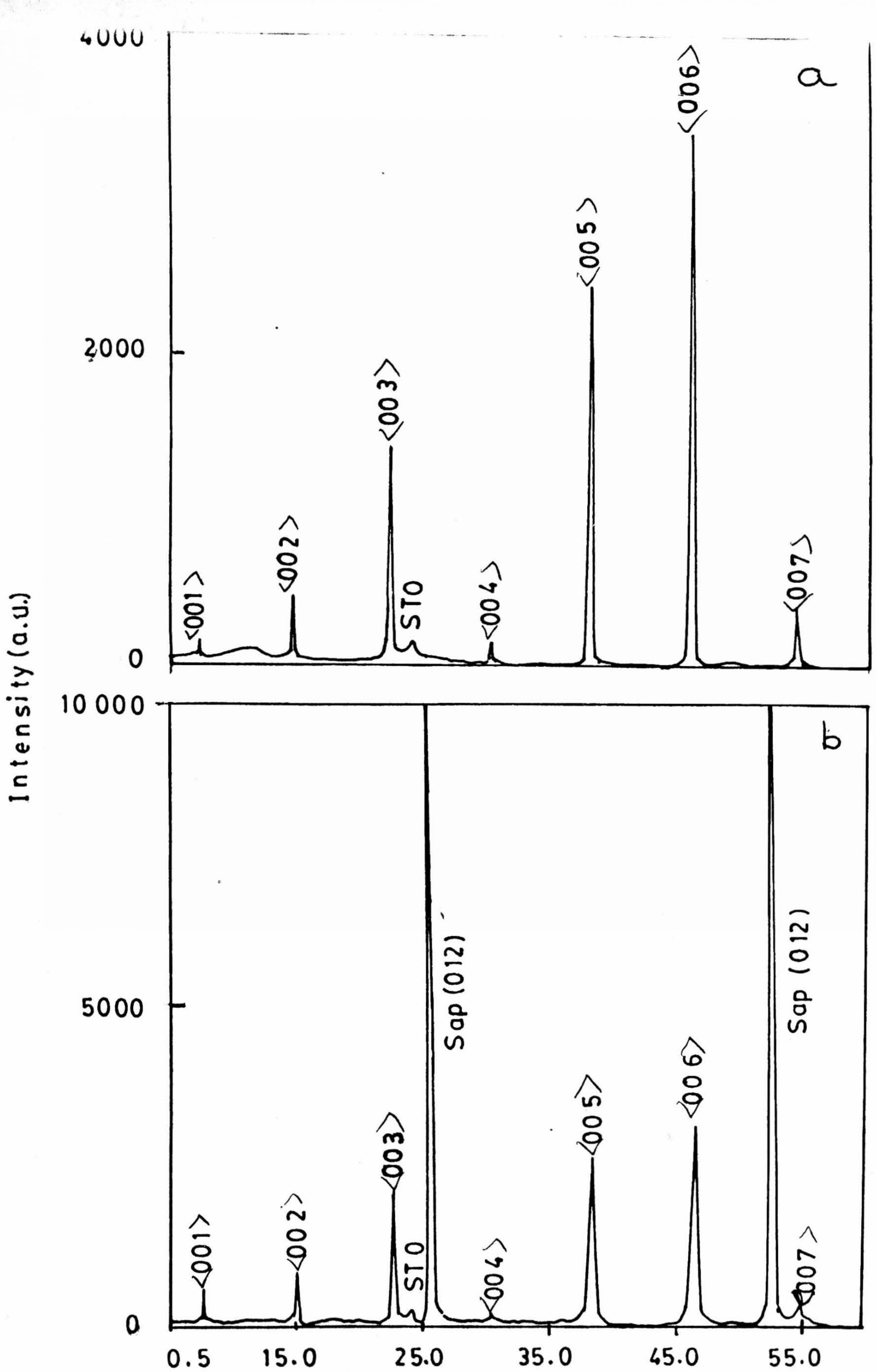

Fig.4.24. XRD pattern of Y-123 deposited on (a) Si <100> and (b) Sapphire substrates buffered with $SrTiO_3$ films.

Table 4.7
Summarized results on STO Buffer layers

Sl. No.	Substrate	Sputtering gas pressure $Ar+O_2$ (9:1) (mTorr)	STO Film Thickness (Å)	Scan length (μm)	Average rougness estimated from AFM study (nm)	Y=123 film thickness Å	Resistivity ρ_{300} cm	T_{co} (K)	J_c at 77 K Å/cm^2
1	Sapphire	5 (9:1)	506	2	0.29	~1000	0.273	88.23	1.3×10^6
				10	0.45				
2	" "	5 (1:1)	975	2	0.42	~1020	0.443	87.18	0.9×10^6
				8	0.63				
3	" "	10 (9:1)	488	2	0.39	~980	0.382	86.80	0.8×10^6
				7	0.40				
4	Si	5 (9:1)	522	2	0.31	~972	0.521	88.00	0.8×10^6
				10	0.46				
5	Si	5 (1:1)	994	2	0.63	~1082	0.973	—	0.4×10^6
				10	0.93				

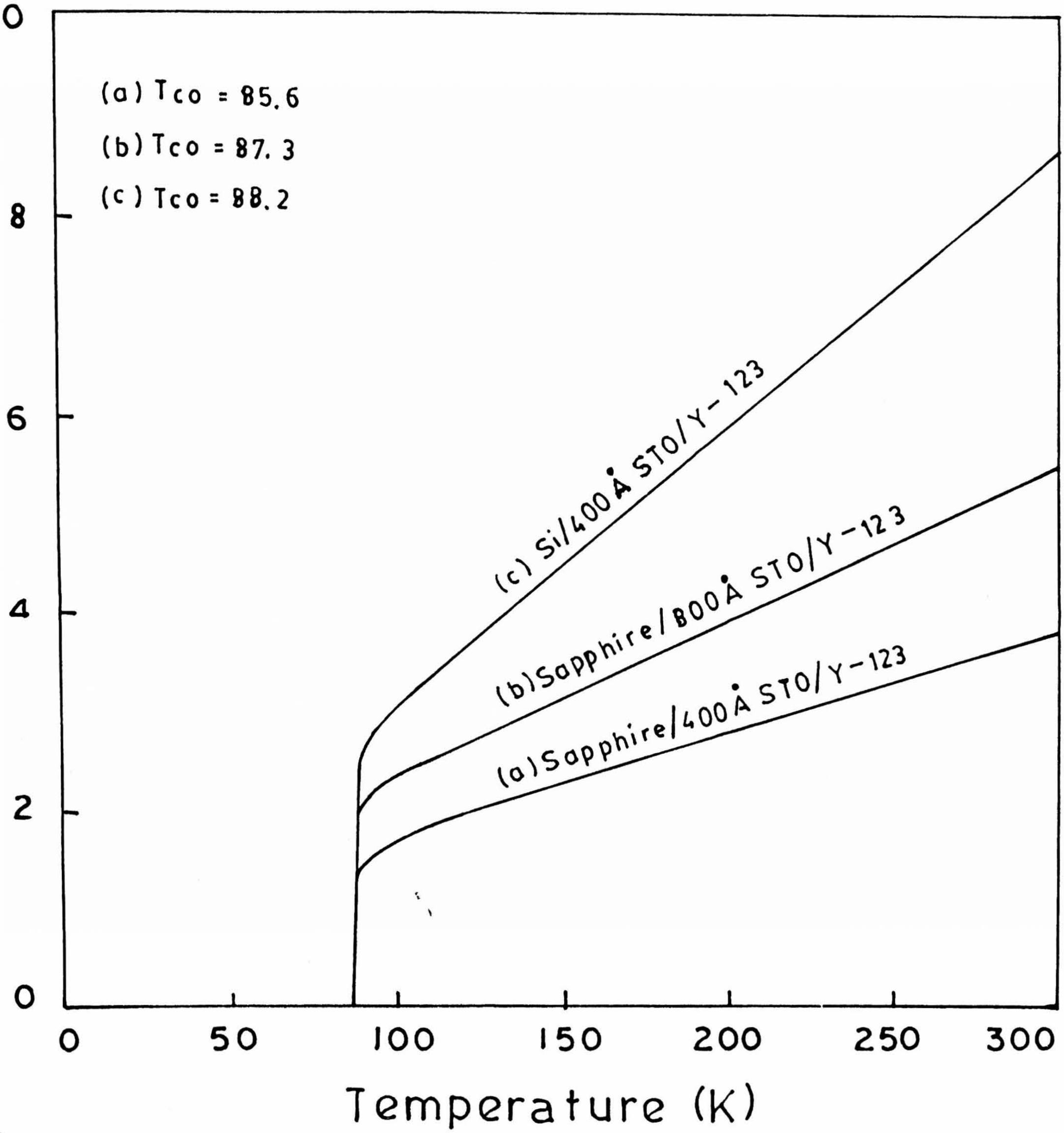

Fig.4.25. R-T plots of (a) Sapphire buffered with 400Å $SrTiO_3$ film; (b) Sapphire buffered with 800Å $SrTiO_3$ films and (c) Si <100> buffered with 400Å $SrTiO_3$

1. A substrate temperature of $800°C$ and 10 mTorr $Ar + O_2$ gas in the 9:1 ratio were the optimized conditions on Si for growing YSZ films with smooth microstructural surface.

2. Above 10 mTorr sputtering gas pressure columnar growth is unavoidable which degrades the T_c and J_c of $Y-123$ thin film deposited on these buffer layer.

3. The thickness of the buffer layer should be around $500A$ and total thickness of buffer layer and $Y-123$ should be preferably below $1500\mathring{A}$ favors high T_c and J_c.

4. Above $500A$ thickness of buffer microcracks develops in thermal cycling due to the large coefficient of thermal expansion mismatch exists.

5. The best T_c and J_c values obtained for $Y-123+5\%\ Ag$ doped films deposited on YSZ buffered Si were 86 K and 1×10^6 A/cm ^{2} at 77 K. Whereas undoped $Y-123$ has a T_c of 86 K and J_c of 10^5 A/cm^2 at 77 K.

6. It is difficult to deposit $< h00 >$ oriented STO layers on Si $< 100 >$ due to the lattice mismatch between Si and STO.

7. A substrate temperature of 800°C and 5 mTorr partial pressure of $Ar+O_2$ gas in 9:1 ratio has resulted in good quality microstructured YSZ/STO films with an average surface roughness of 0.3 nm and 0.28 nm for YSZ and STO films respectively as estimated from AFM studies.

8. Buffer layer thickness effects the T_c and J_c of the $Y-123$ films deposited on YSZ buffered Sapphire substrate and best quality undoped $Y-123$ thin films have a T_c of 88 K and J_c around $2 \times 10^6 A/cm^2$ at 77 K and silver doped $Y-123$ films have a T_c of 89 K and J_c around $4.5 \times 10^6 A/cm^2$ at 77 K.

9. The buffer layer thickness has no drastic effect on $Y-123$ films in the case of STO films. The best quality $Y-123$ films deposited on STO buffered sapphire have a T_c of 88 K and a J_c of $2 \times 10^6 A/cm^2$ at 77 K.

References

[1] R.W. Simon, High J_c th in films, Superconductor Industry, p.22 (1989).

[2] R.W. Simon High Temperature Superconductor for microelectronics Solid state Technology. vol **32** No.9, P141, September 1989.

[3] G.C Liang , RS. Withers, B. F. Cole, S.M. Garrison, M.E. Johansson, W.S. Ruby and W.G. Lyons. IEE Trans Appl. Supercondu., **3** (1993) 3037.

[4] S. Sridhar, D.H. Wu and W. Kennedy, Phys. Rev. Lett. **63** (1989) 1897.

[5] T. Venkatesan, E.W.Chase, X. D. Wu, A. Inam, C.L. Chang, F.K. Shokooli, Appl. Phys. Lett. **53** (1988) 2263.

[6] R.M. Silver, A.B. Berzin, M. Widman, A.L.De Lozanne ibid Vol **52** (1988) 2263.

[7] J. Tate, P. Berberich, W. Dietsche, H.Kinder, ibid **53** (1988) 925.

[8] A. Mogro-Campero, L.G. Turner, ibid **52** (1988) 1185.

[9] L.A. Tietz, C.B.Carter, D.K. Lathrop, S.E. Russek, R.A. Bubruman and J.R. Michael, J. Mater. Res. **4** (1989) 1072.

[10] J. W. Chen and A.G. Milnes, Ann. Rev. Material Sci., **10** (1980) 157.

[11] J. W. Lee, T. E. Schlesinger, A.K. Stamper, M. Migliuolo, D.W. Greve and D. E. Langhlin, J. Appl. Phys. **64** (1988) 6502.

[12] D. K. Fork, J.B. Boyce, F. A. Ponce, R.I. Johnson, G. B. Anderson, G.A.N. Connell, Julia M. Phillips and T.H. Geballe, Appl. Phys. Lett **57** (1990) 1137.

[13] H. Schmidt, K. Hradil, W. Hosler and W. Wersing, G. Gieres and R.J. Seeback, Appl. Phys. Lett. **59** (1991) 222.

[14] H. Schmidt, K. Hradil, S.M. Garrison, W. Hoster and O.Eibl, Physica C **180** (1991) 34.

[15] K. Char, N. Newman, S. M. Garrison, R. W. Bartor, R.C. Taber, S.S. Laderman and R. D. Jacowitz, Appl. Phys. Lett. **57** (1990) 407.

[16] T. Jeffrey, T. Cheung, Isoris, Gergin, M. Janes and Rager E. Dewames, Appl. Phys. Lett. **60** (1992) 3180.

[17] T.Hirano, M. Ueda, K. Motsui, T. Fujii, K. Sakuto and T. Kobayashi, Japn. J. Appl. Phys. **31** (1992) L1345.

[18] U. Poppe, J. Schubert, R.R. Drons, W. Evens, C.A. Freiburg, W. Reichert, K. Schmidt, W. Sybertz and K. Urban, Solid State commn. **66** (1988) 661.

[19] M. Aslam, Soth R.E, Logothetis E.M, Ager *R*, Mikkor M, Wim W chen J.J and Wenger L.E. 1988 Appl. Phys. Lett. **53** (1988) 153.

[20] W.Y. Lee, J. Salem, V.Lee, T. Huang, Savoy R, Deline .V, and Duran. J, Appl. Phys. Lett. **52** (1988) 2263.

[21] Kus *R* and Janos S, Mod. Phys. Lett B. **3** (1989) 37.

[22] Wittanachchi. S, Patel. S, Kuok H.S. and Shaw P.T. Appl. Phys. Lett. **54** (1989) 578.

[23] Aida. T, Tsukamato A, Imagawa. K, Fukazawa. T, Saito S, Shido. K, Takagi. K and Miyavcchi. K, Jpn. J. Appl. Phys **28** (1989) L635.

[24] T. Venkatesan, Chase. E.W, Wu X.D, Inam A, Chang C.C and Shokoohi F.K, Appl. Phys. Lett. **53** (1988) 243.

[25] Koren G, Polturak E, Fisher B, Cohen D and Kinal G, Appl. Phys. Lett. **53** (1988) 2330.

[26] R. K. Singh, J. Naranayan, Singh A.K and Krishnaswamy .J, Appl. Phys. Lett. **54** (1989) 2271.

[27] S. Chromik, Sitt. J, Strbik. V, Schilder J, Smatko V and Benacta S 1989 Jpn. Appl. Phys. **66** (1989) 1472.

[28] Berberich P, Tate J, Dietsche W, and Kinder H, Appl. Phys. Lett **53** (1988) 925.

[29] M. Scheib, I.L. Goebel, L. Hofmann, B. Lengeler, H. Oechsner and G. Zorn. Thin **solid films**

[30] **K. Harada, N. Fujimori and Yazu. S, Jpn. J. Appl. Phys. 27** (1988) 216

[31] Bouteloup. E, Hervieu M, Mercey B, Murray H, Poullain G, Raveau B and Rouillon T, J. Cryst. Growth **91** (1988) 418.

[32] M. Migliuolo, A.K. Stamper, D. W. Greve and T. E. Schlesinger, Appl. Phys. Lett **54** (1989) 859.

[33] Chang C.A, Tsuei C.C, Mc Guire T. R, Yee D.S., Boresh J.P. Lileenthal HR and Farrell C.E. App Phys. Lett. **53** (1988) 916.

[34] Poullain G, Mercey B, Murray H and Raveau B Modern Phys Lett **53** (1988) 916.

[35] Ma Q.Y, Yang E.S and Chang C.A, J. Appl. Phys. **66** (1989) 1866.

[36] Mogro - Campero A, Turner L.G, Hall E.L and Burrell M.C, Appl. Phys. Lett. **53** (1988) 2566.

[37] Mogro - Campero A, Turner L.G, Hall E.L and Burrell M.C, Appl. Phys. Lett. **52** (1988) 2068.

[38] Myoren H, Nishiyama Y, Nasu W, Imura T, Osaka Y, Yamanaka S and Hahori M, Japn. J. Appl. Phys. **27** (1989) L1068.

[39] Myoren H, Nishiyama Y, Nasu W, Imura T and Osaka Y, Japn. J. Appl. Phys. **28** (1989) 351.

[40] P.Tiwari, S.M.Kametkar, S.Sharan and J.Narayan, Appl. Phys. Lett. **57** (1990) 1578.

[41] Wu X.D, Inam A, Hegde M.S, Urilkens B, Chong C.C, Huang D.M, Nazar L, Venkatesan T, Mirua S, Matsubara S, Miyasaka Y, and Shohota N, Appl. Phys. Lett. **54** (1989) 754.

[42] D.K.Fork, D.B.Fenner, R.W.Bartan, Julia M Phyllips, G.A.N.Connell, J.B.Boyce and T.W.Geballe, Appl. Phys. Lett. **57** (1990) 1162.

[43] Ashok Kumar and J. Narayan, Appl. Phys. Lett. **59** (1992) 1785.

[44] Q.X.Jia and W.A.Anderson, Appl. Phys. Lett. **57** (1990) 304.

[45] Li Luo, X.D.Wu, R.C.Dye, R.E.Muarchausen, S.R.Foltin, Y.Coulter and T.Inoue, Appl. Phys. Lett. **59** (1991) 2043.

[46] Mirma S, Yoshitako T, Matsubara S, Miyasaka Y, Shohata N and Satola T, Appl. Phys. Lett. **53** (1988) 1967.

[47] S.Matsubara, Y.Miyasaka, M.Mikani, Japn. J. Appl. Phys. **24** (1985) 10.

[48] E.V.Pechen, R.Schoenberger, B.Brunner, S.Ritzinger, K.F.Renk, M.V.Sidorov and S.R.Oktyabrsky, J. Appl. Phys. **74** (1993) 3614.

[49] Y.Katoh et al, Japn. J. Appl. Phys, **26** (1987) 2136.

[50] R.K. Singh, J.Narayan, A.K. Singh and J. Krishnaswamy Appl. Phys. Lett. **54** (1989) 2271.

[51] X.D. Wu, R.E. Muenchaunsen, N.S. Norgar, A. Pique, R. Edwards, B. Wikens, T.S. Rau, D.M. Huang and C.Y. Chen, Appl. Phys. Lett. **58** (1991) 304.

[52] O. Eibl, K. Hradil and H. Schmidt Physica C **177** (1991) 89.

[53] A.B.Berezin, C.W.Yuon and A.L.de Lozanne, Appl. Phys. Lett. **57** (1990) 90.

[54] D.Kumar, M.Sharan, R.Pinto, P.R.Apte, S.P.Pai, S.C.Purandare, L.C.Gupta and R.Vijayaraghavan, Appl. Phys. Lett. **62** (1993) 3522.

[55] R.Pinto, P.R. Apte, S.P. Pai and Dhananjaykumar, Physica C **207** (1993) 13.

[56] R.Pinto, P.R.Apte, M.S.Hegde and D.Kumar, J. Appl. Phys. **77** (1995)

[57] J. Thornton, J. Vac. Sci. Tech., **11** (1974) 666.

[58] B.A. Movchan and A.V. Demchishin, Phys. Metallogr. **28** (1989) 83.

[59] G. Binng, C.F. Quate, Ch. Gerber, Phys. Rev. Lett. **56** (1986) 930.

[60] T.R. Albrecht and C. F. Quate, J. Vac. Sci. Tech., A **6** (1988) 271.

[61] S.M. Rossnagel and J J Cuomo in "Thin film processing and characterization of of High T_c Sup. (AIP conf. proc. **165**, edited by J.M. E Hamper, R. J. Colton, L.C. Feldman 1987).

[62] **R. Pinto, Navdeep Goyal, S.P. Pai, P.R. Apte, L C. Gupta and R.Vijayaraghavan J.App. Phys. 73. (1993) 13.**

[63] P.G. De Gennes Rev. Mod. Phys. **36** (1964) 225.

[64] J. Clarke Proc. Royal Society London Sen A **308** (1969) 447.

[65] M.S.R. Rao, C.P. D'Souza, P.R.Apte, R.Pinto, L.C. Gupta, S.Srinivas and A.K. Bhatnagar (in press) J. Appl. Phys. **76** (1996).

Chapter 5

Y-123 and Yb-123 Thin Films by PLD Method

5.1 Introduction

The earlier chapters dealt with $Y-123$ films prepared by sputtering techniques. This chapter deals with pulsed laser deposited (PLD) $RBa_2Cu_3O_{7-y}$ or simply $R-123$ thin films (where $R = Y, Yb$). Surface morphology of $R-123$ thin films deposited at different substrate temperatures has been studied using the atomic force microscope (AFM).

It is well established that the superconductivity transition temperature of orthorhombically distorted oxygen deficient perovskite $RBa_2Cu_3O_{7-y}$ (R represents most of the rare-earth elements) is nearly independent of a rare-earth element regardless of its magnetic behaviour [1,2]. However, when R is Ce, Tb, Pr or Lu either single phase 123 compound is not formed or if it is formed then it does not exhibit superconductivity. Lu and Tb fall into the first category while Pr falls in the second category [3-5] and experimental evidence of superconductivity in $Lu-123$ is rather controversial [3]. It is clear that each $R-123$ differ from the other in a number of physical and chemical parameters such as orthorhombicity, oxygen content, orthorhombic-tetragonal transition

temperature, normal state and magnetic properties. Systematic comparative studies have been made on almost all the $R-123$ compound in bulk form only [4]. However, Schwab et al [5] and Pinto et al [6] have shown that $Lu-123$ single phase orthorhombic structure can indeed be formed as thin films on $LaAlO_3$, $SrTiO_3$ and MgO substrates by the pulsed laser deposition (PLD). Rao et al [7] have reported growth of high quality $TmBa_2Cu_3O_{7-x}$ thin films on $LaAlO_3$ substrates using the PLD technique. However, the early efforts to prepare $Yb-123$ films have not been successful [8].

The Yb in $Yb-123$ system can exist in +2 and +3 valence states and its ionic radii in these two states are 0.93 Å and 0.858 Å, respectively. It also has a large magnetic moment ($\mu = 4.5\mu_B$) which can effect superconducting properties of the $Yb-123$ system as well as its transport properties in the normal state. On the otherhand Y in the $Y-123$ system exists only in +3 valence and its corresponding ionic radii is 0.893 Å. Therefore, it is interesting to study the effect of fluctuating valence, and different ionic size of $Yb-123$ superconducting compounds. Moreover, earlier reports on $Yb-123$ system, either bulk or thin films, show disagreement with each other.

The first report on $Yb-123$ thin films is from Kawasaki et al on polycrystalline YSZ substrates by the AC (50 Hz) sputtering [9]. The onset temperature (T_c) and zero resistance (T_{co}) are reported to be 93 K and 66 K respectively. Mukadia et al [10] have prepared $Yb-123$ films on MgO substrates using the e-beam deposition techniques with T_c of 81 K and T_{co} of 79 K. Screen printed $Yb-123$ films on YSZ substrate have been reported by Koinuma et al [11]. Nagata et al [12] reported the light irradiation effect on the preparation of High T_c $Yb-123$ superconducting thin films ($T_{co} = 70$ K) by AC sputtering method. Highly c-axis oriented films are reported by Chen et al [13] on $SrTiO_3$ substrates. They also reported the effect of Ag addition on $Yb-123$ films on $SrTiO_3$ substrates by liquid solidification process [14]. In the first case T_{co} is 82 K and J_C is $\sim 10^4$ A/cm^2 (at 77 K) and in the later case $T_{CO} \simeq 90$ K and $J_C = 3 \times 10^4$ Å/cm^2 (at 77 K). However, Luo et al [15] reported epitaxial $Yb-123$ films on MgO substrate by oxidation of a liquid alloys precursor with $T_{co} = 80$ K and 10^2 A/cm^2 J_c at 50 K. Later Merchant et al [16] have reported the epitaxial growth on $SrTiO_3$ and MgO substrate using the same method. A successful growth of epitaxial $Yb-123$ films has been reported by Lee et al [17] on $SrTiO_3$ having $T_{co} = 82$ K. A recent report by Priscoll [18] on a study of structural disorder in sputter deposited $R-123$ thin films as a function of ionic

radius and film deposition conditions has stated that the structural disorder at Yb site is responsible for the reduced T_c which strongly depends on the deposition conditions. Thus, there is large scatter of results on Yb-123 films. Hence, it was considered worth while to prepare Yb-123 films along with Y-123 by the PLD technique and to study them.

5.1.1 Pulsed Laser Deposition (PLD)

The major drawback in synthesis of stoichiometric R-123 thin films is due to their multi-component, anisotropic and reactive nature of the constituent element which leads to the formation of impurity phases unless care is taken. All the conventional film deposition techniques employed result in poor quality films due to above factors. Conceptually and experimentally PLD is one of the simplest among the various deposition techniques. In simple terms it uses pulsed laser radiation to vaporize /ablate materials and to deposit thin films in a vacuum chamber.

The interaction of short pulse high power (10-100 w/cm^2) laser with a ceramic target and during the growth of a film can be viewed in several stages. The standard picture concerning the ablation from solid surface assumes two step process [fig 5.1]. As the high power laser beam pulse hits the target, photons are absorbed by the surface, forming a molten layer that vaporizes instantaneously. The vaporization process creates a recoil pressure on the liquid layer and expels the molten materials. Thus the material removed is a combination of vapor, liquid and plasma. The second and third mechanisms are higher order perturbations but they affect the film deposition by including changes in the plasma properties. Depending on the optical penetration depth of the material, the thermal diffusivity of the target, and the rate at which energy is dissipated in to the system, the surface of the target is left at

radius and film deposition conditions has stated that the structural disorder at Yb site is responsible for the reduced T_c which strongly depends on the deposition conditions. Thus, there is large scatter of results on $Yb-123$ films. Hence, it was considered wothwhile to prepare $Yb-123$ films along with $Y-123$ by the PLD technique and to study them.

5.1.1 Pulsed Laser Deposition (PLD)

The major drawback of synthesizations of stoichometric $R-123$ thin films is due to their multi-component, anisotropic and reactive nature of the constituent element which leads to the formation of impurity phases unless a care is taken. All the conventional film deposition techniques employed results in poor quality films due to above factors. Conceptually and experimentally PLD is one of the simplest among the various deposition techniques. In simple terms it uses pulsed laserradiation to vaporize/ablate materials and to deposit thin films in a vacuum chamber.

The interaction of short pulse high power (10-100 w/cm^2) laser with a ceramic target and during the growth of a film can be viewed in several stages. The standard picture concerning the ablation from solid surface assumes two step process [Fig.5.1]. As the high power laser beam pulse hits the target, photons are absorbed by the surface, forming a molten layer that instantaneously vaporizes. The vaporization process creats a recoil pressure on the liquid layer and expels the molten materials. Thus the material removed is a combination of vapor and liquid. For effective material removal and congruent evaporation of multi-component targets, short wave lengths (UV) and short pulse width (30 ns) yield superior film quality. While the specific values of the temperature, oxygen back ground pressure, target-substrate distance and other relevant quantities are very system dependent, high-quality thin films of c-axis oriented $Y-123$ (CuO_2 planes oriented parallel to the substrate surface) can be routinely deposited in $\sim$ 100 - 300 mTorr of oxygen from a stoichiometric target onto a lattice matched substrate held at 725 - 800 °C and positioned 4 - 6 cm away. Fig 5.2 shows the laser plasma/plume at the target surface when the pulse interacted with target. The specific values of the oxygen pressure and the substrate temperature determines the orientation of the film (a-axis vs c-axis).

high temperature and it causes emission of many species from the target like thermionic emission of ions and electrons and electrons as well as neutral atoms and molecules that are disoriented from the bulk.

Photoionisation of evaporated material leads to the formation of an expanding plasma above the surface. As the plasma absorbs the laser radiation which results in further heating of the plasma. The plasma generated at the target surface expands away from the target and the electron density decreases and as a result the plasma becomes transparent. The plume of the evaporated material is cone shaped and characterized by a highly forward peak distribution $\cos^n(\theta)$ with $8 \leq n \leq 12$ where θ is measured with respect to the tangent normal. This is in contrast to what one expects from purely thermal evaporation characterized by cos θ distribution. In addition to the highly forward peak distribution a second distribution which is nearly cos θ is also observed. This angular distribution clearly indicates that material removal is a combination of different mechanisms.

For Y-123 it has been shown that in addition to the change in angular distribution of the total material ejected from the target there is also a variation in the composition of the evaporated materials as a function of angle. The sharply forward peaked distribution has the same stoichiometry as the target while the broad distribution is non stoichiometry. While the specific values of the temperature, oxygen back ground pressure, target-substrate distance and other relevant quantities are very system dependent, high-quality c-axis oriented thin films of Y-123 can routinely be deposited in ~ 100-300 mTorr of oxygen from a stoichiometric target onto a lattice matched substrate held at 725 - 800 °C and positioned 4-6 cm away. Fig 5.2 shows the laser plasma/plume at the target surface when the pulse interacted with target.

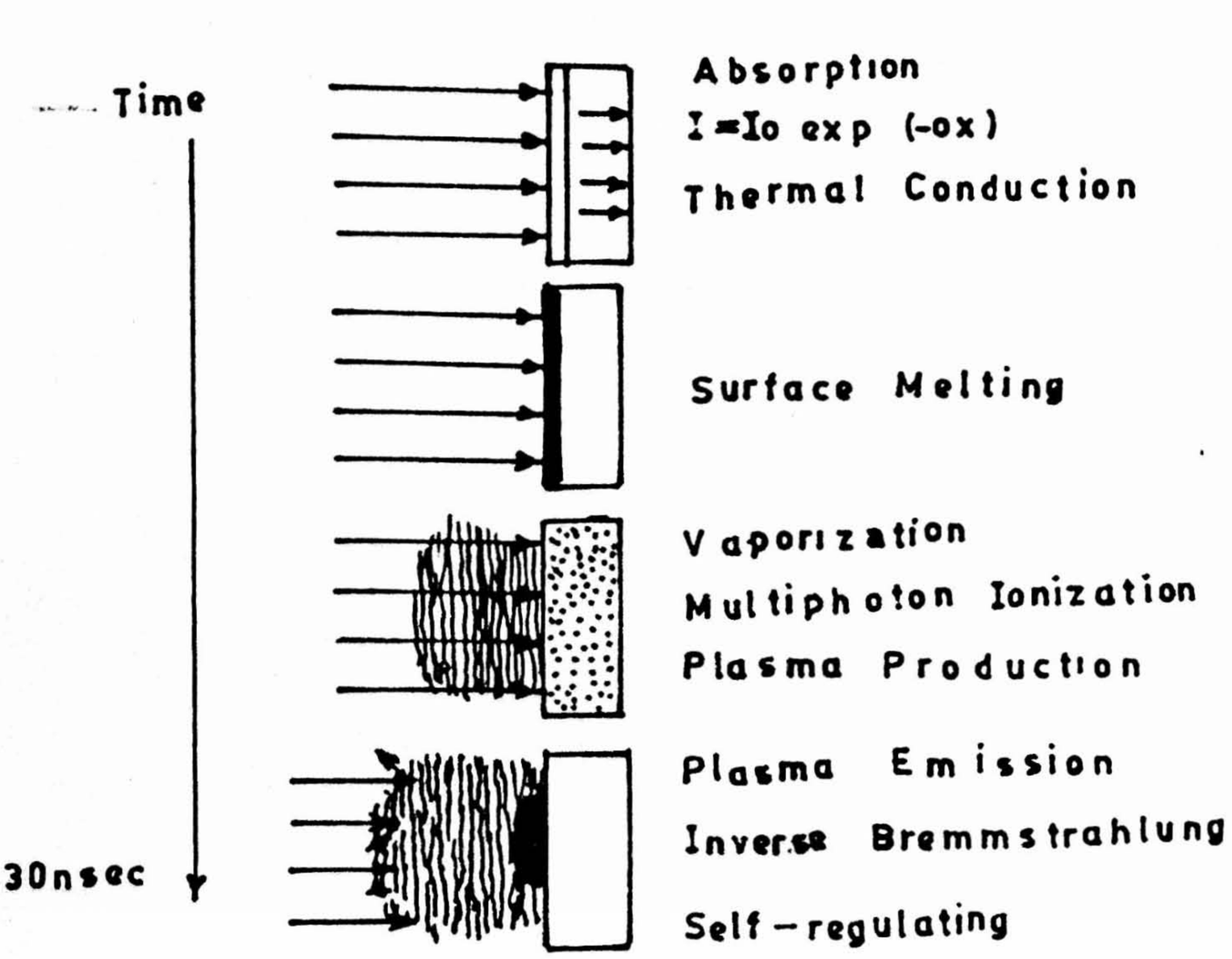

g.5.1. Schematic cross section of laser deposition unit from top side.

Fig.5.2. Photograph of Laser ablation during deposition of Y-123 film white portion indicates laser plume/plasma, red hot plate is substrate holder with substrates and shutter can be seen.

The present investigation is aimed at depositing $Y-123$ and $Yb-123$ thin films by the PLD technique. A comparison between $Y-123$ and $Yb-123$ thin films under the same deposition condition is attempted in order to understand effect of ionic radius of R element on the deposition conditions.

5.2 Experimental Details

$Y-123$ and $Yb-123$ thin films were insitu grown by the PLD technique using half inch diameter targets on $LaAlO_3$ $<l00>$ substrates. $LaAlO_3$ is chosen as a substrate because of its potential applications. These targets were prepared by a high temperature solid state reaction using stoichiometric proportions of 99.99% pure Yb_2O_3, $BaCO_3$ and CuO. X-ray diffraction (XRD) showed that the targets were multi-phase in the case of $Yb-123$ and single phase in the case of $Y-123$. The experimental setup is shown in Fig.5.2. The deposition by laser ablation was carried as described in Chapter 2. Since the intensity profile of the 3 cm× 1 cm laser beam has a Gaussian distribution along the short axis, only 5 mm of central region of the beam along the short axis was allowed to pass through the quartz lens using an aperture having 5 mm height and width variable between 10 - 20 mm. The width of the aperture was varied between 10-20 mm in order to vary the spot size of the laser beams on the target. Typical spots studied were in the range 0.3 mm (width) × 0.8 mm (height) - 6.5 mm × 1.2 mm. The laser fluence was varied by varying the laser output energy and was kept constant at 3 J/cm^2 in all cases. The angle between laser beam and the normal to the target was 45°. The 123 targets of 15 mm diameter and 3 mm thickness were used. The target was rotated at 15 rpm. The substrate temperature was measured using an optical pyrometer. The substrate temperatures studied for depositing $Y-123$ films are 650 °C, 675°, 700°, 725° and 750°C (variation ±5°C). The film composition was measured using energy dispersive X-ray analysis (EDAX) in thin film mode as most of the films studied had thickness varying between 1800 and 2000 Å. Table 5.1 and 5.2 gives the PLD conditions of $Y-123$ and $Yb-123$ thin films.

Films were characterised by XRD. The electrical resistivity was measured by a DC

Table 5.1
Optimized Pulsed Laser Deposition Conditions for Y-123 films.

1.	Target	$YBa_2Cu_3O_{7-y}$ (1 cm dia; 3mm thick, 80% dense; $T_{co} \sim 90$ K).
2.	Substrates	$LaAlO_3 < 100 >$ (0.3×0.8 cm^2)
3.	Substrate Temperature	725°C.
4.	Substrate-traget distance	4.2 cm
5.	Laser Power	600 mJ
6.	Laser Spot size	3×0.8 mm^2
7.	Laser Pulse frequency	8 Hz.
8.	Base Pressure	10^{-6} Torr.
9.	O_2 partial pressure	200 mTorr.

Table 5.2
Optimized Pulsed Laser Deposition Conditions for Y-123 films.

1.	Target	$YbBa_2Cu_3O_{7-y}$ (1 cm dia; 3mm thick, 80% dense; $T_{co} \sim 88$ K).
2.	Substrates	$LaAlO_3 < 100 >$ (0.3×0.8 cm^2)
3.	Substrate Temperature	700°C.
4.	Substrate-traget distance	4.5 cm
5.	Laser Power	600 mJ
6.	Laser Spot size	3×0.8 mm^2
7.	Laser Pulse frequency	8 Hz./sec.
8.	Base Pressure	10^{-6} Torr.
9.	O_2 partial pressure	200 mTorr.

four-probe technique. Silver films of thickness 4000 Åwere evaporated on the HTS films to decrease the contact resistance for the measurement of the critical current density. The films were subsequently patterned by photolithography technique. Typical bridge dimensions were 10 μm $\times$1 mm $\times$200 nm. Critical current density was determined by employing a criterian of voltage drop of 0.15 μV/mm across the sample. In order to check the homogeneity of the films several bridges were fabricated on one film.

The surface morphology of the best quality $Yb-123$ and $Y-123$ films were studied using Atomic Forse Microscope (AFM) digital instruments nanoscope model III.

5.3 Results and Discussion

5.3.1 Optimization of PLD Conditions for Y-123 Films

It has been observed earlier by others that the thickness and composition profiles are more uniform along the short axis of the laser spot as compared to those along the long axis. This is obviously because the plume is much wider along the short axis of the laser spot than along its long axis due to much higher expansion of the alloted material along the short axis. In other words, the major axis of the plume, and hence the film thickness distribution, is perpendicular to the long axis of the laser spot. Therefore, the uniformity of film thickness and composition is mainly governed by plume distribution along the long axis.

The important parameters which govern the plume distribution are laser spot size, fluence, target density and oxygen pressures. Although the effect of fluence has been extensively studied, the effect of spot size has not been discussed extensively. This investigation was aimed at optimizing the growth rate and relative stoichiometry in the long axis, oxygen pressure and target to substrate as a function of the spot size.

The film thickness and composition distribution using $\sim$ 75% density $Y-123$ targets at 200 m Torr oxygen pressure for three spot sizes - 6 mm $\times$ 1.2 mm, 3 mm $\times$ 1 mm and 3 mm $\times$ 0.8 mm were studied. The spots were focussed on the target so that the outermost

edges of the spots were at a distance of 6 mm from the centre of the target, resulting in a circular track of 13 mm outer diameter in all three cases. T-S distance is kept constant at 4.5 cm for this study and deposition time is 100 minutes. Fig.5.3a shows film thickness variation along the long axis. Large uniformity has been observed for 0.8 mm × 3 mm spot size even though it gives a low film growth rate when compare with other two spot sizes. Fig.5.3b shows the variation of $Y-123$ film composition along the long axis for the two spot sizes. It is seen from the figure that the compositional uniformity is slightly better for the smaller spot than the larger spot. Moreover, the former gives films with significantly better stoichiometry when compared to the later. From these results, it can be interpreted that smaller spots give better thickness uniformity and compositional uniformity, under a given set of optimized conditions.

Fig.5.4a shows the R-T plots for films obtained using three laser spots. The film made by the small laser spot shows higher T_c (90 K) than the other two spot sizes. Fig.5.4b shows the R-T plots of films grown at various substrate temperatures at the optimum laser spot. Even though films deposited at 100 mTorr have lower resistance, films deposited at 200 mTorr show $T_c = 90$ K. The primary reason for pressure dependence of T_c is the composition of the film [20]. The variation in a film composition, when the substrates located at various positions along the plume axis, may be traced to the different expansion velocities of the various target species in the plume. Earlier evidences [6,7] indicates that as much as 50% variation in the maximum velocities of different species may occur in the plume. Further, at the tip of the plume, the velocities of different species become equal and hence a stoichiometric film can be realized. Fig.5.5a shows the effect of T-S distance on T_c for $Y-123$. It appears T-S distance around 4.5 cm is optimum for getting stoichiometric films with high T_c.

Fig.5.5b shows T_c vs oxygen pressures at different substrate temperatures of $Y-123$ thin films. At very high or very low oxygen pressures T_c turns out to be much lower. The optimum oxygen pressure in the present case is 200 mTorr.

Fig.5.6 the XRD pattern of $Y-123$ films prepared at 675 °C, 700 °C and 725 °C. All the three films strongly show C-axis orientation. The full width at half maximum (FWHM) values for < 006 > reflection of $Y-123$ films are 0.45°, 0.358° and 0.35° for 675 °, 700 °C and 725 °C respectively. The smaller FWHM corresponds to higher

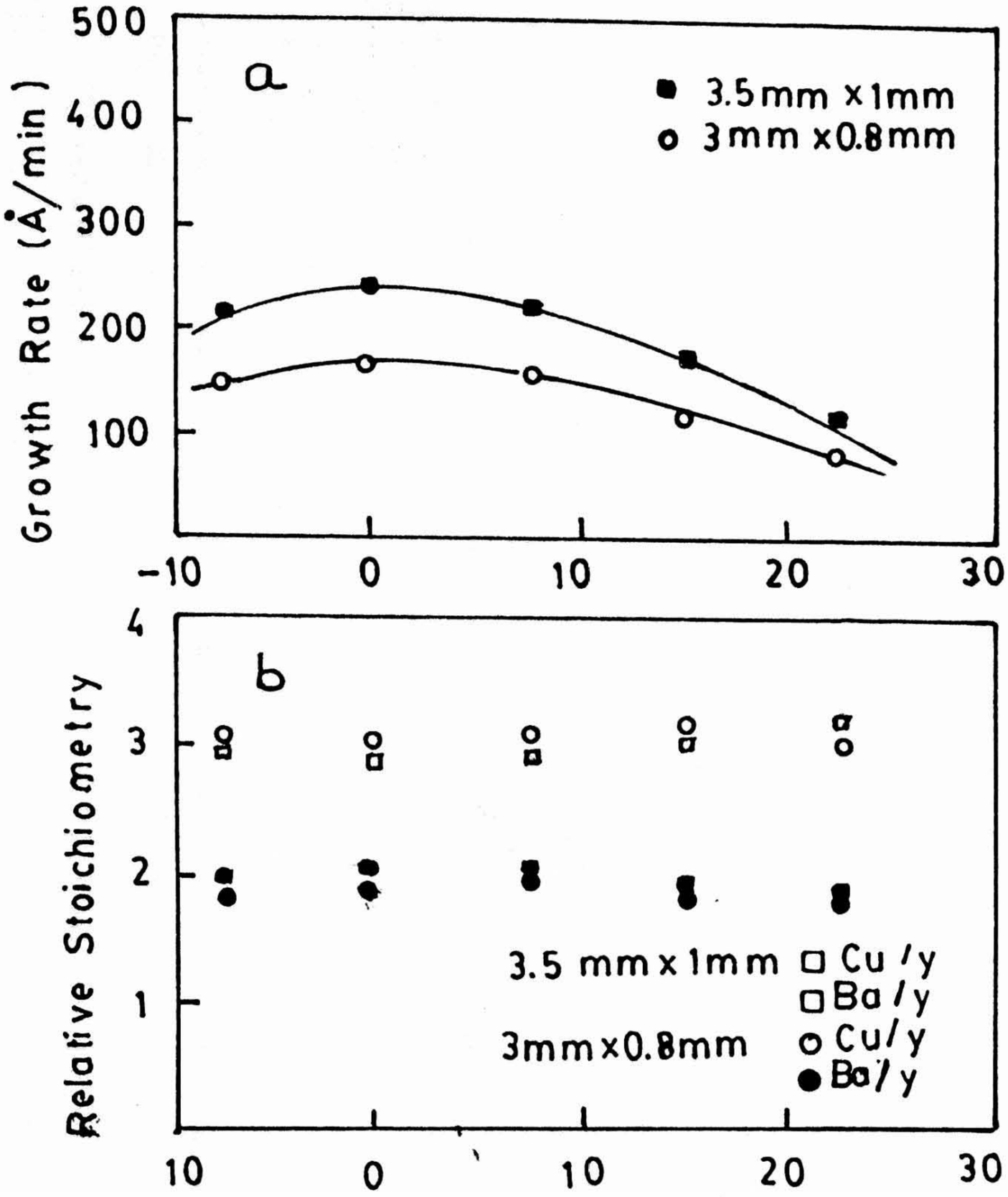

Fig.5.3 (a) Y-123 film thickness variation along long axis for two laser spots; (b) Y-123 film deposition along long axis.

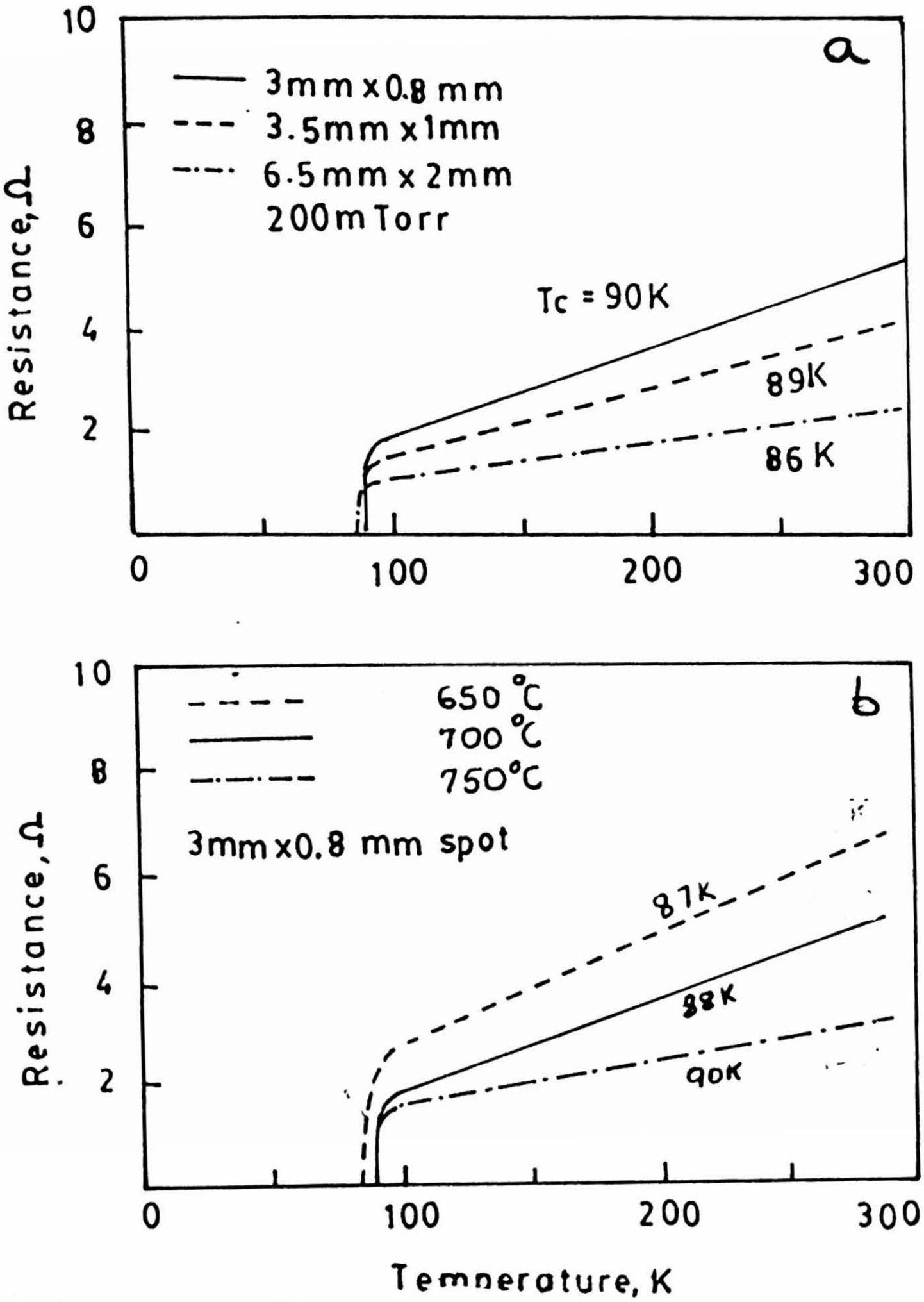

Fig.5.4 (a) R-T plots of Y-123 films for three different laser spots; (b) R-T plots of Y-123 films for three substrate temperatures.

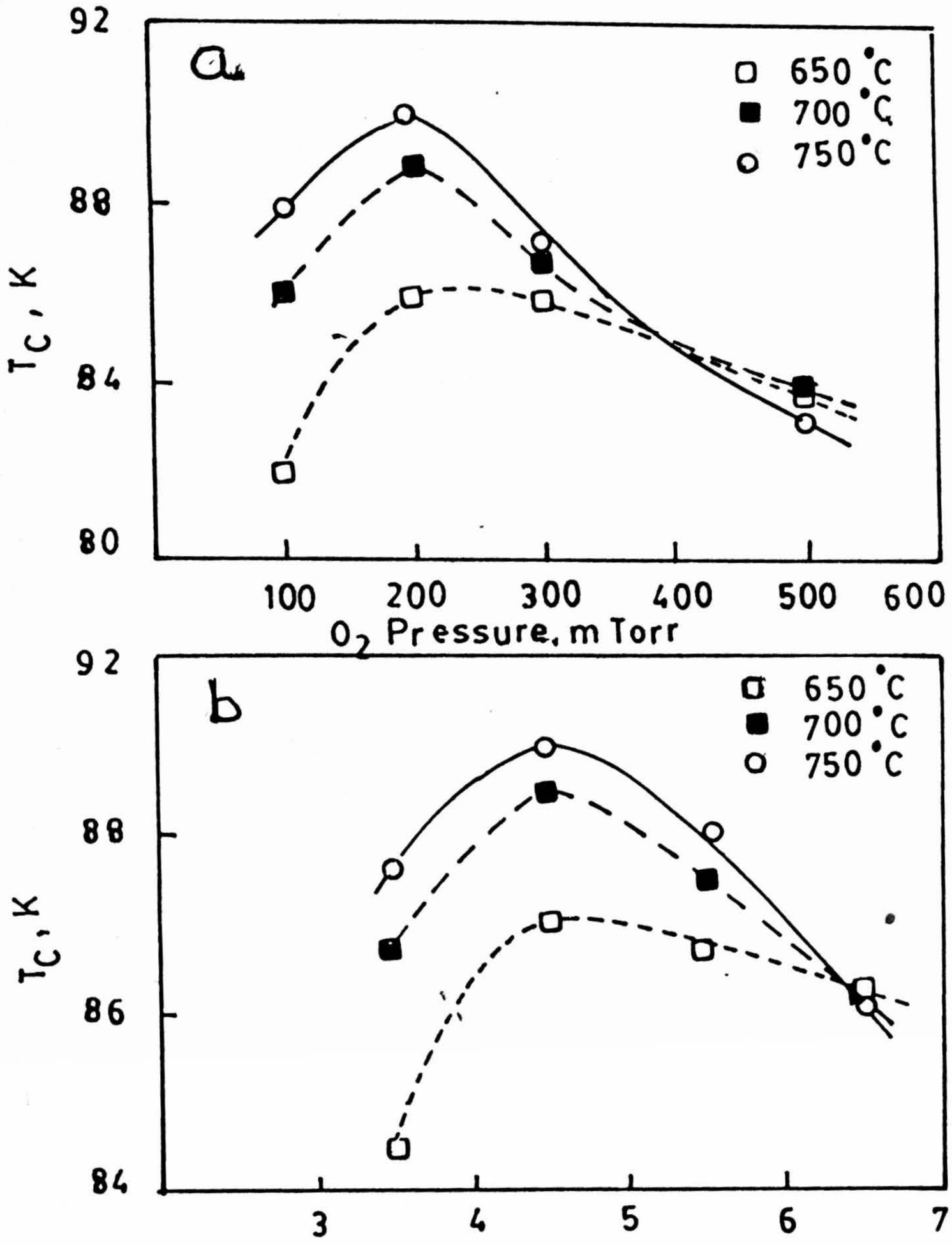

Fig.5.5. (a) T_c vs O_2 plots Y-123 films for deposited at three different temperatures; (b) Target-Substrate distance vs T_c plots for Y-123 films deposited at three substrate temperatures.

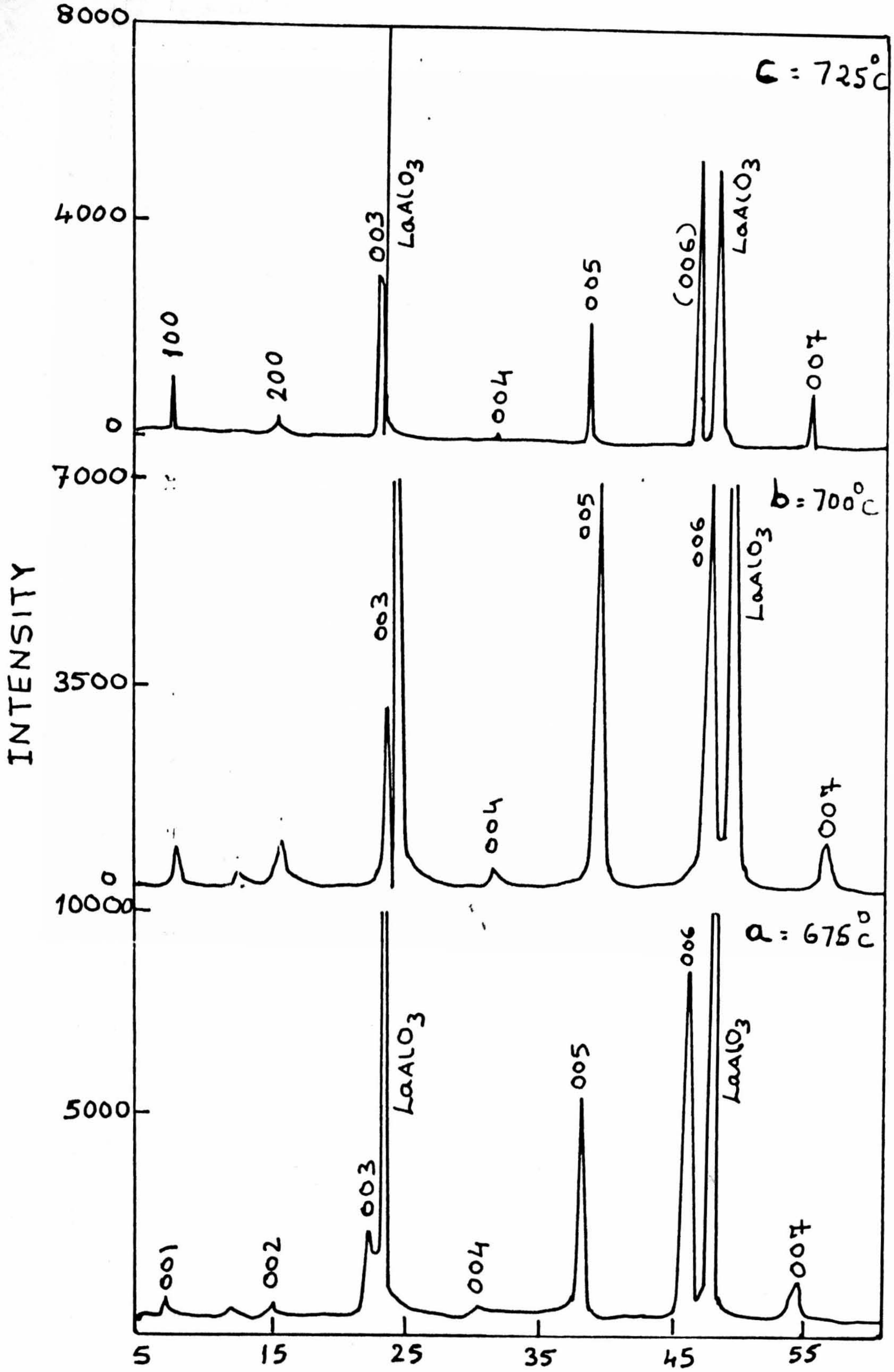

Fig.5.6. XRD traces of Y-123 films deposited at three different substrate temperatures on $LaAlO_3$ <100>.

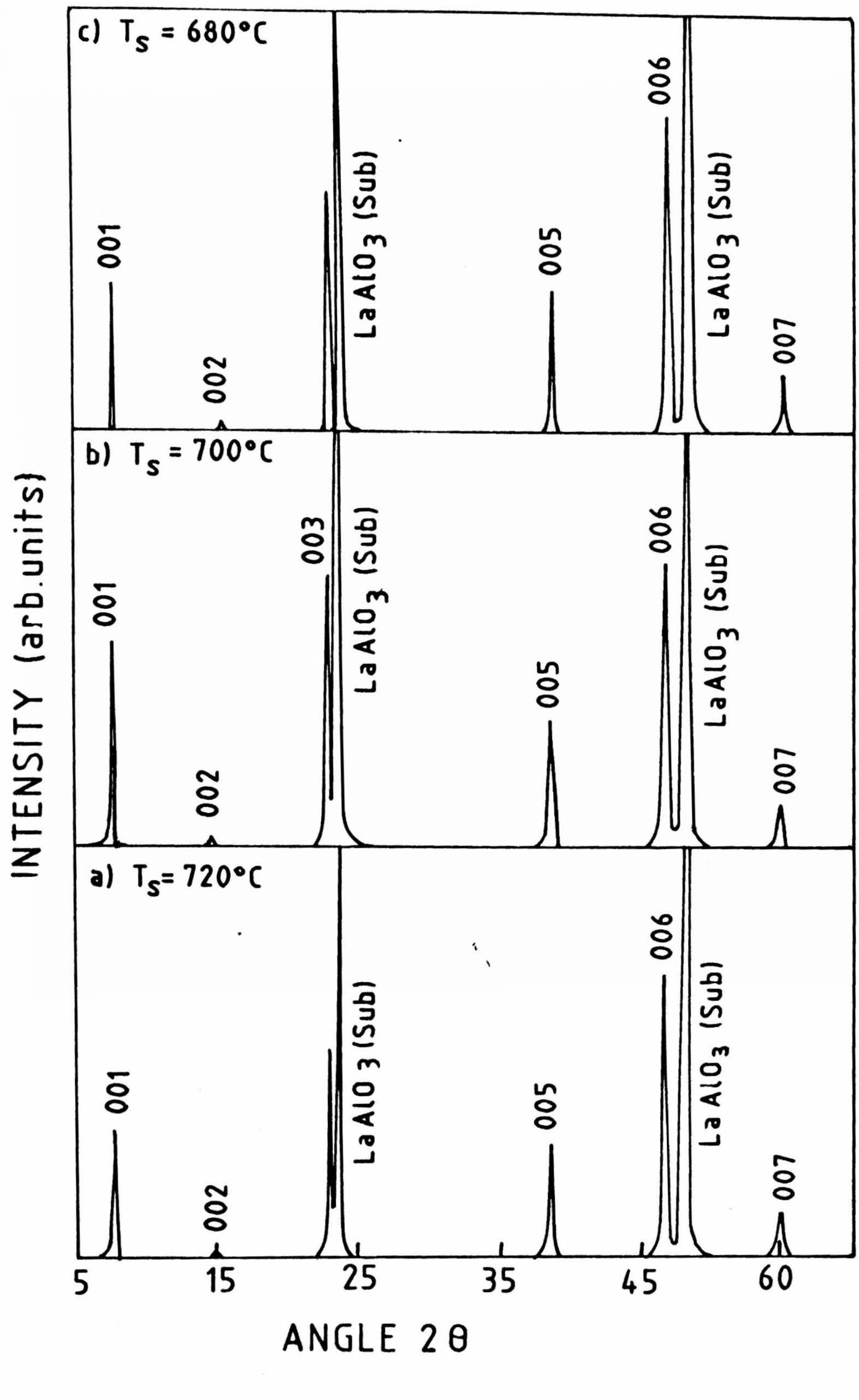

Fig.5.7. XRD plots of Yb-123 at three different substrate temperatures.

order crystalline nature. The results on $Y-123$ thin films are given in Table 5.3. From these results it is obivious that, for $Y-123$ films substrate temperature above 700 °C is preferred for realizing high quality superconducting thin films.

Fig.5.4b and Fig 5.8a shows the R-T plot of the $Y-123$ films grown at 675 °C, 700 °C and 725 °C. Films prepared at 725 °C show $T_c = 89$ K when compared to lower T_cs of other two films prepared at 675 °C and 700 °C. The critical current density of the film grown at optimized conditions (3 mm × 0.8 mm spot T-S distance 4.5 cm and 200 mTorr O_2 pressure and 725 °C substrate temperature) is measured to be 1.5×10^6 Å/cm^2 at 77 K ($T_{co} = 89$ K), which is highly reproducible.

5.3.2 Optimization of Yb-123 Film Growth Conditions

Laser deposition parameters used in the earlier sections were kept constant and only the substrate temperature was varied. Fig.5.7 shows the XRD patterns of $Yb-123$ thin films deposited at (a) 675 °C (b) 700 °C and (c) 725 °C respectively. Most peaks corresponds to the 123 structure. Hence, It is possible to deposite $Yb-123$ film. It is very interesting to observe that $< 001 >$ and $< 005 >$ peak intensities are nearly the same at all deposition temperatures. Moreover, $< 004 >$ reflection which can be seen for all the $Y-123$ films deposited at the same substrate temperatures is absent for all the $Yb-123$ films. This may be the effect of smaller ionic radius of Yb atom when compared with that of Y. The FWHM values for $< 006 >$ reflection are 0.347°, 0.332° and 0.395° for 675 °C, 700 °C and 725 °C, respectively. In the case of $Yb-123$, films deposited at 700 °C showed relatively smaller FWHM which indicates better crystalline quality of the film than other films deposited at lower substrate temperatures.

Fig. 5.8b shows the R-T plots of $Yb-123$ system deposited at 700 ± 25 °C. The T_cs of the films deposited at 675 °C, 700 °C and 725 °C are 84 K, 88 K and 80 K, respectively. Films deposited at 700 °C have relatively low room temperature resistance and small residual resistance (R_o) that indicates high metallic nature of $Yb-123$ thin films when compared to the films deposited at 675 °C and 725 °C. Table 5.4 gives— These results indicate that it is possible to grow quality superconducting $Yb-123$ films

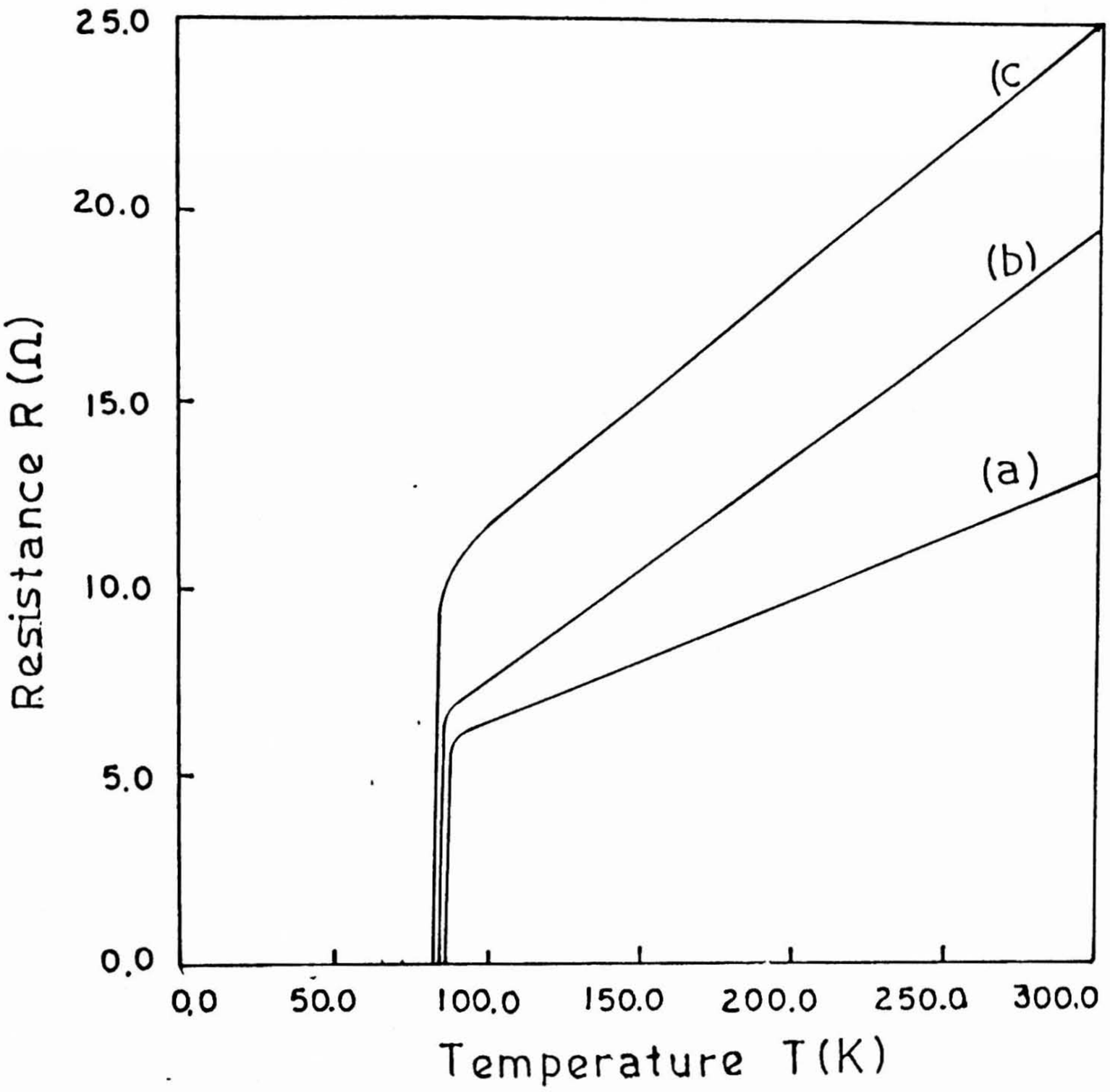

Fig.5.8. (a) R-T plots of Y-123 film deposited at (a) 725°C; (b) 700°C and (c) 680°C.

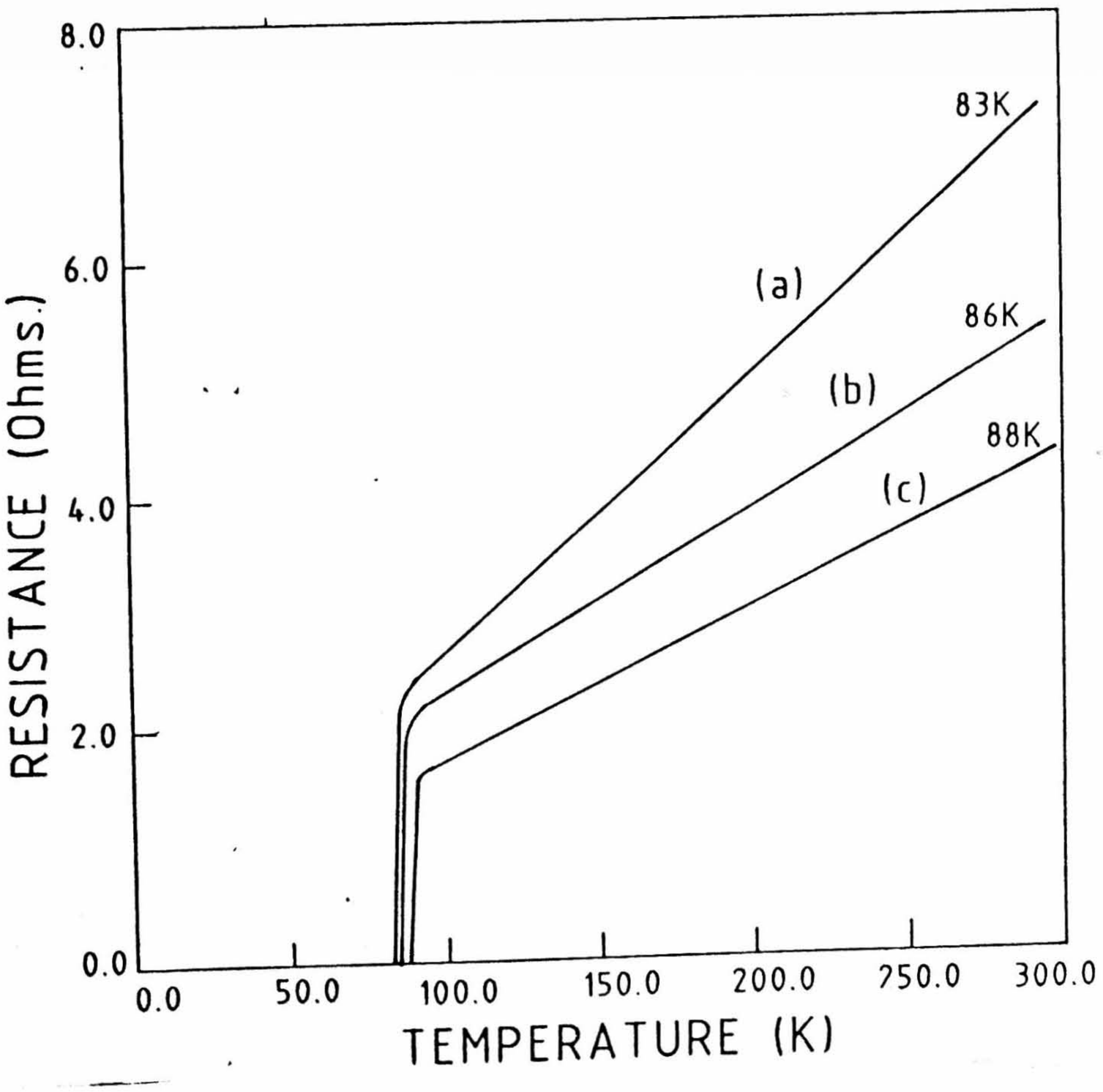

Fig.5.8. (b) R-T plots of Yb-123 film deposited at (b) 725°C; (c) 700°C (a) 680°C.

by PLD method, and the smaller ionic radius of Yb does not have detrimental effect.

5.3.3 Comparative Studies on Y-123 and Yb-123 Films

Following a comparative study on the properties of $Y-123$ and $Yb-123$ films deposited at identical conditions, the properties that are consistent with the substrate temperature in both the cases are listed below.

Fig.5.9a shows c-axis parameter variation with substrate temperature for $Y-123$ and $Yb-123$ films. In both the cases, the c-axis parameter has a lower value at the optimum substrate temperature. Fig.5.9b shows T_c and J_c as function of the substrate temperature. J_c values for $Y-123$ and $Yb-123$ are 1.8×10^{20} and 2×10^{20}, respectively. T_c and J_c of $Yb-123$ films increase initially and exhibit a maximum at the optimum substrate temperature while in the case of $Y-123$ films, T_c and J_c continue to increase with substrate temperature indicating that the optimum substrate temperature to achieve higher T_c and J_c may be higher than 725°C (since the opitimum substrate temperature seems in this case lie well above the maximum substrate temperature used). The variation of T_c and J_c for $Y-123$ films are similar to that of sputter deposited films as explained in Chapter 3. On the otherhand,

smaller ionic radii of Yb atoms which plays a vital role in the growth of unit cell. Similar behaviour was observed in the case of $Lu-123$ and $Tm-123$ films [6,7]. At lower substrate temperatures (below optimum temperature), the film quality is poor probably due to the low adatom mobility of ablated species at the growing surface which limits the phase formation as well the as grain size. On the other hand in the case of $Yb-123$ films, at temperatures higher than the optimum substrate temperature, eventhough the grain size is not limited, increased size of grain boundary domains are responsible for degradation of T_c and J_c. To study this speculation AFM was used to see the surface morphology of the films.

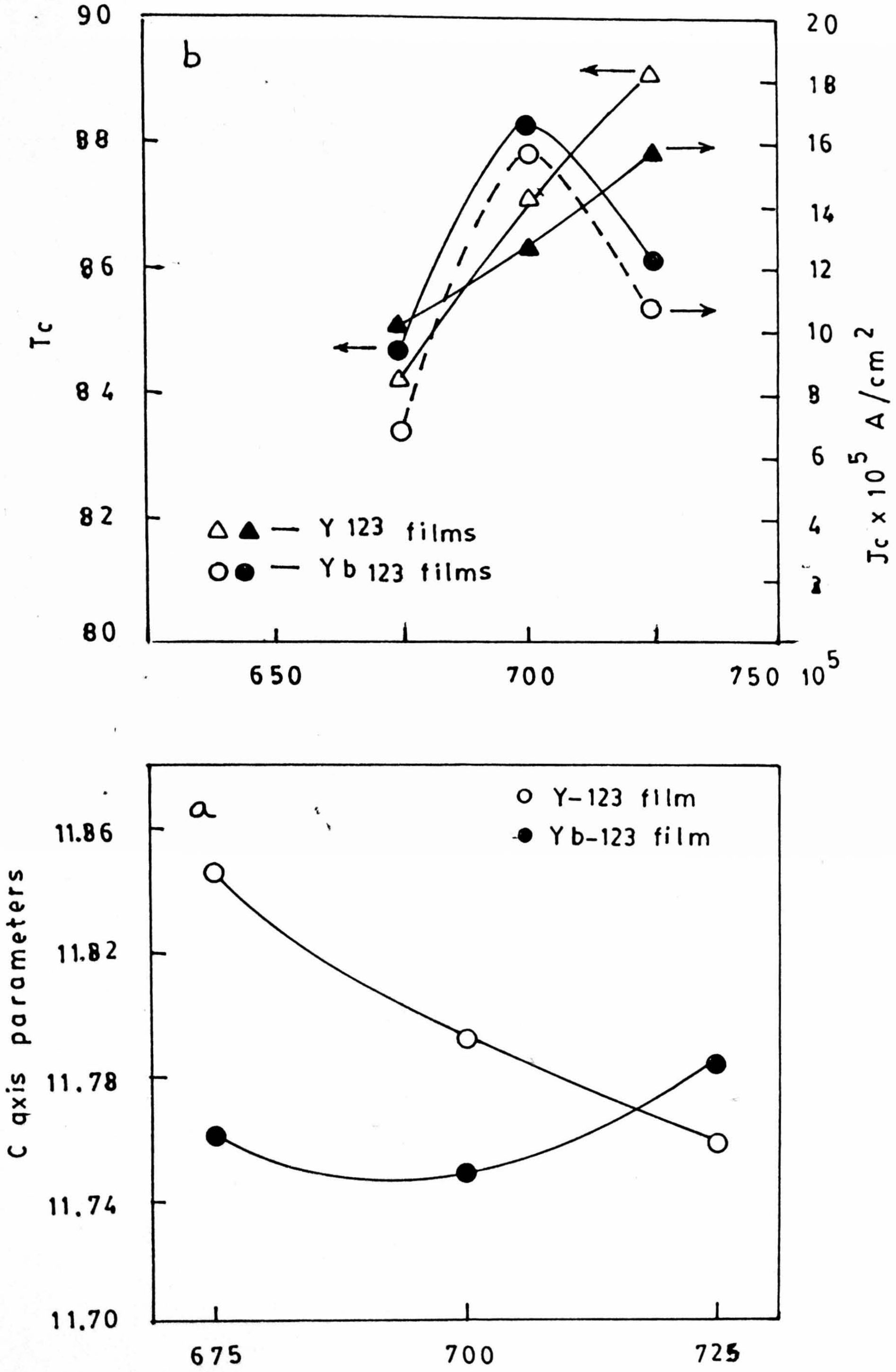

Fig.5.9. (a) C axis vs substrate temperature plots for Y-123 and Yb-123 films; (b) T_c and J_c vs substrate temperature plots of Y-123 and Yb-123 films.

Table 5.3 Results of Y-123 films deposited on $LaAlO_3$ substrates.

S.No	Substrate Temperature (°C)	Thickness (Å)	Resistivity (mΩ-cm)	R_{300}/R_{100}	T_{co} (K)	J_c(77 K) (10^6 A/cm^2)
1	650	1860	0.930	2.25	86.2	0.82
2	675	1852	0.556	2.54	87.1	0.95
3	700	1824	0.547	2.95	88.2	1.02
4	725	1834	0.275	2.88	88.8	1.20
5	750	1812	0.093	3.12	89.2	1.40

Table 5.4 Some reproducible results of Yb-123 films deposited on $LaAlO_3$ substrates.

S.No	Substrate Temperature (°C)	Thickness (Å)	Resistivity (mΩ-cm)	R_{300}/R_{100}	T_{co} (K)	J_c(77 K) (10^6 A/cm^2)
1	680	1860	0.349	3.02	83.8	0.4
2	700	1926	0.272	2.90	88.5	2.1
3	720	1885	0.206	2.64	86.2	0.9

5.3.4 AFM Studies of Y-123 and Yb-123 Thin Films

Surface morphology of the best quality films of $Y-123$ and $Yb-123$ deposited at 700 °C and 725 °C, respectively, have been studied using AFM.

Fig.5.10a,b and c show the AFM picture of $Y-123$ films deposited at 675°, 700° and 725°C respectively. Highly oriented grains were obtained reproducibly at 725 °C temperature. Fig. 5.11a,b and c show the microstructure of the $Yb-123$ films deposited at 675°, 700° and 725°C. $Yb-123$ films prepared at 675°C temperature have poor quality microstructure. Randomly oriented grains with with many weak links or grainboundaries can be seen from AFM pictures for films grown at 675°C in both the cases. However, at 700 °C $Yb-123$ film shows better microstructural characteristics as evident from AFM picture as shown in Fig.5.11b. Which means $Yb-123$ films favour larger size grain and $Y-123$ favour randomly oriented smaller grains at 700 °C. However, $Y-123$ films grow with larger grain sizes and with highly oriented nature at 725 °C, Fig.5.10c. The degradation of superconducting properties of $Yb-123$ can be accounted to the poor microstructure at 725 °C, while the high T_c and J_c of $Y-123$ films prepared at these temperatures could be due to better microstructure. The AFM images confirmed the speculations made and become evidence for the J_c dependance on the microstructure of the films.

Films deposited at 675 °C have show poor quality microstructure in both the cases. Fig.5.11a and b shows the microstructure of $Y-123$ and $Yb-123$ films deposited at 675 °C. In both the cases, degradation in the superconducting properties is observed, i.e., T_c and J_c are lower.

Figure 5.12a,b shows the microstructure of a typical $Yb-123$ thin film deposited at 700 °C. It shows a spiral like growth and screw distortion. This kind of microstructure was earlier observed by a few researchers in $Y-123$ films [21]. The T_c of the film is 88 K and transport J_c at 77 K is 3×10^6 Å/cm^2. The reason for getting this kind of structure is not exactly known. The speculative explanation could be that some variation in the plume characterstics might be responsible for the defective growth of $Yb-123$ film.

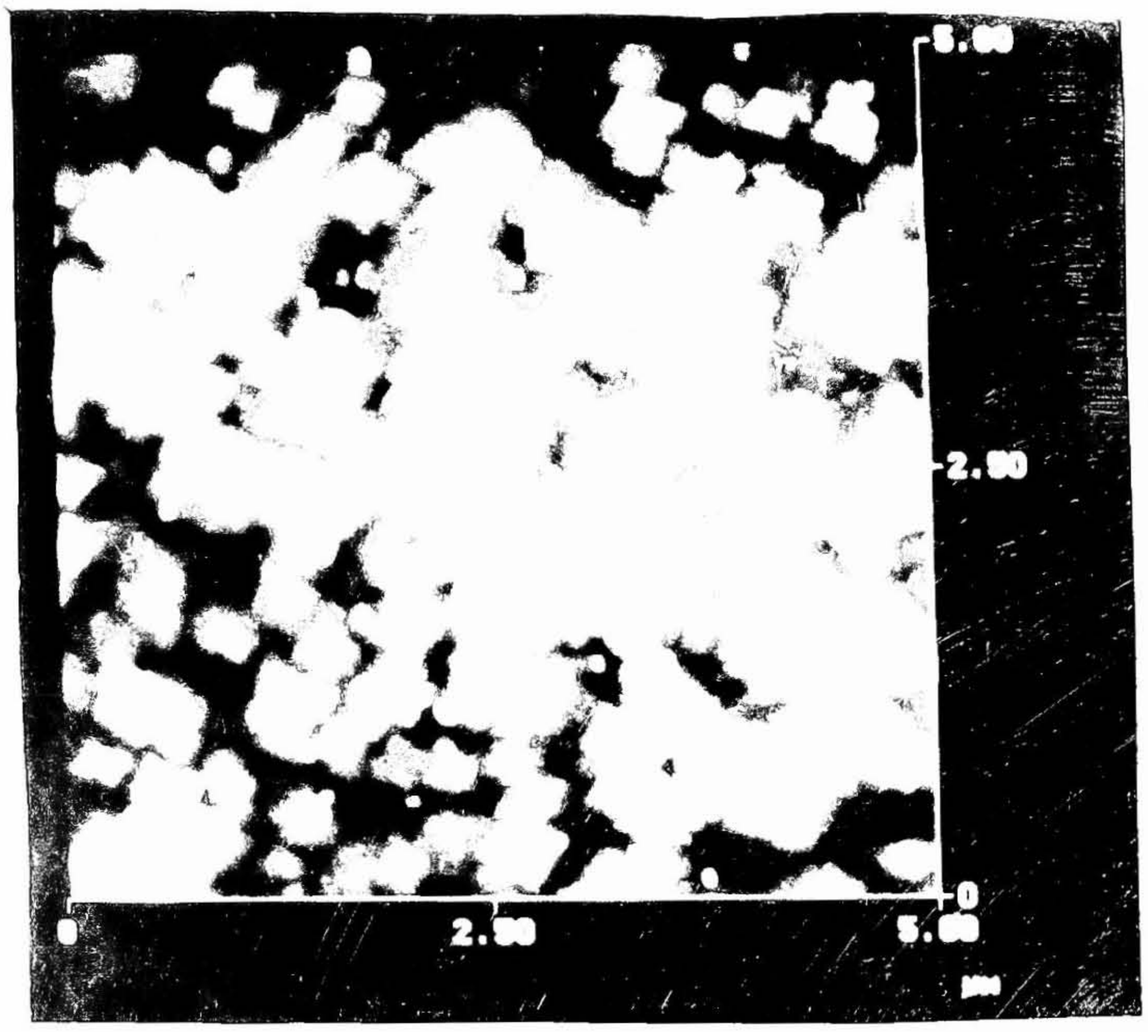

Fig.5.10 (a):
AFM image of Y-123 film surface morphology deposited at 675°C on LAO randomly oriented small grains can be seen.

Fig.5.10 (b):
AFM image of [illegible] morphology [illegible] on LAO [illegible] grains with [illegible] can be seen.

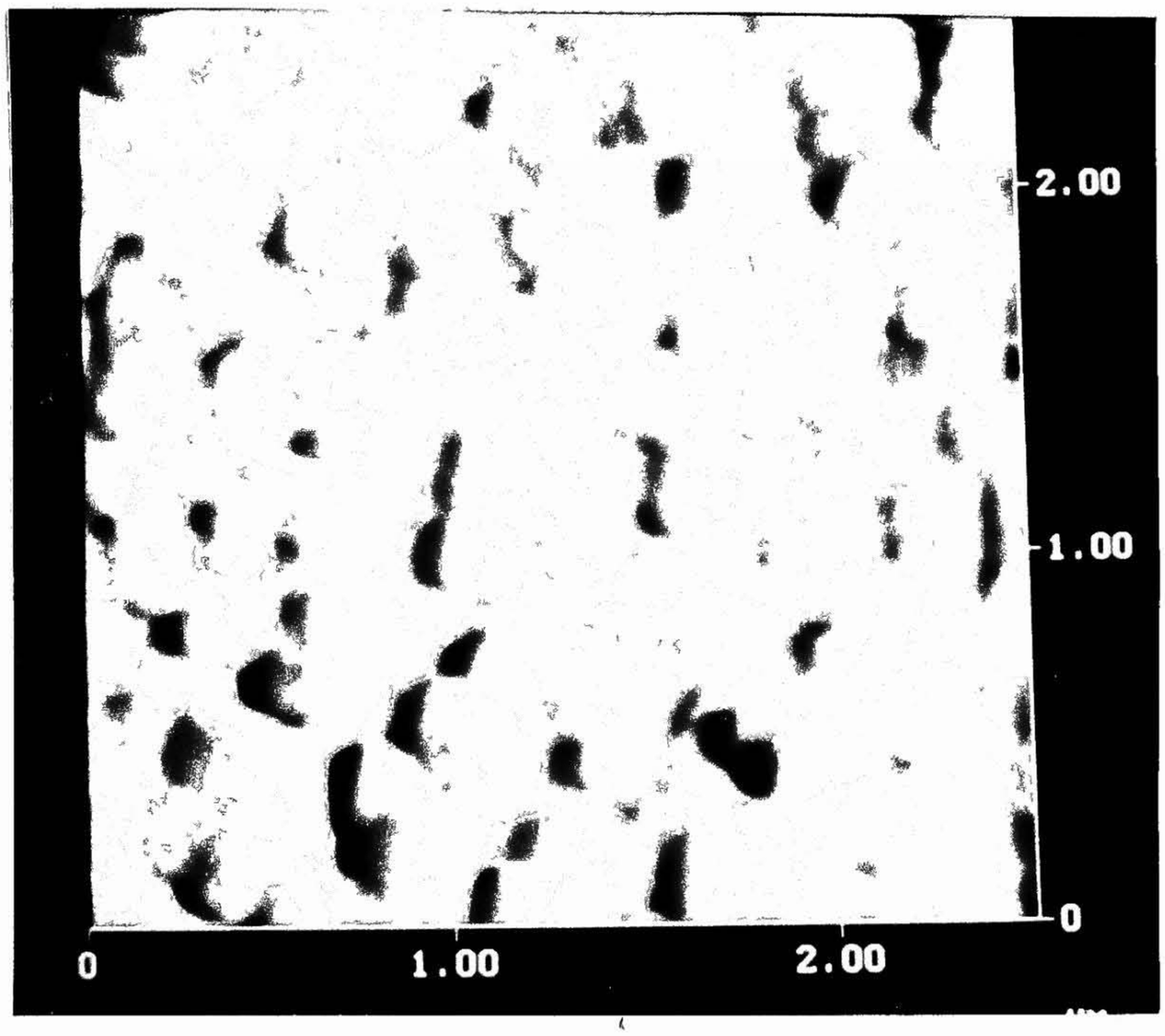

Fig.5.11 (a):
AFM image of Yb-123 film surface morphology deposited at 675°C on LAO - well aligned small grains with poor connectivity.

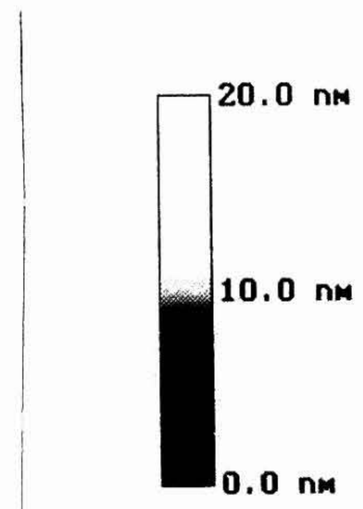

Microscope	NSIII AFM
Scan size	2.000 µm
Setpoint	0 V
Scan rate	25.94 Hz
Number of samples	512

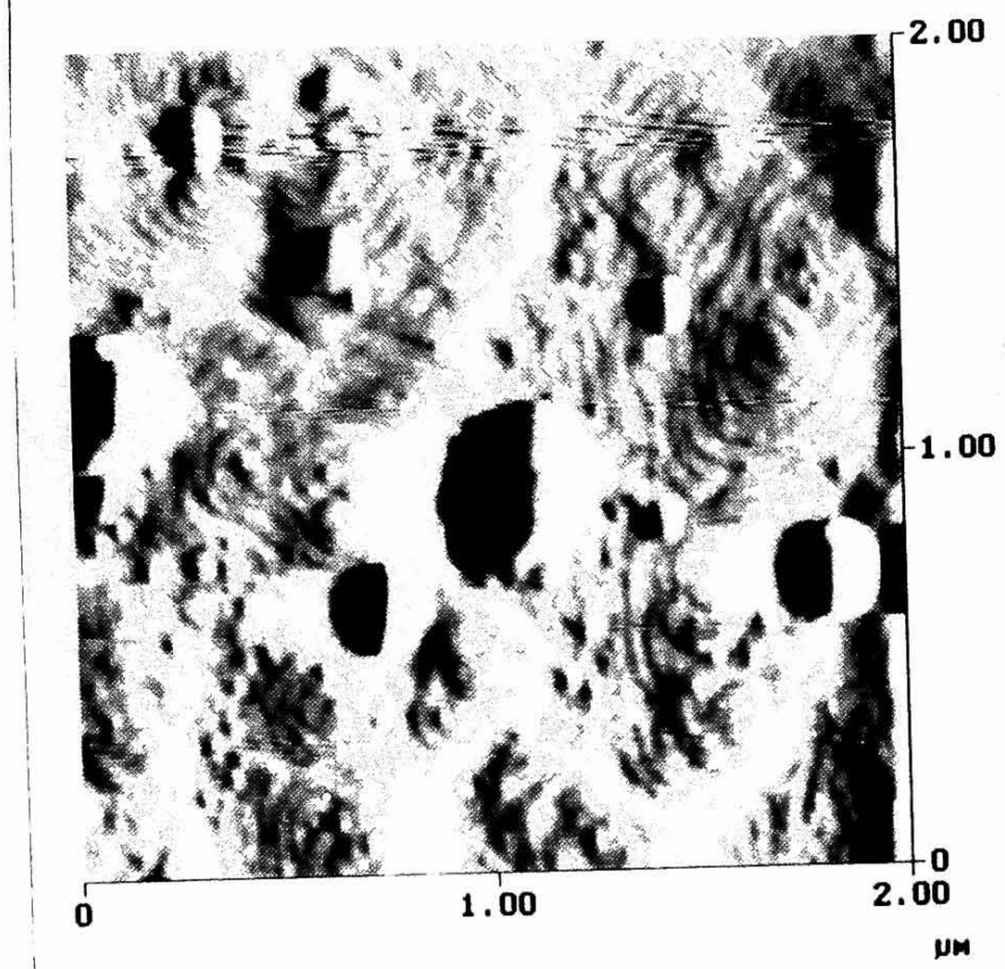

Fig.5.11 (b):
AFM image of Yb-123 film surface morphology deposited at 700°C on LAO - smooth surface with big particulates can be seen.

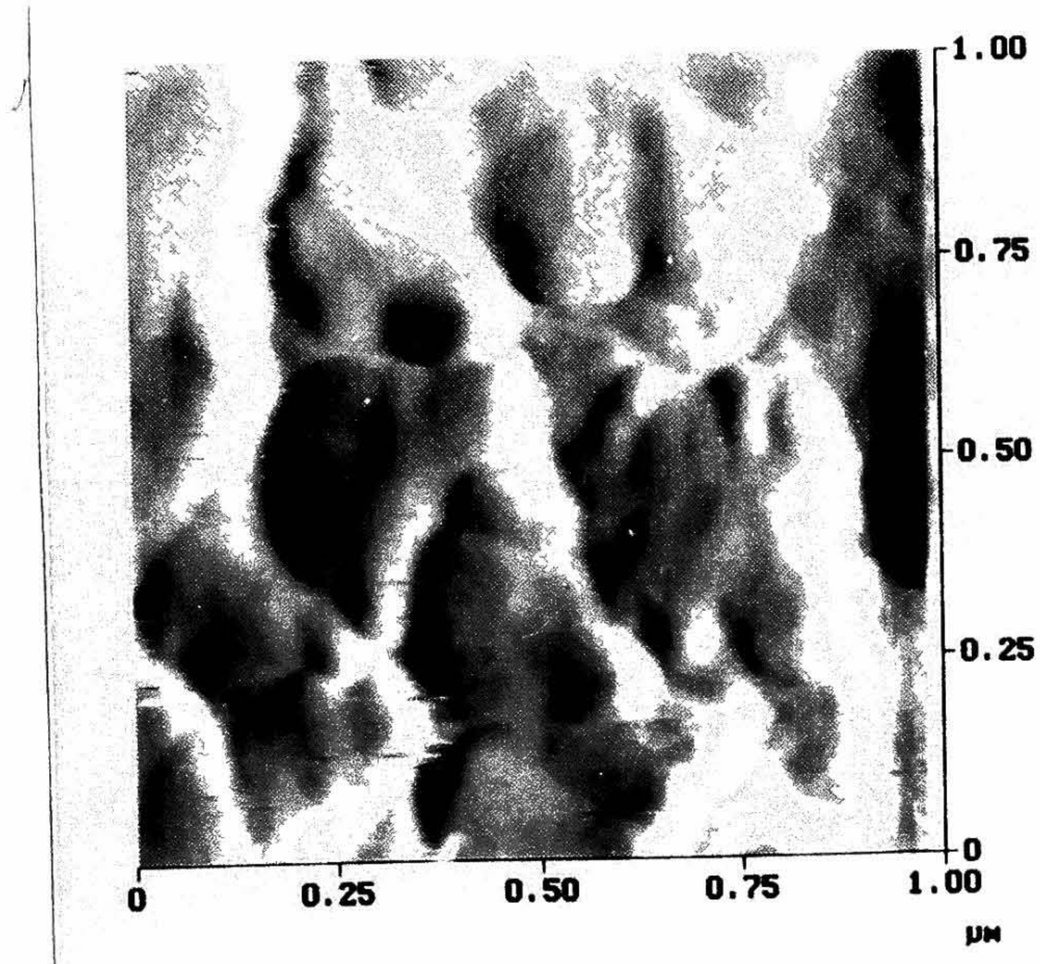

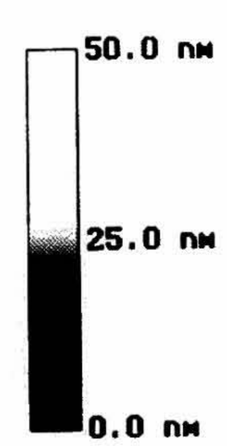

Microscope	NSIII AFM
Scan size	1.000 µm
Setpoint	-0.9500 V
Scan rate	30.52 Hz
Number of samples	512

Fig.5.11 (c):
AFM image of Yb-123 film surface morphology deposited at 725°C on LAO - big grains with grain boundaries can be seen.

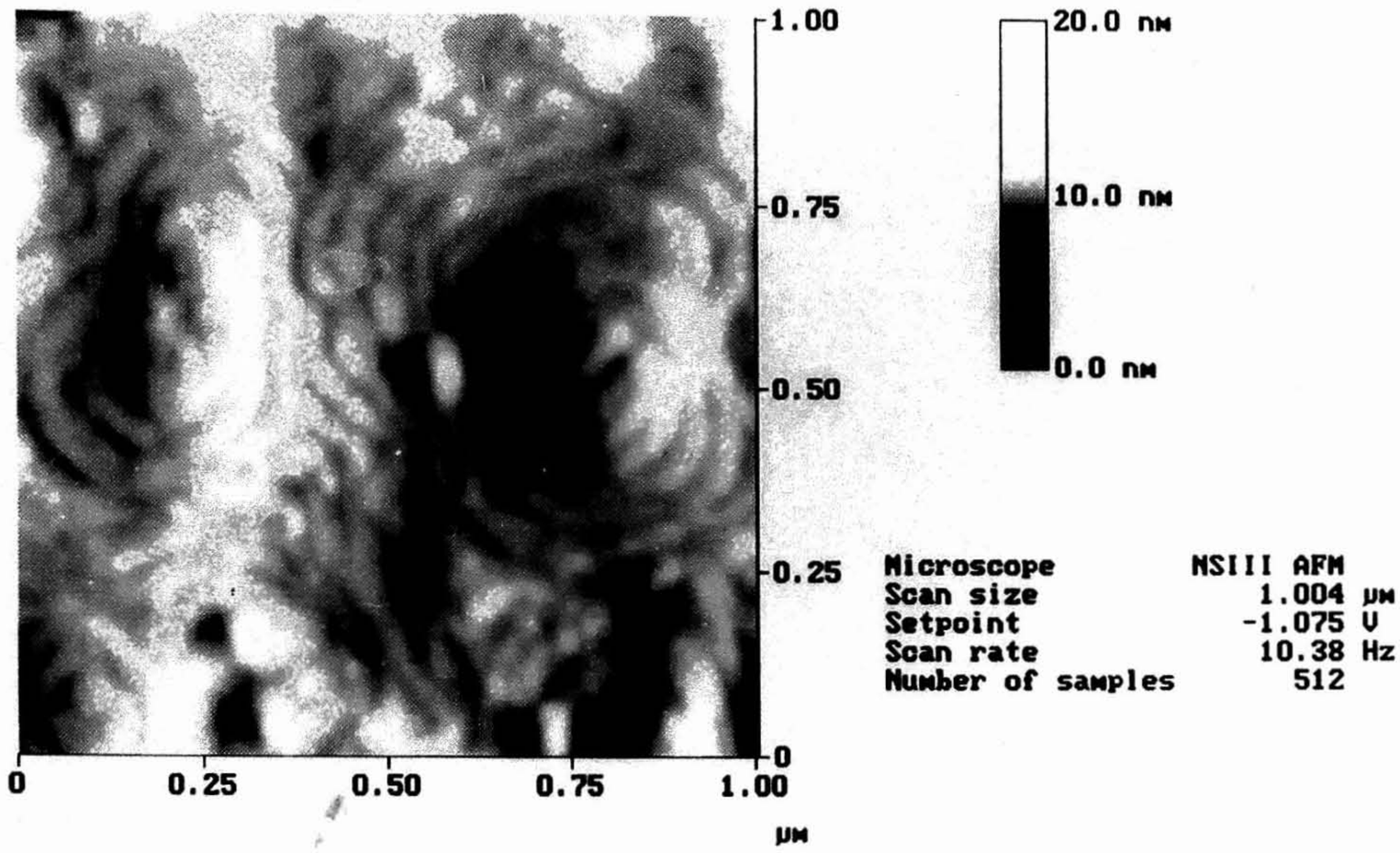

Fig.5.12 (a) AFM image of typical Yb-123 film grown at 700^{o}C - surface morphology shows spiral growth of the film.

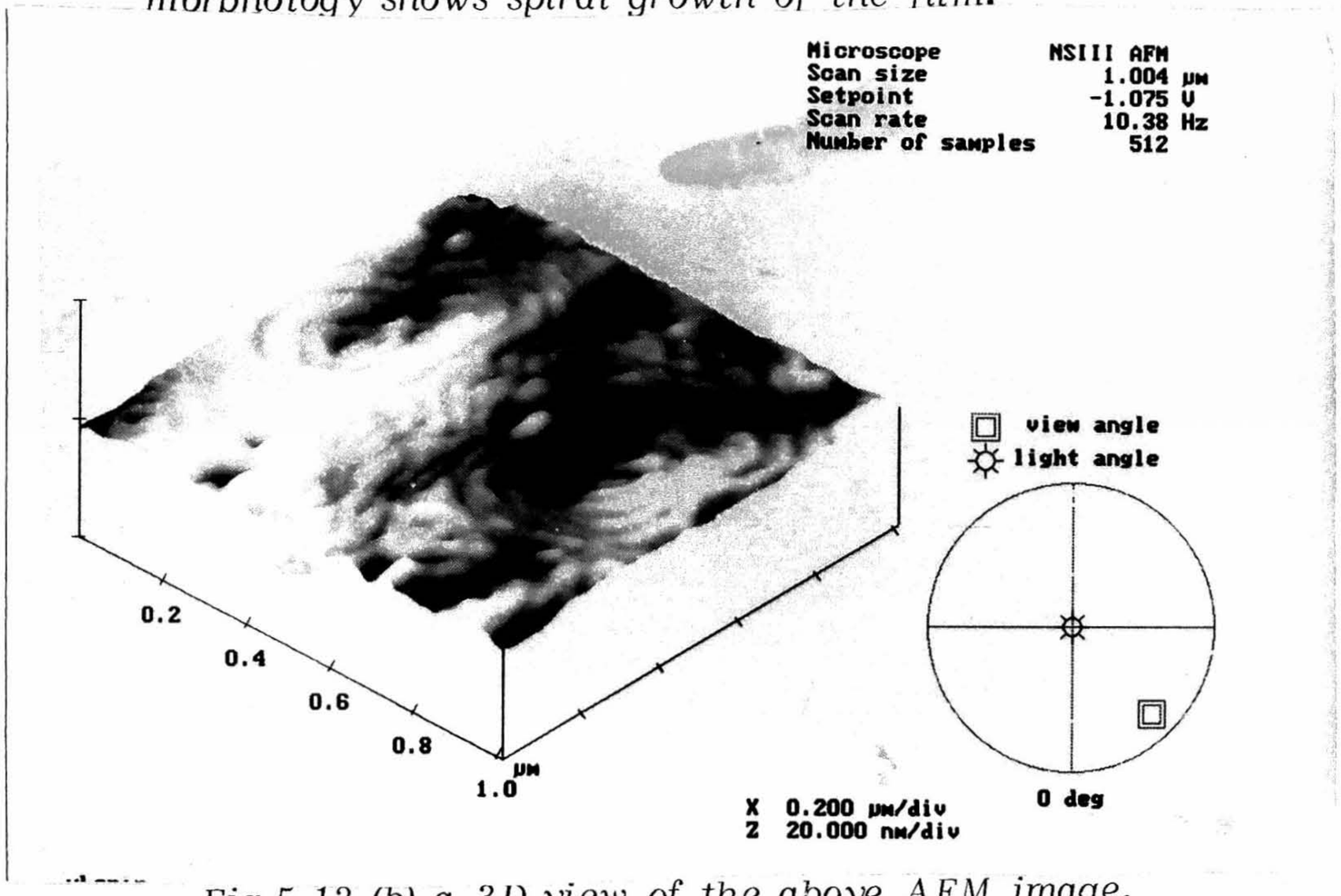

Fig.5.12 (b) a 3D view of the above AFM image.

Overall, AFM studies confirms that the substrate temperature has a influence on microstructure and hence on the quality of superconducting film. To the best of knowledge of the author, so far no such evidence through AFM has been reported in the literature.

5.3.5 Temperature Dependence of J_c

Table 4.2 shows the T_c and J_c values of $Y-123$ and $Yb-123$ thin films grown at different substrate temperatures.

The variation of J_c with temperature of these films are explained using models proposed for granular superconductors by earlier researchers. The basic reason for choosing molecular model is due to their microstructure which confirms the existence of well aligned grains. These grains are homogeneous and are connected by weak links. These weak links can be either grain boundaries or superconducting regions of poor quality, or even normal conducting and insulating barriers.

Close to T_c, the model proposed by De Gennes and Clark [22,23] was adopted to study the nature of grain boundaries. Accoding to this model, current flows between two superconducting grains separated by grain boundary (or weak link) due to tunneling of Cooper pair by the well known proximity effect and J_c is given by

$$J_c \propto (1-t)^2 exp(-d/\xi_N) \tag{5.1}$$

where d is the thickness of the grain boundary layers and ξ_N is the normal metal coherence length. Ignoring the weak temperature dependence of ξ_N compared to the $(1-t^2)$ term, $exp(-d/\xi_N)$ can be neglected at temperatures very close to T_c. The above expression can be rewritten as

$$J_c(t) \propto (T_c - T)^2 \tag{5.2}$$

Fig.5.13 and Fig 5.14 shows the $\sqrt{J_c}$ vs $(T_c - T)$ plot for $Y-123$ and $Yb-123$, thin films. The linear behaviour of these plots very close to T_c indicates that $Y-123$ and

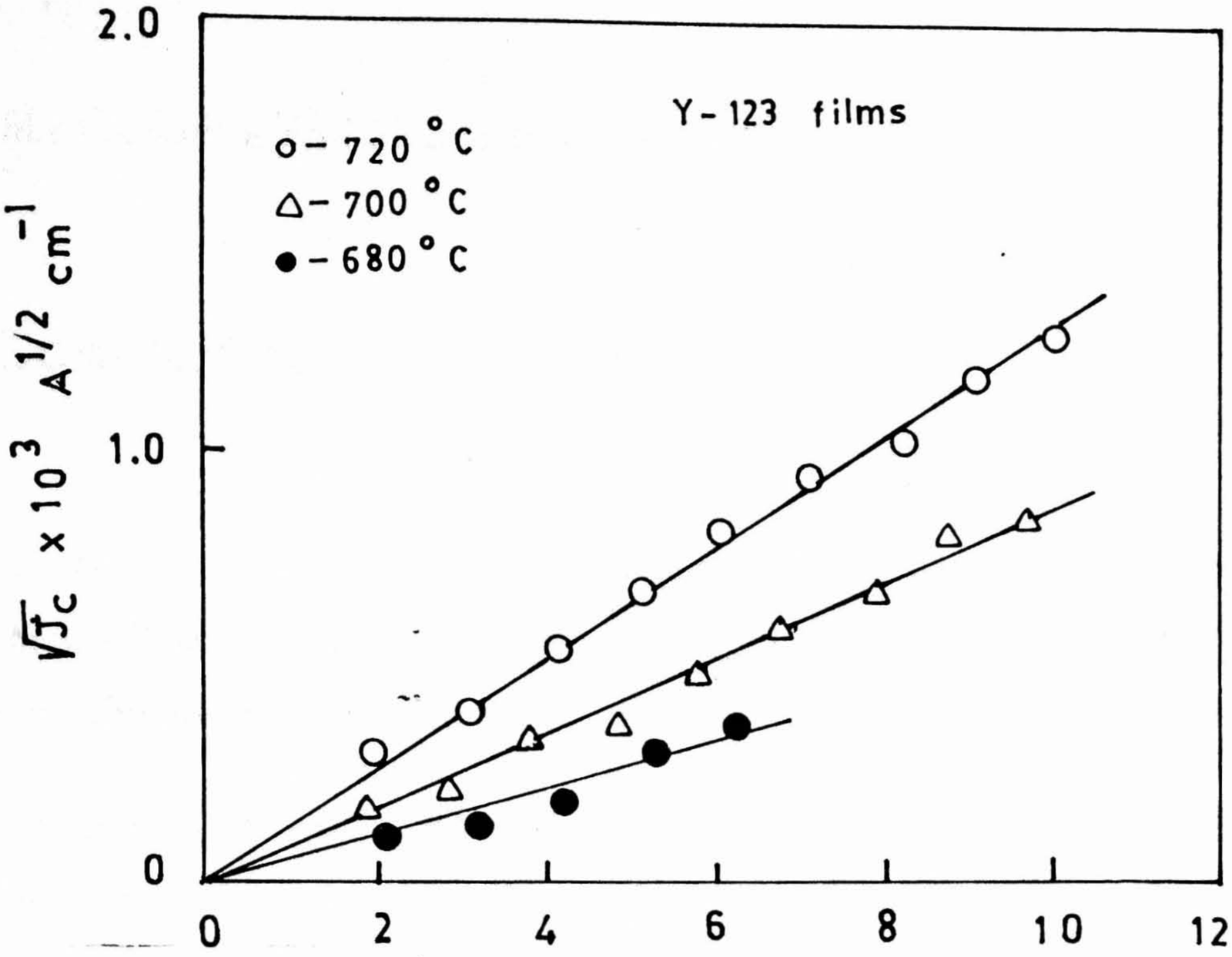

Fig.5.13. $\sqrt{J_c}$ vs Tc-T plot for Y-123 films deposited at three substrate temperatures.

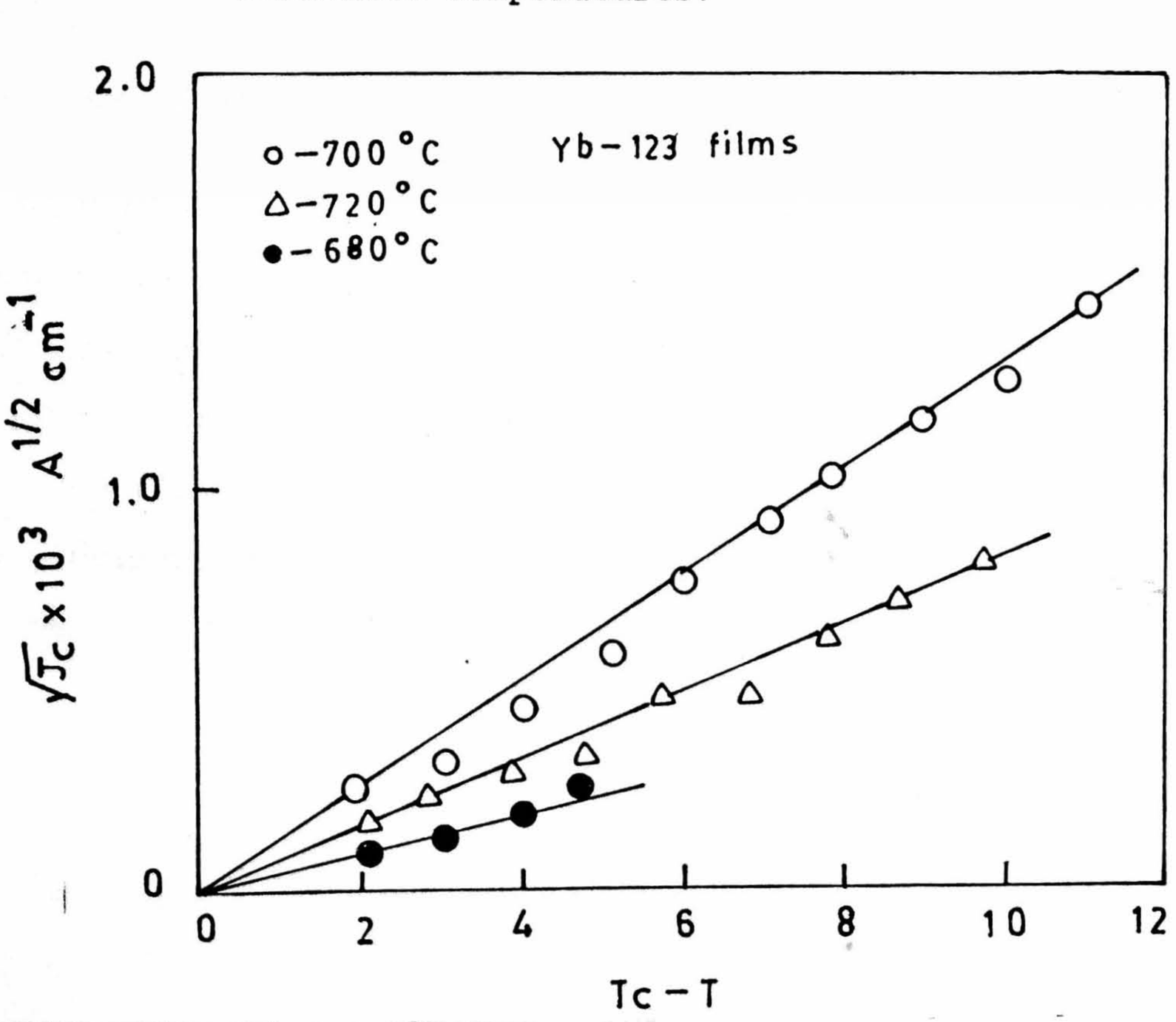

Fig.5.14. $\sqrt{J_c}$ vs Tc-T plot for Yb-123 films deposited at three substrate temperatures.

$Yb-123$ films exhibit a SNS kind of behaviour or grain coupling is metallic in nature..

5.4 Conclusions

1. In the case of $Y-123$ films, no optimization of substrate temperature was done and hence T_c and J_c are showing an increasing tendency with sunstrate temperature whereas the optimiation temperature in the case of $Yb-123$ films is 700 °C.

2. The smaller ionic radii of Yb prefers lower temperature for the formation of 123 phase where as higher ionic radius of Y prefer higher substrate temperature.

3. $Y-123$ thinfilms deposited on LAO substrate at 725 °C have resulted in good quality films with $T_c \cong 89$ K and $J_c \cong 1.8 \times 10^6$ A/cm at 77 K while $Yb-123$ thin films deposited on LAO at 700 °C have high T_c (88 K) and J_c (2×10^6 A/cm^{-2})

4. Surface morphology $Y-123$ fims deposited at 725 °C and above have shown improved microstructure when compared with that of $Y-123$ films deposited on substrates held at below 725 °C temperature. While the surface morphology of Yb-123 films show smooth surface at 700 °C only. Yb-123 films deposited above and below 700 °C substrate temperature have resulted in poor quality microstructure with many weak links.

References

[1] J.M. Taroscon, W.R. McKinnen, L.H. Greene, G.W. Hull and E.M. Vogel, Phys. Rev. B. **36** (1987) 226.

[2] P.H. Hory, L. Gao, R.L. Meng, Z.J. Huang, Y.Q.Q. Wang, K. Forster, J. Varsiliou, C.W. Chu, M.K. Wu, J.R. Ashburn and C.J. Torng, Phys. Rev. Lett. **58** (1987) 911.

[3] P. Somasundaran, A. Mohan Ram, A.M. Umarji and C.N.R. Rao, Mater. Res. Bull. **25** (1990) 331.

[4] R.M. Hazen, 1990. Properties of High Temperature Superconductors II 1990 ed. by D. Ginberg (Singapore World Scientific).

[5] H. Schwab, X.Z. Wang and D. Baurle, Appl. Phys. Lett. **60** (1992) 2023.

[6] R. Pinto, S.P. Pai, A.S. Tanhane, P.R. Apte, L.C. Gupta, R. Vijayaraghavan, K.I. Gnanaseka, and H.V. Keer, Phys. Rev. B**46** (1992) 14242.

[7] M.S. Ramachandra Rao, R. Pinto, S.C. Punandare, P.R. Apte, L.C. Gupta, R. Vijayaraghavan, B.S. Datan and V.S. Shirodkar, Supercond. Sci. Tecnology, **8** (1995) 108.

[8] M. Kanai, T. Kawai and S. Kawai, Jap. J. of App. Phys. **27** (1988) 2001.

[9] M. Kawasaki, S. Nagato, Y. Sato, M. Funabashi, T. Hasegawa, K. Kishio, K. Kitazawa, K. Fueki and H. Koima, Jpn. J. Appl. Phys. **26** (1987) L738.

[10] M. Mukadia, M. Yamamoto, Y. Tazoh, K. Kuroda and K. Hohkai, J. J. Appl. Phys. **27** (1988) L211.

[11] H. Kanuma, T. Hashimoto, T. Nakamura, K. Kishio, K. Kitazawa and K. Fueki, Jpn. J. Appl. Phys. **27** (1988) L761.

[12] S. Nagato, M. Kawasaki and H. Koimuma, Jpn. J. Appl. Phys. **27** (1988) L870.

[13] H.S. Chen, S.H. Liar, A.R. Kortan and L.C. Kinerling, Appl. Phys. Lett. **53** (1988) 705.

[14] H.S. Chen, A.R. Kortan, F.A. Thiel and L.C. Kinerling, Appl. Phys. Lett. **55** (1989) 191.

[15] J.S. Luo, N. Merchant, V.A. Maroni, D.M. Guen and B.S. Tani, K.H. Sandhage and C.A. Craven. Physica C**192** (1992) 356.

[16] N. Merchant, J.S. Luo, V.A. Maroni, D.M. Green and B.S. Tani, S. Sinha, K.H. Sandhage and C.A. Gaven, J. Mater. Res. **7** (1992) 2680.

[17] H.G. Lee, S.D. Park, C.J. Kim, G.W. Hang, H.S. Chang and D.Y. Wan, J. Applied Superconducting **1** (1993) 807.

[18] J.L.M. Driscoll, J.A. Alonso, P.C. Wang, T.W. Geballe and J.C. Bravmun, Physica C**232** (1994) 288.

[19] R.K. Singh and J. Narayan, Phys. Rev. B**65** (1991).

[20] H.F. Sakeck, M. Higgins, W.G. Graham, T. Monow, R.J. Tunner and D.G. Walmsky, J. Appl. Phys. **70** (1991) 2435.

[21] J. Manhert, D. Anselmetti, J.G. Bednorz, A. Catana, Ch. Gerber, K.A. Muller and D.G. Schiom, Z. Phys. B. Cond. Matter **86** (1992) 177.

[22] A.G. De Genner, Rev. Mod. Phys. **36** (1964) 225.

[23] J. Clarke, Proc. Roy. Soci. London A**308** (1969) 442.

Chapter 6

Studies on $YBa_2Cu_{3-x}Nb_xO_{7-y}$ Thin Films

6.1 Introduction

Current research trend in high temperature superconductivity (HTS) has substantially aimed at the improvement of superconducting properties by substitution or addition of other elements. However, numerous investigations into the effects of the substitution of copper in $Y-123$ HTS compound has resulted in only degradation of its superconducting properties. There is a scanty literature on Nb substitution at the Cu site of 123 compounds, and also to the best knowledge of the author no Nb substitution at the Cu site of $Y-123$ films has been reported. Hence it was considered worthwhile to prepare and study the $YBa_2Cu_{3-x}Nb_xO_{7-y}$ films. This chapter gives the details of this work.

The preferential occupancy in two inequivalent copper sites seems to affect the superconductivity in the $Y-123$ system substantially. Consideration of the relative substitutional occupancies of the $Cu1$ (chain) and $Cu2$ (plane) sites is central in the interpretation

of primary features such as degree of degradation of superconducting properties, oxygen site occupancy and substitutional solubility. The superconducdting properties of $Y-123$ have revealed that the $Cu-O$ plane and chains are responsible for the superconductivity and the main contribution to the density of states at the Fermi level is due to the hybridization states of copper 3d and oxygen 2p. Hence, many researchers thought that the substitution for Cu in R-123 by transition metals should produce substantial changes (improvement or degradation) in its superconducting properties.

Numerous investigations into the effects of the substitution of copper in $Y-123$ by a great variety of metallic elements have already been carried out. The most extensively investigated substitutional elements which have resulted in single phase materials are $M = Fe$, Co, Ni, Zn, Ga and Al [1-6]. In the case of trivalent magnetic (Fe and Co) and nonmagnetic (Al and Ga) substitutions, it is reported by many researchers that in $YBa_2Cu_{3-x}M_xO_{7-y}$ maximum dopant concentrations is $x = 0.15$ - 0.25 for $M = Fe$ [1,2], $x = 0.2$ - 0.33 for $M = Co$ [2,3] and $x = 0.13$ - 0.2 for Al and Ga [2,4]. The dependence of T_c on copper dopant is typically only about 2 - 5 K/at.%. In contrast to the trivalent dopants, substitution of Zn (non magnetic) for Cu results in an unusual drastic suppression of T_c, with a typical value of 11 K/atm.%. The Ni (magnetic) substitution resulted in very slow degradation of T_c very slow with the increase of dopant concentration. In the case of pentavalent dopants like V, Nb and Ta etc. [7-9] no significant improvement in superconducting properties have been observed. However, it was noticed that there is an enormous increase in oxygen intake in the case of $Nb/Ta/V$ substituted $Y-123$ compounds. Nb substitution at Cu in $Y-123$ (bulk) system has resulted in improvement of its mechanical properties and increase in the critical current density J_c upto certain level of Nb substitution [8]. Greaves et al have confirmed that the substitution of Nb and Ta at $Cu1$ site in $La-123$ system [10]. They also reported that substitution of Nb_1 at Cu_1 in $Y-123$ system results in formation of single phase YBa_2NbO_6 phase and CuO.

There are very few reports on substitution studies in HTS thin films. Song et al have reported the transport properties of $Y-123$ thin films doped upto 2 at% of Ni, Fe and Co. They found 1×10^6 A/cm^2 J_c for Ni doped film and 5×10^6 A/cm^2 for Fe and Co doped films [11]. But Ogale et al have reported much smaller J_c values in Fe and Zn doped films [12,13]. So far no systematic study has been reported on the pentavalent

element substitution in $Y-123$ thin films. Hence, in the present investigation a systematic study of Nb doping at copper site and its effect on superconducting properties in $Y-123$ thin films is presented.

The reasons for taking the present work are

- No Nb substitution report in 123 films has appeared as yet to the best of the knowledge of the author.

- Nb exists in multivalence states, moreover its ionic radius varies from 0.48 to 0.74 Ådepending upon the valence which is comparable to the ionic radii of different Cu valence states. However, the coordination of Nb, which can be IV to VIII fold, is different than that of Cu. Therefore the substitution of Nb at Cu site may affect the Cu valence and hence one may expect some substantial change in Nb substituted $Y-123$ system.

- Nb is having higher affinity towards oxygen hence it can enhance the oxygen diffusion process for growing a 123 film.

- The formation of $LaBa_2NbCu_2O_8$ has been reported in bulk form but not of $YBa_2NbCu_2O_8$ compound. It is well established that the phases, which may not stabilize in bulk, may stabilize in thin film form [14]. So an attempt is made here to see whether $YBa_2NbCu_2O_8$ phase can be stabilized in thin film form.

- Another interesting thing is that Nb itself is a conventional superconductor and if it does not substitute into the 123 lattice then it may segregate at grain boundaries and may improve the weak link behavior in the granular superconducting films by forming superconductor-metal-superconductor (S-N-S) junctions at the grain boundary domains. Hence an improvement in the microstructure and hence improvement in current density may be expected.

- The present study was also aimed at synthesizing the single phase YBa_2NbO_6 thin films as they can be useful as good buffer layers for depositing $R-123$ films.

Considering all above factors the present work of Nb substitution at Cu site of $Y-123$ system in thin films was taken up, results of which are given below.

6.2 Deposition Details of $YBa_2Cu_{3-x}Nb_xO_{7-y}$ Films

$YBa_2Cu_{3-x}Nb_xO_{7-y}$ powders were prepared using the standard solid state reaction route. Oxide powders were of 99.99% purity. For preparation of powder samples with x = 0.0, 0.025, 0.05 and 0.1, the maximum temperature used was 930°C. For preparation of sample powders with x = 0.02, 0.3, 0.4, 0.5, 0.6, 0.7, 0.8, 0.9 and 1.0. higher synthesization temperature of 1050°C was found to be optimum. The targets having diameter of 1 cm and 4 mm thickness (density around 70 to 80 % of the bulk) were prepared by a standard method. Thin films of varying Nb composition were prepared on $SrTiO_3$ < 100 > and $LaAlO_3$ < 100 > substrates using the PLD method described in Chapt.2. The target to the substrate distance was kept constant at 4.5 cm. Substrates were kept at temperatures between 700 - 800 °C and the oxygen partial pressure was maintained at 200 mTorr. Other deposition conditions were also kept the same for each film deposition including identical geometrical dimensions of each substrate. Details of the deposition conditions are given in Table 6.1-6.2. All the films were characterized by XRD, four probe DC electrical resistivity and SEM. Critical current density (J_c) measurements were done on 15μm wide 1 mm long and 200 nm thick microbridges prepared by a conventional photolithography technique.

6.3 Results and Discussion

Films were deposited on $SrTiO_3$ < 100 > by using targets of $YBa_2Cu_{3-x}Nb_xO_{7-y}$ for x = 0.0, 0.025, 0.05, 0.1, 0.2, 0.4, 0.8 and 1.0 A systematic structural change from the XRD and transport properties for these x values motivated us to study other concentrations (0.1 to 1.0) also. Hence a systematic study of Nb substitution at Cu was studied on $LaAlO_3$ < 100 > substrates was performed. The results of Nb substituted films on $SrTiO_3$ < 100 > and $LaAlO_3$ < 100 > are discussed individually as the deposition conditions are not the same for both the substrates.

Table 6.1
Optimized Laser Deposition Condition on $SrTiO_3$ < 100 >

1.	Targets	$YBa_2Cu_{3-x}Nb_xO_{7-y}$ x=0.0,0.25,0.05, 0.1, 0.2, 0.4, 0.8 and 1.0)
2.	Targets dimensions	1 cm dia 4 mm thick
3.	Substrate	$SrTiO_3$ < 100 > 0.5 × 1 cm.
4.	Substrate-traget distance	4.5 cm
5.	Substrate Temperature	700°C
6.	Laser Power	600 mJ
7.	Laser Spot size	3×0.8 mm^2
8.	Laser Pulse frequency	10 Hz.
9.	Base Pressure	10^{-6} Torr.
10.	O_2 partial pressure	200 mTorr.

Table 6.2a

Laser deposition condition on $LaAlO_3$ < 100 >

1.	Targets	$YBa_2Cu_{3-x}Nb_xO_{7-y}$ x=0.0,0.25,0.05 & 0.1
2.	Targets dimensions	1 cm dia 4 mm thickness
3.	Substrate	$LaAlO_3$ < 100 > 0.5 × 1 cm.
4.	Substrate-traget distance	4.5 cm
5.	Substrate Temperature	725°C
6.	Laser Power	600 mJ
7.	Laser Spot size	3×0.8 mm^2
8.	Laser Pulse frequency	8 Hz.
9.	Base Pressure	10^{-6} Torr.
10.	O_2 partial pressure	200 mTorr.

Table 6.2b

1.	Targets	$YBa_2Cu_{3-x}Nb_xY_{7-y}$ x=0.2 to 1.0
2.	Targets dimensions	1 cm dia 4 mm thickness
3.	Substrate	$LaAlO_3$ < 100 > 0.5 × 1 cm.
4.	Substrate-traget distance	4.5 cm
5.	Substrate Temperature	800°C
6.	Laser Power	600 mJ
7.	Laser Spot size	3×0.8 mm^2
8.	Laser Pulse frequency	8 Hz.
9.	Base Pressure	10^{-6} Torr.
10.	O_2 partial pressure	200 mTorr.

6.3.1 Films on $SrTiO_3$ <100> Substrates

Films were deposited using these targets on $SrTiO_3$ < 100 > substrates maintained at 700°C. The XRD patterns shown in Fig.6.1a-g show strongly c-axis oriented films upto $x \leq 0.1$ since all major lines can be identified as $< 00l >$. For $x \geq 1.0$ XRD patterns also show c-oriented films but with impurity phases. With the increase of Nb concentration the growth of a secondary phase YBa_2NbO_6 [15] has been identified for $x \geq 0.2$ as shown in Fig.6.1d. The best full width at half maxima (FWHM) values for the $< 005 >$ reflection of $Y-123$ for Nb substituted films are 0.21, 0.22, 0.23, 0.28, 0.31, 0.35, 0.52 and 0.75° for $x = 0.0$, 0.025, 0.05, 0.1, 0.2, 0.4, 0.8 and 1.0, respectively. The larger values of FWHM with the increase of Nb concentration indicates that grains are becoming more randomly oriented and/or grain boundary domains are increasing. Since not much variation in the FWHM values are observed for $x = 0.0$, 0.025 and 0.05 it implies that the grain size may be really the same for these compositions. For $x \geq 0.1$ a drastic change in the FWHM values is observed. This suggests a substantial change in the microstructure of the film with $x \geq 0.1$. XRD pattern for increasing x reveal that as Nb concentration increases YBa_2NbO_6 cubic phase starts growing as shown by XRD lines < 200, 300 and 400 $>$ of the compounds, and $Y-123$ phase starts decreasing. Eventually at $x = 1$, almost all $Y-123$ phase is gone and cubic phase of YBa_2NbO_6 dominates in the film. This is clearly shown in Fig.6.1f,g. The FWHM of YBa_2NbO_6 $< 004 >$ reflections whose intensity increases with Nb concentrations for $x = 0.1$, 0.2, 0.4, 0.8 and 1.0 films deposited on $SrTiO_3$ are 0.985, 0.469, 0.284, 0.26 and 0.22 respectively. This suggests that even though YBa_2NbO_6 phase is growing it is not in single phase.

6.3.1a Resisitivity and Transition Temperature Measurements

Resistance vs. Temperature $(R-T)$ plots are shown in Fig.6.2. As seen for R vs. T data, the transition temperatures for $x = 0.0$, 0.025 and 0.05 were around 89 K with sharp transition widths whereas for $x = 0.1$ and 0.2 the T_c has reduced drastically from 85 K to 72 K. Complete loss of superconductivity has been observed for $x = 0.4$ concentration whereas 0.8 and 1.0 show insulating nature i.e., R increases with decrease

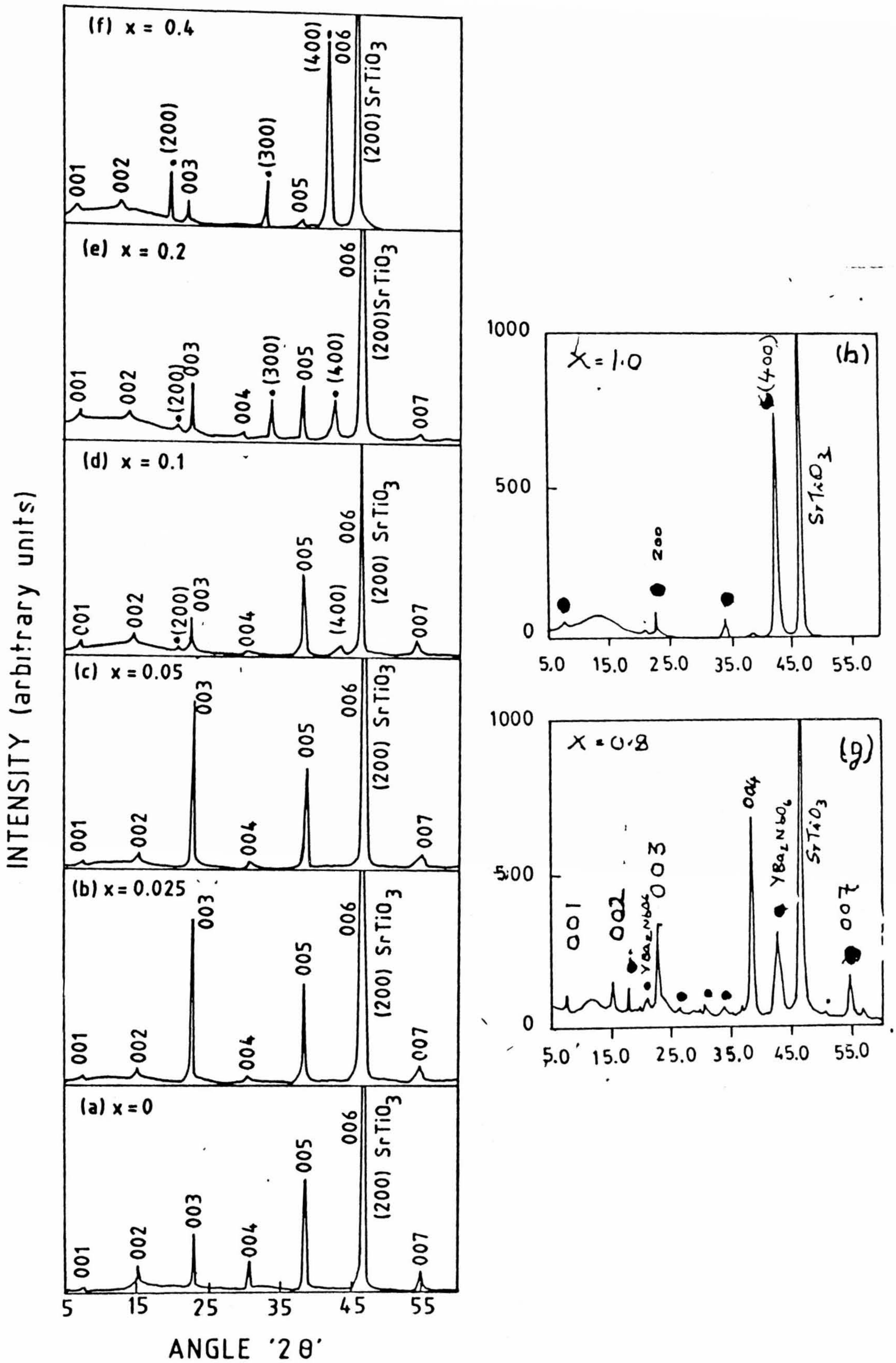

Fig.6.1. XRD patterns of $YBa_2Cu_{3-x}Nb_xO_{7-y}$ films for (a) x = 0 (b) x = 0.025 (c) x = 0.05 (d) x = 0.1; (e) x = 0.2; (f) x = 0.4; (g) x 0.8; (h) x 1.0 deposited at 700°C on $SrTiO_3$ substrates.

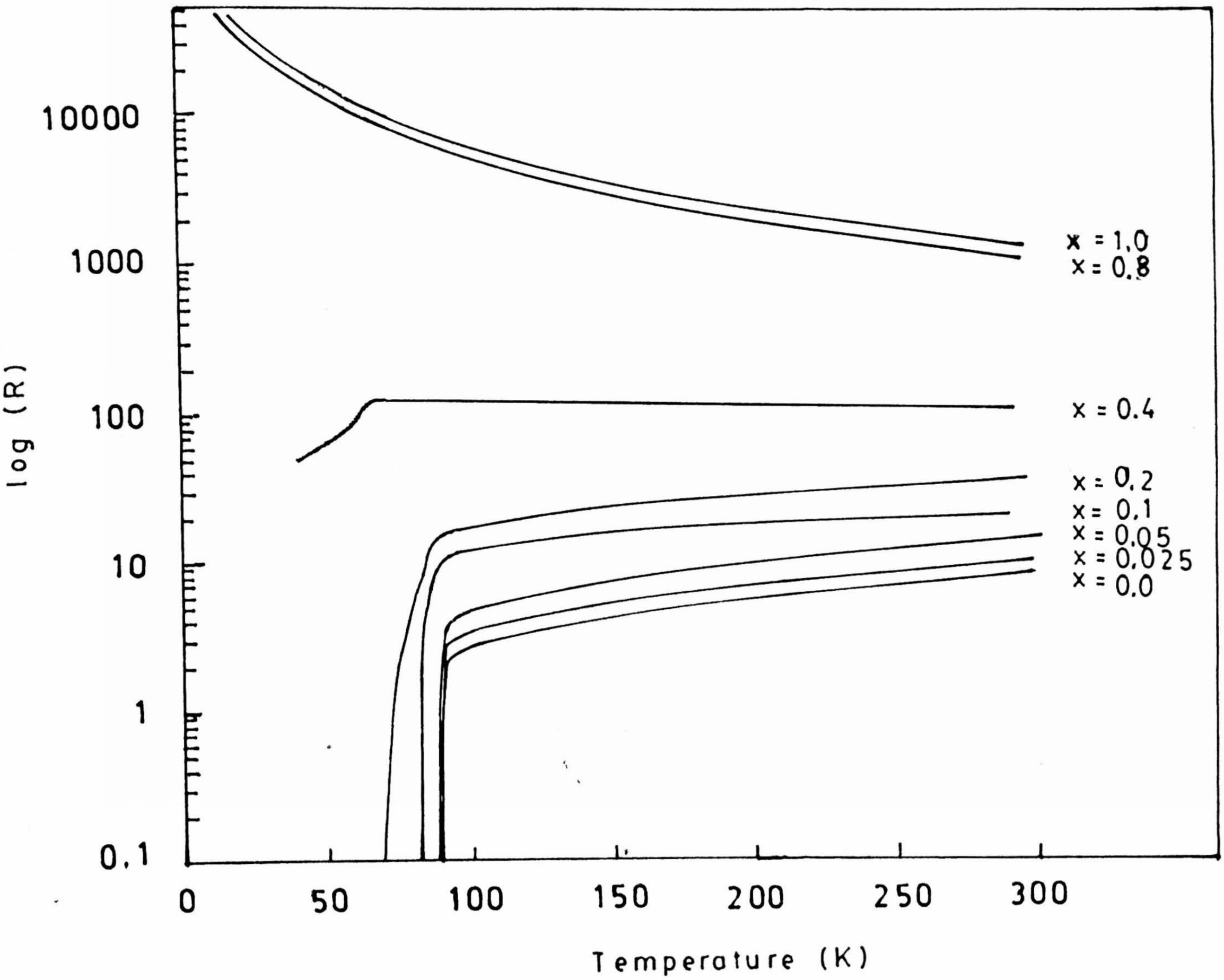

Fig.6.2. Log (R)-T plots of $YBa_2Cu_{3-x}Nb_xO_{7-y}$ thin films, x indicates Nb concentration in the films.

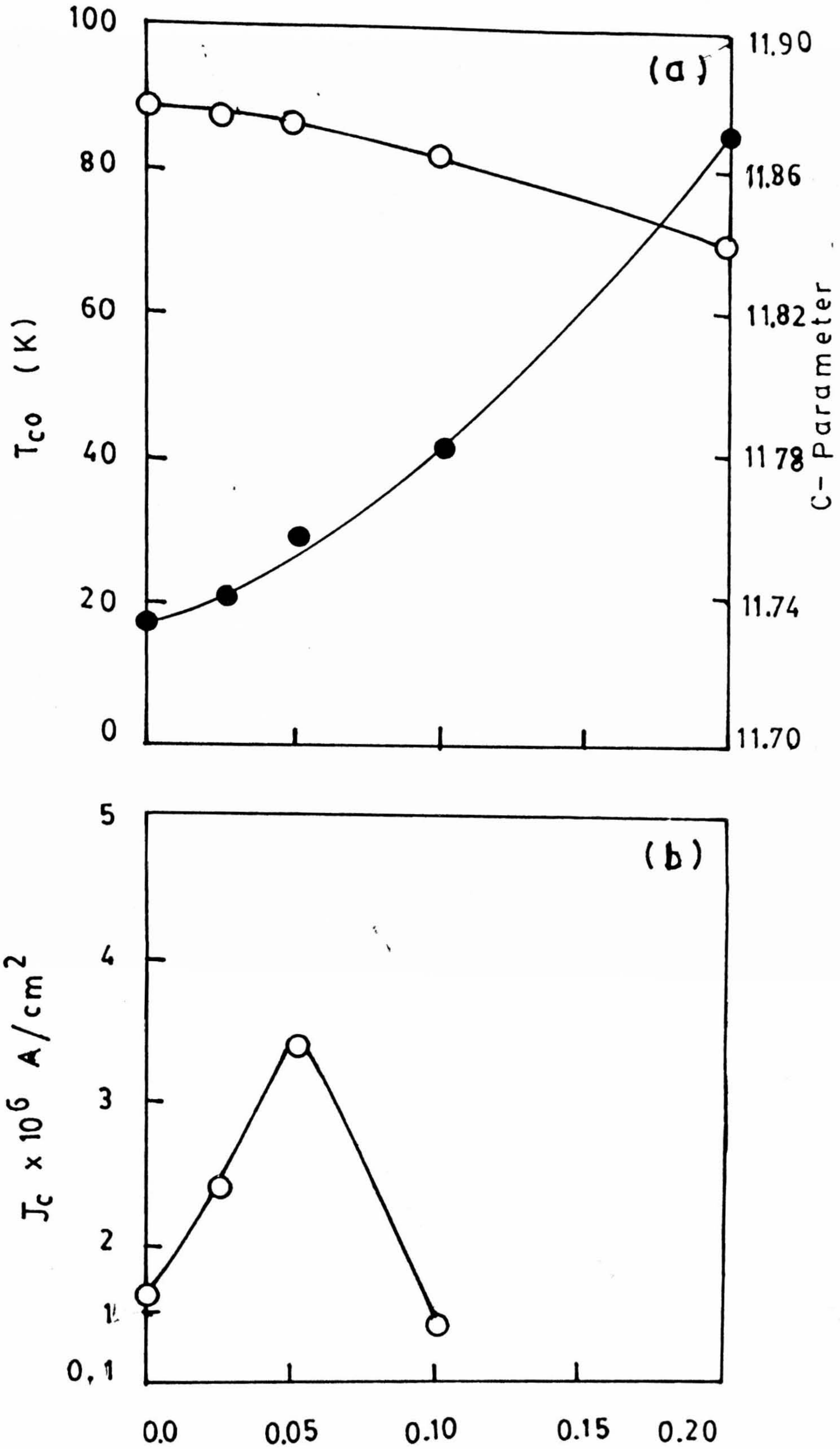

Fig.6.3. (a) T_c vs Nb concentration plots of Nb substituted Y-123 films on $SrTiO_3$ <100>; (b) J_c vs Nb concentration plots for Nb substituted Y-123 films on $SrTiO_3$ <100> deposited at 700°C.

Table 6.3 Results of $YBa_2Cu_{3-x}Nb_xO_{7-x}$ thin films deposited on $SrTiO_3$ substrates

S.No.	Sample x	Thickness (Å)	Resistivity (mΩ-cm)	T_{co} (K)	J_c(77 K) (10^6 A/cm^2)
1	0.0	1860	0.033	89.2	1.4
2	0.025	1906	0.035	88.3	2.4
3	0.05	1854	0.064	87.1	3.2
4	0.1	1796	0.987	85.4	0.2
5	0.2	1792	1.575	69.1	
6	0.4	1765	2.868		
7	0.8	1800	53.28		
8	1.0	1786	61.79		

Table 6.4 Results of $YBa_2Cu_{3-x}Nb_xO_{7-x}$ thin films deposited on $LaAlO_3$ substrates

S.No.	Sample x	Thickness (Å)	Resistivity ($m\Omega$-cm)	T_{co} (K)	J_c(77 K) (10^6 A/cm^2)
1	0.0	1824	0.228	88.8	1.20
2	0.025	1846	0.323	88.6	1.85
3	0.05	1852	0.695	88.3	2.20
4	0.1	1864	0.978	85.4	0.08
5	0.2	1848	2.033		
6	0.3	1872	5.709		
7	0.4	1844	52.55		
8	0.5	1812	1.47×10^2		
9	0.6	1892	2.59×10^2		
10	0.7	1862	5.13×10^2		
11	0.8	1879	7.06×10^2		
12	0.9	1840	8.12×10^2		
13	1.0	1888	1.04×10^3		

forming an intermediate phase YBa_2NbO_6.

The $R-T$ plots show a systematic metal to insulator transition in the electrical resistivity of Nb substituted films. Since it has been shown [18] that the addition of Nb_2O_5 does not reduced the oxygen content, this transition is most probably due to the large growth of the insulating phase YBa_2NbO_6 as indicated earlier. A detailed study of all the concentrations from $x = 0$ to 1 was done on films deposited on $LaAlO_3$ substrate and is discussed later.

6.3.1b J_c Measurements

The critical current density (J_c) measurements show an improvement upto $x = 0.05$ concentration i.e., the range of J_c realized for $x = 0.0$, 0.025 and 0.05 are $1.4 - 1.6 \times 10^6 A/cm^2$, $2 - 2.4 \times 10^6 A/cm^2$ and $2.9 - 3.2 \times 10^6 A/cm^2$ at 77 K on $SrTiO_3 < 100 >$ substrates. For $x > 0.05$ there is a drastic decrease in the J_c. Fig.6.3b shows the concentration J_c (at 77 K) vs. x which shows a peak around $x = 0.05$. The J_c values at different temperatures have been listed in Table 6.2.

D. Kumar et al [19] have reported that the nature of grain boundaries in undoped and Ag doped films can be studied using a model proposed by De. Gennes [20] and Clarke [21] as described in Chapter 3, section 3.5.4. As per this model, the slope of the $\sqrt{J_c}$ vs. $T - T_c$ will give a measure of the grain boundary domain thickness. Fig.6.4 shows the $\sqrt{J_c}$ vs. $T - T_c$ plots for $x = 0.0$, 0.025, 0.05 and 0.1 of Nb substituted thin films. It shows linear behavior for all the films. If the slope is large, it indicates good alignment of grains and hence reduction of weak links which results in good quality film. From Fig.6.4, it is evident that the slope of Nb substituted films for the concentrations 0.025 and 0.05 is larger compared with the undoped $Y-123$ film and also for $x = 0.1$ Nb doped $Y-123$ film. This indicates the metallic nature at the junctions (SNS) which implies a proximity junction like behavior as proposed by Clarke [21]. But our results indicates that the resistivity of 123 films increase with Nb_2O_5 concentration. This indicates presence of the insulating phase between the superconducting grains which may imply that Nb is not substituting at Cu site.

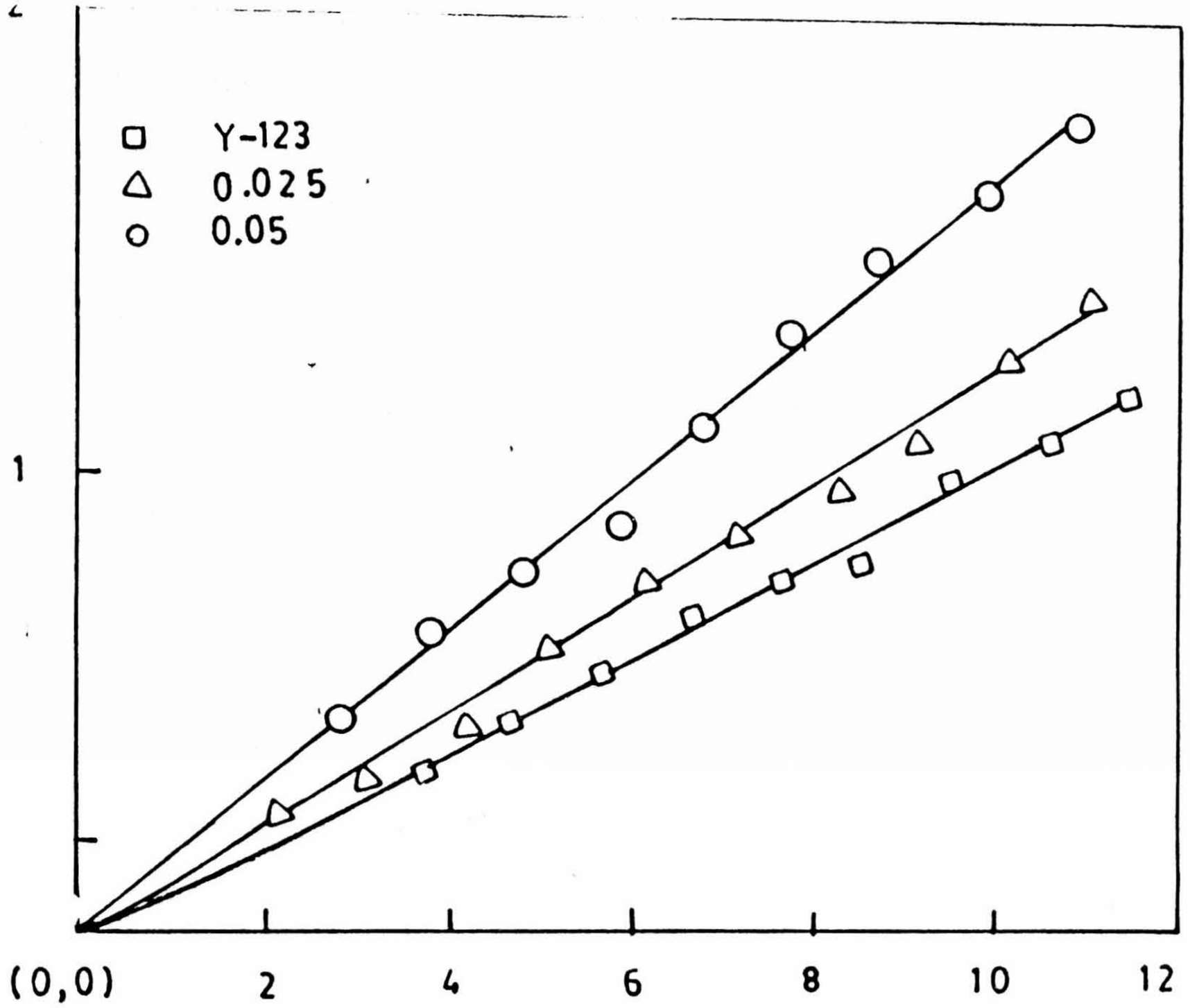

Fig.6.4 $\sqrt{J_c}$ vs (T_c-T) plots for Nb substituted Y-123 films deposited at 700°C on $SrTiO_3$ <100>.

6.3.1c Scanning Electron Microscope Studies

J_c of HTS films directly depends on their microstructure. The microstructure varies with the grain size, grain orientation and grain boundary weak links which critically depend upon the complexity of the growth process and the quality of the substrate used. The main reason for the occurrence of a large number of grain boundaries in $Y-123$ thin films are due to the dominant island growth mechanism than the layer by layer growth mechanism [22]. C-axis oriented $Y-123$ thin films show $J_c \approx 10^6 A/cm^2$ at 77 K irrespective of the deposition technique [23]. To observe the surface morphology SEM studies were performed. Fig.6.5a,b shows SEM photographs for $x = 0.0$ and 0.05 concentrations. As deposited film photographs show featureless grain structure which may be due to the alignment of grains during growth process. However, particulates still exists. To improve the contrast, films were partially etched and surface morphology was observed again. Fig.6.5a,b shows the partially etched films for $x = 0.0$ and 0.05 of Nb. The etched portions (black rectangular portions in the photographs) represents the grain size. From these micrographs it is seen that there is a grain alignment in the film with the increase of Nb concentration up to 0.05 as evident from the systematic etching of grains. From SEM studies it can be interpreted that Nb substitution may be helping in the alignment of grains.

6.3.2a Nb Substituted Films on $LaAlO_3$ <100> Substrates

The concentrations for $x = 0.0, 0.025, 0.05, 0.1, 0.2, 0.3, 0.4, 0.5, 0.6, 0.7, 0.8$ 0.9 and 1.0 were also studied to investigate the systematic changes in structural and electrical properties of Nb substituted $YBa_2Cu_{3-x}Nb_x)_{7-y}$ films.

The XRD patterns of the films deposited on $LaAlO_3 < 100 >$ are shown in Fig.6.6 $< 00l >$ orientated superconducting $Y-123$ films were obtained (which means the orthorhombic $Y-123$ exists upto $x \leq 0.2$) upto $x \leq 0.2$ concentration, and for $x \geq 0.2$ the formation of single phase YBa_2NbO_6 has been observed when deposited at a substrate temperature of 750°C. The increase in intensity of the YBa_2NbO_6 phase was observed for $x = 0.4, 0.6, 0.8$ and 1.0 concentrations. The larger values of FWHM with the increase in

Fig.5 (a) SEM photograph of Y-123 fibers [illegible] indicate grains and their orientation

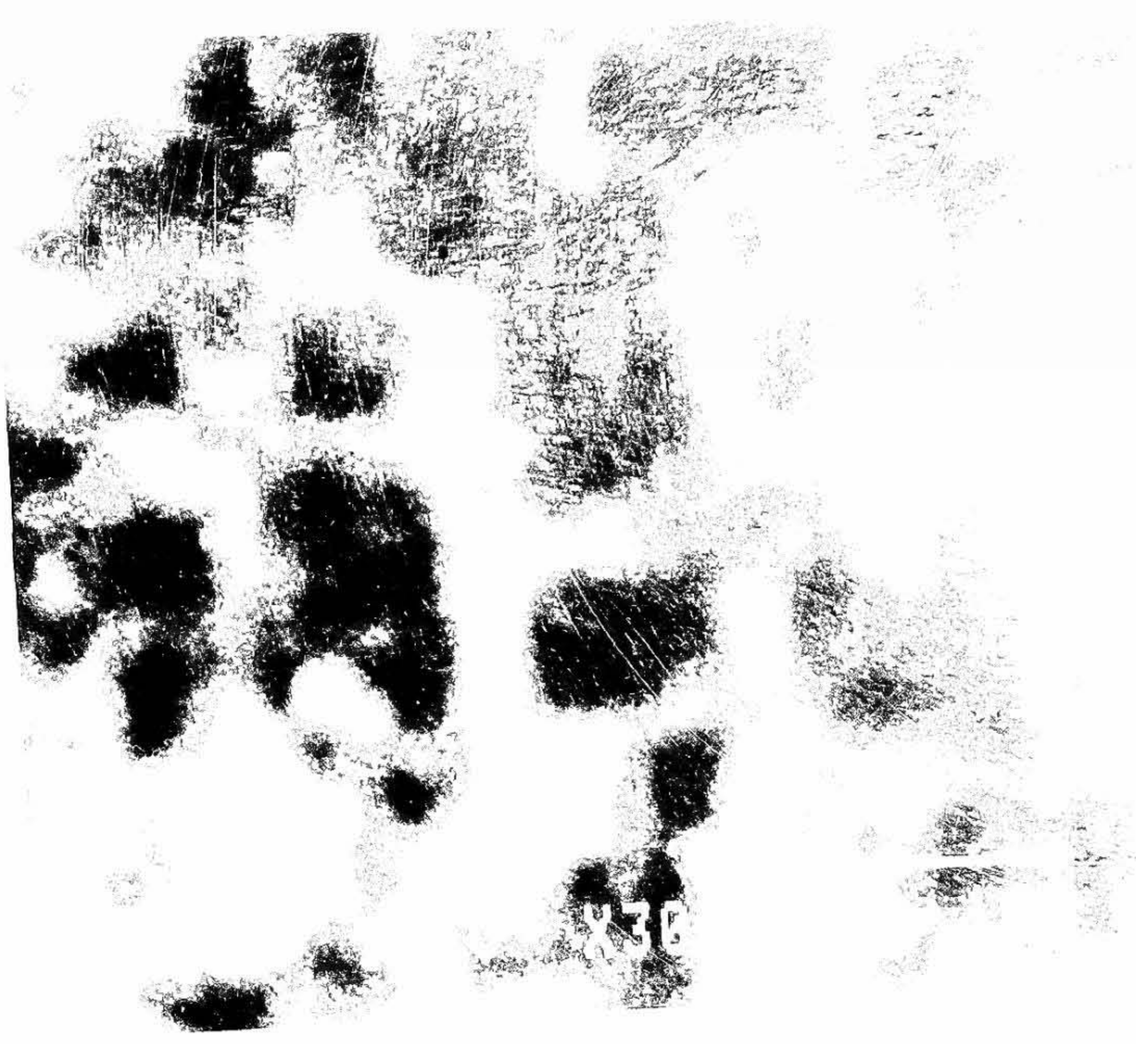

Fig.5 (b) SEM photograph of YBa[illegible] portions indicate well aligned grains.

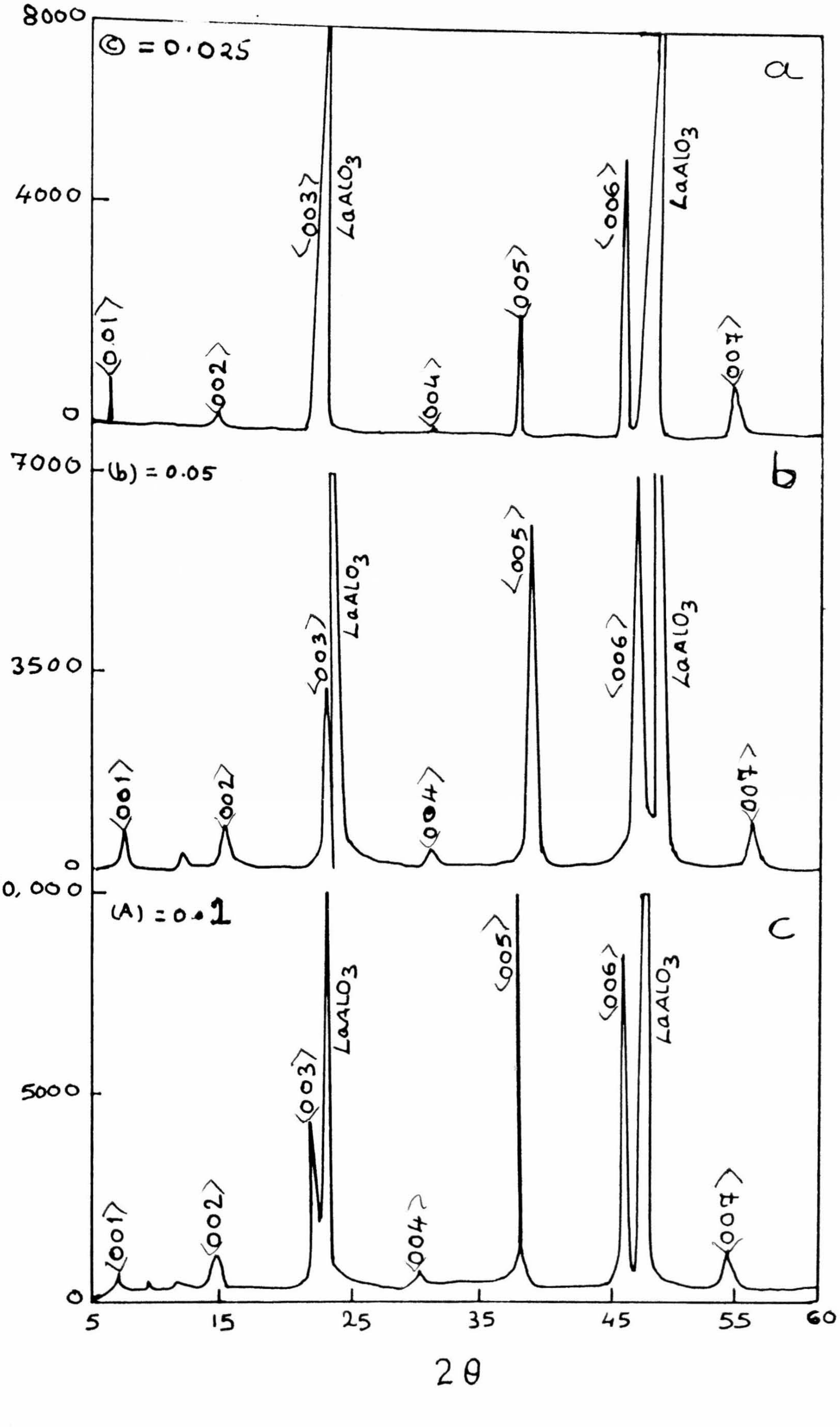

Fig.6.6. XRD patterns of $YBa_2Cu_{3-x}Nb_xO_{7-y}$ films (a) x = 0.025; (b) x = 0.05 and (c) x = 0.1 deposited on $LaAlO_3$ <100> substrate at 720°C.

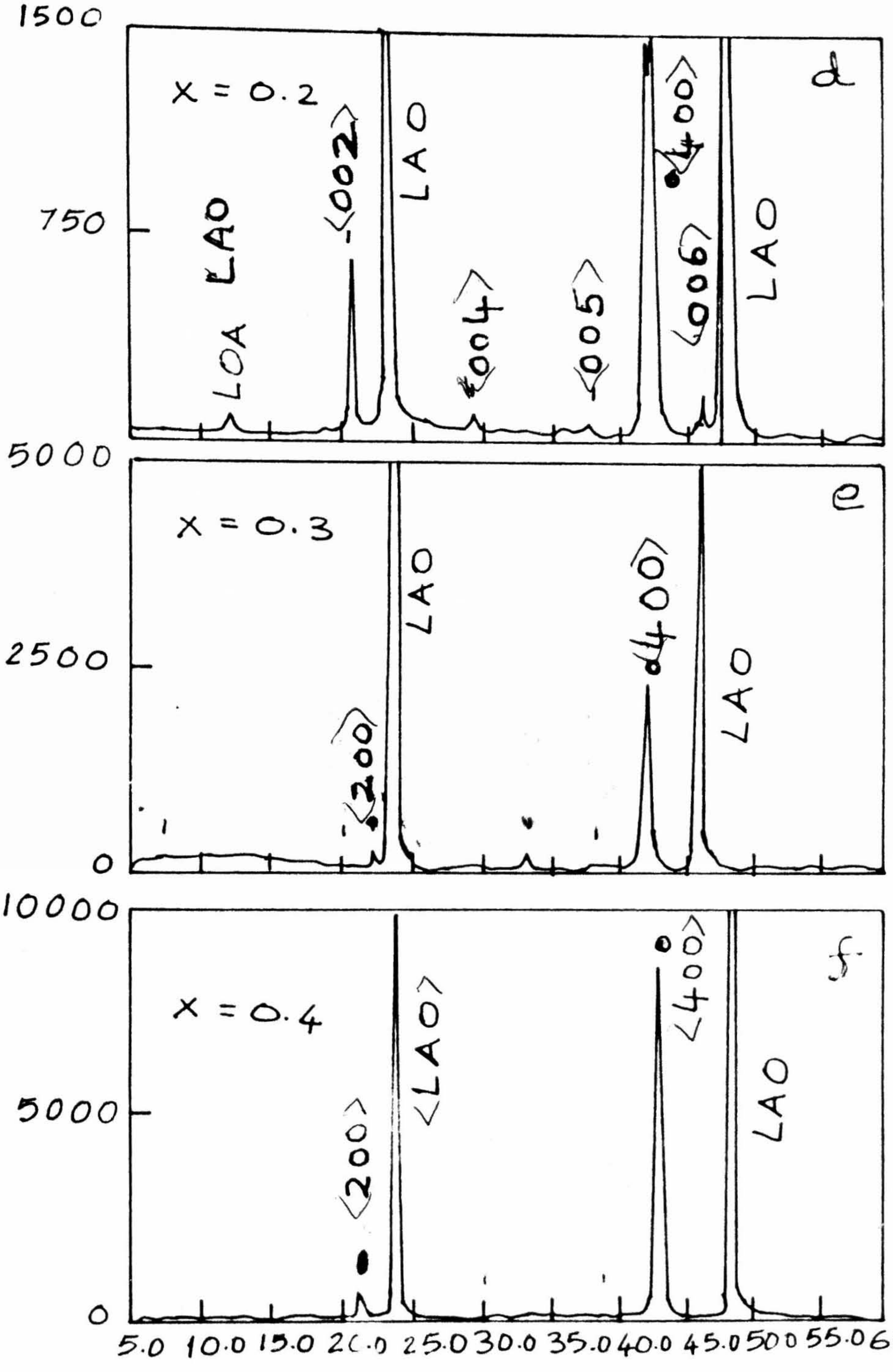

Fig.6.6. XRD patterns of $YBa_2Cu_{3-x}Nb_xO_{7-y}$ films (d) x = 0.2; (e) x = 0.3; (f) x = 0.4 at 750°C.

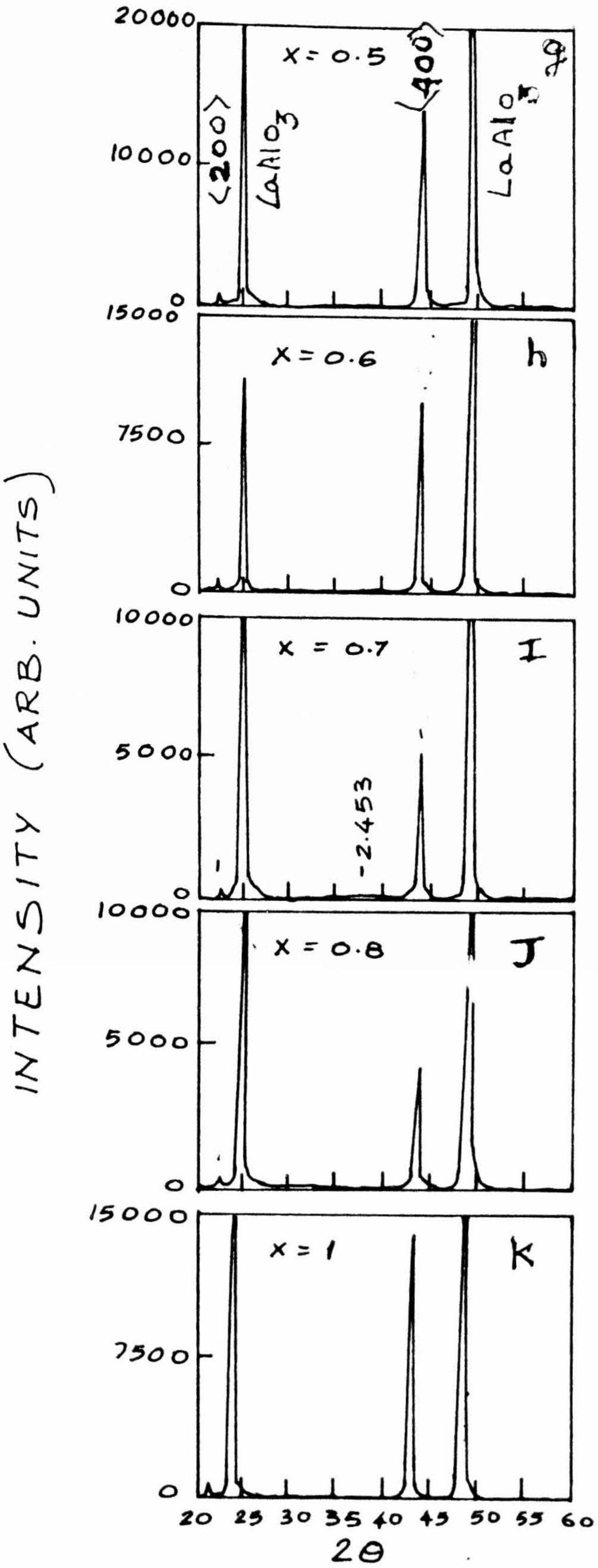

Fig.6.6. XRD patterns of $YBa_2Cu_{3-x}Nb_xO_{7-y}$ films (g) x = 0.5; (h) x = 0.6; (i) x = 0.7 (j) x = 0.8; (k) x = 1.0 at 800°C.

x above 0.1, indicates that Nb of Nb_2O_5 may be segregating at the grain boundaries or forming the secondary phase YBa_2NbO_6. The FWHM of $YBa_2NbO_6 < 004 >$ reflection whose intensity increases with Nb. FWHM values for $< 400 >$ reflection of YBa_2NbO_6 phase are 0.21, 0.25, 0.22, 0.25, 0.21, 0.22, 0.20, 0.21 and 0.22° for 0.2, 0.3, 0.4, 0.5, 0.6, 0.7, 0.8, 0.9 and 1.0, respectively. This clearly indicates that with the increase of Nb concentration and an increase in film deposition temperature makes it possible to deposit single phase YBa_2NbO_6 which is highly $< h00 >$ oriented from $x = 0.4$ onwards. Even though copper is more in the target, no X-ray detectable CuO reflection was observed.

6.3.2b T_c Measurements

Fig.6.7 shows $R - T$ curves of the films deposited on $LaAlO_3 < 100 >$ substrates. Table 6.4 gives the summary of the $R - T$ curves. It is observed that there is an increase in room temperature resistance with the increase in x and there is a linear decrease in T_c upto $x = 0.1$ and drastic suppression of T_c is observed for $x = 0.2$ as shown in Fig.6.8a. The variation of c-parameter with Nb concentration is similar to that discussed in the case of films deposition on $SrTiO_3$ substrates. Superconductivity was completely absent for films having $x \geq 0.3$. A systematic metal to insulator transition was observed from $x = 0.2$ to 0.4 concentrations from the $R - T$ plots and insulator nature is stabilized for $x = 0.6$ - 1.0 concentrations. This metal to insulator transition appears to be sudden. When the concentrations were doubled i.e 0.2 to 0.4 then the charge balance is affecting drastically (see table). Due to the imbalance and also due to the chemical reactive nature of Nb with Y and Ba results in the stable cubic phase YBa_2NbO_6 (i.e. MO_6) to form at the grain boundaries which increases with the increase in Nb concentration and complete transformation of $Y - 123$ phase into YBa_2NbO_6 takes place around $x = 0.4$ of Nb concentration.

6.3.2c J_c Measurements of Films on $LaAlO_3 < 100 >$ Substrate

As there is a lattice mismatch between $LaAlO_3$ and $Y - 123$ it is relatively difficult

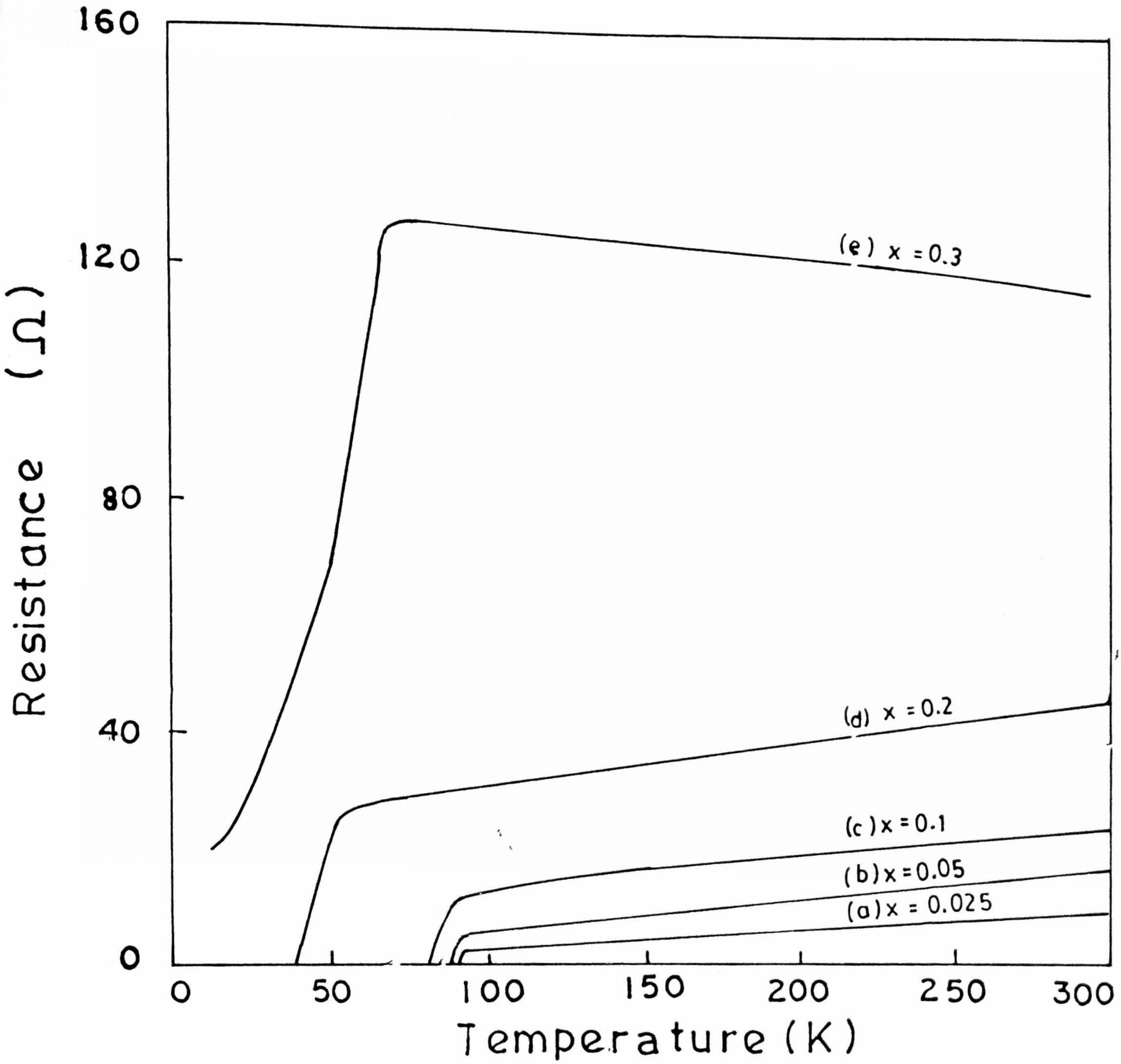

Fig.6.7. Resistivity vs temperature plots of $YBa_2Cu_{3-x}Nb_xO_{7-y}$ films deposited on $LaAlO_3$ <100> for (a) x = 0.025; (b) x = 0.05; (c) x = 0.1; (d) x = 0.2 and (e) x = 0.3.

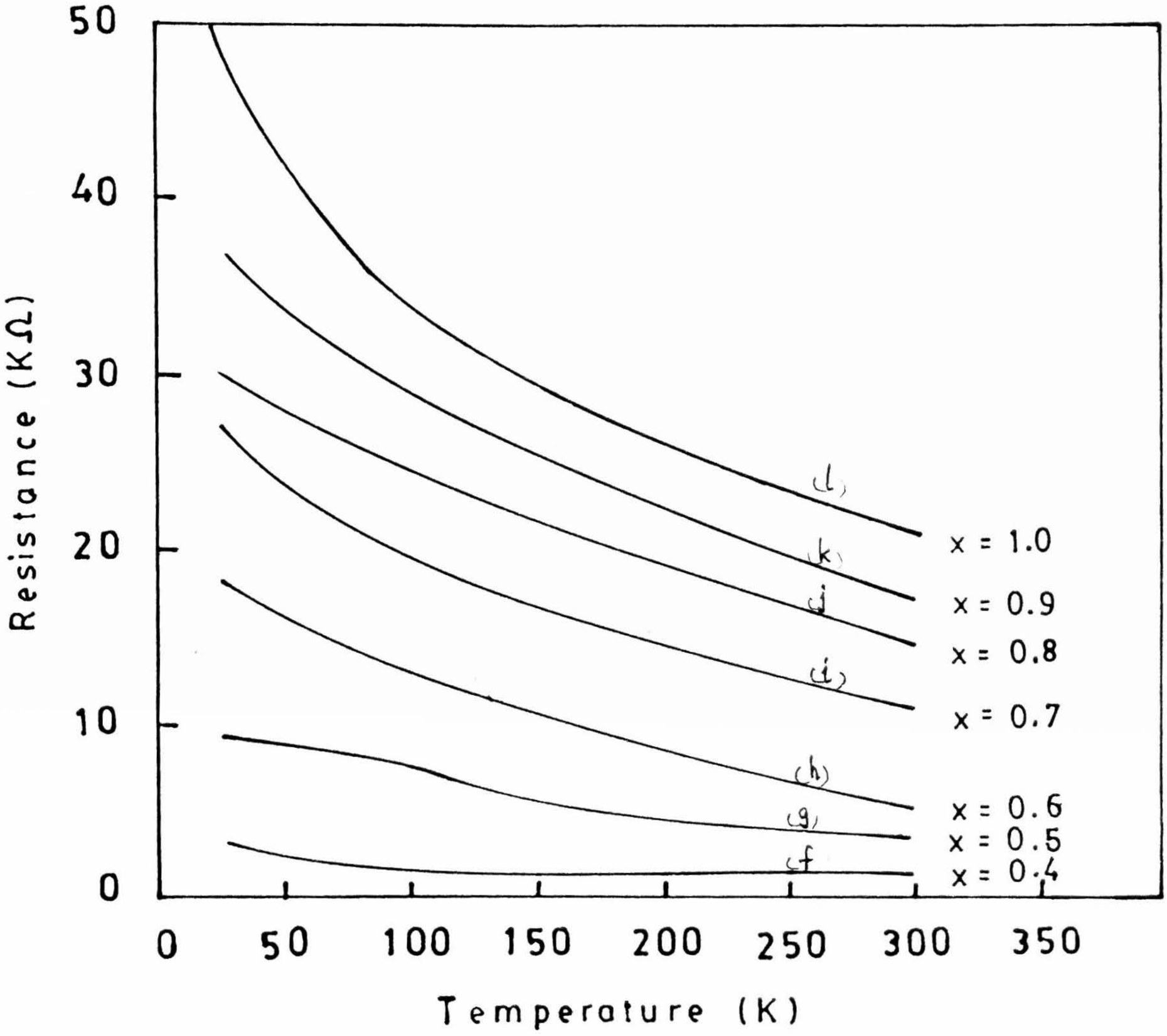

Fig.6.7. Resistivity vs temperature plots of $YBa_2Cu_{3-x}Nb_xO_{7-y}$ films deposited on $LaAlO_3$ <100> for (f) x = 0.4; (g) x = 0.5; (h) x = 0.6; (i) x = 0.7 and (j) x = 0.8; (k) x = 0.9; (l) x = 1.0

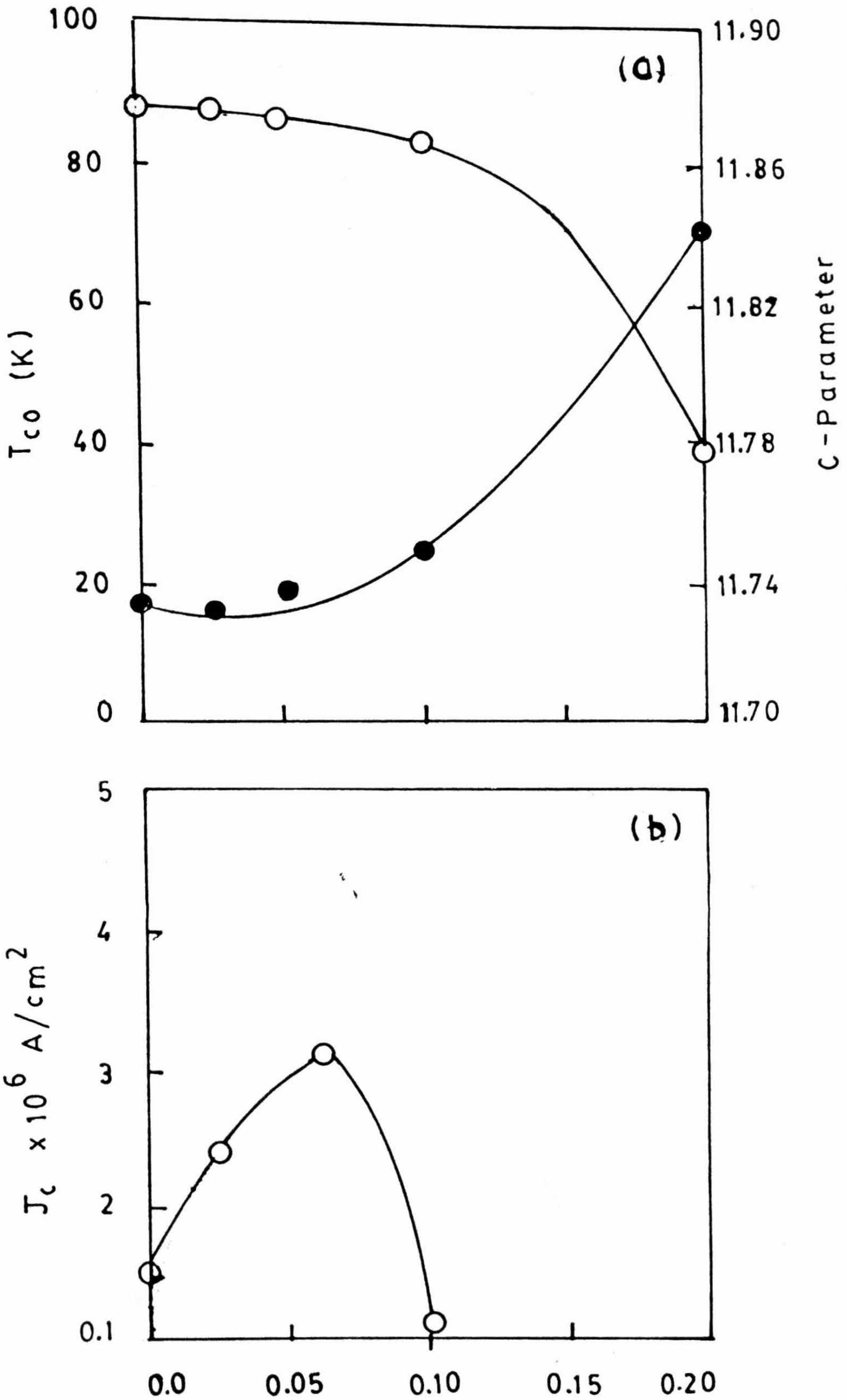

Fig.6.8. (a) T_c vs Nb concentration of Y-123 films deposited on $LaAlO_3$ <100> at 720°C.

Fig.6.8. (b) J_c vs Nb concentration of Nb substituted Y-123 films deposited on $LaAlO_3$ <100> at 720°C.

to achieve high J_c on $LaAlO_3$ < 100 > substrates. Fig.6.8b shows T_c and J_c vs. x, concentration of Nb substituted films on $LaAlO_3$ < 100 > substrates. Here also J_c peaks around $x = 0.05$. The highest J_c achieved on $LaAlO_3$ substrate for $x = 0.05$ is $2.9 \times 10^6 A/cm^2$ at 77 K. The $\sqrt{J_c}$ vs. $T_c - T$ plots shown in Fig.6.9 have linear behavior for concentrations $x = 0.0$, 0.025 and 0.05 and indicates films having interconnecting grains. However, undoped $Y - 123$ films have the lowest slope when compared with that of Nb doped films. This clearly indicates that there is a relative improvement in the Nb doped films upto $x = 0.05$ when compared to that of undoped $Y - 123$ thin films. Since $SrTiO_3$ has a very good lattice match relatively higher J_c were realized on $SrTiO_3$ stubstrates whereas $LaAlO_3$ has a lattice mismatch of nearly 5% which could be responsible for realizing relatively lower $J_c s$ on $LaAlO_3$ < 100 > substrates.

6.4 Conclusions

The effect of Nb substitution for Cu, on the superconducting properties of $Y - 123$ thin films has been studied. These studies reveals the following.

1. It is noticed that no significant change in the crystal structure or in T_c has been observed in $Y - 123$ thin films for Nb substitution for Cu upto $x = 0.05$. Above this concentration there is a change in crystal structure from < $00l$ > orientation to < $h00$ > orientation (i.e orthorhobic $Y - 123$ to cubic YBa_2NbO_6) phase and drastic suppression in T_c and complete loss of superconductivity for $x \geq 0.3$ of Nb substitution.

2. There is a relative improvement in the superconducting properties of Nb substituted films upto $x = 0.05$ concentration when the same is compared with undoped films. The T_c of the films for $x = 0.0$, 0.025 and 0.05 is around 88 K and J_c has shown an increasing tendency and peaks around $x = 0.05$ and above which it decreases drastically.

3. **The best $J_c s$ realized on $SrTiO_3$ < 100 > substrate are J_c $(x = 0.05) = 3.2 \times 10^6 A/cm^2$, $J_c(x = 0.025) = 2.4 \times 10^6 A/cm^2$ and J_c $(x = 0.0) = 1.4 \times 10^6 A/cm^2$**

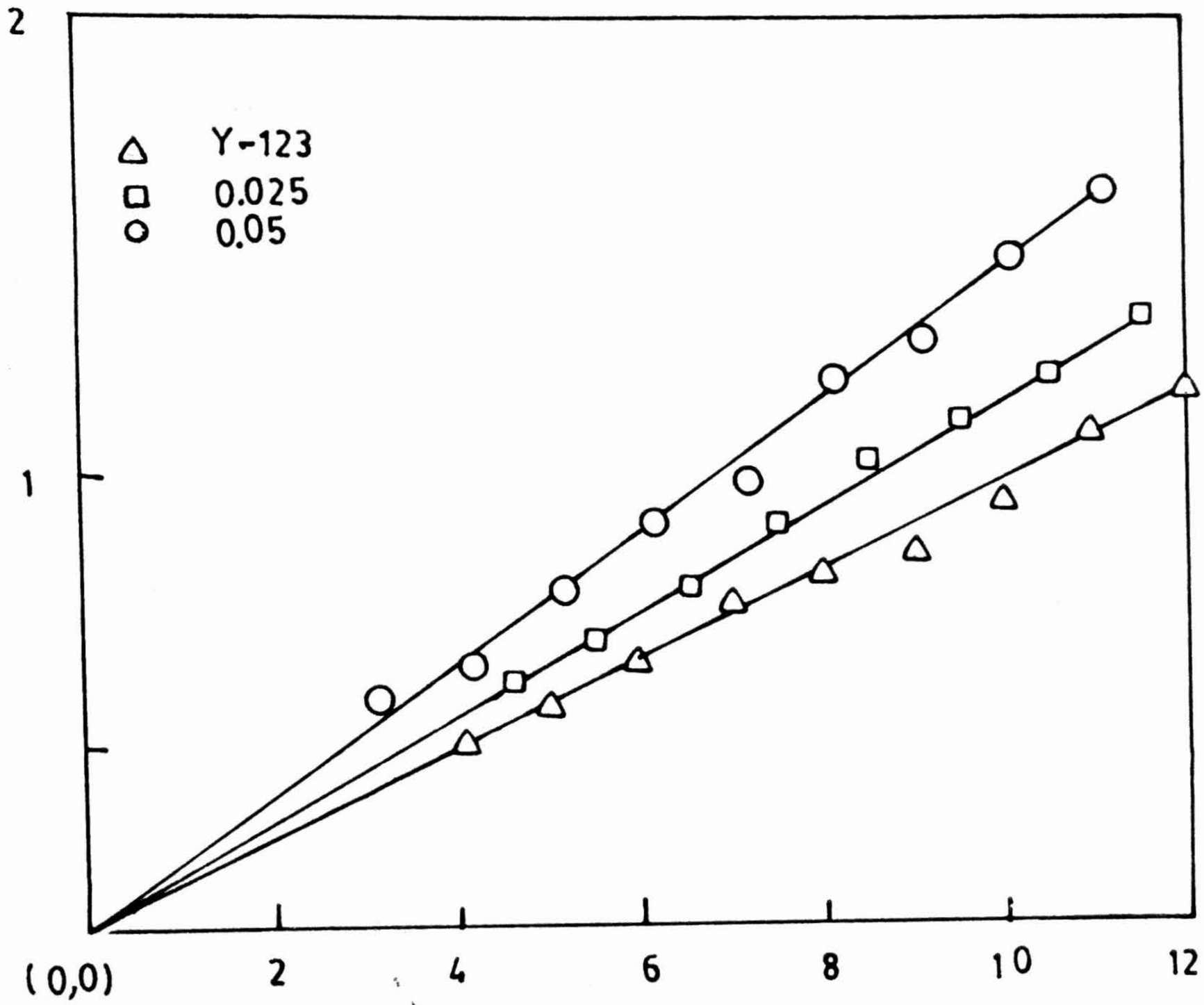

Fig.6·9· $\sqrt{J_c}$ vs (T_c-T) plots for Nb substituted Y-123 films deposited on $LaAlO_3$ <100> at 720°C.

where as the best $J_c s$ realized on $LaAlO_3 < 100 >$ are 1.2×10^6, 1.95×10^6 and $2.85 \times 10^6 A/cm^2$ at 77 K, respectively. It confirms that substrate nature also play an important role in getting high J_c superconducting thin films.

4. The SEM studies reveal that proper grain alignment occurs in $YBa_2Cu_{3-x}Nb_xO_{7-y}$ films upto $x = 0.05$ as evident from the surface morphology of partially etched films.

5. The linear behaviour of $\sqrt{J_c}$ vs. $T_c - T$ plots for $x = 0.0$, 0.025, and 0.05 Nb substituted films suggests the proximity effect of the grain boundary junctions.

6. It is realized from these studies that $YBa_2Cu_2Nb_1O_8$ phase does not form even in thin films.

References

[1] M. Mehbod, P. Wyder, R. Deltour, Ph. Duvigneaud and G. Maessens, Phys. Rev. B **36** (1987) 8819.

[2] J.M. Tarascon, P. Barboux, P.F. Mieceli, L.H. Greene, G.W. Hull, M. Eibschutz and S.A. Sunshine, Phys. Rev. B **37** (1988) 7458.

[3] J. F. Bringley, T.M. Chen, B. A. Averill, K. M. Wong and S. J. Poon, Phys. Rev. B. **38** (1988) 7458.

[4] Gang Xiao, M.Z. Cieplak, A. Gavrin, F. H. Streitz, A. Bakhshai and C. L. Chein, Phys. Rev. Lett **60** (1988) 1446.

[5] M. S. Islam and Baetzold, Phys. Rev. B **40** (1989) 10926.

[6] Y. Maeno, T. Tomita, M. Kyogogoku, S. Awaji, Y. Aoki, K. Hoshino, A. Minami and T. Fujita, Nature, **328** (1987) 512.

[7] V.P.N Padmanaban and K. Shahi, Physica C **208** (1993) 263.

[8] M. Kuwabara and N. Kusaka, Jpn. J. Appl. Phys. **27** (1988) L1504.

[9] G. V. Subba Rao, S. Natarajan and U. V. Varadaraju, Physica C **153** (1988) 501.

[10] C. Greaves and P.R. Slater : Physica C **161** (1989) 245.

[11] L. W. Song, G. Narumi, F. Yang et al Physica C **174** (1991) 303.

[12] S. B. Ogale, S. T. Bendre, P. Guptasarma and M. S. Multani, Solid State Comm. **78** (1991) 285.

[13] S. B. Ogale, M. Vedavyas, G.S.T. Bendre and S.M. Kanetkar, Appl. Phys. Lett **61** (1992) 2105.

[14] R. Pinto, S.P. Pai, A.S. Tanhane, P.R. Apte, L.C. Gupta, R. Vijayaraghavan, K.I. Gnanaseka, and H.V. Keer, Phys. Rev. B**46** (1992) 14242.

[15] K.V. Paulouse, J. Koshy and A.D. Damodaran, Physica C **193** (1992) 2105.

[16] H. Obara, H. Oyaanagi, K. Murata, H. Yamasaki, H. Ihara, M. Tokumot, Y. Nishihara and Y. Kimuara, Jpn. J. Appl. Phys. **27** (1988) L603.

[17] G. K. Strukova, I.S. Smirnova, S. A. Shevchenko, A. I. Kolyubakin, I.I. Zver Kova, V. Sedykh, A. A. Polyanskii, L. A. Dorosinskii and V. Sh. Shekhtman, Supercon. Sci. Technol., **6** (1993) 589.

[18] K.V. Paulore, J. Koshy and A.D. Damodaran, Jpn. J. App. Phys. **30** (1991) L458.

[19] D. Kumar M. Sharon, P.R. Apte, S. P. Pai, R. Pinto, Appl. Phys. Lett., **61** (1992) 2105.

[20] P.G. Dennes, Rev. Mod. Phys. **36** (1964) 225.

[21] J. Clarke : Proc. R. S. London A **308** (1969) 447.

[22] H. U. Krebs, Ch. Krauns, X. Yang and U. Geyer, Appl. Phys. Lett. 59 (1991) 2180.

[23] R. Kromann, J. B. Blide-Sorensen, R. Dereus, N. H. Andersen, P. Vase and T. Freltoft, J. Appl. Phys. **71** (1992) 3419.

Chapter 7

V_2O_5 and Nb_2O_5 Doped Y-123 Thin Films

7.1 Introduction

In the previous chapter variation of transport properties with Nb substitution at Cu site in Y-123 thin films have been discussed in detail. The present chapter deals with the addition effect of of V_20_5 and Nb_2O_5 to Y-123 system in thin film form.

There are two main obstacles in using HTS oxide superconductor for high current applications; Primarily due to the the large H_{c2} anisotropy, and weak coupling between grains resulting in disappointingly low transport currents [1-3]. Several attempts have been made to modify the nature of the grain boundary e.g., in the case of bulk $YBa_2Cu_3O_{7-y}$ $(Y-123)$ by doping with appropriate metals or oxides. As many metals and metal oxides adversely react with $Y-123$ and suppress the T_c, the choice of elements for the doping is rather limited and the degree of doping has to be carefully controlled[4]. Such studies conclude, that the J_c could be raised by an order of magnitude

by doping an optimal concentration of metal oxides having either low melting point (less than 800°C) or decomposition temperatures (less than 800 °C) and less chemical reactivity with $Y-123$ system [5-9]. Kammlott and his coworkers reported that a complete recovery of 90 K superconductivity can be achieved by natural melt processing of the material doped with certain transitional metals, which is attributed to second phase particles draining the dopant element away from the matrix [6]. Panlose et al have reported that widely accepted slow cooling procedure is not essential to obtain $Y-123$ (bulk) samples with high T_c and J_c if the samples are doped with small amount of Nb_2O_5 [7,8]. It is well established that a T_c of 90 K could still be obtained by quenching [8,9].

Moreover, as the current density (J_c) of the superconducting films is more relevant to practical applications, it is important to study factors which influence J_c in metal oxide doped $Y-123$ films. Addition of Au [10], Ag_2O [11], Pt [12], and Sb_2O_3 [13] in $Y-123$ films revealed that certain dopants can improve quality (T_c and J_c) of $Y-123$ films when deposited at relatively lower substrate temperatures due to their surfactant like nature.

In addition to above reasons, the main motivation to carry the present work is,

- Both vanadium and Niobium can exist in +5 valence as well as other state and both are conventional superconductors. So it is interesting to see how their addition affects the superconducting properties of $Y-123$ thin films.
- The melting point of V_2O_5 is 690°C and decomposition temperature is 1750°C. Whereas for Nb_2O_5 melting point is 1460°C. Hence it is quite interesting to study their addition affects on superconducting properties of $Y-123$ thin films using PLD technique.
- In $Y-123$ thin films the grain boundaries are the main passage for diffusing oxygen out. As the additives usually occupy the grain boundary domains, these inhibit oxygen diffusion resulting in lesser degradation of doped $Y-123$ thin films to that of undoped $Y-123$ thin films with time.

Considering all above, the addition of V_2O_5 and Nb_2O_5 to $Y-123$ thin films have

been studied to investigate their effect on the superconducting properties of $Y-123$ thin films.

7.2 Experimental Details

Targets for pulsed laser deposition were made by the standard solid state method using $Y-123$ powder (99.,9%) and, V_2O_5 (99.999%) and Nb_2O_5 (99.9%) powders. The doping concentrations chosen for V_2O_5 and Nb_2O_5 in this study were 0.00%, 0.25%, 0.5%, 1% and 2 wt% by weight. Thin films were made using pulsed laser ablation (PLD) method on $SrTiO_3$ < 100 > substrates of same geometrical dimension under identical deposition conditions. Table 7.1 shows the deposition conditions. The substrate temperatures were maintained at 725±5°C. Each film thickness was nearly 2000 Åfor all depositions. J_c measurements were done on 100 μm × 1.5 mm × 200 nm microbridges prepared by the laser pattern technique. Structural characterization of films was done using XRD. Using SEM, microstructure was studied on partially etched films.

7.3 Results and Discussion

7.3.1 V_2O_5 doped Y-123 thin films

XRD patterns of V_2O_5 doped $Y-123$ films are shown in Fig.7.1. Strongly c-axis oriented films were grown on $SrTiO_3$ substrate upto 1 wt% of V_2O_5 doped $Y-123$ thin films. An impurity peak is seen around $2\theta = 43°$ for 2 wt% of V_2O_5 doped $Y-123$ thin films in Fig. 7.1(d). This impurity peak reflection corresponds to < 400 > orientation of $YBa_2V_3O_8$ phase.

The FWHM values of < 005 > reflections for V_2O_5 doped $Y-123$ films are 0.28°,

Table 7.1

Laser deposition conditions for addition studies in Y-123 thin films

1	TARGETS	1. V_2O_5 (by wt%) doped $Y-123$ targets a)0.25% b) 0.5% c)1.0% and d) 2.0% concentrations 2. Nb_2O_5 (by wt% doped Y-123 targets a) 0.25% b) 0.5% c) 1.0% and d) 2.0% concentrations.
2	Substrates	$SrTiO_3$ < 100 > substrates.
3	T-S distance	4.5 cm.
4	Laser Energy	620 mJ.
5	Pulse frequency	10 Hz
6	Substrate temperature	700 q 5°C.
7	Base pressure	10^{-5} Torr.
8	Oxygen pressure	200 mTorr.

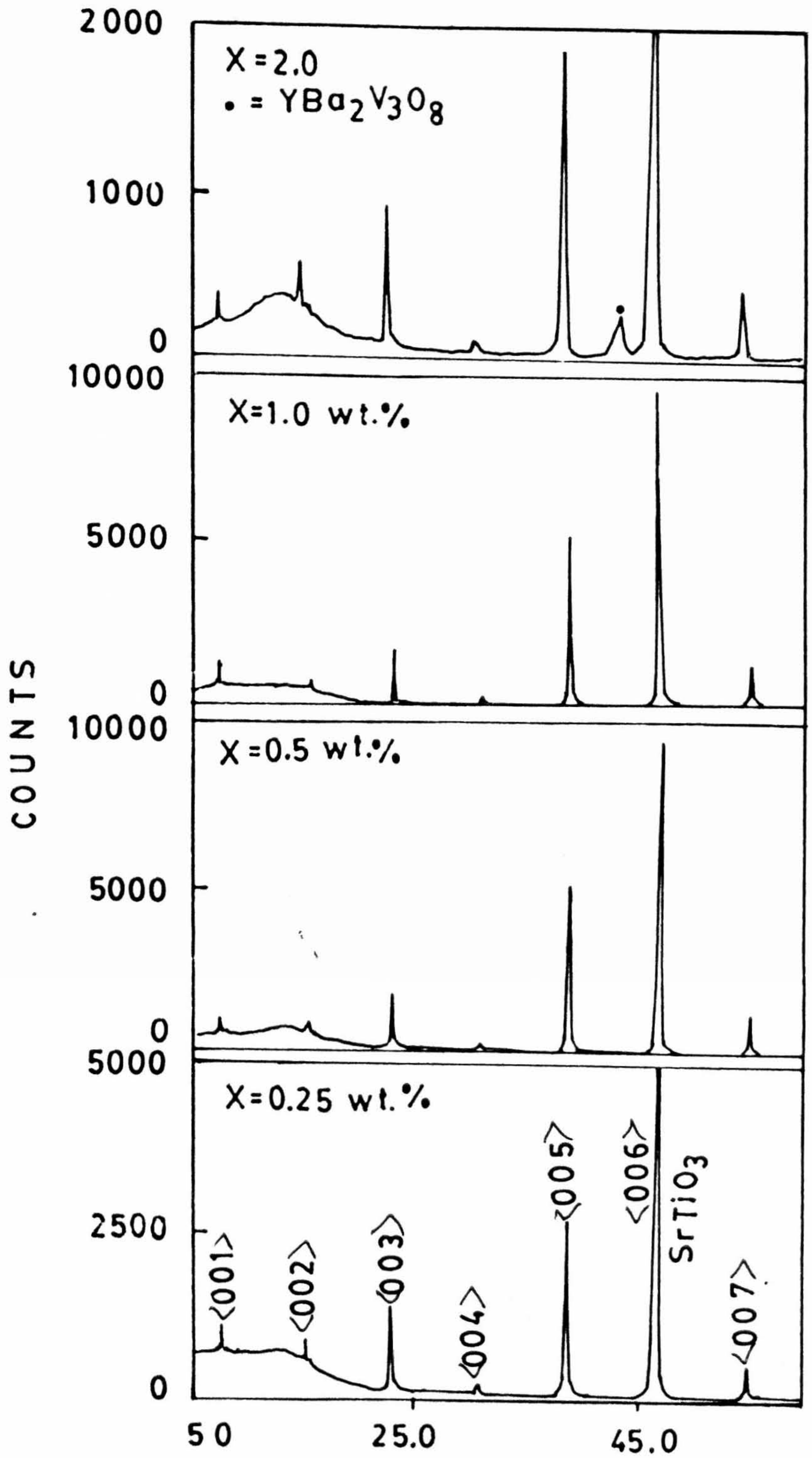

Fig.7.1. XRD patterns of V_2O_5 added Y-123 films on $SrTiO_3$ <100>.

0.2^o, 0.24^o, 0.34^o and 0.38^o for 0.0%, 0.25%, 0.5 wt.%, 1 wt% and 2 wt% concentrations of V_2O_5, respectively. These values indicate that there is some relative improvement in the crystallinity of the films when compared to that of undoped $Y-123$ film upto 0.5 wt% i.e., FWHM decreases and then degradation of the crystallinity takes place from 1 wt% onwards, since FWHM show larger values. The improved crystallinity indicates larger grain size and proper grain alignment with respect to the substrate in these films. Above 0.5 wt%, the formation of some intermediate phase at the grain boundaries may be responsible for the observed larger FWHM values.

Fig.7.2 shows c-axis parameter and T_c vs concentration of V_2O_5 doped $Y-123$ films. The c-axis parameter decreases upto 0.5 and then increases rapidly. T_c is stabilized around 88 K upto 0.5 wt% concentration addition of the dopants and above which it decreases rapidly. The decrease in c-parameter can be attributed to well oxygenation of the $Y-123$ film [14] . However, for higher concentrations above 0.5 wt% c-parameter increases sharply which indicates insufficient oxygenation. Reduced T_c can be attributed to less oxygenation in the presentc case. Moreover, growth of impurity phase at 2 wt% confirms that insufficient oxygenation to the $Y-123$ cell and hence local defects at oxygen sites might be responsible for decrease in T_c and increase in the c-axis parameter. This explanation is based on the earlier reports [14] and present data in this work clearly reflects their confirmed results.

Table 7.2 shows the T_c, T_{co}, resistivity ρ and J_c values of the V_2O_5 doped $Y-123$ thin films. Fig.7.3 shows R vs T_c plots for V_2O_5 doped $Y-123$ films. Above all the curves show linear behaviour with temperature. The increase in resistivity for samples above 0.5 wt% can be attributed to the growth of $YBa_2V_3O_8$ phase. Increase in residual resistance also clearly suggests that widening between the superconducting grains by nonsuperconducting region and hence degradation in microstructural properties of these films. From these results 0.5 wt% appears to be the optimum level of doping without affecting the $Y-123$ structure in the case of V_2O_5 addition.

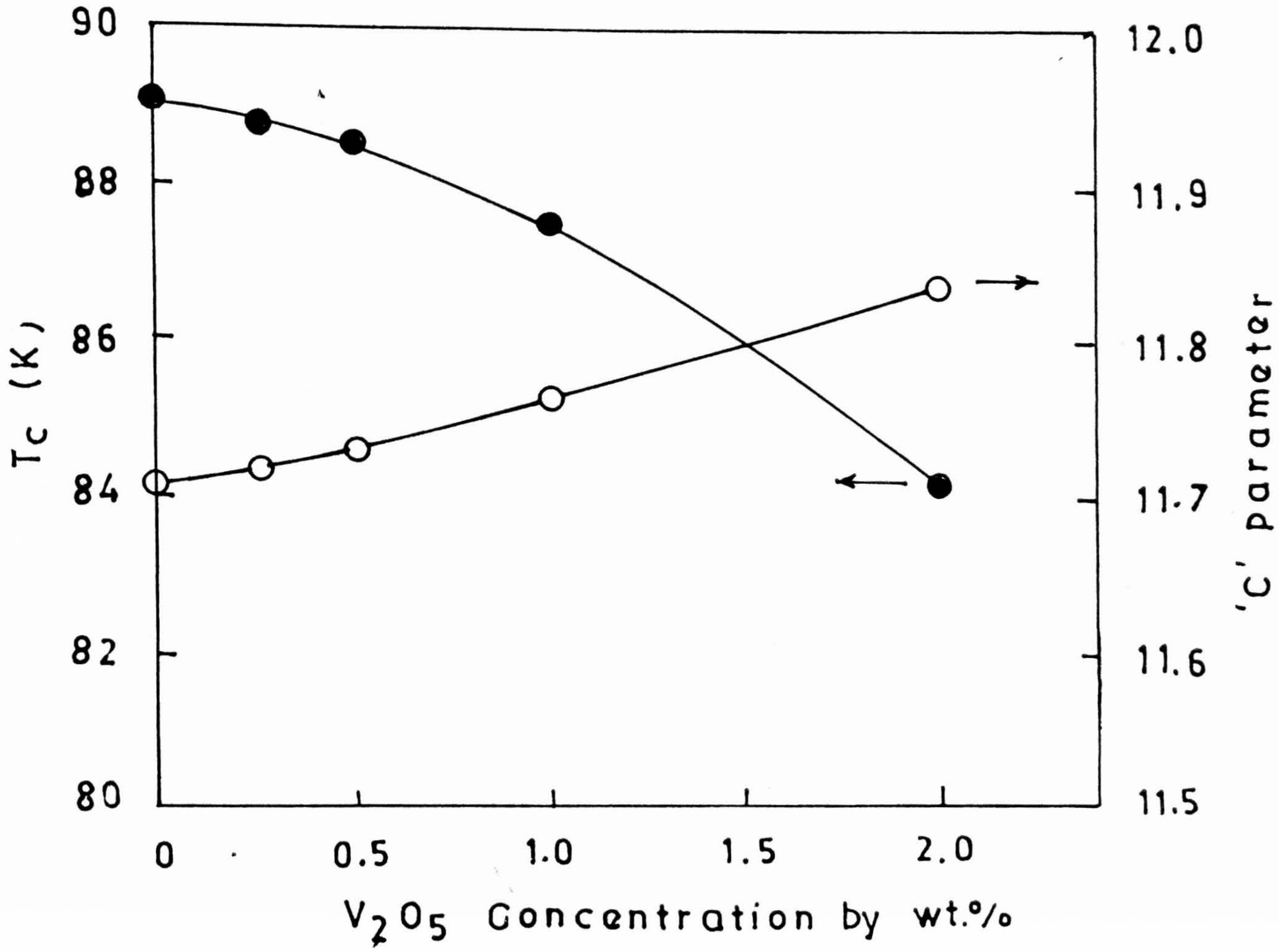

Fig.7.2. Transition temperature T_c C-parameter vs V_2O_5 concentrations.

Table 7.2
V_2O_5 Addition Results

Sl. No.	Doping conc.wt.%	Thickness Å	ρ_{300} mΩ-cm	R_{300}/R_{100}	T_{co} (K)	$J_c(77K)$ (10^6 A/cm^2)
1.	0.00	2040	0.182	2.962	89.25	1.4
2.	0.25	2015	0.111	3.106	88.9	2.2
3.	0.5	1985	0.253	3.175	88.1	3.4
4.	1.0	1890	0.350	2.586	86.0	0.8
5.	2.0	1924	0.654	2.586	84.2	0.5

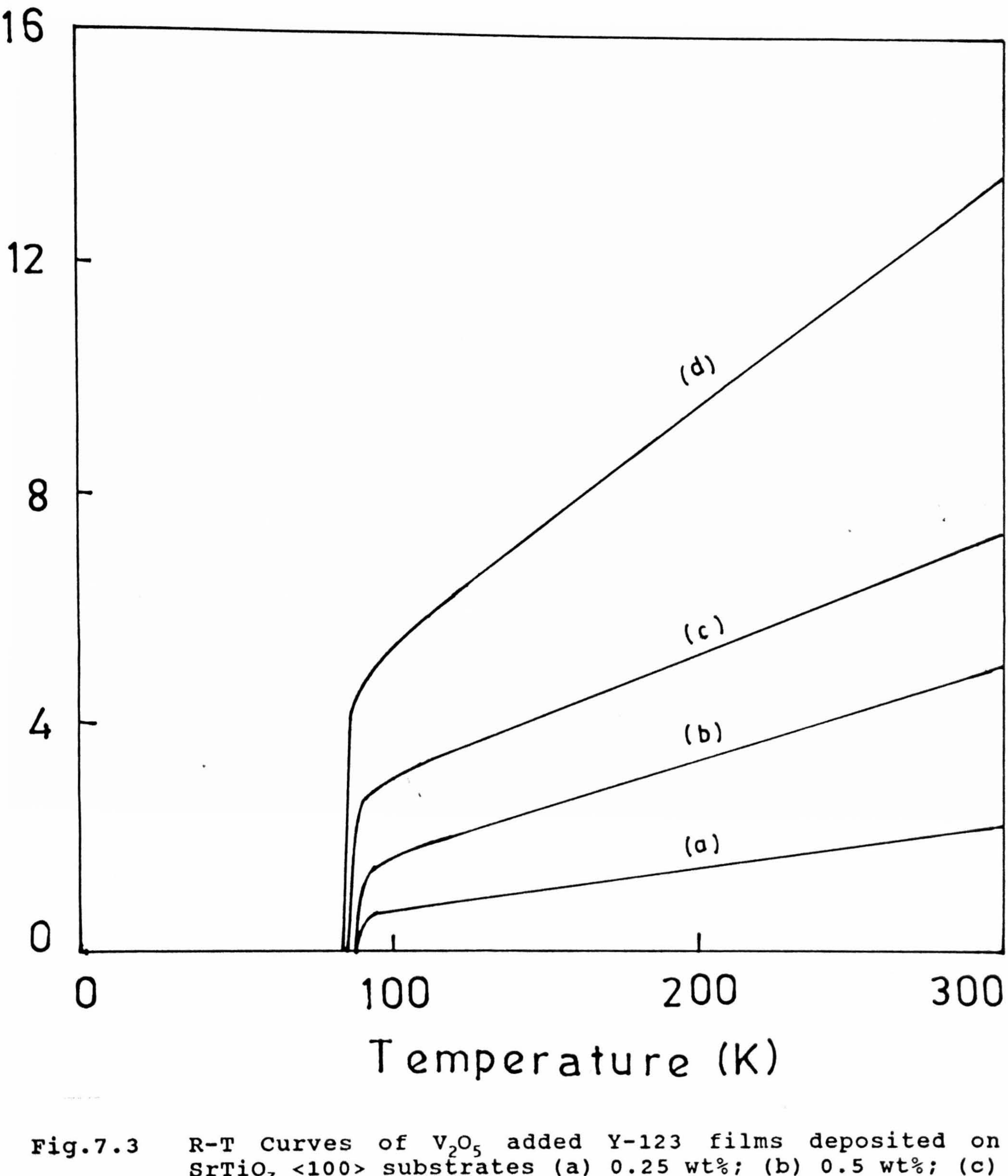

Fig.7.3 R-T Curves of V_2O_5 added Y-123 films deposited on $SrTiO_3$ <100> substrates (a) 0.25 wt%; (b) 0.5 wt%; (c) 1.0 wt% and (d) 2.0 wt%.

(a) J_c Measurements :

Since the high T_c films are granular in nature, the grain boundary limits the current density (J_c). The nature of grain boundaries in doped and undoped $Y-123$ thin films was discussed in earlier chapters using a model proposed by De Gennes and Clarke [15,16] which predicts that near T_c the critical current density of SNS junctions can be expressed as

$$J_c(T) \propto (T_c - T)^2 \exp\left(\frac{-d}{\xi_N}\right)$$

or

$$\sqrt{J_c}(T) \propto (T_c - T) \exp\left(\frac{-d}{2\xi_N}\right)$$

This indicates that the slope of $\sqrt{J_c}(T)$ vs $(T_c - T)$ plot is an inverse expeonential function of d. If the same proportionality constant in above eequation and the same coherence length ξ_N is taken to be unchanged for both doped and undoped films, the slopes of $\sqrt{J_c}$ vs $T_c - T$ will give a measure of the grain boundary thickness in the two types of films. This holds good strictly close to T_c.

Fig.7.4a shows the $\sqrt{J_c}$ vs $(T_c - T)$ behaviour of V_2O_5 doped films upto 0.5 wt% concentration of V_2O_5. Y-123 film doped with 0.5 wt% has relatively higher slope when compared with that of 0.025 doped and undoped (0.0%) $Y-123$ thin films, i.e., the grain boundary is relatively more metallic for 0.5 wt%. It indicates that the microstructure of the V_2O_5 doped films is improved over $Y-123$ thin films, upto 0.5 wt%. However, this SNS model do not fit to 1 wt% and 2 wt% concentrations of the V_2O_5 deped films. Hence, other models like SIS were tried to fit this data. If the barrier between the superconducting grains are of an insulating nature, the maximum supercurrent (I_o) is given by the expression of Ambegaokar and Baratoff (AB) [17]. The AB theory gives for a Josephson junction between two identical superconductors. Near T_c one has

$$J_c \propto (T_c - T)$$

for SIS kind junctions, as illustrated in chapter 3 sec. 5.4(a).

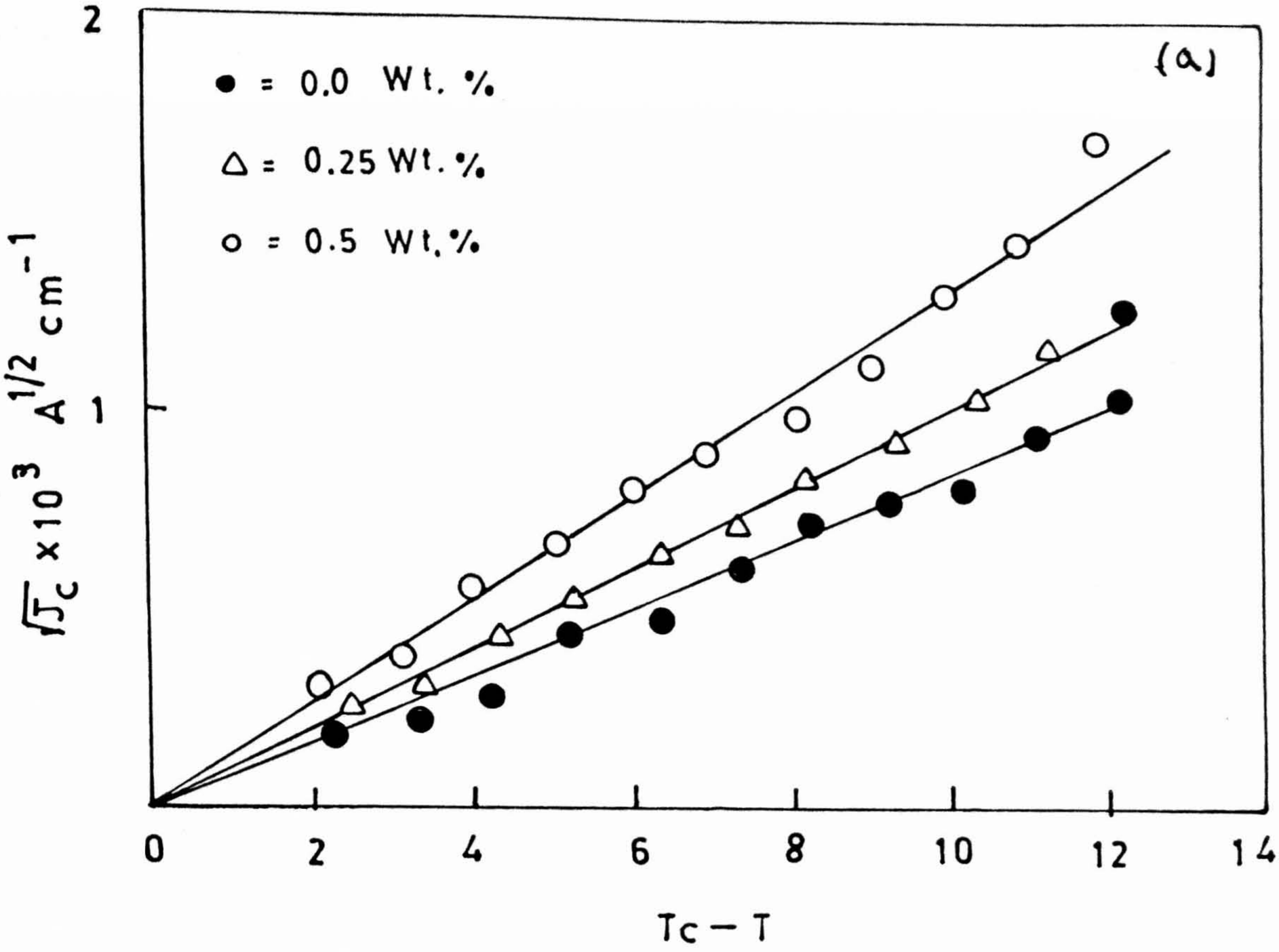

Fig.7.4 (a) $\sqrt{J_c}$ vs T_c - T plots for V_2O_5 doped Y-123 films for 0.0, 0.25 and 0.5 concentrations

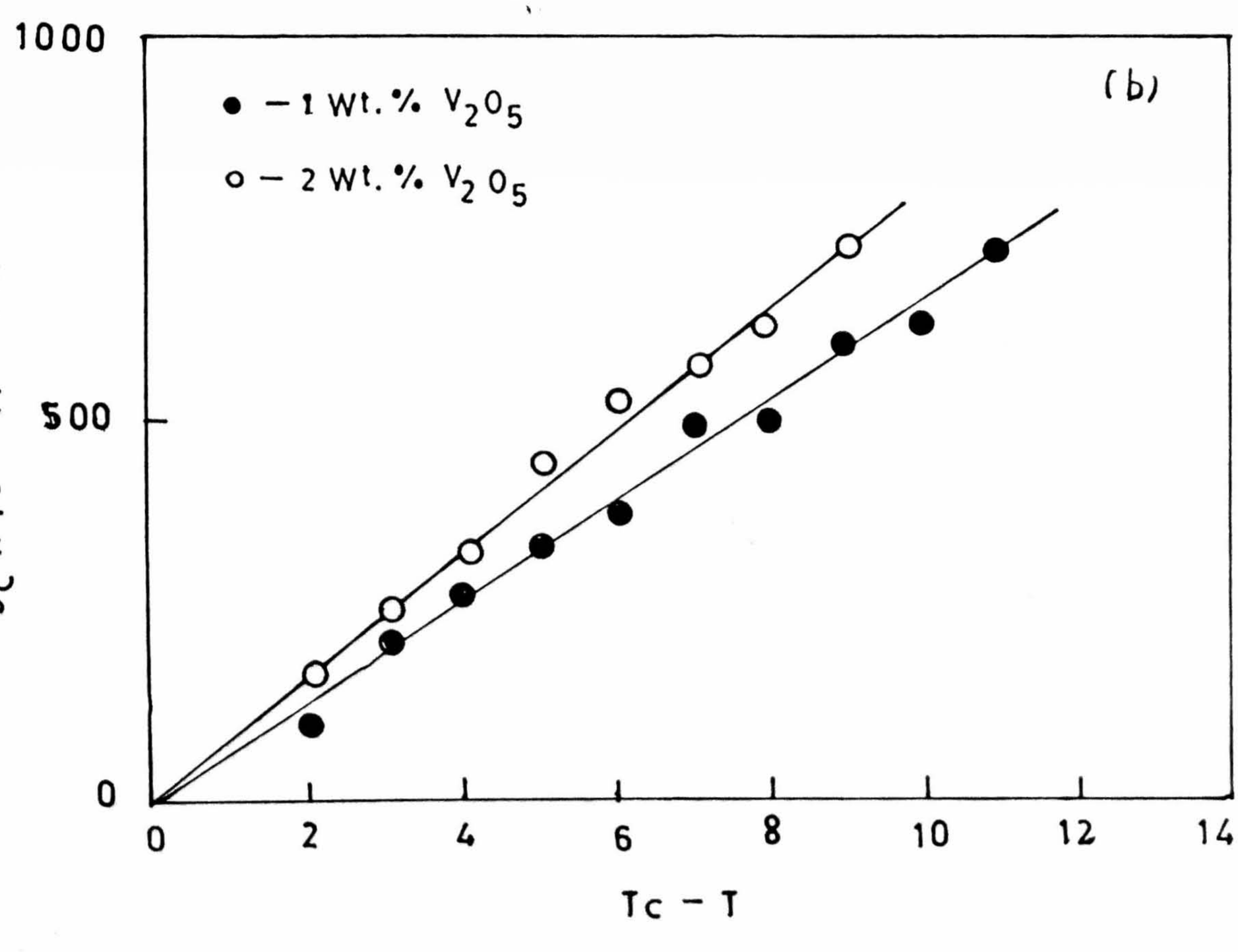

Fig.7.4 (b) J_c vs T_c - T plots for V_2O_5 doped Y-123 films for 1.0, and 2.0 concentrations

Fig.7.4b shows J_c vs $(T_c - T)$ behavior for 1 wt% and 2 wt% of V_2O_5 doped $Y-123$ thin films. The linear behaviour of the graph indicates the existence of insulating phase at the grain boundaries which may be responsible for the limiting T_c as well as J_c in the present case.

Overall, the experimental results have shown some improvement in V_2O_5 doped $Y-123$ thin films upto 0.5 wt% than undoped $Y-123$ thin films prepared at the same deposition conditions. The improvement can be speculated by few possible mechanisms.

The first mechanism is based on the high mobility of V_2O_5 on the high temperature substrate (~700°C) due to its low melting point which is less than the deposition temperature of $Y-123$. As the $Y-123$ lattice can accommodate V or V_2O_5 atoms, they segregate as agglomerates in localized regions. Furthermore the high mobility of V_2O_5 atoms is expected to increase the surface mobility of other atoms forming $Y-123$ lattice by importing their momentum. This enhanced surface mobility may be responsible for the significant increase in grain size and grain alignment. These factors might be responsible for the improvement in microstructure and hence J_c, of laser deposited V_2O_5 doped $Y-123$ thin films when compared with that of undoped $Y-123$ thin films prepared under identical deposition conditions.

Another mechanism which one can imagine is, the laser deposition process itself. When high energy laser pulse hits the target surface, it generates local heat, having temperature greater than 2000°C and produces plasma. This plasma consists of many species. Because of such high temperature V_2O_5 may decompose and reaching the substrate surface and may be segregating at the grain boundaries and forming SNS type microstructure. However, the possibility of reoxidation of vanadium can not be ruled out in the high oxygen environment (200 mTorr) in the plume after ablation. But, the SNS type behaviour of the $\sqrt{J_c}$ vs $T_c - T$ curves upto 0.5 wt% V_2O_5 doped $Y-123$ thin films indicates that the grain boundary junctions are metallic. So it can be suggested that V_2O_5 is acting as a flux due to its low melting point (690°C) and improving the microstructure of $Y-123$.

However, above 1 wt% of V_2O_5 doped $Y-123$ thin films confirm the impurity phase growth, which is due to the intermediate phase grown at grain boundaries with the increase of V_2O_5 concentration. Also the linear behaviour of J_c vs $(T_c - T)$ confirms the insulating nature of the grain boundary domains.

From these observations, it can be interpreted as upto 0.5 wt% of V_2O_5 addition one can improve superconducting properties of $Y-123$ thin films when compared with undoped $Y-123$ films deposited under identical deposition conditions due to V_2O_5 surfactant like nature [13].

7.3.2 Nb_2O_5 doped Y-123 thin films

Highly c-axis oriented films with $< 00l >$ reflections were grown on $SrTiO_3 < 100 >$ substrates Fig.7.5 shows the XRD of the $Y-123$ films added with 0.0%, 0.25%, 0.5%, 1% and 2% of Nb_2O_5 by weight. However, an impurity phase peak was observed around 43^o of 2θ. It was identified as YBa_2NbO_6 phase. The FWHM values correspond to $< 005 >$ reflection of Nb_2O_5 doped $Y-123$ films are 0.20^o, 0.25^o, 0.27^o, 0.34^o and 0.37^o for 0.0%, 0.25%, 0.5%, 1% and 2% respectively. With Nb_2O_5 addition there is an improvement in the crystallinity upto 0.5 wt% and above which degeneration of crystalline quantity has been observed from these FWHM values.

Fig.7.6 shows the variation of T_c and c-parameter with concentration. The c-parameter varies slowly upto 0.5 wt% and increases rapidly beyond 0.5 wt% of doping concentration. Drastic decrease in T_c is observed for dopant concentration beyond 0.5 wt%. Fig.7.7 also shows R T curves of Nb_2O_5 doped films. Increase of room temperature resistance with the increase of Nb_2O_5 concentration has been observed. Table 7.3 shows the results of Nb_2O_5 doped Y-123 films. From these results it is noticed that T_c remains around 88 K and J_c increased from 1.2 to 1.8 times 10^6 A/cm^2. Above 0.5 wtaddition of Nb_2O_5tY-123 films

The critical current density variation near T_c in Nb_2O_5 doped $Y-123$ films was

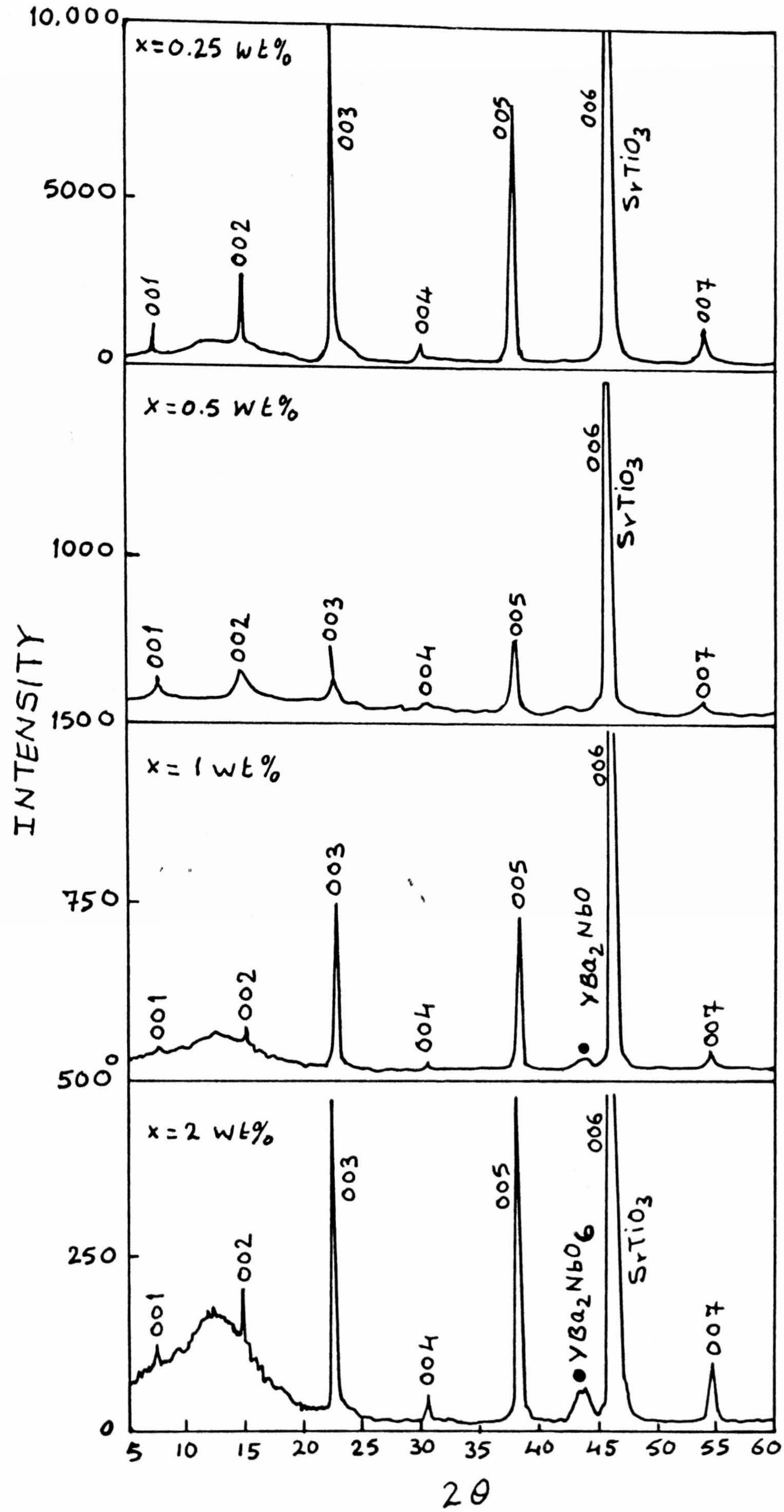

Fig.7.5 XRD patterns of Nb_2O_5 added Y-123 films on $SrTiO_3$ <100>.

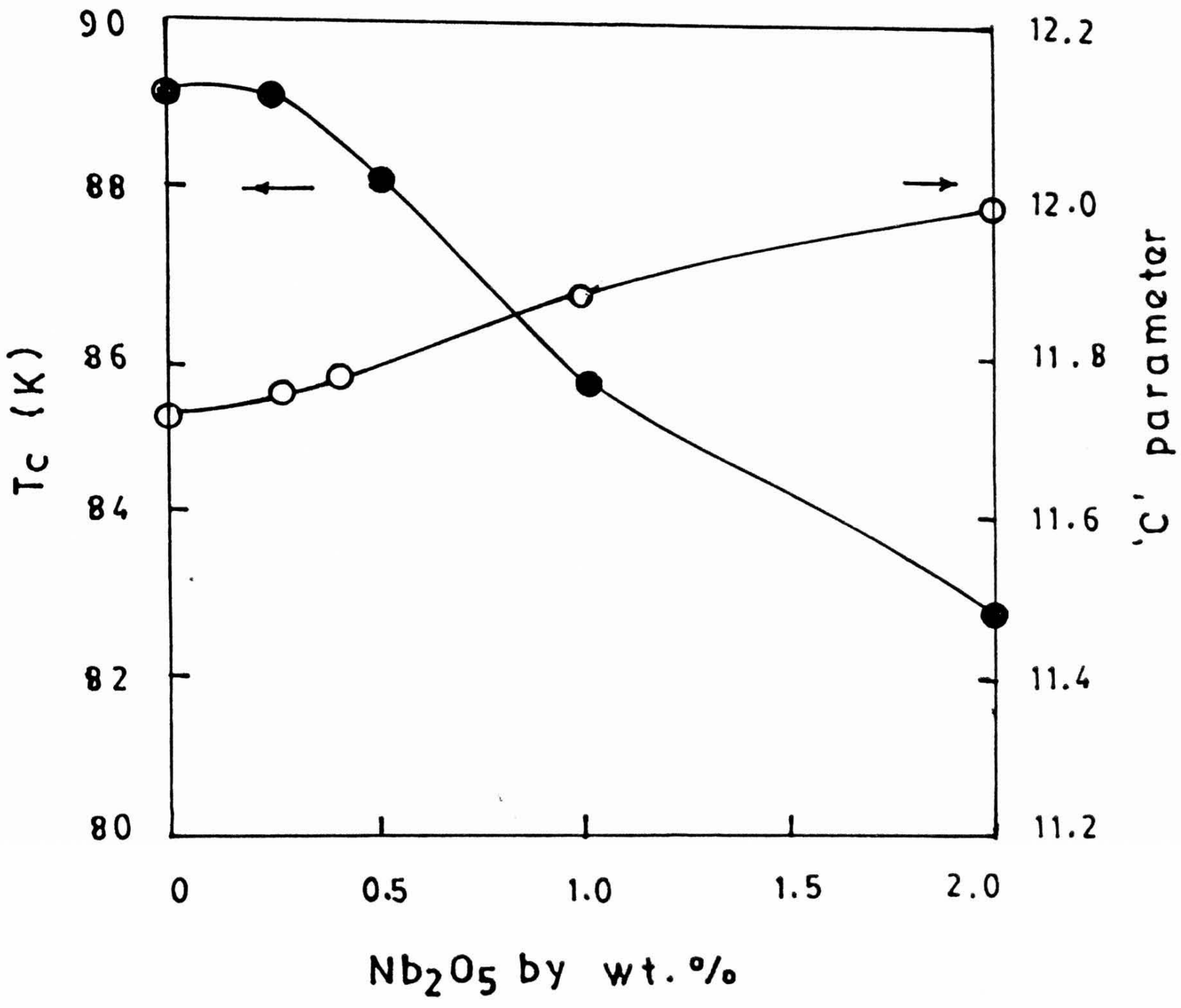

Fig.7.6. Variation of C parameter and T_c vs with Nb_2O_5 doping in Y-123 thin films.

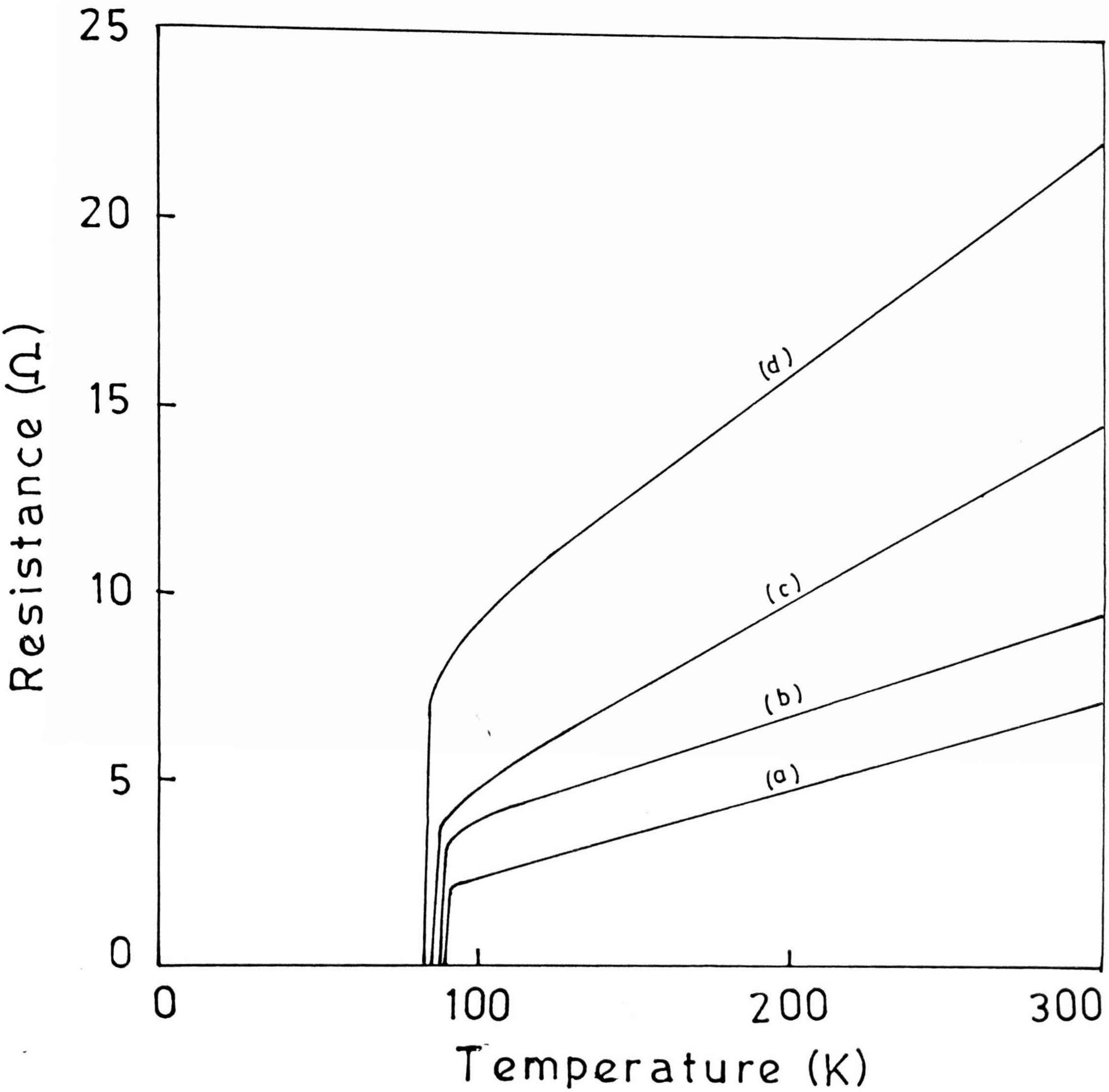

Fig.7.7. Resistivity vs Temperature plot Nb_2O_5 doped in Y-123 thin films for (a) 0.25; (b) 0.5; (c) 1.0 and (d); 2.0 wt% doped concentrations.

Table 7.3
Addition of Nb_2O_5 to Y-123

Sl. No.	Doping conc. by wt.%	Thickness (Å)	ρ_{300} (mΩ-cm)	R_{300}/R_{100}	T_{co} (K)	$J_c(77K)$ (10^6 A/cm^2)
1.	0.00	2040	0.183	2.96	89.3	1.4
2.	0.25	1992	0.374	3.06	89.3	1.6
3.	0.50	1954	0.423	3.20	88.1	1.8
4.	1.00	1860	0.684	3.09	85.7	0.8
5.	2.00	1910	1.064	2.43	82.8	0.3

explained on the basis of the model proposed by De Gennes and Clark (upto 0.5 wt%) and Ambegaoker and Bartoff model for above 0.5 wtbehavior of $\sqrt{J_c}$ with $T_c - T$ for 0.0%, 0.25%, and 0.5% by weight and Fig.7.8b shows the linear behaviour of J_c with $T_c - T$ nearer to T_c (i.e., upto 77 K).

It clearly indicates that addition of Nb_2O_5 may be segregating at grain boundaries and grain boundary contact is of insulating nature above 0.5 wt%. However, the J_c values of Nb_2O_5 added $Y-123$ films for 0.25 and 0.5 concentration have shown small improvement instead of decreasing. This improvement suggests that lower level Nb_2O_5 doping can improve microstructure in laser ablated films and hence there is a little improvement when compared with that of $Y - 123$ thin films prepared under the same deposition conditions. The improvement can be attributed to well oxygenation and sealing the oxygen leak path with the Nb_2O_5 at grain boundary. However, well oxygenation was confirmed in the case of Nb_2O_5 added bulk $Y - 123$ sample [5]. So the same mechanism can be applied to thin films also.

But above 0.5 wt% addition, the growth of YBa_2NbO_6 phase takes place and increases with the increase of Nb_2O_5 concentration. That means, the insulating phase at the grain boundaries is increasing and widening the weak links and limiting the intergrain J_c. Moreover reduction in T_c for 1 wt% and 2 wt% film may be due to the oxygen deficiency caused by YBa_2NbO_6 phase growth at grain boundary. That means, oxygen supply to the $Y - 123$ has been reduced during the film growth as YBa_2NbO_6 phase growth also requires.

Overall Nb_2O_5 addition has not produced any substantial changes in the superconducting properties of $Y - 123$ thin films as it did in the case of bulk samples [6-9]. But when compared with undoped $Y - 123$ films there is little improvement. The speculative explanation could be due to the higher melting point of Nb_2O_5 and also faster reoxidation on substrate surface and higher chemical reactivity with $Y - 123$ lattice at grain boundaries, which results in degradation and structure collapse of $Y-123$ faster when compared with that of V_2O_5 added thin films. Nb_2O_5 addition of further concentrations study is not at all necessary as it is very clear from earlier chapter that YBa_2NbO_6 dominates

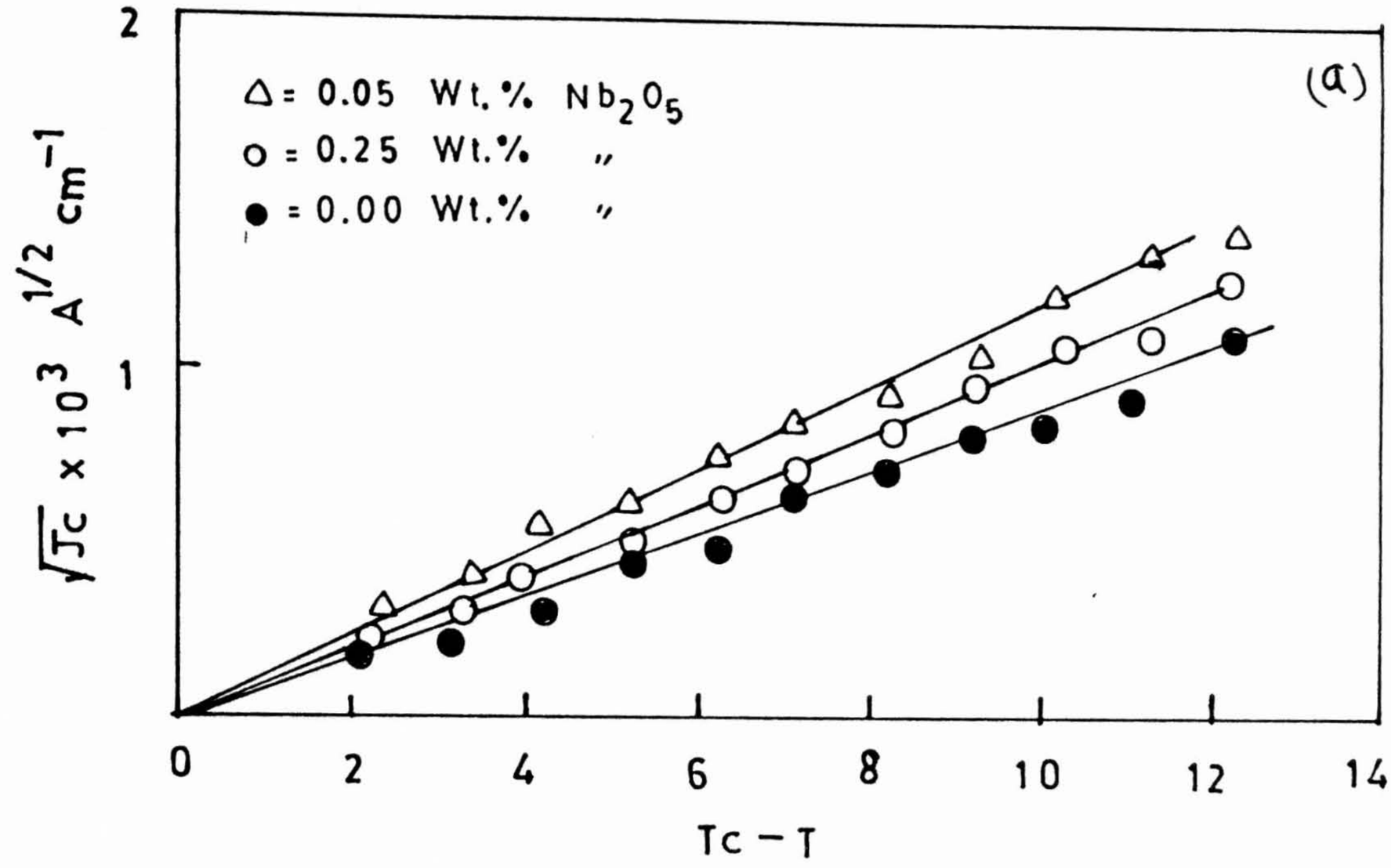

Fig.7.8 (a) $\sqrt{J_c}$ vs T_c- T plots for Nb_2O_5 doped Y-123 films for 0.0, 0.25 and 0.5 wt% concentrations

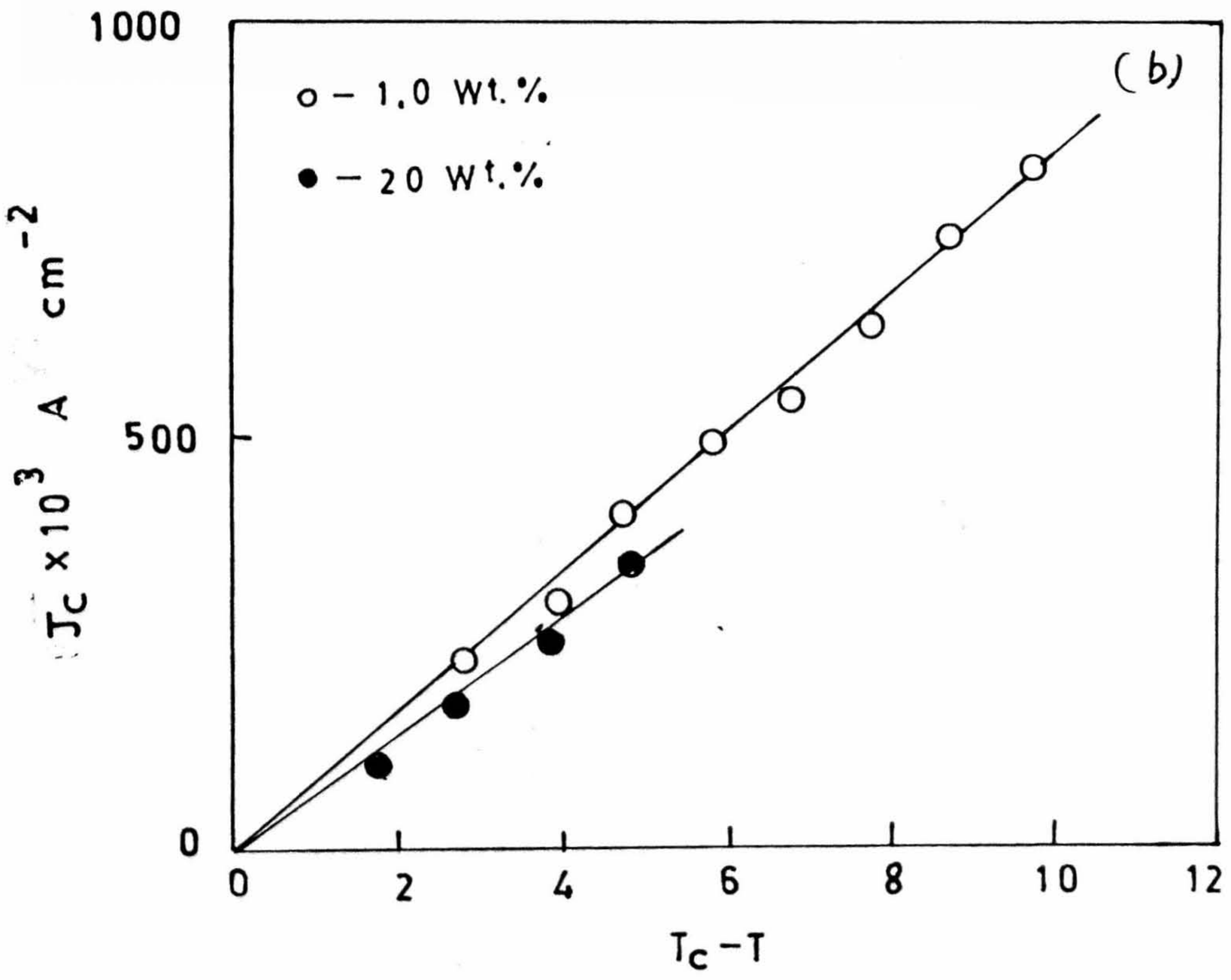

Fig.7.8 (b) $\sqrt{J_c}$ vs T_c- T plots for Nb_2O_5 doped Y-123 films for 0.0, 0.25 and 0.5 concentrations

and the $Y-123$ has completely transformed into YBa_2NbO_6 at higher concentrations of Nb substitution. The same can be expected here. Moreover present study aimed at synthesization of good quality $Y-123$ thin films using metal oxides as surfactants.

7.3.3 Ageing studies

0.5 wt% of V_2O_5 and Nb_2O_5 doped $Y-123$ thin films and undoped $Y-123$ thin films were preserved in a desicator at laboratory conditions and its resistivity measurement and J_c measurements were carried out on every 10th day periodically upto 60 days. Fig.7.9 shows the T_c vs number of days plot. Table 7.4 gives the summary of the ageing effect results.

0.5 wt% V_2O_5 doped $Y-123$ thin films have shown hardly any degradation with time. But 0.5 wt% Nb_2O_5 doped $Y-123$ and undoped $Y-123$ have shown significant degradation of superconductivity with time. The possible explanation for the better ageing effect in the case of V_2O_5 added $Y-123$ film may be due to the surfactant nature and metallic nature of vanadium at grain boundary junctions (SNS). Whereas in the case of Nb_2O_5 addition, even though the contact is SNS type at the grain boundary it exhibits poor ageing effect due to possible enhancement of porosity leading to the escape of oxygen from the lattice. But in the case of the $Y-123$ there is no dopant material at the grain boundary which can seal off the escape path of oxygen, and hence random orientation of grains and large weak links are responsible for the degradation of superconducting properties with time when deposited at relatively lower substrate temperatures (i.e., around 700°C).

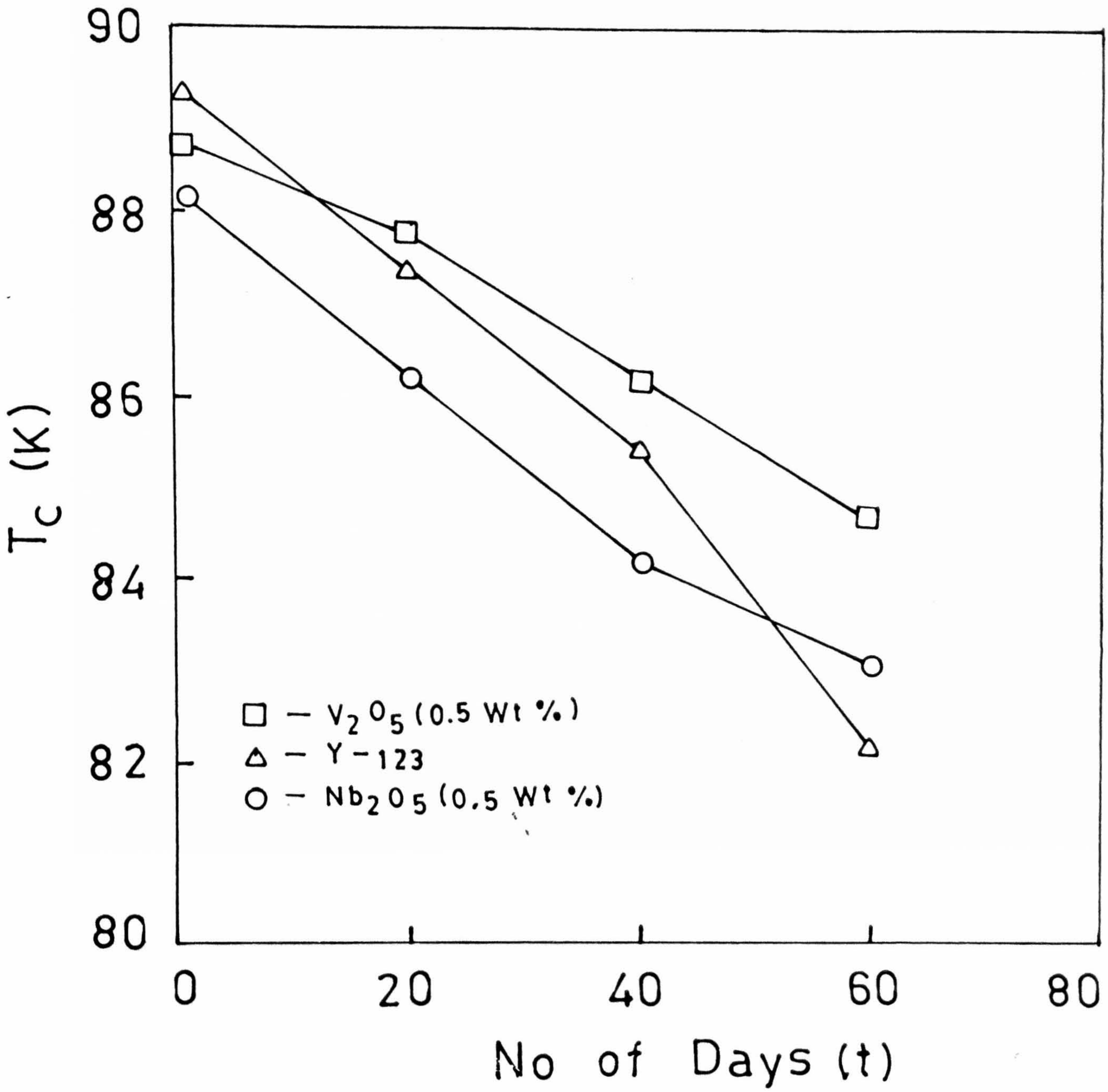

Fig.7.9 A comparitive graph of variation of Tc with time (days) for 0.5 wt % dopant concentration of V_2O_5, Nb_2O_5 doped Y-123 and undoped Y-123 films.

Table 7.4
Aging Studies Results

Sl No	Sample Name	time days.	R_{300} Ω	ρ Ωcm	$\frac{R_{300}}{R_{100}}$	T_c			J_c - A/cm^2 at 77 K
						T_c onset	T_{co}	ΔT_c	
1	Undoped Y-123 film 2040Å (Y123)	1st day	3.5838	0.182774 $\times 10^{-3}$	2.962	90.50	89.25	1.25	1.2×10^6
		10th day	8.2340	0.41490 $\times 10^{-3}$	2.420	89.10	87.40	1.70	7.2×10^5
		40th day	16.26	0.82926 $\times 10^{-3}$	2.12	88.3	85.4	3.0	4.0×10^5
		60th day	25.142	0.1.282 $\times 10^{-3}$	1.9	87.4	82.2	5.2	9.0×10^4
2	0.5 wt.% V_2O_5 doped Y-123 film 1954 Å (VA5)	1st day	5.0312	0.25345 $\times 10^{-3}$	3.175	88.7	88.7	1.0	3.2×10^6
		20th day	7 2135	0.35796 $\times 10^{-3}$	2.850	89.7	87.8	2.00	1.8×10^6
		40th day	9.452	0.48405 $\times 10^{-3}$	2.50	89.4	76.62	3.2	7.0×10^5
		60th day	10.425	0.54215 $\times 10^{-3}$	2.05	88.5	84.7	3.8	5.0×10^5
3	0.5 wt.% Nb_2O_5 doped Y 123 film 1954 Å NBA7	1st day	3.656	0.42284 $\times 10^{-3}$	3.2	89.18	88.14	1.04	1.8×10^6
		20th day	10 512	0.51332 $\times 10^{-3}$	2.81	87.;7	86.2	1.5	8.5×10^5
		40th day	14.82	0.77395 $\times 10^{-3}$	2.45	87.5	84.2	3.5	6×10^5
		60th day	18 265	0.891805 $\times 10^{-3}$	1.45	87.2	83.1	4.1	3.5×10^5

7.3.4 A comparative study of V_2O_5 and Nb_2O_5 doping in Y-123 thin films

There is a significant improvement in the microstructure and superconductivity properties of V_2O_5 doped thin films than that of Nb_2O_5 of thin films. V_2O_5 acted as a surfactant due to its melting temperature (690°C) and hence was responsible for the improvement of superconducting properties upto 0.5 wt% addition. As Nb_2O_5 has very high melting temperature, it could not provide any surfactant like nature. But still there is little improvement when compared with pure/undoped $Y-123$ thin films. Fig. 7.10 shows the comparative graph which shows J_c vs dopant concentration of the Y-123 films at 77 K. In both the cases it exhibits a peak around 0.5 wt% dopant concentrations. Fig 7.11 (a) shows the SEM micrographs of the 0.5 wt% doped V_2O_5 and Fig. 7.11 (b) Nb_2O_5 Y-123 films. Smooth surface and reduced particulate growth can be seen on 0.5 wt% V_2O_5 doped thin films while big particulates with increased roughness can be seen in the case of 0.5 wt% dope thin films. Nb_2O_5 doped thin films.

The impurity phase grows at 1 wt% in the case of Nb_2O_5 doped films where as for V_2O_5 added films it grows at 2.0 wt%. The possible explanation for this may be due to less reactive nature of V_2O_5 and $Y-123$ lattice can accommodate relatively more concentration of V_2O_5 than Nb_2O_5.

From ageing studies, it appears upto 0.5 wt% any oxide dopant seems to improve the properties of $Y-123$ films when compared with that of undoped $Y-123$ thin films deposited under similar conditions. V_2O_5 doped $Y-123$ films have shown relatively less degraded properties when compared with that of Nb_2O_5 doped or undoped $Y-123$ thin film, with time

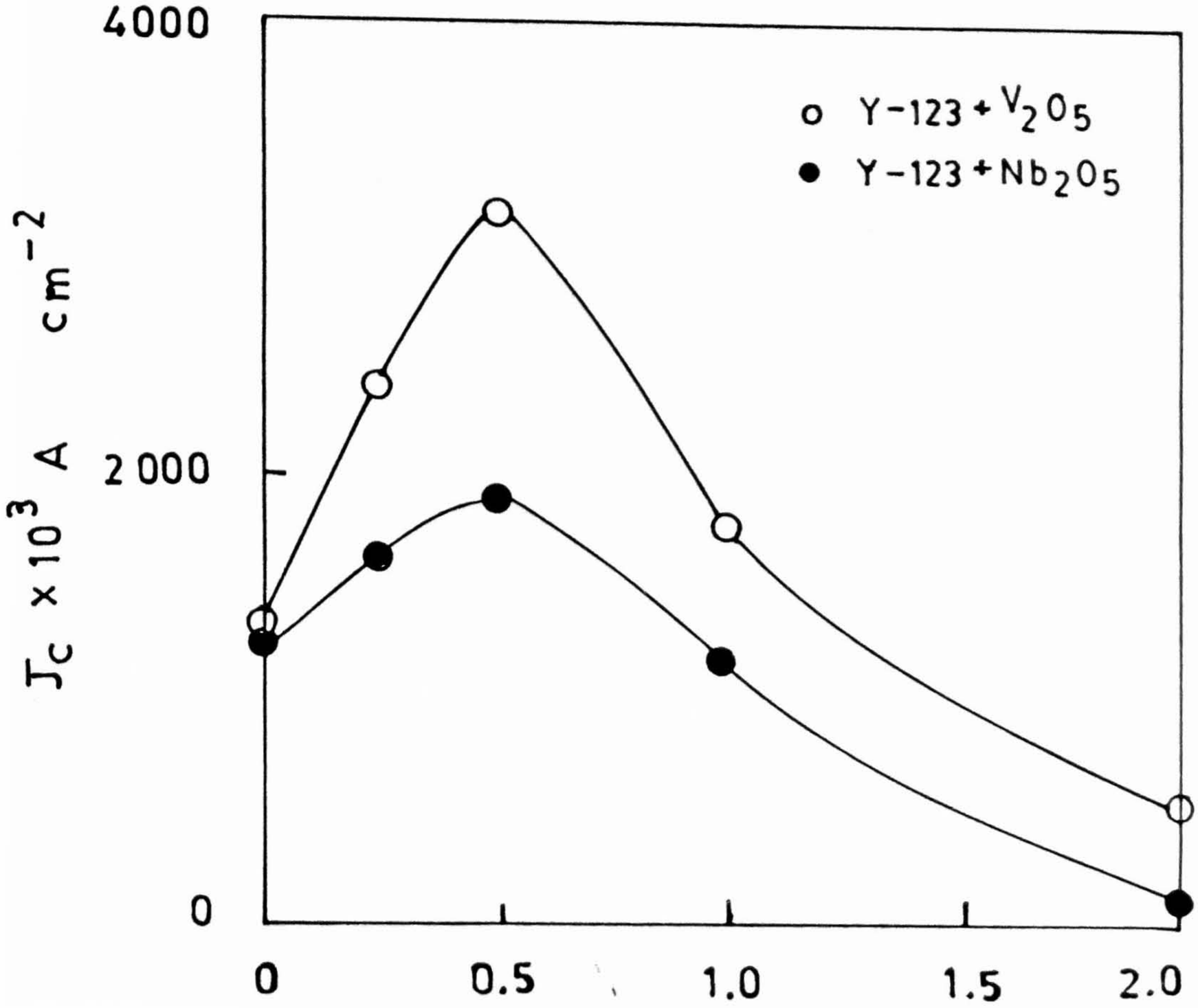

Fig.7.10 J_c vs dopant concentration plot of (o) V_2O_5 and Nb_2O_5 (●) doped Y-123 films.

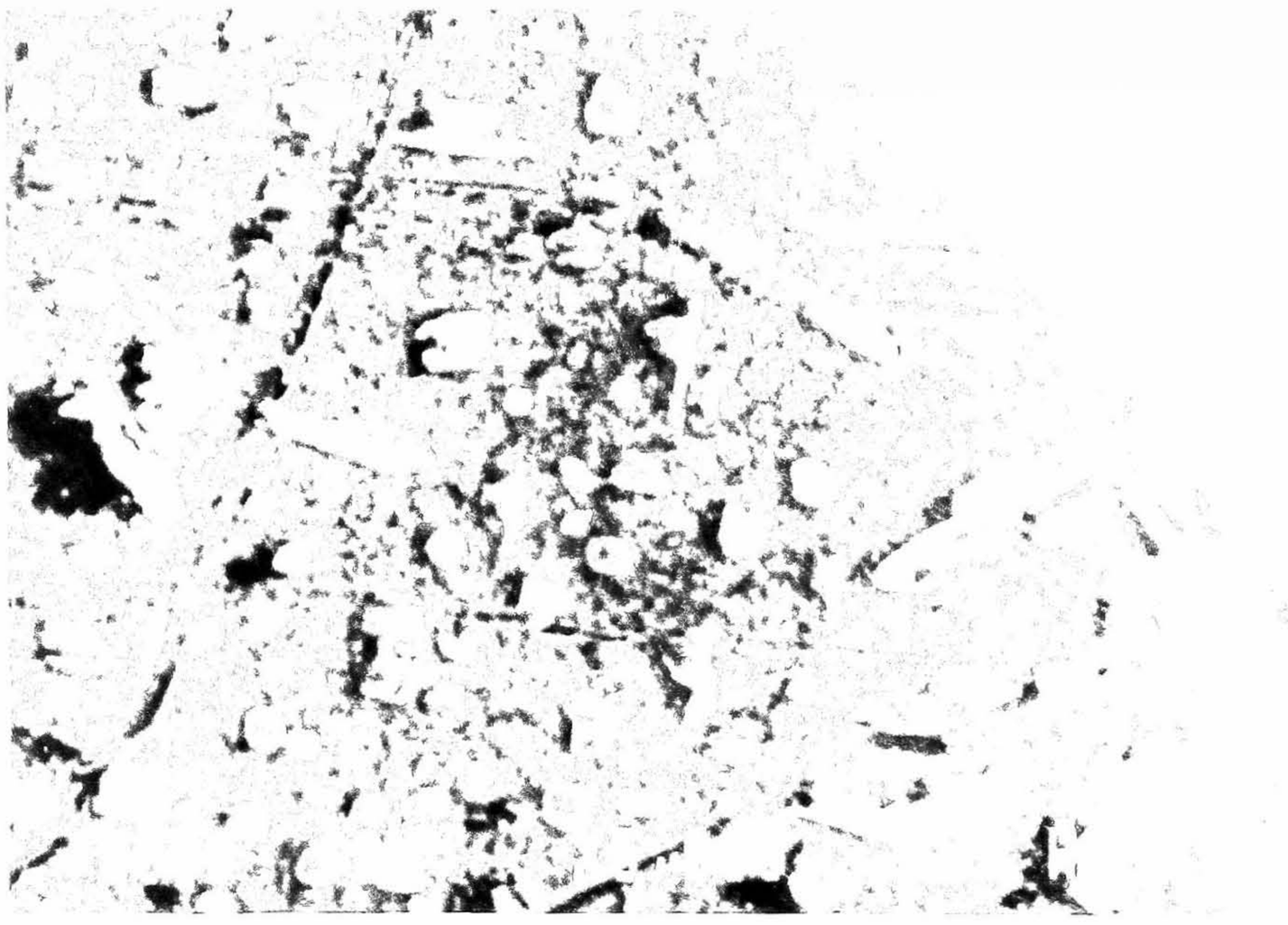

7.4 Conclusions

The addition of V_2O_5 and Nb_2O_5 in $Y-123$ thin films have been studied and analysed. These studies reveal,

1. Upto 0.5 wt% concentration of both the dopants, an improvement in the superconducting properties have been observed when compared with that of undoped $Y-123$ films.

2. 0.5 wt% of V_2O_5 doped $Y-123$ thin film has significant improvement in J_c at 77 K. The best possible J_c has been obtained is 3.4×10^6 Å/cm^2 at 77 K.

3. The best possible J_c for 0.5 wt% doped $Y-123$ thin film as observed is 1.8×10^6 Å/cm^2 at 77 K and for undoped $Y-123$ thin film is 1.2×10^6 Å/cm^2 at 77 K in the case of Nb_2O_5 addition.

4. Above 0.5 wt% addition of dopants have shown growth of impurity phase which slowly degrades the superconducting grains in both the cases.

5. The J_c variation with temperature is well described by using SNS and SIS models for granular superconductor.

6. The surfactant like nature of V_2O_5 (due its low melting point) was attributed to the significant improvement in the microstructure of V_2O_5 doped $Y-123$ thin films upto 0.5 wt%. The high melting point and hence less mobility of Nb_2O_5 on substrate surface and high chemical reactivity with $Y-123$ lattice at grain boundaries are responsible for the degraded properties of Nb_2O_5 doped $Y-123$ films.

7. These studies reveals the fact that certain level of transition metal oxide doping can relatively improve the superconducting properties of $Y-123$ thin films when compared with that of undoped $Y-123$ thin films.

References

[1] P. Chowdhary, R.H. Koch, R.B. Laibouitz, T.R. McGuire and R.J. Garedino, Phys Rev. Lett. **58** (1987) 2684.

[2] T.R. Digner, T.K. Worthington, W.J. Gorllagher and R.I. Sandstrom, Phys. Rev. Lett. **58** (1987) 2687.

[3] S. Jin and J.E. Gaeboner, Mater. sci. Eng. **137** B7 (1991) 243.

[4] S. Jin, T.H. Tiefel, R.A. Fastnarth and G.W. Kammlott, Appl. Phys. Lett. 60 (1992 3307.

[5] Y. Hikichi, T. Maruta, S. Suzuk, M. Niyamoto, S. Okada and K. Kudore. JJAP **31** (1992) L1232.

[6] G.W. Kammlott, T.H. Tiefel and S. Jin, Appl. Phys. Lett. **56** (1990) 2459.

[7] K.V. Paulore, J. Koshy and A.D. Damodaran, Jpn. J. App. Phys. **30** (1991) L458.

[8] K.V. Paulore, J. Koshy, P. Umadevi and A.D. Damodaran, Appl. Phys. Lett. **59** (1991) 1251.

[9] Y. Hikechi, T. Maruta, S. Suzuki, M. Miyamoto, S. Okada and K. Kudou, Jpn. J. Appl. Phys. **31** (1992) L1232.

[10] F.H. Streitz, M.Z. Cieplak, Gang Xiao, A. Courim, and C.L. Chein, Appl. Phys. Lett. **52** (1988) 927.

[11] D. Kumar, M. Sharan, R. Pinto, P.R. Apte, S.P. Pai, S.C. Purandare, L.C. Gupta and R. Vijayaraghavan, J. Appl. Phys. **62** (1993) 3522.

[12] J.A. Leins, M. Vegmann, C.E. Platt and M. Teepl, Appl. Phys. Lett. **64** (1994) 103.

[13] **M. Murugesan, R. Pinto, S.P. Pai, P.R. Apte, M. Sharan and L.C. Gupta, Physica C 234 (1994) 339.**

[14] J.M. Tarascon, L.H. Gune, P. Barboux, W.R. McKinaon, G.W. Hull, T.P. Orlando, K.A. Dehn, S. Fopner and E.J. McNiff, Phys. Rev. B**36** (1987) 8393.

[15] P.G. DeGenner, Rev. Mod. Phys. **36**, 225 (1964).

[16] J. Clarke, Proc. R. Soc. London A**308** (1969) 442.

[17] V. Ambegaokar and Baratoff, Phys. Rev. Lett. **10** (1963) 486.

Summary

Ever since the discovery of the High T_c the researchers are trying to improve the superconducting properties of the newly invented compounds. This thesis work is one such successful attempt. A focus was given to fabricate high quality thin films by using Sputtering and Pulsed Laser ablation techniques. In that process, initially a planar magnetron sputtering system with one inch dia target electrode was designed and fabricated for growing better quality films. Using this system thick and thin $Y-123$ film (nearly $1000A$) superconducting films have been grown having critical current densities (J_c) between $10^4 - 10^5 A/cm^2$ at 77 K. An attempt was made to grow insitu single phase $Y-124$ films. It is observed that films deposited on substrates held at above $650°C$, show $Y-123$ phase and substrates held at below $600°C$ favours $Y-124$ phase.

It is well known that for technological applications and device fabrication one needs to deposit good quality of HTS films on Si and Sapphire substrates. In this thesis another such a successful attempt was made using YSZ and STO buffer layer. The dependence of microstructure of buffer layers on growth conditions was studied using a very recent technique Atomic Force Microscopy (AFM). YSZ films grown on substrates held at $800°C$ with sputtering chamber pressure held at 5 mTorr $Ar+O_2(9:1)$ gas mixture are found to have a very good microstructure with average roughness of 3 nm. $5\%Ag$ doped $Y-123$ thin films deposited on YSZ buffered Sapphire substrate, show high $J_c(4.5x10^6 A/cm^2)$ This result was found highly reproducible.

The Pulsed Laser Deposition (PLD) is one of the simplest among the various thin film deposition techniques for depositing multicomponent HTS films. In the present study, PLD parameters were varied and studied for growing good $Y-123$ and $Yb-123$ films on $LaAlO_3(LAO)$ substrates. Using AFM the surface morphology of the films deposited was studied and found there is a direct relationship between film microstructure and

superconducting properties (T_c and J_c).$Yb-123$ films grown on substrates held at $700°C$ show better superconducting properties ($88K$ and $1.5x10^6 A/cm^2$ at $77K$) than the films grown at 725 and $675°C$ substrate temperature. $Y-123$ films grown at $725°C$ and above have shown better superconducting properties than the films deposited at 675 or 700°C. $Yb-123$ films have shown spiral like growth reproducible around $700°C$ and they have aJ_c of $3x10^6 A/cm^2$ at 77 K. So far the reported J_c was never crossed more than $5x10^5 A/cm^2$ at $77K$ in $Yb-123$ films irrespective of the growth technique. Moreover this is the first report on $Yb-123$ films by using PLD method to the best of the author's knowledge.

Using PLD technique, $YBa_2Cu_{3-x}Nb_xO_{7-y}$ thin films for $x = 0-1$ were prepared and examined. For that the Nb substitution at Cu site upto $x = .05$ atomic concentration in $YBa_2Cu_{3-x}Nb_xO_y$ films, J_c was found to improve when compared the same with that of the undoped $Y-123$ films. It is observed that single phase $YBa_2NbO_6(YBNO)$ grows when $x \geq 0.1$ with $< h00 >$ orientation which is cubic phase having lattice constant 8.304 Å. This is the first report of growth of YBa_2NbO_6 in the form of thin films to the best of authors knowledge. Results presented here indirectly indicate that Nb is difficult to substitute because it prefers to form an intermediate compound YBa_2NbO_6. Single phase $< h00 >$ oriented YBNO films were obtained at $x = 0.5$ when deposited at 800°C.

Addition of V_2O_5 which is having low melting temperature and addition of Nb_2O_5 which is having high melting temperature, to $Y-123$ films is studied and found that oxides having melting temperatures less than $700°C$ are good candidates for improving microstructure of $Y-123$ and hence superconducting properties of $Y-123$ thin films. However, there is a optimum for doping concentration above which degradation of superconductivity takes place.

Models proposed by DeGennes and Clarke and Ambegaokar and Bartoff for granular superconductors to explain the temperature dependence of J_c of conventional superconductors was applied to HTS films prepared in this work. Critical current density measurements close to T_c are were done to all the films. Using the $J_c(T)$ data close to T_c. Some conclusion with respect to the microstructure of which is good the films were drawn which seem to agree qualitatively with the SEM and AFM results. films was predicted and confirmed through SEM and AFM studies is well in agreement with the SNS and

SIS microstructure models.

Over all this work reviews a study on the affect of substrate temperature and deposition parameters on the microstructural properties of growth of HTS $R-123$ films. Optimization of deposition conditions are reported for YSZ and STO buffer layers for depositing high quality HTS films on Sapphire and Silicon substrates. Substitution and addition effects of metal oxides on the superconducting properties of $Y-123$ films were studied.

Scope of the Future Work

The research on SUPERCONDUCTIVITY is a very exciting ever green challenging field for theoreticians as well as experimentalists. Research itself is a continuing process. There is a lot of scope for further work in the reported results of this thesis. The extension for the future scope of this thesis work is mentioned below.

The magnetron geometry (transverse field) mentioned in this thesis can be studied in detail in order to obtain a relationship between fields *vs* microstructural properties of the films by keeping other deposition parameters constant or by varying the deposition parameters and keeping the field constant. Moreover, thickness variation is another major topic was not covered here can be continued.

In the buffer layers work the thermal recycling effect of the buffer layers is a very interesting point of study for technological applications should be studied in detail

In this thesis an attempt was made to study the Nb substitution at Cu site in detail. But lot many things like metal to insulator transition and the underlying physics have yet to be explained. The impurity phase YBa_2NbO_6 was found to be grow preferentially when Nb substitution at the Cu site exceeds 0.1 at%. Further studies on this phase as buffer layer for HTS films deposition on Si or Sapphire need to be explored. Magnetic properties of the HTS films grown in this work were not studied. It is very important to study these properties for eventual applications.

List of Publications

1. **Microstructural study of yittria stabilized zirconia buffered sapphire for $YBa_2Cu_3O_{7-y}$ thin films.**

   M. S. R. Rao, C.P. *D*' Souza, P. R. Apte, R. Pinto and L. C. Gupta, S.Srinivas and A.K. Bhatnagar

   J. Appl. Physics 79 (1996).

2. **A New Magnetron Geometry for *RF* sputtering deposition of $YBa_2Cu_3O_{7-y}$ thin films.**

   S.Srinivas

   Proc. SSP symp 1990 Vol 33*cp*454.

3. **Study on the phase formation of YSZ films.**

   S. Srinivas, R. Pinto, S. P. Pai, D. Kumar, C. P. *D*'Souza, S. C. Purandare and A.K. Bhatnagar

   Proc. of SSP symp. 1993 vol.36*C*477.

4. **Polycrystalline $YBa_2Cu_4O_8$ thin films on Polycrystalline YSZ substrates.**

   S. Srinivas and A. K. Bhatnagar

   Proc. of SSP symp. vol36*C*(1993)5444.

5. **Superconducting properties of $YBa_2Cu_{3-x}Nb_xO_{7-y}$ thin films.**

   S. Srinivas, A. K. Bhatnagar, R. Pinto, S. P. Pai, P. R. Apte, S. C. Purandare and C.P.D'Souza

   NASA Proc. 3290 Vol II (1995) 762.

6. Growth and microstructural study of YSZ and STO buffer layers on Si and Sapphire substrates.

   S. Srinivas, R. Pinto, S. P. Pai, D. Kumar, C. P. *D*'Souza, S. C. Purandare and A. K. Bhatnagar

   NASA conf. Proc 3290 Vol 2(1995)770

7. Effect of V_2O_5 and Nb_2O_5 addition on the superconducting properties of $YBa_2Cu_3O_{7-\delta}$ films.

   S. Srinivas, A. K. Bhatnagar, R. Pinto, S. P. Pai, S. C. Purandare and C. P. *D*'Souza

   NASA Proc. 3290 Vol I (1995)241.

8. Growth of Insulating Buffer layers by *RF* Magnetron sputtering

   S. Srinivas, C. P. *D*' Souza, M.S.R. Rao, R. Pinto and A. K. Bhatnagar

   INCOVAST conf. Proc. vol 2. (1995) 353.

9. $YbBa_2Cu_3O_{7-x}$ thin films by PLD.

   S. Srinivas, M. S. R. Rao, S.P. Pai, S. C. Purandare, R. Pinto and A. K. Bhatnagar

   National Conf. Proc. on Thin films and applications (1995) *p*21

10. A Study on the Deposition of $YBa_2C_4O_8$ thin films.

    V. V. Saikumar, S.Srinivas, A.K. Bhatnagar, S.B Ogale and R.D. Vispute

    National Conf. proceedings on Thin films and applications (1995)

Communications

1. STUDY ON $Yb_{1-x}Dy_xBa_2Cu_3O_{7-\delta}$ SUPERCONDUCTOR.

   S. SRINIVAS, A.K. BHATNAGAR, V.R. PALKAR AND M.S. MULTANI

   (COMMUNICATED TO INT. J. OF MODERN PHYSICS).

2. STUDIES ON $YBa_2Cu_4O_8$ THIN FILMS.

   S.SRINIVAS, A.K.BHATNAGAR, S.B OGALE AND R.D.VISPUTE

   (COMMUNICATED TO PHYSICA C)

3. $YBa_2Cu_{3-x}Nb_xO_{7-\delta}$ THIN FILMS

   S.SRINIVAS, A.K. BHATNAGAR, S.P. PAI AND R. PINTO

   (COMMUNICATED TO JOURNAL OF APPLIED PHYSICS)

4. $Yb_1Ba_2Cu_3O_{7-x}$ THIN FILMS
   (COMMUNICATED TO RAPID COMMUNICATION PHYSICAL REVIEW B)

5. A STUDY ON GROWTH CONDITIONS AND THE MICROSTRUCTURE OF YSZ BUFFER LAYERS ON Si< 100 > SUBSTRATES.
   S.SRINIVAS, M.S.R. RAO, R.PINTO, S.C. PURANDARE AND A.K. BHATNAGAR
   (TO BE COMMUNICATED TO PHYSICA *C*)

6. A STUDY ON YSZ AND STO BUFFER LAYERS
   S.SRINIVAS, R.PINTO, S.P. PAI AND A.K. BHATNAGAR
   (TO BE COMMUNICATED TO PHYSICA *C*)

7. A STUDY ON *Nb* SUBSTITUTION AT *Cu* IN $YBa_2Cu_3O_{7-y}$ SYSTEM.
   S.SRINIVAS, A. K. BHATNAGAR, S.P. PAI AND R. PINTO.
   (TO BE COMMUNICATED TO PHYSICAL REV. *B*)

BIO-DATA

NAME : SATHIRAJU SRINIVAS

DATE OF BIRTH : 09-08-1962

NATIONALITY : INDIAN

ADDRESS FOR CORRESPONDENCE : B-7, 38/2RT, MUNCIPAL COLONY, MALAKPET, HYDERABAD -500 046, INDIA.
PHONE : 091-040-548954.

EDUCATIONAL QUALIFICATIONS :

DEGREE	UNIVERSITY	SUBJECT	YEAR	Class
M. Sc. (App.Phys)	J.N.T.Univ. Hyderabad	ELECTRONICS	1987	I (72.95%)
Ph. D.	UNIVERSITY OF HYDERABAD	PHYSICS	(Thesis submitted in January 1996)	

THESIS TITLE : STUDIES ON DOPED AND UNDOPED HIGH TEMPERATURE SUPERCONDUCTING THIN FILMS

SUPERVISOR : Prof. ANIL K BHATNAGAR.
School of Physics, University of Hyd.

RESEARCH EXPERIENCE : Nearly 7 years research experience in the field of thin films and HTS thin films.

TECHNICAL EXPERTISE : RF/DC Magnetron Sputtering techniques and Pulsed laser deposition techniques. Solid State ceramic Powder preparation, Metal Alloy preparation, Characterization techniques like XRD, EDAX, SEM, AFM, AES, Photolithography etc.

RESEARCH PUBLICATIONS : 9 PAPERS

REFERENCES :

1. PROF. ANIL KUMAR BHATNAGAR,
SCHOOL OF PHYSICS,
UNIVERSITY OF HYDERABAD,
HYDERABAD - 500 046.

2. PROF. R. PINTO,
SOLID STATE ELECTRONICS,
T.I.F.R.,
BOMBAY - 400 005.

3. Dr.(Mrs.)V.R.PALKAR,
SOLID STATE PHYSICS,
T.I.F.R., BOMBAY-400 005

4. Dr. V.S. RAGHUNATHAN,
HEAD OF PHYSICAL METALLURGY
IGCAR, KALPAKKAM 603201.

5. Dr. V.D. Vankar,
CMST, Thin film Laboratory,
IIT Delhi, Delhi -110 016.